

Title of thesis

**A Study on Enhanced Oil Recovery by Surfactants for a
Malaysian Sandstone Reservoir**

I, MUHAMMAD NADEEM

hereby allow my thesis to be placed at the Information Resource Centre (IRC) of Universiti Teknologi PETRONAS (UTP) with the following conditions:

1. The thesis becomes the property of UTP.
2. The IRC of UTP may take copies of the thesis for academic purpose only.
3. This thesis is classified as

Confidential

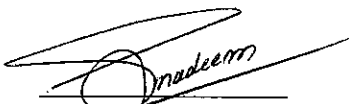
Non-confidential

If this thesis is confidential, please state the reason:

The contents of the thesis will remain confidential for _____ years.

Remarks on disclosure:

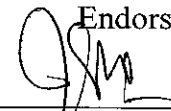
The contents or any part of the thesis should not be copied or published by anyone without the written permission by the author.



Signature of Author

Permanent: Department of Chemistry,
Address University of Agriculture,
Faisalabad-38040, Pakistan.

Date: 25/02/08

Endorsed by


Signature of Supervisor

Name of Supervisor
Assoc. Prof. Dr. Isa Bin Tan

Date: 25/02/08

Assoc. Prof. Dr. Isa Mohd Tan
Lecturer
Chemical Engineering Programme
Universiti Teknologi PETRONAS
31750 Tronoh
Perak Darul Ridzuan, MALAYSIA.

UNIVERSITI TEKNOLOGI PETRONAS

Approval by Supervisor

The undersigned certify that they have read, and recommend to The Postgraduate Studies Programme for acceptance, a thesis entitled

A Study on Enhanced Oil Recovery by Surfactants for a Malaysian Sandstone Reservoir

submitted by

Muhammad Nadeem

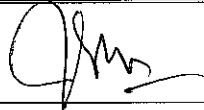
for the fulfillment of the requirements for the degree of

Doctor of Philosophy in Chemical Engineering

Date

Signature

:



Main Supervisor

:

Assoc. Prof. Dr. Isa Bin Tan

Date

:

25/02/08

Assoc. Prof. Dr. Isa Mohd Tan
Lecturer
Chemical Engineering Programme
Universiti Teknologi PETRONAS
31750 Tronoh
Perak Darul Ridzuan, MALAYSIA.

UNIVERSITI TEKNOLOGI PETRONAS

A Study on Enhanced Oil Recovery by Surfactants for a Malaysian Sandstone Reservoir

By

Muhammad Nadeem

A THESIS

SUBMITTED TO THE POSTGRADUATE STUDIES PROGRAMME

AS A REQUIREMENT FOR THE

DEGREE OF DOCTOR OF PHILOSOPHY IN

CHEMICAL ENGINEERING

BANDAR SERI ISKANDAR,

PERAK

December, 2007

DECLARATION

I hereby declare that the thesis is based on my original work except for quotations and citations which have been duly acknowledged. I also declare that it has not been previously or concurrently submitted for any other degree at UTP or other institutions.

Signature:



Name:

Muhammad Nadeem

Date:

25/02/08

Dedicated To My Late Father

ACKNOWLEDGEMENT

First and foremost, I owe an unrepayable debt to Almighty Allah; before Him are exposed all my weaknesses and shortcomings but His blessings have always come upon me boundlessly. He is indeed the only one worthy of being worshipped. And peace is upon the Prophet Muhammad who declared the pursuit of knowledge as the noblest of deeds, and set forth his own example as to how to arrive practically at the ultimate nature of things. He is truly the one worthy of being followed in that great mission of acquiring and disseminating knowledge that can bring about a renewed vigor and life to many an unanimated potentialities of man.

Many sincere thanks to my supervisor, Dr. Isa Bin Mohammad Tan, for his research-oriented attitude, faith, support, consistent guidance, quite liberal disposition and encouragement through out the research. His kind concern, generous supervision through good and hard times, required for the accomplishment of this task, is highly appreciated. I am also thankful to my initial supervisor, Prof. Syed Sakhawat Shah, for his valuable suggestions in the earlier days of this project. I would also like to take this opportunity to express my gratitude to the program head, Chemical Engineering Department, Assoc. Prof. Dr. Kamarul Ariffin Amminudin and all other faculty members for their kind concern and support throughout this period. I am grateful to research enterprise office for providing the short term internal funding for this project.

Lot of thanks to my mother, brother and sisters for their patience, understanding and encouragement during this whole period of research. It is my pleasure to thankfully offer the heartiest appreciation to my loving and caring wife (Rubina Siddique) and kids (Fatima Nadeem & Muhammad Jamil) for their great sacrifice, patience, encouragement, moral support and prayers for the completion of this work.

Thanks to all the technical and non technical staff from UTP and PRSS for their prolonged assistance in the collection of data and assistance for analyzing the samples. I would also like to take this opportunity to express my gratitude to all of my friends for their continuous support.

Muhammad Nadeem

ABSTRACT

A laboratory scale investigation into the utilization of conventional and non-conventional surfactants for Enhanced Oil Recovery (EOR) was conducted using an in-house imbibition cell flooded with formation water in the presence of polymers and alkaline mixtures. The success of chemical enhanced recovery treatment hinges on many factors; firstly there is a need for the selected chemical mixture to be sufficiently benign towards the aggressive components of the formation water. Secondly there is a need for the components of the chemical flooding mixture to possess certain desirable properties namely, stability, viscosity, extend of IFT reduction, partition coefficient, adsorption and wettability alteration. Formation water from Angsi field was analyzed for mineral contents using volumetric analyses and Atomic Absorption Spectroscopy (AAS). Surfactants and polymers have been examined for temperature stability using Thermo Gravimetric Analyses (TGA). The viscosities of the polymers have been determined using a rotary viscometer. The presence of alkali, surfactants and a raise in temperature led to a decrease in the viscosity of the polymers. Reduction in IFT at the oil/water interface has been recorded using an interfacial tensiometer. Partition coefficients of the surfactants in oil and water phases have been calculated. Emulsification and wettability alterations have been evaluated by an Atomic Force Microscopy (AFM) and contact angle measurements respectively. BET surface and micropore areas of the cores have been measured. Sandstone cores possessing suitable porosity and permeability have been characterized and used for the imbibition studies. The internal structure and mineral profiles of the sandstones have been illustrated and analyzed using a Scanning Electron Microscopy (SEM) and an Energy Dispersive X-ray (EDX) respectively. Molecular interactions between the various components have been elaborated by Fourier-Transform-Infra red (FTIR) spectroscopy. It was concluded that oil recovery can be significantly enhanced, when an appropriate mixture of non-conventional anionic surfactants (Aerosol OT & TR) has been utilized along with alkali and polymer. The preliminary screening results obtained by an in-house imbibition cell have also been adequately verified by industry accepted coreflooding experiments. Adsorption mechanism of the surfactants on sandstone cores is well elaborated by the Langmuir isotherm instead of the Freundlich isotherm.

Adsorption kinetics obeys the Pseudo-second-order kinetics. It can be concluded that the polymer is responsible to increase the macroscopic displacement efficiency, whereas the synergistic effect of the surfactants and alkali are responsible to produce an ultra-low IFT (10^{-3} dyne/cm) resulting in a pronounced microscopic displacement efficiency. Non-conventional surfactants can produce an ultra-low IFT even in minuscule amounts of alkali and polymer. It was concluded that Low-Alkaline-Surfactant-Polymer (LASP) is not only an economical technology but it can also enhance oil production drastically.

ABSTRAK

Satu penyelidikan berskala makmal terhadap penggunaan surfaktan konvensional dan bukan konvensional bertujuan untuk meningkatkan pengeluaran minyak telah dijalankan dengan menggunakan alat penyerapan yang dibanjiri dengan cecair reserboir berserta dengan kehadiran polimer dan sebatian alkali. Kejayaan usaha pemulihan pengeluaran secara kemikal bergantung kepada banyak faktor; pertamanya keperluan campuran kemikal yang dipilih sepatutnya tidak akan bertindak dengan komponen komponen cecair reserboir. Keduanya, komponen campuran kemikal seharusnya memiliki beberapa sifat yang diperlukan seperti kestabilan, kelikatan, tahap penurunan IFT, partition coefficient, adsorption dan wettability. Cecair reserboir dari lapangan Angsi telah dianalyses menentukan kandungan mineral secara volumetric dan Atomic absorption spectroscopy (AAS). Surfaktan dan polimer telah di uji menggunakan Analyses Thermo Gravimetrik. Tahap kelikatan polimer telah di uji menggunakan viscometer berpusing. Kehadiran alkali, surfaktan dan peningkatan suhu telah menyebabkan kelikatan polimer berkurangan. Penurunan nilai IFT di permukaan antara minyak dan air telah dicatatkan menggunakan interfacial tensiometer. Koefisyen pemisahan (Partition coefficient) surfaktan fasa diantara minyak dan air telah ditentukan. Emulsifikasi dan perubahan pembasahan telah dinilai dengan menggunakan Mikroskop Daya Atomik (AFM) dan analisis sudut kontak. Keluasan permukaan BET dan mikropora empulur telah ditentukan. Empulur batu pasir yang memiliki keliangan dan ketelapan yang sesuai telah dikaji dan digunakan untuk siasatan penghirupan (imbibition studies) Struktur dalaman dan profil mineral batu pasir telah di kaji masing masing menggunakan Mikroskop Imbasan electron (SEM) dan X Ray Tenaga Terurai (EDX). Interaksi molecular antara komponen komponen telah dihuraikan menggunakan Spektroskopi Fourier Transform Infra red (FTIR). Kesimpulanya pemulihan minyak boleh ditingkatkan menggunakan campuran surfaktan anionik tidak konvensional digunakan berserta dengan alkali dan polimer. Keputusan saringan awal menggunakan sel penghirupan rekaan sendiri telah disahkan menggunakan eksperimen ketepuan empulur yang diperakui oleh industri. Mekanisma penyerapan surfaktan atas batu pasir di jelaskan melalui isoterma Langmuir dan bukan Freundlich. Kinetik penyerapan adalah menurut keteraturan kedua palsu (pseudo second order). Boleh

disimpulkan bahawa polimer bertindak untuk meningkatkan keupayaan pemindahan, manakala kesan paduan sinergi antara surfaktan dan alkali bertanggung jawab menghasilkan IFT terendah. Surfaktan bukan konvesyenal boleh menghasilkan IFT terendah walaupun dalam amaun alkali dan polimer yang amat rendah. Bolehlah disimpulkan Polimer Surfaktan Beralkali bukan sahaja merupakan teknologi yang ekonomik malahan ia boleh meningkatkan pengeluaran minyak yang ketara Polimer-Alkali.

TABLE OF CONTENT

STATUS OF THESIS	I
DECLARATION	IV
ACKNOWLEDGEMENT	VI
ABSTRACT	VII
ABSTRAK	IX
TABLE OF CONTENT	XI
LIST OF TABLES	XVIII
LIST OF FIGURES	XIX
ABBREVIATIONS AND SYMBOLS	XXIV
1. INTRODUCTION	1
1.1 ENHANCED OIL RECOVERY (EOR)	1
1.2 ALKALINE-SURFACTANT-POLYMER (ASP) FLOODING	3
1.3 SURFACTANTS IN EOR	3
1.3.1 Critical Micelle Concentration (CMC)	5
1.3.2 Adsorption	6
1.3.3 Interfacial Tension (IFT)	8
1.3.4 Emulsification	9
1.3.5 Wettability Alteration	10
1.3.6 Partition Coefficient/Function	13
1.4 POLYMERS IN EOR	14
1.4.1 Hydrolysable Polyacrylamides (HPAM)	14
1.4.2 Polysaccharides	15

1.4.3	Requirements of a Polymer.....	16
1.4.4	Viscosity and Shear Thinning of Polymer Solution	16
1.4.5	Inaccessible Pore Volume (PV) in Polymer Flooding.....	19
1.4.6	Polymer Retention in Porous Media.....	20
1.5	ALKALIS IN EOR	24
1.6	MOTIVATION FOR THE PROJECT.....	27
1.7	PROBLEM STATEMENT.....	28
1.8	OBJECTIVES AND SCOPE OF THE STUDY	28
1.9	ORGANIZATION OF THESIS	29
1.10	SUMMARY.....	30
2.	LITERATURE REVIEW	31
2.1	BASIC PARAMETERS IN CHEMICAL FLOODING PROCESSES	34
2.1.1	Wettability.....	34
2.1.2	Amott Wettability Index	37
2.1.3	USMB Wettability Index	39
2.1.4	Wettability and Contact Angle.....	40
2.1.5	Techniques for Measuring Contact Angles.....	42
2.1.6	Wettability and Water-advancing Contact Angle Relationship.....	43
2.2	CAPILLARY PRESSURE	45
2.3	RELATIVE PERMEABILITY	48
2.4	SIGNIFICANCE OF ASP FLOODING.....	50
2.5	SYNERGISM AND ANTAGONISM	51
2.6	SIGNIFICANCE OF ETHOXYLATION DEGREE	56

2.7	SURFACTANT'S STRUCTURE EFFECTS	61
2.8	SIGNIFICANCE OF HYDROPHOBICALLY ASSOCIATING POLYMERS	62
2.9	TRANSPORTATION THROUGH POROUS MEDIUM	64
2.10	ROLE OF VISCOELASTICITY IN EOR.....	67
2.11	EFFECTS OF DIVALENT IONS IN SURFACTANT FLOODING.....	68
2.12	OPTIMIZATION OF A SURFACTANT FLOODING PROCESS	71
2.13	EFFECT OF HYDROPHILIC POLYMER ON SURFACTANT FLOODING.....	73
2.14	SUMMARY.....	81
3.	EXPERIMENTAL	82
3.1	WATER ANALYSES.....	82
3.1.1	pH Measurement	83
3.1.2	Conductivity (Salinity/Total Dissolved Solids) Measurement	84
3.1.3	Total Hardness- EDTA Titration Method.....	85
3.1.4	Estimation of Total Hardness, ppm as CaCO ₃	86
3.1.5	Calcium Hardness- EDTA Titration	86
3.1.6	Estimation of Calcium Hardness, ppm as CaCO ₃	87
3.1.7	Magnesium Hardness (Calculation method).....	87
3.1.8	Chlorides– Mohr Titration Method.....	87
3.1.9	Testing Procedure, Chlorides (ppm as Cl).....	88
3.1.10	Sulfates.....	89
3.1.11	Titration Test for Sulfate (ppm as SO ₄) Using THQ.....	89
3.1.12	Procedure (Phosphate Absent).....	89
3.1.13	Procedure (Phosphate Present)	90

3.1.14	Estimation of Carbonate and Bicarbonates.....	91
3.2	ANALYSES OF SODIUM, POTASSIUM, IRON, BARIUM AND STRONTIUM	91
3.2.1	Atomic Absorption Spectroscopy (AAS)	92
3.2.2	Instrumentation of Atomic Absorption Spectrometer.....	93
3.3	MATERIALS CODING	95
3.4	VISCOSITY AND SHEAR THINNING OF HIGH MOLECULAR WEIGHT PAM	96
3.4.1	Working Principle of Rotary Viscometer	99
3.5	TEMPERATURE STABILITY OF USED CHEMICALS	101
3.5.1	Thermogravimetric Analyses (TGA).....	102
3.5.2	TGA-Principle of Operation	103
3.5.3	Instrumentation of TGA.....	103
3.5.4	Factors Affecting the TGA Curve.....	104
3.5.5	Procedure for Thermogravimetric Analyses.....	104
3.6	MOLECULAR INTERACTIONS BETWEEN VARIOUS CHEMICALS	104
3.6.1	FTIR-ATR Spectroscopy.....	105
3.6.2	Sample Preparation and Analyses.....	107
3.7	INTERFACIAL TENSION (IFT)	108
3.7.1	Techniques for Measuring Surface Tension	109
3.7.2	Capillary Rise Method	109
3.7.3	Du Noüy Ring Method.....	110
3.7.4	Pendant Drop Shape Analyses.....	112
3.7.5	Drop Weight or Drop Volume Method.....	113
3.7.6	Maximum Bubble Pressure Method (MBPM).....	115

3.7.7	Selection of an Appropriate Method.....	117
3.7.8	Spinning Drop Tensiometer.....	117
3.8	CALCULATION OF PARTITION COEFFICIENTS	120
3.9	CHARACTERIZATION OF OIL-IN-WATER EMULSIONS	121
3.9.1	Atomic Force Microscopy (AFM).....	121
3.9.2	Emulsion Stability.....	123
3.10	WETTABILITY THROUGH CONTACT ANGLE MEASUREMENTS	124
3.11	CHARACTERIZATION OF SANDSTONE CORES	125
3.12	SPONTANEOUS IMBIBITION STUDIES	126
3.13	BET SURFACE AREA AND PORE STRUCTURE MEASUREMENTS	127
3.14	SCANNING ELECTRON MICROSCOPY/ENERGY DISPERSIVE X-RAY ANALYSES ...	130
3.14.1	Principle of SEM.....	130
3.14.2	Principle of EDX.....	131
3.15	CORE FLOODING STUDIES.....	133
3.16	SURFACTANTS ADSORPTION AND KINETICS STUDIES	137
3.16.1	Langmuir and Freundlich Adsorption Isotherms.....	138
3.16.2	Adsorption Kinetics	140
3.16.3	Pseudo-first-order Model	140
3.16.4	Pseudo-second-order Model	141
3.16.5	Intra-particle-diffusion Model	141
3.17	SUMMARY.....	142
4.	RESULTS AND DISCUSSION	143
4.1	CHARACTERISTICS OF ANCSI FIELD	144

4.1.1	Angsi Crude Assay	145
4.1.2	Angsi Sea Water Analyses.....	147
4.2	VISCOSITY MEASUREMENTS OF POLYACRYLAMIDE.....	148
4.2.1	Effect of Polymer Concentration	148
4.2.2	Effect of Temperature	149
4.2.3	Effect of Alkalinity and Surfactants	150
4.3	THERMOGRAVIMETRIC ANALYSES.....	153
4.3.1	Thermal Stability of Polymers.....	153
4.3.2	Thermal Stability of Surfactants	155
4.4	FTIR-ATR SPECTROSCOPIC ANALYSES	158
4.4.1	FTIR-ATR Spectroscopy of Polymers.....	158
4.4.2	FTIR-ATR Spectroscopic Analyses of Angsi Crude Oil.....	159
4.4.3	FTIR-ATR Spectroscopic Analyses of Surfactants	160
4.4.4	FTIR-ATR Spectroscopic Analyses of Various Combinations.....	163
4.5	IFT MEASUREMENTS	169
4.6	ATOMIC FORCE MICROSCOPY OF OIL-WATER EMULSIONS.....	172
4.6.1	Stability of O/W Emulsions.....	174
4.7	ESTIMATION OF PARTITION COEFFICIENTS	174
4.8	WETTABILITY THROUGH CONTACT ANGLE MEASUREMENTS	177
4.9	CHARACTERIZATION OF SANDSTONE CORES	178
4.10	SPONTANEOUS IMBIBITION STUDIES	179
4.10.1	Oil Recovery from Low and High Permeability Cores	179
4.10.2	Oil Recovery by ASP Imbibition with SDS	180

4.10.3	Oil Recovery by ASP Imbibition with ATR.....	180
4.10.4	Oil Recovery by ASP Imbibition with AOT.....	181
4.10.5	Oil Recovery by ASP Imbibition with ATR and AOT.....	182
4.10.6	Oil Recovery by ASP Imbibition with CTAB	183
4.11	BET SURFACE AREA AND PORE STRUCTURE MEASUREMENTS	184
4.12	SEM/EDX ANALYSES OF CORES.....	185
4.13	CORE FLOODING STUDIES.....	189
4.14	SURFACTANT ADSORPTION AND KINETICS STUDIES	193
4.14.1	Langmuir and Freundlich Adsorption Isotherms.....	193
4.14.2	Adsorption Kinetics of Surfactants.....	196
4.15	SUMMARY.....	198
5.	CONCLUSIONS AND RECOMMENDATIONS.....	201
5.1	CONCLUSIONS.....	201
5.2	RECOMMENDATIONS.....	204
	REFERENCES.....	205

LIST OF TABLES

Table 1.1: Comparison of primary, secondary and tertiary recovery processes.	26
Table 2.1: Relationship between wettability and common measurements.	37
Table 3.1: Standard atomic absorption conditions for Na, K, Fe, Ba and Sr.	94
Table 4.1: Characteristics of Angsi Field.	145
Table 4.2: Angsi Crude Assay	146
Table 4.3: Angsi sea water analyses.	147
Table 4.4: Stability of Alkaline-Surfactant-Polymer Formulations.	151
Table 4.5: Viscosities of A-P and A-S-P formulations.	152
Table 4.6: Chemical assignments for absorption bands for polymer 1 and 2.	159
Table 4.7: Volumes of hydrocarbon phase separated from O/W emulsions	174
Table 4.8: Partition coefficients of various surfactants in O/W systems.	176
Table 4.9: Basic properties of sandstone core samples.	178
Table 4.10: BET surface and micropore areas of sandstones.	184
Table 4.11: Elemental profiles of core samples 1 and 7.	188
Table 4.12: Chemically enhanced oil recoveries by various components.	191
Table 4.13: Adsorption constants for Langmuir isotherm.	194
Table 4.14: Adsorption constants for Freundlich isotherm.	195
Table 4.15: Kinetic parameters for the adsorption of surfactants by sandstone.	198

LIST OF FIGURES

Figure 1.1: Trapping of oil in reservoir rocks.....	1
Figure 1.2 : Structural architecture of conventional and non-conventional surfactant.....	5
Figure 1.3: Various micellar forms of surfactant aggregates.....	6
Figure 1.4: Growth of aggregates for various regions of the adsorption isotherm	8
Figure 1.5: IFTs of heavy oil/brine as a function of surfactant concentration	9
Figure 1.6: Photographs by an optical electron microscope for W/O emulsions stabilized by conventional and gemini surfactant	10
Figure 1.7: The wettability of an oil-wet solid surface in contact with a water droplet	10
Figure 1.8: Advancing and receding contact angles of surfactant solution on pre-equilibrated mica surface.....	12
Figure 1.9: Molecular structure of water-soluble polyacrylamide.....	15
Figure 1.10: Molecular structure of water-soluble polysaccharide	16
Figure 1.11: Viscosity as a function of SDS concentration for various PAMs concentrations at pH 4	18
Figure 1.12: Polymer breakout curves.....	20
Figure 1.13: Interaction between glass probe and glass surface bearing an adsorbed layer of polymer.....	22
Figure 1.14: Reduction in the hydraulic conductivity of a capillary tube expressed as layer thickness during polymer injection.....	23
Figure 1.15: Pictures of oil/brine systems with different surfactants at various stages of emulsification.....	24
Figure 1.16: Original oil in place around the globe	27
Figure 2.1: CO ₂ contacts the residual oil allowing it to flow out of the tight pores	33
Figure 2.2: Schematic diagram of surfactant-polymer flooding process	34
Figure 2.3: A liquid droplet in equilibrium with horizontal surface surrounded by gas ...	35
Figure 2.4: Capillary pressure-saturation curves for Amott/USBM method	39
Figure 2.5: Five ways in which the contact angle can be measured.....	42
Figure 2.6: Depiction of the dual-drop-dual-crystal contact angle technique	43
Figure 2.7: Oil-wet case of Beaverhill Lake oil on calcite under reservoir conditions	44

Figure 2.8: Capillary tube containing oil and water exposed to the atmosphere.....	46
Figure 2.9: Schematic of pore cross-section in a water-wet porous media	47
Figure 2.10: Capillary pressure curve for an oil-wet core	47
Figure 2.11: Relative permeability curves	49
Figure 2.12: Effect of salinity on DIT behaviors.....	52
Figure 2.13: Interfacial tension vs. wt% of the mixtures of Aerosol TR and Aerosol OT. 54	
Figure 2.14: Determination of the CMC for surfactant ENP95 and ENP150.	57
Figure 2.15: The three types of phase behavior for surfactant (S)–oil (O)–water (W) systems according to Winsor.	58
Figure 2.16: The picture of the foam in porous medium.	66
Figure 2.17: Schematic model of the suggested mechanism for the wettability alteration induced by seawater.	70
Figure 2.18: Experimental liquid–liquid equilibria phase diagram of the system brine–oil–surfactant at 25 °C.	75
Figure 3.1: Energy transitions during atomic absorption spectroscopy.....	92
Figure 3.2: Schematic of an atomic absorption spectrometer	93
Figure 3.3: Hitachi AA 6800 atomic absorption spectrometer.	95
Figure 3.4: Brookfield LVDV-14 digital viscometer.	99
Figure 3.5: Major components of a rotary viscometer.....	100
Figure 3.6: Perkin Elmer TGA7 Bench Model Thermogravimetric Analyzer.	102
Figure 3.7: Major components of thermogravimetric analyzer.	103
Figure 3.8: Perkin Elmer-2000 FTIR-ATR spectrometer.....	105
Figure 3.9: Schematic of the FTIR spectrometer [131].	106
Figure 3.10: Schematic diagram of Michelson-Interferometer [149].	107
Figure 3.11: Capillary rise method	110
Figure 3.12: The position of Du Noüy ring right before the film rupture [156].	111
Figure 3.13: The liquid interface of pendant drop.	112
Figure 3.14: A drop breakaway process	114
Figure 3.15: Pressure curves during bubble formation as a function of time	116
Figure 3.16: SVT 20 spinning drop video tensiometer.....	118
Figure 3.17: Geometry of a spinning drop of denser liquid in less dense liquid	119

Figure 3.18: ATAGO RX-5000 model digital refractometer.	119
Figure 3.19: Agilent series 4500 AFM.	122
Figure 3.20: Schematic of AFM	123
Figure 3.21: Contact angle analyzer Phoenix300.	124
Figure 3.22: Extended range helium porosimeter.....	125
Figure 3.23: Air permeability meter.	125
Figure 3.24: Actual and self designed imbibition cells.	126
Figure 3.25: Micrometrics ASAP 2000 surface area and pore size analyzer.	129
Figure 3.26: Schematic of scanning electron microscope.	131
Figure 3.27: Interaction of an electron beam with specimen in EDX	132
Figure 3.28: Zeiss DSM-950 SEM/EDX electron microscope.....	133
Figure 3.29: Coreflooding system by Temco, USA.	133
Figure 3.30: Schematic diagram of coreflooding system.	134
Figure 3.31: Specifications and views of core holder.....	135
Figure 3.32: Schematic of circulation process.....	139
Figure 4.1: Viscosities of polymer 1 and 2 in brine Vs. concentration at 90 °C.	149
Figure 4.2: Temperature Vs. viscosities of polymers 1 and 2 with 1500 ppm in brine....	150
Figure 4.3: TGA curve for polymer-1.	154
Figure 4.4: TGA curve for polymer-2.	154
Figure 4.5: TGA curve for SDS.....	156
Figure 4.6: TGA curve for CTAB.	156
Figure 4.7: TGA curve for AOT.....	157
Figure 4.8: TGA curve for ATR.	158
Figure 4.9: FTIR-ATR spectrums of polymers 1 and 2.....	159
Figure 4.10: FTIR-ATR spectrum of pure Angsi crude oil.	160
Figure 4.11: FTIR spectra of pure SDS and CTAB.....	161
Figure 4.12: FTIR-ATR spectra of ATR (A), AOT (B) and mixture of ATR:AOT (C)..	163
Figure 4.13: FTIR-ATR spectrum of SDS and Angsi crude in combination with SDS...	164
Figure 4.14: FTIR-ATR spectrum of Angsi crude in combination with CTAB.....	165
Figure 4.15: FTIR-ATR spectra of Angsi crude in combination with ATR, AOT and ATR:AOT (1:9) surfactants.	167

Figure 4.16: FTIR-ATR spectra of Angsi crude recovered by ASP flooding with SDS and ATR:AOT.	169
Figure 4.17: Normal (L) and elongated (R) oil droplet.....	169
Figure 4.18: IFTs at crude oil-water interface in combination with various surfactants..	170
Figure 4.19: IFTs at crude oil-water interface in combination with various ASP formulations.	171
Figure 4.20: Oil recovery and IFT correlation	172
Figure 4.21: AFM micrographs of oil-water emulsions	172
Figure 4.22: Phase separation in oil-water emulsions [60].....	173
Figure 4.23: Surfactant's concentration and contact angles of brine solution droplet.	177
Figure 4.24: Wettability alteration mechanism by surfactants.	178
Figure 4.25: Oil recovery from the cores with low and high permeability.	179
Figure 4.26: Oil recoveries by spontaneous imbibition with ASP by SDS.	180
Figure 4.27: Oil recoveries by spontaneous imbibition with ASP by ATR.	181
Figure 4.28: Oil recoveries by spontaneous imbibition with ASP by AOT.	181
Figure 4.29: Oil recoveries by spontaneous imbibition with ASP by ATR:AOT.	182
Figure 4.30: Oil recoveries by spontaneous imbibition with ASP by CTAB.....	183
Figure 4.31: Adsorption, desorption isotherms for liquid nitrogen on sandstone.	184
Figure 4.32: BET plot for the adsorption of liquid nitrogen on sandstone.....	185
Figure 4.33: SEM image of original sandstone.....	185
Figure 4.34: SEM image of an oil saturated sandstone.	186
Figure 4.35: SEM image of sandstone after ASP flooding with ATR:AOT.	186
Figure 4.36: SEM image of sandstone after ASP flooding with CTAB.....	187
Figure 4.37: EDX analyses of sandstone core sample 1.....	188
Figure 4.38: EDX analyses of sandstone core sample 7.....	188
Figure 4.39: Oil recoveries in coreflooding with ASP by ATR:AOT.	189
Figure 4.40: Oil recoveries in coreflooding with ASP by SDS.	189
Figure 4.41: Oil recoveries in coreflooding with ASP by ATR.	190
Figure 4.42: Oil recoveries in coreflooding with ASP by AOT..	190
Figure 4.43: Pictures of sandstone cores	192

Figure 4.44: Langmuir adsorption isotherms for SDS, ATR, AOT and ATR:AOT in the absence and in the presence of alkali..... 194

Figure 4.45: Freundlich adsorption isotherms for SDS, ATR, AOT and ATR:AOT in the absence and in the presence of alkali..... 194

Figure 4.46: Pseudo-first-order, Pseudo-second-order and intra-particle diffusion kinetics for the adsorption of surfactants on sandstone..... 197

ABBREVIATIONS AND SYMBOLS

ΔS_{ot}	Residual oil saturation
ΔS_{wt}	Residual water saturation
AA	Acrylic acid
AAS	Atomic absorption spectrometer
AES	Alkyl ether sulfate
AFM	Atomic force microscopy
AMNS	Alkyl methylnaphthalene sulfonate surfactant
AOT	Aerosol OT
AR	Analytical reagent
ASP	Alkaline-surfactant-polymer
ATR	Aerosol TR
BET	Bruner-Emmet-Teller
CEOR	Chemically enhanced oil recovery
CMC	Critical micelle concentration
COBR	Crude oil-brine-rock
CTAB	Cetyltrimethyl ammonium bromide
DBSA	Dodecyl benzene sulfonic acid
DDDC	Dual-drop-dual-crystal
DIFT	Dynamic interfacial tension
DIW	Deionized water
DPR	Disproportionate permeability reduction
DSC	Differential scanning calorimetry
DTA	Differential thermal analyses
DTAB	Dodecyltrimethyl ammonium bromide
EBT	Eriochrome black T
EDTA	Ethylenediaminetetraacetic acid
EMF	Electric and magnetic field
EOR	Enhanced oil recovery
ESR	Electron spin resonance

FTIR-ATR	Fourier transformation infra red-attenuated total reflectance
η	Viscosity
HLB	Hydrophile-lipophile balance
HM	Hydrophobically modified
HM-PAM	Hydrophobically modified polyacrylamide
HPAM	Hydrolysable polyacrylamide
HPLC	High performance liquid chromatography
I_{a-h}	Amott-Harvey wettability index
IFT	Interfacial tension
IOIP	Initial oil in place
IOR	Improved oil recovery
IOR	Improved oil recovery
k	Absolute permeability
K	Partition coefficient
K_1^{st}	First order rate constant
K_2^{nd}	Second order rate constant
K_{id}	Intra-particle diffusion model rate constant
LASP	Low-alkaline-surfactant-polymer
LASP	Low alkaline surfactant polymer
LPG	Liquefied petroleum gas
LTPWF	Low tension polymer waterflood
Nc	Capillary number
O/W	Oil-in-water
OCD	Organic conception diagrams
OIS	Optimal injection strategies
OOIP	Original oil in place
P_c	Capillary pressure
POE	Polyoxyethylene
ppm	Parts per million
PV	Pore volume
RI	Refractive index

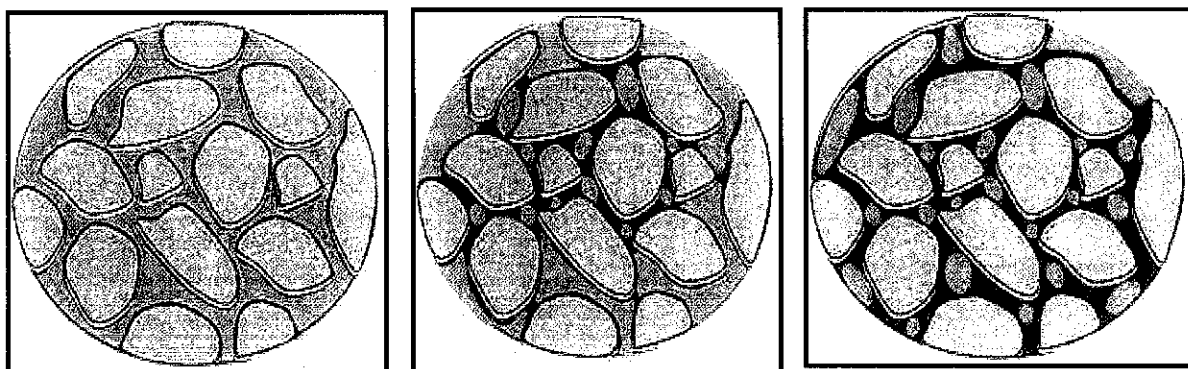
ROIP	Residual oil in place
RPM	Relative permeability modification
SDS	Sodium dodecyl sulfate
SEM/EDX	Scanning electron microscopy/energy dispersive X-ray
τ	Shear stress
TDS	Total dissolved solids
TGA	Thermogravimetric analyses
THQ	Tetrahydroxyquinone
TPCL	Three phase contact line
USBM	United States bureau of mines
v	Velocity
V_{osp}	Oil volume displaced by spontaneous imbibition
V_{ot}	Oil volume displaced by both water and forced displacement
V_{wsp}	Water volume displaced by spontaneous imbibition
W/O	Water-in-oil
γ	Interfacial tension
$\gamma_{s,g}$	IFT of solid-gas interface
$\gamma_{s,l}$	IFT of solid-liquid interface
δ	Ratio of volumes displaced by spontaneous and forced imbibition
θ	Contact angle
μ	Viscosity
σ	Surface tension
Φ	Porosity

CHAPTER 1

1. INTRODUCTION

1.1 Enhanced Oil Recovery (EOR)

The global economy is highly dependant on the production and accessibility to crude oil. Much of today's geopolitical tension centers on the ability to secure an uninterrupted supply of crude oil. The provision of heat, light and transport depends on oil and there has not been a single energy source that is able to replace crude oil fuel. Primary recovery produces oil and gas using the natural pressure of the reservoir as the driving force to push the material to the surface. In a secondary recovery process gas is reinjected and is often assisted with waterflooding to extract the residual oil and gas remaining after the primary recovery phase. Traditional primary and secondary production methods typically recover one third of the Original Oil in Place (OOIP), the total hydrocarbon content of an oil reservoir, leaving two third behind [1]. This is attributed to the high capillary forces, viscous forces and reservoir heterogeneities which results in poor microscopic and macroscopic displacement efficiencies. Tertiary recovery involves the injection of gases (carbon dioxide, air), heat (steam or hot water) and fluids (alkali, surfactant and polymer) to stimulate oil and gas flow that were left behind after primary and secondary recovery phases.



(a)

(b)

(c)

Figure 1.1: Trapping of oil in reservoir rocks: (a) oil and water saturation early in waterflood with high oil saturation (b) pore system with higher water saturation during waterflood (c) pore system with trapped waterflood residual oil.

During the life of a well, from production to abandonment, there is always a point at which the cost of producing an additional barrel of oil is higher than the price the market will pay for that barrel. Enhanced oil recovery (EOR) is a generic term used for the techniques being implemented to increase the amount of oil that can be extracted from an oil field. Except for brief periods in which EOR was not economical, or perceived to be so, there were good economic reasons not to nurse every drop of oil from a well. Oil was easy to find in the other giant fields and the cost of newly found barrel of oil was far less than the cost of an EOR incremental barrel. But with the passage of time the situation has begun to change because the reserves in the aging oil fields are declining faster than the addition of new oil discoveries.

Nowadays research and development on many fronts indicate that the economical risks of EOR are being reduced while the potential of profitability is on the rise [2]. Following a waterflooding process, the residual oil is believed to be in the form of oil ganglia trapped in the pores of the rocks in the reservoir. The water-oil mixture prevents oil flow within the pores of reservoir and well bore. EOR methods are the only way to recover that trapped oil. Using EOR techniques, 30 - 60 %, or more, of the reservoir's original oil can be extracted compared with 20 - 40 % using primary and secondary recovery techniques. EOR is also known as Improved Oil Recovery (IOR) or tertiary recovery. Any process involving the injection of a fluid or fluids into a reservoir to supplement the natural energy present in a reservoir is known as EOR process. The injected fluids interact with the reservoir rock/oil/brine system to create favorable conditions for maximum oil recovery [3]. These interactions are intended to maximize oil recovery due to oil swelling, lowering of IFT, rock wettability alteration, oil viscosity reduction and favorable phase behavior which are the central theme of the work described in this report.

Generally EOR methods can be categorized into two major groups namely thermal and non thermal processes. The in-situ combustion, steam injection, wet combustion and electrical heating fall under thermal processes, whereas, miscible-, micellar-, emulsion-, alkaline-, surfactant-, polymer-, alkaline-surfactant-, alkaline-surfactant-polymer-, inert gas- and carbon dioxide flooding fall under non thermal processes.

1.2 Alkaline-Surfactant-Polymer (ASP) Flooding

ASP flooding is one of the EOR techniques that can be utilized for the production of light to medium viscosity crude oil that is left behind in the reservoir after primary and secondary flooding processes. The trapped oil ganglia possess high interfacial tension (IFT) of about 20 - 30 dyne/cm which makes it immobile. In an ASP process, a very low concentration of the surfactant is used to achieve an ultralow IFT between the trapped oil and the injection fluid/formation water i.e. $10^{-3} - 10^{-4}$ dyne/cm [4]. The ultralow IFT also allows the alkali present in the injection fluid to penetrate deep into the formation and establish an intimate contact with the trapped oil globules. The alkali then reacts with the acidic components in the crude oil to form additional surfactant in-situ, thus, continuously providing an ultralow IFT and freeing the trapped oil. In an ASP process, a polymer is used to increase the viscosity of the injection fluid, to minimize channeling, and provide mobility control. Production of such ultralow IFT can mobilize the trapped oil through the narrow necks of the pores in the form of microemulsion. However, the stability of this emulsion depends on the concentration of the reservoir formed alkali-oil surfactant at the interface. This again depends on the concentration of the potential acidic components from crude oil that forms interfacially active soap components [5].

The major challenges of an ASP flooding process include the loss of surfactants due to an increased adsorption on reservoir rocks, precipitation due to the presence of inorganic minerals, entrapment of immobilized crude oil and its retention in the porous media and electrostatic interactions with the polymer present in micellar slug reducing oil mobility.

1.3 Surfactants in EOR

Surfactants/surface-active agents are amphipathic substances with lyophobic and lyophilic groups making them capable of adsorbing at the interfaces between liquids, solids and gases. They form self-associated clusters, which normally lead to organized molecular assemblies, monolayers, micelles, vesicles, liposomes and membranes. Their capability of reducing surface tension allows them to mix or disperse readily. Depending upon the nature of hydrophilic groups, surfactants are classified as **Anionic**: the surface-active portion of

the molecule bearing a negative charge e.g. RCOO^-Na^+ (soap), **Cationic**: surface-active agents bearing a positive charge e.g. $\text{RN}^+(\text{CH}_3)_3\text{Cl}^-$ (poly quaternary ammonium chloride), **Zwitterionic**: both positive and negative charges may be present in the surface-active portion e.g. $\text{R}^+\text{NH}_2\text{CH}_2\text{COO}^-$ (long chain amino acids) and **Nonionic**: the surface-active portion bears no apparent ionic charge e.g. $\text{RCOOCH}_2\text{CHOHCH}_2\text{OH}$ (mono glyceride of long chain fatty acid). The minimum concentration of the surfactant required to form micelles/aggregates is known as Critical Micelle Concentration (CMC).

Surfactants are among the most versatile products of the chemical industry and play an important role in many human endeavors ranging from very mundane (trivial e.g. washing clothes) to very sophisticated applications such as microelectronics. Apart from traditional applications such as detergents, emulsifiers, dispersants, wetting and flotation agents, they have tremendous and not yet fully appreciated potential for engineering functional interfaces and surface coatings. Emerging technologies represent a vibrant and challenging area in understanding the physico-chemical properties and phase behavior of surfactant based processes involved in the preparation of emulsions, dispersions, suspensions and their subsequent characteristics i.e. stabilization, formation, breaking of interfaces, wetting, emulsification, spreading, solubilisation and adhesion, etc. Emulsification of crude oil in displacing water is one of the mechanisms of ASP flooding for conventional oils. In the presence of a suitable surfactant or a combination of surfactants, mass transfer can occur, near the oil–water interface that can result in an ultralow IFT and interfacial instability. Oil ganglia can be broken down into fine droplets or emulsified into the aqueous phase.

Modifications in the molecular structure of surfactants to improve their existing properties such as surface activity have attracted the attention of scientists and they have been in search of newer surfactants. This has led to the synthesis of new generation such as branched chain, gemini, viscoelastic and non-migratory surfactants [6, 7]. Nowadays, many scientists around the world are involved in the study of surfactants and a number of scientific journals are devoted for this particular area. Structural architecture of conventional, straight chain and non-conventional, branched chain surfactant is presented in Fig. 1.2.

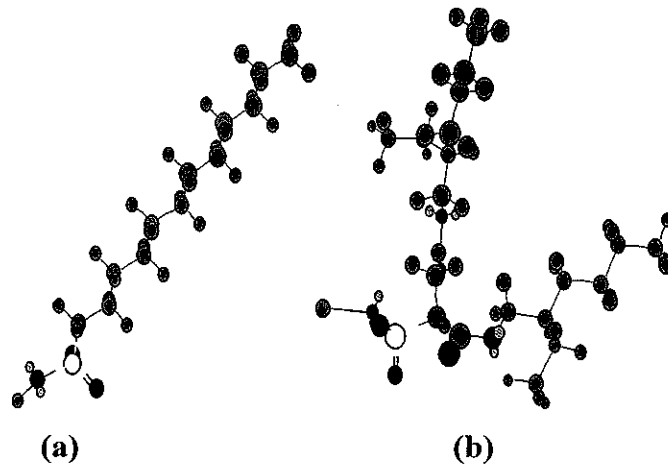


Figure 1.2: Structural architecture of conventional (a) Sodium dodecyl sulfate and (b) non-conventional Aerosol OT surfactant.

Surfactants may be applied at all stages in the petroleum recovery and processing industry, from oilwell drilling, reservoir injection, oilwell production, and surface plant processes, to pipelines and seagoing transportation of petroleum emulsions [8]. The selection criteria of surfactants intended in EOR applications depends upon the interplay of various fundamental parameters including IFT reduction, partition coefficient, adsorption on reservoir rocks, wettability alterations, compatibility with alkali and polymers, etc. It is therefore essential that a detailed understanding of the fundamental properties and principles involved in the use of surfactants for EOR applications is needed.

1.3.1 Critical Micelle Concentration (CMC)

Both of the components of a surfactant i.e. lyophilic and lyophobic differ in their affinity towards a solvent. The part of the molecule which has an affinity for polar solvents, such as water, is said to be hydrophilic. The part of the molecule which has an affinity for non-polar solvents, such as hydrocarbons, is said to be hydrophobic. Such molecules display a distinct behavior when interacting with water. The polar part of the molecule seeks to interact with water while the non-polar part does not favor an interaction with water.

A surfactant molecule is organized at the surface of water such that the polar part interacts with the water and the non-polar part is held above the surface (either in the air or

in a non-polar liquid). Another possible arrangement of these molecules involve each component to interact with its favored environment. Molecules can form aggregates in which the hydrophobic portions are oriented within the cluster and the hydrophilic portions are exposed to the solvent. Such aggregates are known as micelles. Critical micelle concentration (CMC) is defined as the concentration of surfactants in free solution which is in equilibrium with surfactants in aggregated form. The regions before and after CMC are known as pre- and post micellar regions respectively. Micelles can have various forms as shown in Fig. 1.3 [9].

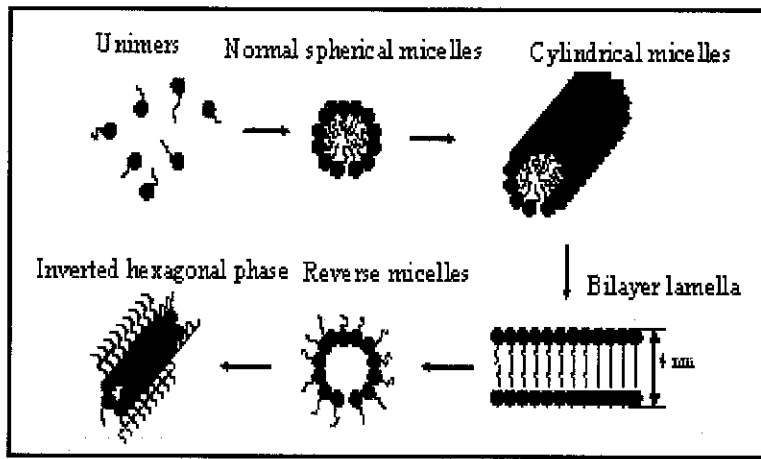


Figure 1.3: Various micellar forms of surfactant aggregates [9].

1.3.2 Adsorption

The amphipathic behavior of a surfactant molecules influences their adsorption on solid surfaces and is responsible to change a variety of interfacial phenomena such as wetting behavior (oil displacement, flotation, detergency) and colloid stability (dispersion, flocculation). There are a number of mechanisms for adsorption such as electrostatic attraction/repulsion, ion-exchange, chemisorption, chain-chain interactions, hydrogen and hydrophobic bonding. The nature of the surfactants, minerals and solution conditions as well as the mineralogical composition of reservoir rocks play a major role in determining the interactions between the reservoir minerals and externally added reagents (surfactants/polymers) and their effect on solid-liquid interfacial properties such as surface charge and wettability. The wettability of the minerals and hence the oil displacement is determined by the adsorption of surfactants on the minerals and the orientation that

surfactant assumes. Adsorption of surfactants on the solid itself has been studied extensively [10]. The adsorption isotherms of long chain ionic surfactants on minerals are illustrated in Fig. 1.4. The S–F isotherm as shown in Fig. 1.4 was originally proposed by Somasundaran and Fuerstenau, exhibits four characteristic regions [10-13].

The adsorption in various regions is contributed by electrostatic, hydrophobic and micellar interactions in the system. In Region I, the surfactant adsorbs mainly by electrostatic interactions between the surfactant headgroup and the charged sites on the mineral surface. In region II, there is a marked increase in the adsorption resulting from the interaction of the hydrophobic chains of ongoing surfactants with those of previously adsorbed surfactants. This aggregation of hydrophobic groups occurs at concentrations far below the CMC of the surfactant with the microstructures formation known as solloids (surface colloids, also termed as hemimicelles in some cases) [14]. In this region adsorption is attributed to electrostatic attraction between the surface sites and the oppositely charged surfactant species and hydrophobic interactions between the hydrocarbon chains. At the end of the region II, the surface is electrically neutralized and further adsorption in region III takes place due to chain–chain hydrophobic interactions alone, countered by electrostatic repulsion that builds up as the surface begin to acquire the same charge as the adsorbing surfactant ions. Above the CMC of the surfactant in Region IV, monomer activity is essentially constant and under these conditions adsorption remains constant.

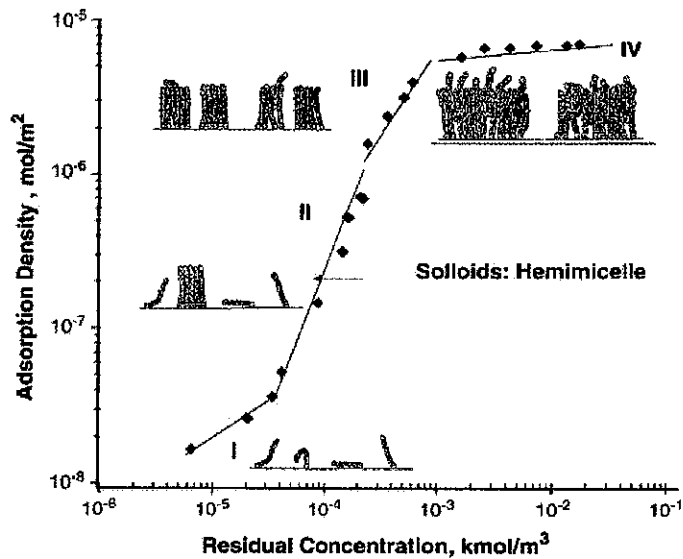


Figure 1.4: Schematic representation of the growth of aggregates for various regions of the adsorption isotherm [10].

1.3.3 Interfacial Tension (IFT)

IFT is the surface tension at the surface separating two immiscible liquids. It is a measurement of the cohesive (excess) energy present at an interface arising from the imbalance of forces between molecules at an interface (gas/liquid, liquid/liquid, gas/solid, and liquid/solid). It can be quantified as the force acting normal to the interface per unit length (force/unit length, mN/m or dyne/cm). Direct measurement of surface free energy of solids is not possible through techniques used for liquids. Polar liquids, such as water, have a strong intermolecular interaction and thus high surface tension. Any factor which is responsible to decrease the strength of this interaction will lower the surface tension. Any contaminant, especially by surfactants, will lower the surface tension. Since a lower IFT will cause a corresponding lowering of the capillary force between oil and brine, it is possible to improve oil recovery by lowering IFT to ultra-low values i.e. 10^{-3} dynes/cm [15]. It has been reported in Fig. 1.5 that such an ultra-low IFT can be achieved by the combination of alkali and surfactant which is the result of the reaction of alkali with the acid in oil and mass transfer of the surfactant across the oil/water interface respectively [16].

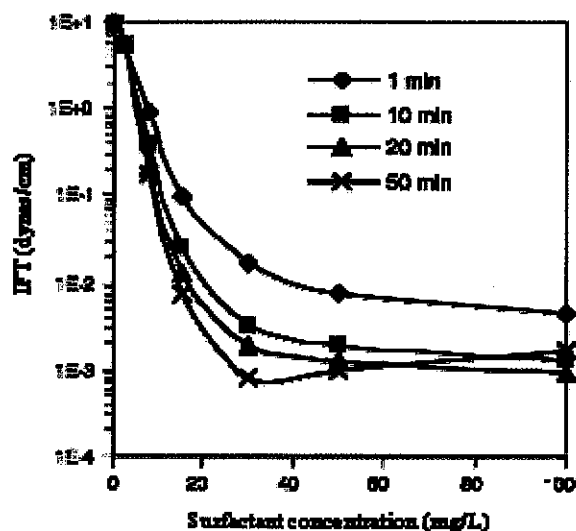


Figure 1.5: Interfacial tensions of heavy oil/brine as a function of surfactant S_4 concentration at different measurement times. Na_2CO_3 concentration: 0.15 wt% [16].

1.3.4 Emulsification

An emulsion is defined as the mixture of two immiscible liquids wherein droplets of one phase (the dispersed or internal phase) are encapsulated within sheets of another phase (continuous or external phase). There are two forms of emulsions: oil-in-water (O/W) emulsion in which oil droplets are dispersed and encapsulated within the water and water-in-oil (W/O) emulsion in which droplets of water are dispersed and encapsulated within oil. The most important factor in the preparation of emulsions is the selection of a suitable surfactant, blend of surfactants and/or additives which can satisfactorily emulsify the chosen ingredients at a specific temperature. Emulsification is greatly influenced by hydrophile-lipophile balance (HLB) of any surfactant/emulsifier. Generally water-oil (W/O) emulsifiers have a low HLB value, solubilizing agents have a high HLB value and oil-water (O/W) emulsifiers have intermediate HLB values. The stability of W/O emulsion depends on various factors, including the presence or absence of the surfactant, temperature, viscosity, specific gravity and water contents [6]. In EOR, emulsification requires very little energy input induced at an oil-water interface that is initially in a state of equilibrium. The process involves destabilization through contraction, of local interfacial regions. For emulsification to occur, it is necessary for the interfacial structure to have no or reduced resistance to surface shearing. Such a mechanism of emulsification may have

important implications in EOR and petroleum refining processes [17]. It has been reported that the branched chain, gemini and other novel surfactants are better emulsifiers as compared to the conventional surfactants because of the enhanced surface activity of the modified surfactants [6].

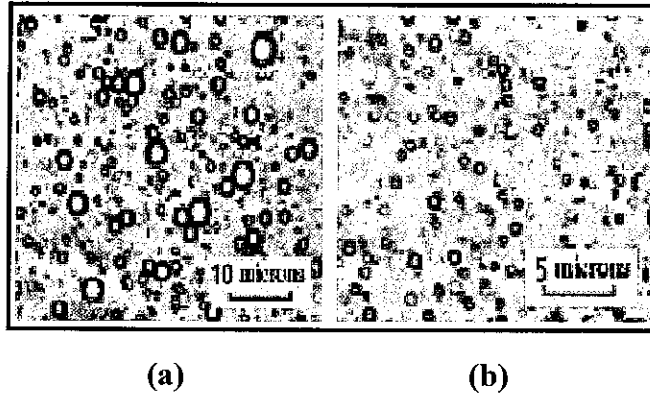


Figure 1.6: Photographs by an optical electron microscope at a magnification of 500 for W/O emulsions stabilized by conventional (a) and gemini (b) surfactant [6].

1.3.5 Wettability Alteration

Wettability is the ability of a fluid to spread or adhere on a rock surface in the presence of other immiscible fluids. Knowledge of wettability is important to decide what production strategy needs to be employed for an optimum oil recovery. Wettability is affected by several factors including rock mineralogy, rock surface roughness and chemical structure of surfactant and brine compositions. The mechanisms involved in surfactant flooding of fractured, oil-wet formations are mainly attributed to wettability alteration and IFT reduction.

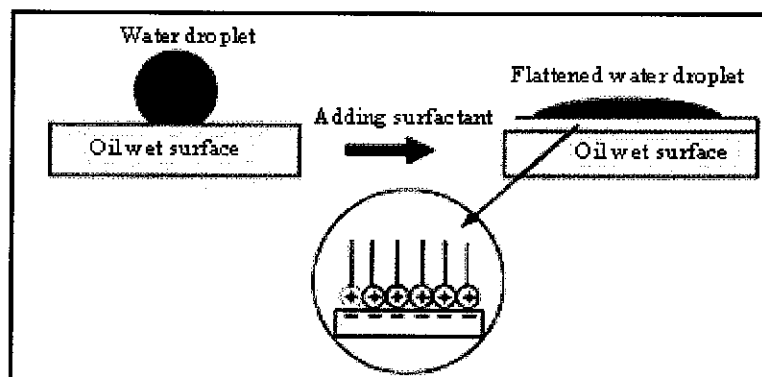


Figure 1.1: The wettability of an oil-wet solid surface in contact with a water droplet increases when surfactant molecules adsorb on to the surface [19].

The extent to which crude oil wets the porous media is directly related to the work required to bring this oil to the surface. Wetting of a solid surface by a liquid can be determined by the contact angle (measured through the liquid) which that liquid makes with the surface. Surfactants are responsible to affect wetting dynamics dramatically compared to pure fluids. Simple observation of the wetting behavior of soluble surfactants indicates that the dramatic impact on wetting is due to the mass transfer from one phase to the other. For systems with strongly attractive surfactant-solid interaction, receding surfactant solutions leave behind surfactant adsorbed at the solid-liquid interface. However, when this interaction is weak, the solid emerges with a reduced concentration of surfactant. To get to the solid-liquid interface, a very complex mass transfer and surfactant rearrangement must occur as the surfactant exchanges among the solid/liquid, solid/vapor and liquid/vapor interfaces, as well as the bulk. Strategies to promote or control the wetting/spreading on solid surfaces are important to many industrial as well as biological processes.

The manipulation of surface tension and contact angle by the addition of surfactants to the bulk liquid may be used to alter the contact angle of a liquid on a solid surface. The wetting nature of a particular fluid on the rock surface in preference to the other can be measured in terms of contact angle. Contact angle is the angle between a tangent drawn on the surface of the drop resting and a tangent to the supporting surface.

It is well known that surface and capillary forces account for most of the oil being left behind in the reservoirs after a secondary production. Capillary forces are generally quantified by the capillary number, N_c , which is the ratio of viscous to capillary forces and can be presented by the relation given below [20]:

$$N_c = v\mu / \sigma \cos \theta \text{ ----- (1.1)}$$

where,

v = velocity,

μ = viscosity,

σ = interfacial tension

θ = contact angle

The greater the capillary number, the lower is the residual oil saturation and hence a superior recovery is expected. In this way the recovery of residual oil can be linked to capillary number, which in turn is dependent on the viscosity of the fluid, interfacial tension between the fluids, and the contact angle. In the development of EOR processes, most of the attention has been directed towards the reduction of oil-water IFT to a minimum so that capillary number would increase thereby yielding a higher oil recovery. However, as it can be observed from Eq. 1.1, the capillary number can be increased to infinity without altering the IFT by just increasing the contact angle. The influence of the concentration of surfactants and composition of aqueous solution on the wettability of various hydrophobic surfaces has been reported in recent years [18, 19].

Fig. 1.8 shows the dynamic advancing (circles) and receding (diamonds) contact angles of aqueous imidazolium BF_4 surfactant solutions wetting a pre-equilibrated mica surface. The wetting solution and the pre-equilibrated solution were of the same concentration. The contact angle data shows a measurable adsorption onto the mica surface initially at approximately 10^{-6} mol/L and forms a hydrophobic surface at approximately 7×10^{-5} mol/L. A contact angle of $84^\circ \pm 2^\circ$ was measured at this concentration. It can be assumed that a monolayer has been formed at this concentration. At higher concentrations, the measured contact angle decreased, presumably due to the formation of a bilayer [19].

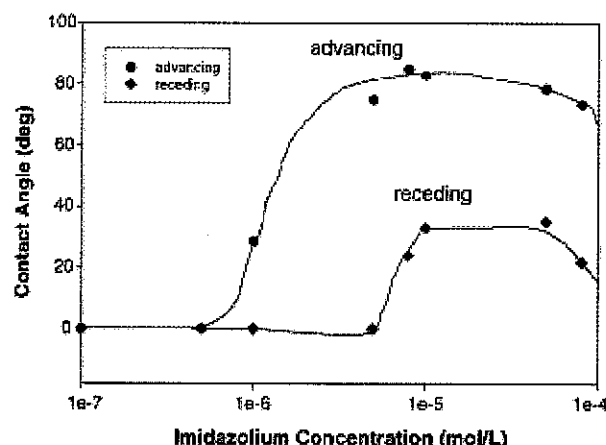


Figure 1.2: Advancing (circles) and receding (diamonds) contact angles of ImBF_4 surfactant solution on pre-equilibrated mica surfaces measured as a function of ImBF_4 concentration. The values of the contact angle were measured to $\pm 3^\circ$. The immersion speed

was 5 mm/min. The solid lines are drawn through the data and are meant to guide the eye [21].

1.3.6 Partition Coefficient/Function

Partition coefficient or distribution coefficient is a measure of differential solubility of a compound in two different solvents. In case of surfactants it is a measure of the hydrophobicity and hydrophilicity. In EOR the partition coefficient represents the ratio of surfactant concentration in oil phase to that in the water phase. When an oil phase is present in contact with the aqueous phase, the water/oil partition coefficient of the surfactant, degree of surface activity and molecular structure determine whether an oil-in-water (o/w) emulsion, water-in-oil (W/O) emulsion, or liquid crystalline structure is formed [22]. Surfactant aggregates are dynamic systems. Thermal energy and columbic forces are responsible to keep surfactant monomers and aggregates in motion, and influence mass transfer from aqueous to organic and organic to aqueous phase, the rates of formation and break-up of these structures. Micellar systems exhibit two characteristic “relaxation” times, known as τ_1 and τ_2 . The first corresponds to the rate at which single monomers enter and exit a micellar aggregate, and the second involves the rate of formation and break-up of an entire micelle. The kinetics of micellization has been shown to strongly affect such interfacial phenomena as wetting time, foamability, emulsion droplet size, oil solubilization rate and detergency [23].

Partitioning of surfactant out of the aqueous phase can occur when it encounters with other fluids which are either of too high or too low salinity. The surfactant-containing fluid should therefore be intensively analyzed by mixing with several samples of the water at different salinity levels. In this manner the upper and lower salinity bounds for an effective water formulation that will not cause partitioning of the surfactant out of the water phase can be determined. Optimized water can be selected that falls within these salinity boundaries for injection in an EOR processes. Following the injection of the polymer slug, injection of this controlled salinity drive water can either be performed in a continuous manner until the termination of the surfactant flooding process or takes the form of a discreet slug following the injection of the polymer slug, followed by a drive water of unspecified salinity.

1.4 Polymers in EOR

The main objective of polymer injection during waterflooding of oil reservoir is to decrease the mobility of the injected water by increasing its viscosity and decreasing the rock permeability to water through the formation of a water soluble high molecular gel with the injected water. Water breakthrough is an unwanted problem during the course of waterflooding in an oil field. Polymer solution has been widely applied to resolve the water-channeling problem in a deep formation. In practice, polymers are used in deep formation treatment either to form a gel blockage plug high permeability zones in-situ, or to act as mobility control agent and increases the viscosity of the injected fluids.

A polymer solution has to be injected at a relatively high concentration so as to maximize its penetration. However, the traditional polymer flooding may become ineffective mainly due to the viscosity loss caused by mechanical and chemical degradations of the polymer molecular structure. Thus such a treatment may not be economical as an oil displacement agent in a heterogeneous reservoir. Different polymers have different properties. The transportation of a polymer in porous media is also affected by many other factors. Generally the polymers for EOR processes can be categorized into two types: polyacrylamides and polysaccharides (biopolymer).

1.4.1 Hydrolysable Polyacrylamides (HPAM)

In HPAM the monomeric unit is the acrylamide molecule. When used in polymer flooding, polyacrylamides are susceptible to partial hydrolysis, which causes the scattering of anionic (negatively charged) carboxyl groups (-COO-) along the backbone chain. For this reason these polymers are called partially hydrolyzed polyacrylamides. Typical degrees of hydrolysis are 30 - 35% of the acrylamides monomers; hence the HPAM molecule is negatively charged, which accounts for many of its physical properties. This degree of hydrolysis is responsible to optimize certain properties such as water solubility, viscosity, and retention. If hydrolysis is too small, the polymer will not be water-soluble. If it is too large, the polymer will be too sensitive to salinity and hardness [24].

The viscosity-increasing features of HPAM depend upon its large molecular weight. This feature is accentuated by the anionic repulsion between polymer molecules and segments of the same molecule. The repulsion forces cause the molecule in solution to elongate and snag; an effect that accentuates the mobility reduction at higher concentrations. If the brine salinity or hardness is high, this repulsion is greatly decreased through ionic shielding since the freely rotating carbon-carbon bonds allow the molecule to coil up. The shielding causes a corresponding decrease in the effectiveness of the polymer since snagging is greatly reduced. The molecular structure of typical water-soluble polyacrylamide is presented in Fig. 1.9. HPAM is inexpensive and relatively resistant to bacterial attack, and exhibits permanent permeability reduction but they are sensitive to salinity and hardness.

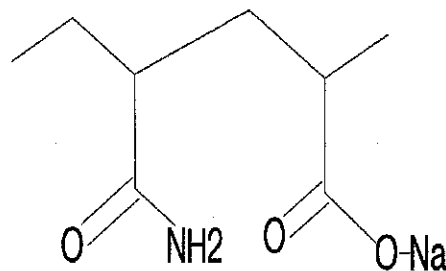


Figure 1.3: Molecular structure of water-soluble polyacrylamide.

1.4.2 Polysaccharides

Formed from the polymerization of saccharide molecules, polysaccharide generation leaves a substantial amount of debris in the polymer product that must be removed before the polymer is injected. The polymer is susceptible to bacterial attack after it has been introduced into the reservoir. The disadvantages are offset by the insensitivity of polysaccharide properties to brine salinity and hardness. The polysaccharide molecule is relatively non-ionic and, therefore, free of the ionic shielding effects of HPAM. Polysaccharides are more branched compared to HPAM, and the oxygen-ringed carbon bond does not rotate freely; hence the molecule increases brine viscosity by snagging and adding a more rigid structure to the solution. Polysaccharides do not exhibit permeability reduction. Molecular structure of a typical water-soluble polysaccharide is presented in Fig. 1.10. Molecular weights of polysaccharides are generally around 2 million. HPAM is

much cheaper than Polysaccharides so it is being widely used in most of the polymer flooding projects.

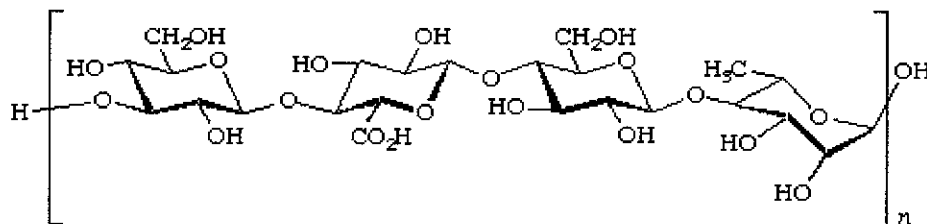


Figure 1.4: Molecular structure of water-soluble polysaccharide used for EOR.

1.4.3 Requirements of a Polymer

For EOR applications polymers must contribute to the oil ganglia mobility by providing the needful communication with other oil droplets. Polymers must be capable to play both the roles of thickening and viscosity control to reach the millipores and microspores. They must be hydrophilic and brine tolerant especially when the fluids contain divalent cations like Ca^{2+} and Mg^{2+} . Polymers should possess good thermal, dimensional stability but does not possess an initial mechanical strength unless it is constrained within a porous structure or narrow fracture within the pores and fine sand grains. The polymers are expected to enhance the inflow of oil relative to water because they provide a selective restriction of aqueous fluid flow through the entrapment of water hence reducing formation water permeability and decreasing water flow. They must be thin enough and maintain the viscosity until the commencement of gel formation (through solvation effects).

1.4.4 Viscosity and Shear Thinning of Polymer Solution

Generally, with the increase in polymer concentration, the viscosity of polymer solution increases quickly. However, all polymers are susceptible to shear thinning; their viscosity decreases with a corresponding increase in shear rate. The shear thinning behavior of the polymer solution is caused by the uncoiling and unsnagging of the polymer chains when they are elongated in high shear rate regime [25]. This elongation in combination with the other factors like temperature, concentration, pH, salinity, surfactants, rheological behavior, gelation range, can affect the gel strength leading to a reduction in shear

viscosity. This is often the case for polymer solutions exiting a gap or made to flow through a narrow orifice and opening. In order to use a polymer for EOR applications intensive care should be taken to evaluate the effects of all the mentioned contributing factors.

Recently, much effort has been focused on the synthesis of water-soluble polymers that demonstrates a favorable behavior when exposed to an external stimulus such as pH, temperature, or added electrolyte. The interactions between hydrophobically modified (HM) polymers and surfactants in solution have become the subject of extensive research. The reason for this intense interest can be found in the unusual rheology of HM polymer/surfactant mixtures, with a wide variety of possible applications. Polymers based on polyacrylamide (PAM) and polyacrylic acid (or acrylate, AA) containing a small fraction of hydrophobic groups is often employed in these studies. The general picture that emerges is that the binding between HM-PAM and surfactants strongly affects the rheology. The viscosity affects are larger with anionic surfactants compared to cationic surfactants [26 - 28].

Viscosity data have been reported for aqueous solutions of a series of acrylamide-based co- and terpolymers with added surfactants. Various surfactants like sodium dodecylsulfate (SDS), diethylhexyl sulfosuccinate (AOT) and dodecyltrimethyl ammonium bromide (DTAB) have been investigated. In the presence of anionic surfactants, the polymer solutions exhibit a dramatic increase in solution viscosity at concentrations around the surfactant CMC. This is attributed to interpolymer crosslinking through the formation of mixed micelles involving the hydrophobes from different polymer chains and the surfactant molecules. The viscosity enhancement is found to increase with increasing hydrophobicity of the hydrophobe (alkylacrylamide) and decreased with increasing acrylic acid (AA) incorporation in the polymer. The ionic fraction of the polymer chain also plays an important role in unfolding the polymer chain through electrostatic repulsion contributing to the viscosity increase at high solution pH. Both rheology and electric and magnetic field, EMF-derived binding isotherms suggest that the viscosity maximum occurs

at a low ratio of bound surfactant and hydrophobe monomers of approximately two surfactant molecules per hydrophobe [28].

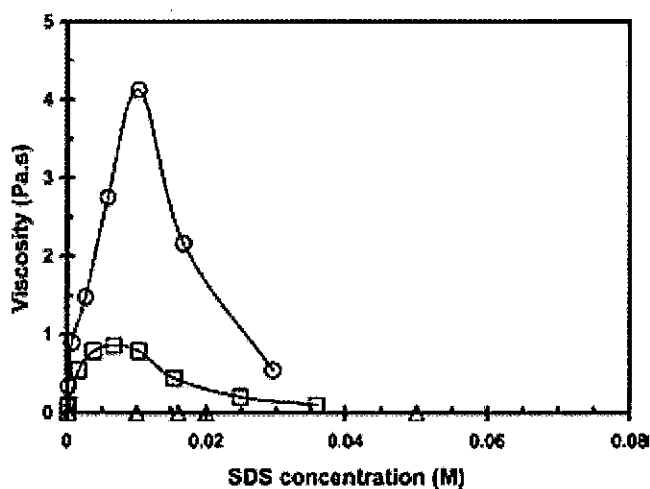


Figure 1.5: Viscosity as a function of SDS concentration for (Δ) PAM-C10-2%-AA-20%, (\square) PAM-C12-2%-AA-20% and (\circ) PAM-C14-2%-AA-20% at 2%wt polymer concentration and at pH 4 [28].

A plot of viscosity as a function of SDS concentration for a series of 2%wt aqueous solutions at pH 4 is presented in Fig. 1.11 for the terpolymers with C_{10} , C_{12} and C_{14} hydrophobe substitution and 20% AA incorporation. The addition of SDS to aqueous solution of the alkylacrylamides modified terpolymers leads to a strong viscosity increase. This viscosity behavior is commonly observed for HM polymers and can be ascribed to the formation of mixed micelles containing both surfactant molecules and the polymer hydrophobes. The viscosity curve reaches a maximum at concentrations close to the CMC of the surfactant and decreases again as the surfactant concentration is increased further. From this behavior it is assumed that SDS is not only compatible with the modified polymers but also play an important role to control the viscosity through enhanced solubilization of sparingly soluble mineral contents.

In EOR applications polymers act as mobility controlling agents, however, if the viscosity is too high it cannot invade or penetrate the millipores and micropores. There is an opportunity to use polymers in combination with surfactants to perform the dual task. In the presence of surfactant, mixed micelle formation involves surfactant molecules and polymer hydrophobes belonging to two or more polymer chains. Such mixed micelles act as effective interpolymer cross-linkers; this dynamic polymer network is responsible for

controlling the solution viscosity. The negatively charged mixed micelles on the polymer chain produce repulsive forces in the presence of anionic surfactants causing the polymer backbones to assume a more extended conformation [28 – 31]. On the basis of these findings various surfactants like SDS, cetyltrimethyl ammoniumbromide; CTAB, dodecyl benzene sulphonic acid; DBSA, AOT and ATR have been selected for this project to further evaluate their properties related to emulsification, partitioning in aqueous and oleic phases, IFT reduction, compatibility with polymers, stability towards temperature, alkalinity and salinity.

1.4.5 Inaccessible Pore Volume (PV) in Polymer Flooding

Gelled polymer treatments are applied to oil reservoirs to increase oil production and to reduce water production by altering the fluid movement within the reservoir. Polymer flooding has the capability of increasing the water viscosity, providing the mobility control of water phase and at the same time improving the driving efficiency. The treatment of porous rocks with gelled polymer system like polyacrylamide is expected to reduce the permeability of water at residual oil saturation to a much greater extent than the reduction of permeability of oil at the water saturation that is immobile after treatment. This is termed as Disproportionate Permeability Reduction (DPR). During polymer flooding, inaccessible pore volume, polymer shear thinning, polymer adsorption and relative permeability reduction must be considered. It has been reported [32] that during the passage of polymer solution through the porous media, it can not occupy all of the effective pore volume.

The remainder of the pore volume is inaccessible to polymer solution. This inaccessible pore volume is occupied by water that contains no polymer. This allows changes in polymer concentration to be propagated through the porous media more rapidly than similar changes in salt concentration as shown in Fig. 1.12. The disproportionate effect of polymer solution in the aqueous phase and the pore accessible polymer solution plays a significant role in controlling the mobility of aqueous phase.

At the front edge of a polymer bank, the effect of inaccessible pore volume opposes the effect of adsorption and may completely remove it. Generally, oil permeability develops as oil penetrates into the polymer-filled pore space, dehydrating the polymer gel

by displacing brine from the gel structure and creating “new flow” channels within or around the polymer gel. This “new pore space” is a fraction of the original pore space, and the permeability to oil is reduced substantially from its value before placement and in-situ gelation of the polymers.

Subsequent brine injection displaces oil from these flow channels but traps some of the oil in the “new pore space” as oil residual saturation. The trapping of residual oil in the new pore space causes the disproportionate reduction in brine permeability because the brine flows primarily in the pore channels created by dehydration of the polymer gel even though the gel has some brine permeability. However, the permeabilities to oil and water in the new pore space are functions of imposed pressure gradient. Pressure gradient has a much larger effect on water permeability than on oil permeability, thus the magnitude of the DPR is expected to decrease as pressure gradient increases. However, the large DPR values can be expected at the lower range of pressure gradients which attributes to relatively large residual oil saturation in the new pore space and the extremely water-wet nature of the new pore space. As a consequence of disproportionate solubility of polymers in the presence of brine in porous media the saturation of polymer solution is not equal to the saturation of aqueous phase.

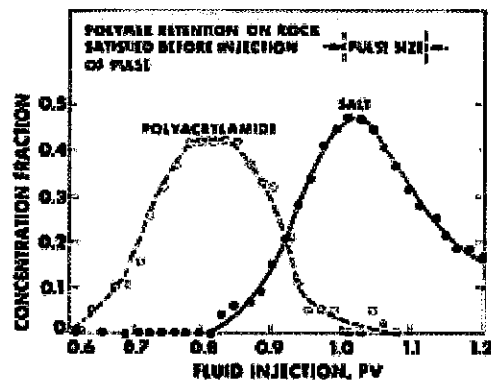


Figure 1.6: Polymer breakout curves [32].

1.4.6 Polymer Retention in Porous Media

Poor sweep efficiency due to reservoir heterogeneity is a major concern for the production of oil and gas from reservoirs. Improving reservoir sweep efficiency is important for a successful reservoir management. To control premature production of

water or gas, and if the motivation is to improve reservoir sweep efficiency, then polymer gels will be employed as a conformance control agent. However, when polymer solution flows through porous media, polymer molecule can be adsorbed onto solid surface or trapped within the small pores.

Polymer retentions vary with polymer structure, molecular weight, polymer concentration, rock composition, permeability, brine salinity, brine hardness, flow rate and temperature. For a given rock, the adsorption function can be adequately described by a Langmuir-type isotherm. Polymer adsorption can be harmful for polymer flooding; due to adsorption, the polymer solution gradually loses its viscosity during propagation [33]. For oil-wet rock, this polymer layer may change the rock to water-wet and induce a dramatic drop of residual oil saturation. Although the polymer has little effect on the IFT between phases, the adsorbed polymer layer changes the irreducible water saturation by decreasing the radius of the pore throats of the rock. As a result capillary pressure increases. Increase in capillary pressure originates from the increase of irreducible wetting phase saturation. For oil-wet reservoir rock capillary pressure causes a significant change, ranging from negative to positive. For no-wetting phase (oil) the effect of polymer adsorption is not so marked as that for the wetting phase (water).

With the advancement of polymerization techniques, nowadays, various varieties of polymers are available that contain a hydrophilic block and another block that is tunably hydrophilic/hydrophobic. The use of alternate polymer structures to overcome the deficiencies in polyacrylamide based flooding systems is being extensively explored. A common type of hydrophobically modified polymer contains a relatively small number of hydrophobic groups (usually alkyl groups) attached along the polymer backbone. In aqueous solution, the hydrophobic groups tend to associate together to diminish their direct contact with water, leading to substantial rheological effects. In the dilute regime the associations may occur between hydrophobic groups of the same chain, which leads to coil contraction and, consequently, a decrease in the viscosity of the solution. In the semi-dilute regime, hydrophobic groups of different chains may associate, leading to the formation of temporal intermolecular networks and a viscosity increase [34 – 37]. A vital factor in determining the suitability or lack of polymers for water control is whether or not the

polymer will adsorb on a rock surface. However, the size of a monolayer of adsorbed polymer or polymer molecules may not be large enough to reduce the permeability to the measured levels [38].

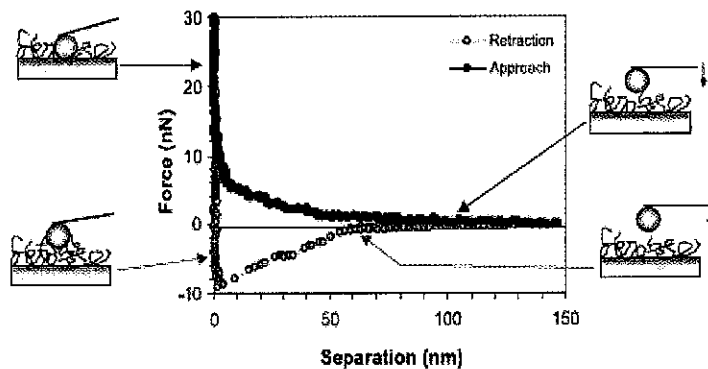


Figure 1.7: Interaction between glass probe and glass surface bearing an adsorbed layer of polymer B (1.0% of polymer in nanopure water). The drawings give a schematic representation of the events occurring along the force–distance curves [38].

Polymer retention in a porous medium generally decreases the permeability to water. This phenomenon can be modeled by a layer of adsorbed polymer onto the pore walls, which reduces the pore sizes. Most of the research effort has been directed at testing polymer/gels in cores and sand-packs to improve the understanding of water control by polymers and gels. However, the causes of Relative Permeability Modification (RPM) could vary with the polymer/gel system and the particular conditions studied. As a consequence, several theories have been proposed but there is a lack of general agreement between researchers on the basic mechanisms and the conditions under which they are applicable [38 – 45].

It is also commonly known that certain polymers and modified starch additives which were traditionally used for EOR applications tend to adsorb or to be retained by, and sometimes plugging and restricting the water-wet reservoir pores impairing formation permeability. Despite the careful selection of less-damaging polymeric viscosifiers, reduced mobility of oleic phase still remains as a major challenge. Depending on the compatibility of the aqueous phase with the reservoir fluids, strong water/oil emulsions with high viscosities may also be formed, damaging the reservoir pores.

Fig. 1.13 explains the adsorption of polyacrylamide when nanopure water was used during measurement; the approach curve is almost similar to the curve that was obtained in the presence of brine, but the thickness is slightly smaller (ca. 110nm) and the dense domain of adsorbed polymer seems to be less than 7 nN. However, on retraction a strong adhesion is observed. The probe remains in contact with the surface until 0 nN, and starts departing from the surface to a value of 5 nm (-10 nN), whereupon it slowly separates until it is finally released at 60 nm. This behavior is due to the polymer attaching onto the glass probe on the cantilever, which is typically termed polymer bridging, wherein polymer molecules form bridges between the two surfaces.

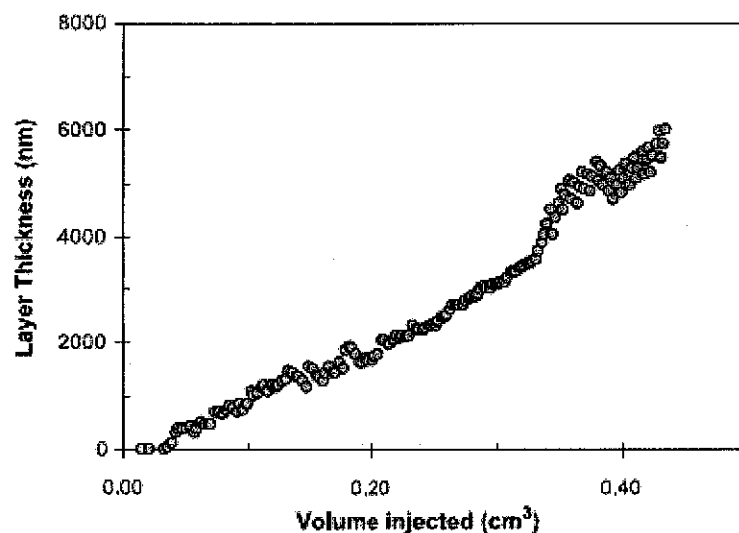


Figure 1.8: Reduction in the hydraulic conductivity of a capillary tube expressed as layer thickness during polymer injection. The increase in thickness shows the dynamic formation of a thick polyacrylamide layer [38].

Fig. 1.14 indicates that at the end of the first injection, an equivalent layer of 6000 nm (6 μm) is formed. Further injection of polymer did not produce an increase of the layer thickness, while some oscillations in conductance were observed as a function of time. It is an indication that during the injection of low molecular weight polymer; a slow pressure is building up. The conductance was calculated using the average flow rate and pressure drop during the same time interval. If the extra resistance to flow is interpreted as a reduction of the capillary size (modeled as two parallel plates), a continuous increase in the polymer layer thickness can then be inferred [38].

1.5 Alkalis in EOR

The interactions between alkalis and surfactants in ASP flooding have great technological importance and are being widely investigated. Synergistic effect of surfactants and alkalis is responsible to produce spontaneous emulsification and ultra-low IFT at oil-water interface [16, 46]. Interfacial properties of acidic oil/caustic systems have been investigated by Dong *et al.* [47] using kerosene/oleic acid as the oil phase and a NaCl/NaOH solution as the water phase. The pre-equilibrium of the oil/water phase produced the anionic surfactant sodium oleate. The results showed that the minimum IFT was measured in the range of 50 - 200 mg/L NaOH depending on the salinity of the water phase. In the vicinity of the NaOH concentration of minimum IFT, the oil-in-water emulsion had the highest electrophoretic mobility. Electrophoretic mobility describes the motion of charged species in a fluid due to an external charge. It is proportional to ionic charge and the external field applied.

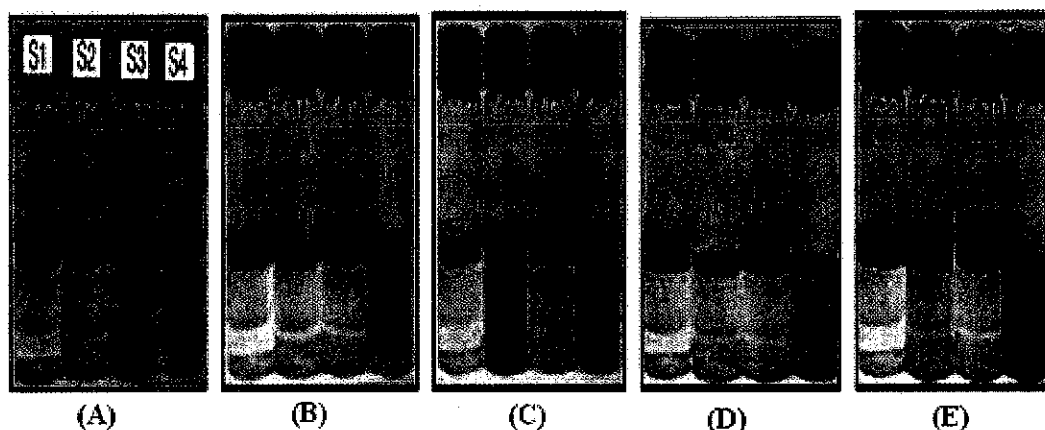


Figure 1.9: Pictures of oil/brine systems with different surfactants at five stages of emulsification test. Oil/water ratio: 3/100, Na_2CO_3 concentration: 0.15 wt.%, surfactant concentration: 50 mg/L: (A) the prepared samples; (B) after being gently turned three times; (C) after being gently turned four more times; (D) at 50 h before the third re-emulsification mixing; and (E) after the third re-emulsification mixing [16].

Chan and Shah [48] studied the effects of surfactant concentration, NaOH concentration, and salt concentration on IFT and electrophoretic mobility. It was reported that the minimum IFT corresponded to a maximum electrophoretic mobility. They concluded that the maximum adsorption of the surfactant at the oil/water interface led to the highest surface charge density, contributing to the lowering of the IFT to a minimum

value. Verzaro *et al.* [49] have emulsified a Venezuelan acidic heavy oil (API gravity = 7.8) in tap water when the organic acids in oil were ionized and became effective emulsifiers by adding ammonia or NaOH to the water phase to react with the acids. Qiang *et al.* [46] have reported the emulsification behavior of the heavy oil in the original formation brine (2.7 wt.% salinity) using bottle tests. They showed that the heavy oil could be emulsified and re-emulsified in the bottle tests with Na₂CO₃ concentrations from 0.2 to 0.6 wt.% and surfactant S4 concentrations higher than 80 mg/L. The emulsification behavior was very similar to that of the heavy oil in dilute brine (1.4 wt.% salinity), at a narrower range of alkaline concentrations and with a slightly higher surfactant concentration.

An emulsion of viscous heavy oil can be applied in EOR applications through in-situ production in a reservoir. Heavy oils usually contain some organic acids that can react with alkalis to form in-situ surfactants. If these in-situ surfactants can emulsify heavy oil in the injection water during the displacement process in the reservoir, heavy oil can be produced out of deposits in emulsion, which is relatively easier than production of the heavy oil without emulsion. Therefore, emulsification of heavy oil in formation brine under a very slight interfacial disturbance is of immense practical interest for EOR. In heavy oil reservoirs, formation brines have a high salinity and high concentration of bivalent cations (mainly Ca²⁺ and Mg²⁺), which are detrimental to the formation of oil-in-water emulsions. Under these conditions, emulsification of heavy oil in the formation brine provides a formidable challenge to EOR strategies.

As a summary Table-1.1 provides a general comparison of primary, secondary and tertiary recovery processes highlighting the mechanisms, advantages, areas of ambiguities and technical challenges associated with each processes.

Table 1.1: Comparison of primary, secondary and tertiary recovery processes.

Processes	Primary recovery	Secondary recovery	Tertiary recovery
Mechanisms	Being a natural process the available energy of the reservoir act as driving force for the processes like gas cap drive, solution gas drive and bottom water drive [2].	Using waterflooding to maintain pressure and displace oil by improving the sweep efficiency, viscous fingering controlled by the difference in relative permeabilities and viscosities of the fluids [1-5].	Using thermal recovery methods, gas injection, chemical injection, in-situ heat generation, etc. IFT reduction, control of miscibility, emulsification and wettability change, etc [3-5, 8-10, 15].
Advantages	Typically covers 15% of the OOIP. Only suitable for lighter crude oils. The driving force is naturally available, no need for additional energy to run the process.	Economically feasible, typical oil recoveries range from 15 to 40% of OOIP after primary recovery. Appropriate for the enhanced recovery of lighter to medium crude oils.	Typically covers 5 - 30% OOIP after a primary and secondary recovery. Having the potential to maximize the oil recovery to another level.
Complications	Pressure of the reservoir is always declining with the passage of time causing a gradual decrease in oil recovery due to the lack of driving force. It is less or not suitable for the recovery of medium and heavier crude oils.	Poor sweep efficiency. Formation of scale and other deposits causing localized permeability damage. Generation of transition zone, an interval tens of feet below the traditionally defined producing oil-water-contact (OWC) where the oil saturation falls rapidly. Waterflooding is only operated via long-distance displacement [2, 3].	Lack of reliable technology particularly for ASP flooding at indigenous level. Excessive loss of injected chemicals and fluids due to high temperature, adsorption, production of in-situ emulsion with high viscosities, precipitation and incompatibility among different components. Poor relationship between lab and in-situ investigation [3-6, 8-22, 24, 32-37, 46, 48].

1.6 Motivation for the Project

No matter how extensive the primary, secondary and improved oil recovery strategies that are put in place; there is still a huge amount of crude oil remaining in the existing reservoirs. EOR strategies take a centre stage, motivated by high crude oil prices and a need to squeeze more from the existing mature fields.

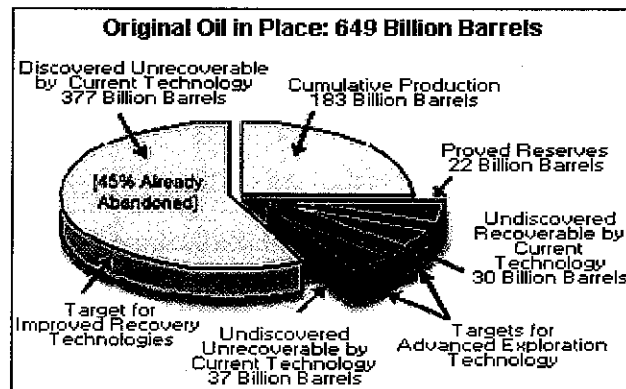


Figure 1.10: Original oil in place around the globe [50].

Fig. 1.16 provides an overview of OOIP around the globe and indicates that there is still a huge amount of oil trapped in the proven reserves which requires advanced and improved technologies for their recovery. Capillary forces are responsible to control oil and water mobilities in petroleum reservoirs. Current chemical methods involved in EOR processes widely used to overcome these capillary forces include the use of conventional and non conventional modified surfactants and polymers.

Most important preconditions for polymer flooding are reservoir temperature and the chemical properties of reservoir water. At high temperature or with high salinity in reservoir water, polymers and surfactants cannot be kept stable and their concentrations keep on declining causing a reduction in the effectiveness of the process and jeopardizing economic returns. Significant problems associated with CEOR involve the incompatibility between surfactants and polymers, temperature instability, reduction in polymer thickening ability in formation due to the presence of various salts, excessive loss of chemicals due to adsorption, precipitation and degradation of chemicals either by the breakdown of the polymer chains, molecular scission or permanent hydrolysis of PAM. The main reason for this is the complex relationship between surfactants, polymer rheology and their

adsorption, retention and precipitation. These factors strongly depend on the porous medium structure, salinity, temperature, crude composition, etc.

1.7 Problem Statement

Chemical flooding is an important process for enhanced oil recovery. A substantial amount of oil is present in the reservoirs, especially the oil reservoirs that have low primary and waterflood oil recoveries. Various EOR techniques have been reported on different types of reservoirs. However, limited success of CEOR methods was attributed to the sensitivity of the oil price, huge up-front investment with unpredictable return, accessibility, limitations of chemicals supply and mismatch between the lab and field studies. Nowadays, increase in oil price has led to a new look at more cost intensive CEOR methods especially for declining oil fields. Successful implementation of CEOR methods requires that the basic mechanisms (improved microscopic displacement efficiency, wettability alteration and IFT reduction) governing the processes are well understood.

Most of the previously reported chemical flooding studies have been performed in water-wet sandstone reservoirs. However, in most of the cases reservoirs are either oil-wet or mixed-wet in nature. As a consequence, the effects of chemical flooding on heterogeneity and wettability alteration of oil-wet reservoirs are fairly unknown. Higher concentrations of the required chemicals, poor tolerance to harsh conditions of temperature and salinity, viscous stable emulsion formation, blockage and residual harmful additives in the produced oil are the major challenges that need to be adequately addressed. The use of chemical flooding is no longer restricted to tertiary recovery activities but is being incorporated right at the beginning of the production cycle.

1.8 Objectives and Scope of the Study

ASP flooding has been widely tested for its ability to improve oil recovery, but little effort has been made towards the understanding of the controlling mechanisms and variables. Although much scientific work has been accomplished, underlying principles of CEOR is not well established. The objectives and scope of this study is to overcome the

ambiguities of the previous studies and to provide the detailed critical elaboration of the involved mechanisms in CEOR process.

Systematic studies will be conducted by screening the various conventional, non-conventional surfactants and polyacrylamide based modified polymers towards their temperature stability, mutual compatibility, adsorption and retention by sandstone rocks, IFT reduction on oil-water inter phase, emulsification, viscosity reduction of polymer due to increase in temperature, salinity, higher pH and partition coefficient of surfactants in oil and water phases. Adsorption behavior and kinetics of the surfactants on reservoir rocks will be elaborated using appropriate models. Evaluation of all these parameters will be helpful in designing a suitable ASP flooding formulation for a Malaysian sandstone reservoir.

Detailed studies will be conducted to understand the complex relationship involved in the aggregation of polymer and surfactants. This aggregation phenomenon can have drastic effects on the EOR processes. Adsorption of surfactants on the reservoir rocks can be determined by a large number of variables such as chemical and structural properties of the surfactants, polymers, porosity of the medium, solubility, interfacial charge, salinity, hardness, pH and temperature. Porous structure plays an important role towards these factors and is expected to behave differently in the bulk phase. The aim was thus to contribute to an understanding of this complex field paying due attention to the physico-chemical interactions involved in oil recovery applications.

1.9 Organization of Thesis

The primary objectives of this project was to develop a suitable chemical formulation, to enhance oil recovery from sandstones, based upon surfactants, polymers and alkalis by evaluating their stability towards various contributing factors like temperature, salinity and alkalinity, etc. This was accomplished in four separate stages. Chapter 1 provides a brief introduction to EOR, fundamentals of surfactants, ASP flooding and role of surfactants, polymers and alkalis in oil recovery processes. It discusses the various basic properties of these chemicals. Chapter 2 provides a detailed literature review

on the main topic of this thesis, enhanced oil recovery by surfactants with the help of previously reported work. The review also includes a detailed description of the effects of, wettability, emulsification, IFT reduction and the mechanisms in which are responsible to control these parameters. Chapter 3 deals with the experimental portion including water analyses, thermogravimetric analyses, optical microscopy, partition coefficient measurement, viscosity estimation, IFT analyses, contact angle measurement, oil recovery experiments using imbibition cell under ambient conditions and core flooding experiments using reservoir conditions, BET surface area measurement and scanning electron microscopy. Chapters 4 deals with the analyses of the results and description of adsorption and kinetics using appropriate models. Chapters 5 summarize the main conclusions of the thesis and provide recommendations for further work.

1.10 Summary

In this chapter basic concepts of EOR, ASP flooding, CMC, IFT, emulsification, partition coefficient, wettability alteration, viscosity and shear thinning of polymer solution, inaccessible pore volume in polymer flooding and polymer retention in porous medium have been explained. A general comparison of primary, secondary and tertiary recovery processes has been presented in order to highlight the importance of tertiary oil recovery and in particular ASP flooding. Organization of the thesis has also been presented. It can be summarized that the traditional recovery methods have limitations and can be exploited further through EOR strategies. Implementation of ASP flooding was previously hindered due to the lack of appropriate technology, economical and environmental factors, etc. but it has a bright future. The present work provides laboratory data to adequately demonstrate the benefits of surfactant molecules engineered to maximize oil recovery.

CHAPTER 2

2. LITERATURE REVIEW

Aging fields and an ever diminishing prospect for finding new large reserves are enough reasons for the intensification of efforts directed at maximizing the oil recovery from existing fields. Crude oils from different fields vary widely in appearance and viscosity from each other. They range in color, odor, and have variation in the physico-chemical properties. While all crude oils are essentially hydrocarbons, the difference in properties, especially the variations in molecular structure, means that crude is more or less easy to produce, pipeline, and refine from diverse reservoirs. Crudes can be roughly classified into three groups, Paraffin-, Asphaltene-, and Mixed- base crude oils, according to the nature of the hydrocarbons which they contain. Even though crude oils are a continuum of thousands of different hydrocarbon molecules, the proportions of the various elements like N, O, S, Ni, V, Fe, etc in crude oils vary over fairly narrow limits [51]. Nevertheless, a wide variation in properties is found from the lightest crude oils to the highly asphaltic crudes. The carbon content normally is in the range of 83 – 87%, and the hydrogen content varies between 10-14%. Knowledge of the distribution of major structural classes of hydrocarbons in crude oils is essential not only for reservoir evaluation, migration, degradation and environmental safety but also for ultimate utilization. The SARA-separation is an example of such group type analyses, separating the crude oils in four major chemical classes based on differences in solubility and polarity. The four SARA-fractions are saturates (S), aromatics (A), resins (R), and the asphaltenes (A). Asphaltenes are the heaviest and most polar fractions found in crude oil and are considered as responsible for the formation of deposits. Due to this phenomenon asphaltene is also known as the “cholesterol of petroleum” [52].

Although the current recovery rates from the mature oilfields are declining, the deposits due to asphaltenes will further hinder the production and transportation processes. The structure of the asphaltene has been the subject of several investigations but is now believed to consist of polycyclic aromatic clusters, substituted with varying alkyl side

chains [53]. Figure 2.1 shows a hypothetical asphaltene monomer molecule. The molecular weight of asphaltene molecules has been difficult to measure due to the asphaltene's tendency to self aggregate, but is believed to be in the range of 500-2000 g/mole. Asphaltene monomer molecular size is in the range 12-24 Å [54]. The presence of high asphaltene contents may result in productivity losses and sometimes even production shutdowns due to pressure loss during production, or a change in the composition of the fluids in the reservoir during recovery operations enhanced by the injection of gas (e.g. CO₂). Asphaltenes could lead firstly to an increase in the viscosity of crude and secondly to the formation of a deposit causing partial or total blocking of the porous medium.

During the past few decades, varieties of EOR methods have been developed and implemented in mature and near depleted reservoirs. The methods, or phases of oil recovery, can have the following divisions: primary, secondary and tertiary phases of recovery. The tertiary oil recovery can be categorized at least into three phases: thermal, chemical and solvent, methods. These tertiary phase recovery categories utilize various methods, such as, non-hydrocarbon gas injection (CO₂, N₂, air, combustion gases) into the reservoir, LPG injection (liquefied natural gas or propane), waterflooding methods (injection of water enhanced by surface-active agents, polymers or other chemical agents), the use of heat to decrease the viscosity of oil (underground combustion, steam or hot water injection), the use of metabolic activity of anaerobic bacteria, etc. The main objective is to intensify the flow of "residual" oil that has not been exploited during the primary and secondary phases of recovery [55]. Of the many methods developed to improve oil recovery, thermal and gas injection were considered as economical and most successful in the last few years. Fig. 2.1 elaborates the drive mechanism when CO₂ contacts with the trapped residual oil and allows it to flow out of the channels [56].

Despite the many researches on CO₂ injection, the interactions between CO₂ and residual oil and the actual mechanisms by which residual oil might become mobilized during a CO₂ injection is not yet fully understood. This knowledge is not only essential for an economic evaluation of CO₂ sequestration but also for the prediction of migration and ultimate fate of CO₂ after it has been injected into a depleted oil reservoir. It is anticipated that the injection of steam or CO₂ has always resulted in a poor sweep efficiency due to

reservoir heterogeneity, low gas density (causing gravity override) and low gas viscosity (causing fingering).

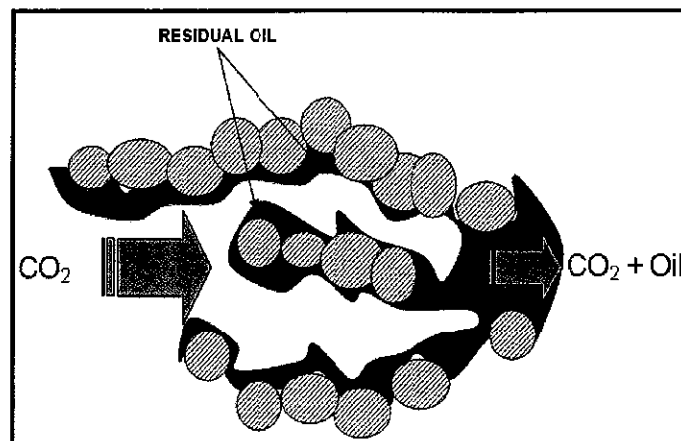


Figure 2.1: CO₂ contacts the residual oil and allows the oil to flow out of the tight pore channels [56].

The potential of CEOR by advanced injection techniques has been known for many decades, but unstable economic climate and the complex nature of the reservoir processes often involved in EOR have hindered the implementation of many CEOR projects [34,42,48]. A lot of work has been reported on CEOR methods involving microbial and chemical techniques [2 - 5,8,15,16,22,28,41 - 45,48]. Microbial and chemical techniques were not popular in the early days due to the lack of understanding of the process and the cagey cost effectiveness factors. Although CEOR methods are slightly expensive as compared to steam or gas flooding, with improved drilling technologies, better production, improved reservoir knowledge, and higher oil prices, these methods are becoming more attractive. The main mechanisms accomplished through the EOR methods for the displacement of oil from the pores of the reservoir rocks can be explained by the attainment of miscibility, a reduction in IFT, wettability alteration, change in oil or water viscosity and an increase in pressure due to injected medium [57]. A surfactant-polymer flooding process is shown in Fig 2.2 explaining that the surfactant-polymer slug is responsible to disperse the oil ganglia by controlling the mobility, reducing IFT and altering the wettability.

Most common chemical flooding methods that have been shown to be effective in recovering unswept oil involve the combination of polymer, alkali and surfactants. They

can be categorized as surfactant/polymer (SP), alkaline/surfactant/polymer (ASP) and microbial enhanced oil recovery (MEOR).

An SP flood is accomplished by injecting a surfactant to reduce the IFT and mobilize the residual oil saturation mixed with a polymer for mobility control of the chemical slug. ASP flood on the other hand involves an alkaline chemical such as sodium carbonate mixed with a surfactant or combination of surfactants and polymer to generate an in-situ surfactant, producing an ultra-low IFT and with an added advantage of reducing the surfactant adsorption on reservoir rocks [16].

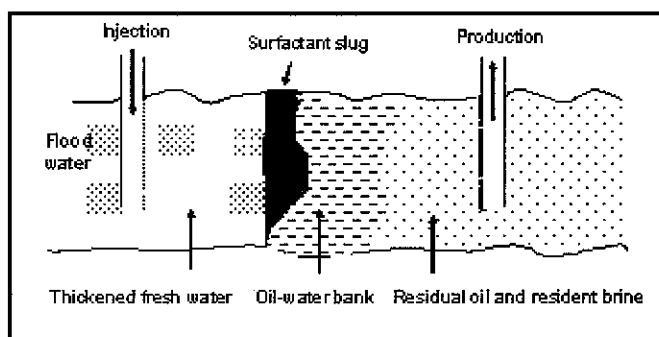


Figure 2.2: Schematic diagram of surfactant-polymer flooding process [58].

2.1 Basic Parameters in Chemical Flooding Processes

It is important to understand the basic properties involved in CEOR processes such as wettability, capillary pressure, residual oil saturation and relative permeability. These properties play a vital role to oil recovery during chemical flooding.

2.1.1 Wettability

Wettability is a manifestation of rock-fluid interactions associated with fluid distribution in porous media. It is defined as the contact angle between a droplet of the liquid in thermal equilibrium placed on a horizontal surface. Wettability can also be defined as the tendency of one fluid to spread on or adhere to a solid surface in the presence of other immiscible fluids [59]. When the fluids are water and oil trapped in reservoir pores, the wettability can be defined as the tendency for the rock to preferentially imbibe oil, water, or both. Depending on the type of surface and liquid the droplet may

take a variety of shapes as illustrated in Fig. 2.3. The wetting angle ' θ ' is given by the angle between the interface of the droplet and the horizontal surface. The liquid is considered wetting when $90^\circ \leq \theta \leq 180^\circ$ and non-wetting when $0^\circ \leq \theta \leq 90^\circ$. A contact angle $\theta = 0^\circ, 180^\circ$ corresponds to a perfect wetting surface and the drop spreads on the surface forming a uniform film.

The wetting angle ' θ ' is a thermodynamic variable that depends on the IFT of the surfaces. Let $\gamma_{l,g}$ denotes the IFT due to the liquid-gas surface, $\gamma_{s,l}$ refers to the IFT due to the solid-liquid surface and $\gamma_{s,g}$ indicates the IFT of the solid-gas surface. In thermodynamic equilibrium the wetting angle ' θ ' is given by Young's law [60]:

$$\gamma_{s,l} = \gamma_{s,g} + \gamma_{l,g} \cos \theta \text{ ----- (2.1)}$$

For two-phase flow in porous media the wetting angle influences the strength of the capillary pressure. Let ' θ ' denote the wetting angle between the interface and the pore wall, then the capillary pressure ' P_c ' in a pore of size ' a ' becomes as follows:

$$P_c \approx (2\gamma/a) \cos \theta \text{ ----- (2.2)}$$



Figure 2.3: A liquid droplet in equilibrium with a horizontal surface surrounded by a gas. The wetting angle ' θ ' between the horizontal layer and the droplet interface defines the wettability of the liquid. To the left: A non-wetting fluid with $0^\circ \leq \theta \leq 90^\circ$. To the right: A wetting fluid with $90^\circ \leq \theta \leq 180^\circ$ [56].

A fundamental understanding of the wettability of rock surfaces by crude oil and brine requires a good description of the intermolecular interactions between the different phases in contact. In order to have a clear picture about the flow and allocation of fluids within reservoir rocks it is extremely important to have proper information about the wettability. Generally, when a rock is water-wet, the aqueous phase will be retained by the capillary forces in the smaller pores and on the walls of the larger pores. Alternatively, the

“oleic” phase will occupy the center of the larger pores and form globules that are extendible to numerous pores. Whereas the oil phase is usually referred to as the “oleic” phase since its density and viscosity change with the amount of gas (solvent) dissolved. A rock can have a neutral, fractional and mixed wettability. Neutral wettability represents no clear preference for one fluid or another. Fractional wettability condition on the other hand arises due to the occurrence of multifarious mineral constituents of the reservoir rocks. Different minerals have diverse surface chemistry and adsorption properties, which can lead to variations in wettability within a single reservoir [10]. The concept of mixed wettability was introduced by Salathiel in 1973 [61]. A mixed-wet rock may have the oleic phase completely occupying the oil-wet large pores and the aqueous phase occupying the water-wet small pores or different minerals within the same pore.

The understanding about the nature of a mixed-wet reservoir is based on the assumption that the rock was strongly water-wet prior to hydrocarbon migration. During migration, the oleic phase is supposed to expel the aqueous phase from the large pores which will not enter the small pores due to surface and capillary forces. In the mean time the oleic phase can start to wet the surface of the large pores converting them to oil-wet. However, the traditional definition of an oil-wet rock involving, the oleic phase occupying the small pores and coating the walls of the large pores, whereas the aqueous phase occupying the center of the large pores is now modified. As the terms oil-wet and mixed-wet are interchangeable, all reservoirs that claimed to be oil-wet were actually mixed-wet by definition because the oleic phase does not occupy the small pores. Various studies on core handling effects and crude oil/brine/rock (COBR) interactions have revealed the wettability of a core sample is altered when retrieved from a reservoir. It is also reported that wettability of a core will affect almost all types of physical parameters necessary for reservoir management, such as capillary pressure [62 – 64]. However, the most accurate results can be obtained using the native virgin or restored-state cores with native crude oil and brine at reservoir temperature and pressure. The wettability of originally water-wet rock can be altered by the adsorption of polar compounds and/or the deposition of organic material that was originally in the crude oil. The degree of wettability alteration can be

estimated by the interactions between the oil constituents, the mineral surface, and the brine chemistry and the factors that influence wettability alterations.

Due to the capillary pressure dependence on water saturation, the effect of wettability alteration on reserve estimation through the initial water saturation can be predicted. Several methods have been presented in the literature for the determination of rock wettability. The three most common quantitative methods are contact angle measurements, the Amott method, and the U.S. Bureau of Mines (USBM) method. Many qualitative methods such as relative permeability have also been presented. The contact angle method only measures the wettability of a single solid surface, while the Amott and USBM methods measure the average wettability of a core sample. Contact angle measurements involve a fluid drop (typically water) coming in contact with a solid surface (mineral crystal plate or rock surface) and surrounded by an additional fluid (typically oil). The fluids are allowed to come to equilibrium and the contact angle between the fluid drop and the solid surface is measured. The magnitude of the contact angle gives a direct indication of the wettability of the rock [65 – 70]. Table 2.1 provides the ranges of contact angles and the respective wetting state.

Table 2.1: Relationship between wettability and common measurements [67].

Techniques	Water-wet	Neutral-wet	Oil-wet
Contact Angle (Minimum)	0°	60° – 75°	105° – 120°
Contact Angle (Maximum)	60° – 75°	105° – 120°	180°
USBM Wettability Index	~1	~0	~-1
Amott Wettability Index: Displacement by water ratio	>0	0	<0
Amott Wettability Index: Displacement by oil ratio	<0	0	>0
Amott-Harvey Wettability Index	$0.3 \leq I_w \leq 1.0$	$-0.3 \leq I_w \leq 0.3$	$-1.0 \leq I_w \leq -0.3$

2.1.2 Amott Wettability Index

The first quantitative wettability measurement method that is used for rock cores was described by the Amott [65]. This method utilizes a sequence of imbibition and forced displacement tests. After the centrifuged core has obtained residual oil saturation under brine, the following steps are adhered to: a) spontaneous imbibition of oil to record the volume of water displaced; b) forced displacement of water by oil under centrifuge to record the volume of water displaced; c) spontaneous imbibition of water to record the volume of oil displaced; d) forced displacement of oil by water under centrifuge to record

the volume of oil displaced. One problem with the Amott method is its insensitivity near neutral wettability. The obtained results can be expressed in terms of a ratio of the displaced volume by spontaneous imbibition and the displaced volume by forced displacement (δ_o , δ_w).

$$\delta_o = V_{wsp}/V_{wt} \text{ ----- (2.3)}$$

where, V_{wsp} is the water volume displaced by spontaneous imbibition and V_{wt} is the water volume displaced by both oil imbibition and forced displacement.

$$\delta_w = V_{osp}/V_{ot} \text{ ----- (2.4)}$$

where, V_{osp} is the oil volume displaced by spontaneous imbibition and V_{ot} is the oil volume displaced by both water imbibition and forced displacement. For a water-wet core, δ_w is positive and δ_o is zero, whereas the reverse is true for an oil-wet core. Wettability index is the difference between water index and oil index. For fractional or mixed wettability cores, both indices may be positive as reported in Table: 2.1. The method is insensitive for neutrally-wet cores. Because in this region, liquids do not spontaneously imbibe and both displacement ratios are close to zero.

A modification to the Amott method otherwise known as the Amott-Harvey method is commonly used. The Amott-Harvey wettability index (I_{a-h}) is a combination of Equations 2.3 and 2.4 as follows:

$$I_{a-h} = \delta_w - \delta_o = V_{osp}/V_{ot} - V_{wsp}/V_{wt} \text{ ----- (2.5)}$$

Eq. 2.5 is preferred to Eqs. 2.3 and 2.4 as it has a better sensitivity within certain ranges of wettability. The main problem with the Amott and its modifications involves its insensitivity near neutral wettability. The Amott-Harvey index ranges from +1 for a completely water-wet medium to -1 for a completely oil-wet medium [70].

2.1.3 USMB Wettability Index

The USBM method was first introduced by Donaldson *et al.* 1969 [71]. This method is useful to determine the average wettability of a rock core. One benefit of the USBM method over the Amott method is that the USBM is sensitive near neutral wettability, while the Amott method is not. The USBM method is based on the fact that the work required for the wetting fluid to displace the non-wetting fluid is less than the work required for the opposite displacement. It compares the work done by one fluid to displace the other, as given by the capillary pressure relationships (Figure 2.4). The USBM wettability index is defined by:

$$W = \log(A_1/A_2) \text{-----} (2.6)$$

Where A_1 = area under the secondary drainage curve, and A_2 = area under the forced imbibition curve. Several experiments have been performed to confirm that the work is proportional to the area under the capillary pressure curve. The capillary pressure curve for each phase was generated using standard centrifuge methods. For positive values of W , the core is water-wet; for negative values, the core is oil-wet, and for W close to zero, the core is neutrally wet. One disadvantage of the USBM method is that it can only be conducted on plug-sized samples.

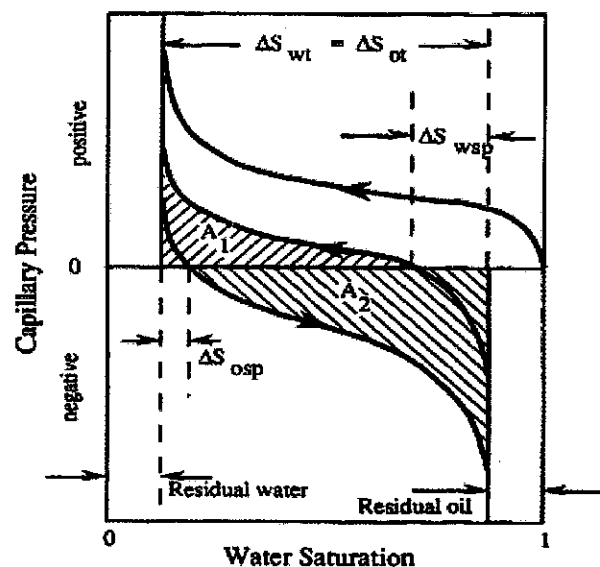


Figure 2.4: Capillary pressure-saturation curves for Amott/USBM method [71].

Areas under the water and oil capillary pressure curves are shown by A_1 and A_2 , whereas, ΔS_{wt} , ΔS_{ot} , ΔS_{wsp} , ΔS_{osp} represent residual water and oil saturations before and after spontaneous imbibitions respectively.

2.1.4 Wettability and Contact Angle

The contact angle is the angle at which a liquid/vapor interface meets the solid surface. The contact angle is specific for any given system and is determined by the interactions across the three interfaces. Contact angle is a widely used quantity to measure the wettability of surfaces. Hence, the idea of applying the contact angle concept in reservoir crude oil–brine–rock systems to quantify reservoir wettability is an old one. The concept of contact angle has been widely adopted in studies involving the characterization of solid–fluid–fluid interfacial interactions between reservoir rock surface, brine and crude oil in petroleum reservoirs. The idea of relating rock–fluids interactions in petroleum reservoirs to contact angle appears sound to make experimental measurements and develop meaningful correlations with expected success. In the studies concerning surface phenomena wettability term has been used interchangeably with spreadability. If a liquid spreads spontaneously on a given solid surface, it is said to be wetting the solid. On the other hand, if the liquid beads up into droplets on a solid surface instead of spreading, then it is said to be non-wetting. The contact angle concept has been helpful in determining whether a given liquid spreads or not on a given solid. A non-spreading liquid means that the contact angle (measured through the liquid droplet resting on a solid surface and in the environment of its vapor) is nonzero; and when the liquid wets the solid completely and spreads freely over the surface at a rate depending on the liquid viscosity and solid surface roughness, the contact angle is zero.

There is always some adhesion of any liquid to any solid. On a homogeneous solid surface contact angle is independent of the volume of the liquid drop. Obviously, since the tendency for the liquid to spread increases as the contact angle decreases, the contact angle is a useful inverse measure of spreadability or wettability. Equilibrium contact angles are functions of the surface free energies of the solid substrate and the liquid in contact with it and of the free energy of the interface between the two phases.

Much useful information can be obtained through the studies of contact angles. This equilibrium, however, represents the extent to which the liquid spreads over the substrate and not the extent of wetting at the interface. This indicates that contact angles, while being a direct measure of spreadability of liquids over solids, may not represent all the interactions taking place at the fluid–solid interface [72]. The solid surfaces generally used in these contact angle measurements are usually quartz, calcite or dolomite depending upon the predominant mineral content present on the reservoir rock surface. In pure surface science studies, such as those of Zisman [73], the system consisted of a pure smooth solid substrate upon which a drop of a pure liquid was placed surrounded by atmospheric air or vacuum. The contact angle made by the liquid on the substrate was a measure of the extent to which the liquid spread and hence wettability.

In the study of wettability of petroleum reservoirs, two liquid phases, namely brine and crude oil, compete to wet the solid rock surface. The three-phase equilibrium in a reservoir is further influenced by the injected fluids such as water in a waterflood or gases or solvent in tertiary enhanced oil recovery processes. Reservoir wettability has been defined so as to have a close association with waterflooding since it is the predominant secondary recovery process. In waterflood oil recovery takes place due to water-advancing over the rock surface that has been previously occupied by oil, water-advancing contact angles have been treated in the literature as defining the reservoir wettability. However, a different consideration evolves if by considering the native state reservoir wherein crude oil migrates into an originally water filled porous rock matrix. This migrating oil could cause water to recede from the pores depending upon the water film stability within the reservoir environment of brine salinity and pH. This raises a question whether the water-receding angle defines the native state reservoir wettability. A similar question arises while producing heavy oils by huff-and-puff steam injection where water from steam condensation would be receding from the reservoir while oil is advancing during the production cycle. The reservoir engineering literature does not appear to address this issue mainly due to the fact that it is generally concerned with moving the oil out of the reservoir by pushing it with injected water. It is essential to consider water-advancing angles as accepted measure of reservoir wettability. Water-advancing contact angle mean the

limiting contact angle obtained after the water has been advanced over the solid surface previously covered by oil [74,75].

2.1.5 Techniques for Measuring Contact Angles

There are five common techniques that can be employed to measure the contact angle namely, Sessile or Static drop method, Wilhelmy plate method, Captive air bubble method, Capillary rise method and Tilting substrate method. These methods have been summarized in Figure 2.5. The chosen technique depends principally on the geometry and location of the surface or coating to be studied. In all the methods, the contact angle (θ) is the angle of the liquid at the interface relative to the plane of the model surface.

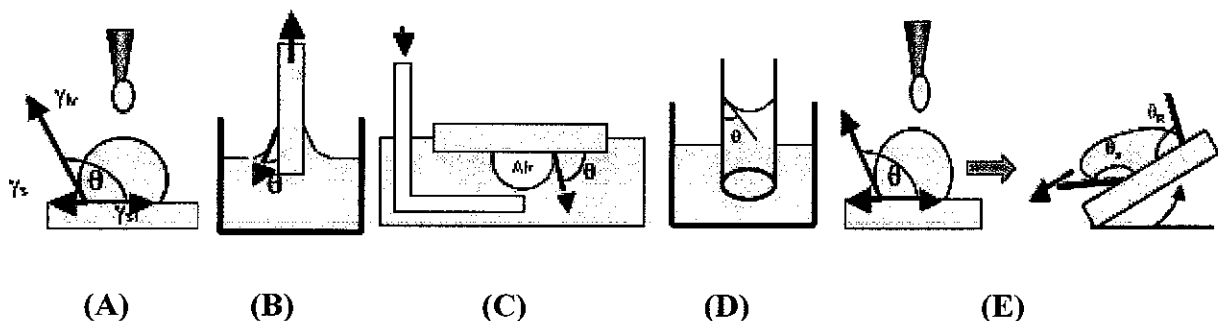


Figure 2.5: Five ways that the contact angle (θ) can be measured. (A.) Sessile or Static drop. (B.) Wilhelmy plate method. (C.) Captive air bubble method. (D.) Capillary rise method. (E.) Tilting substrate method [72].

Dandina N. Rao [72] has reviewed the measurements of dynamic contact angles in solid–liquid–liquid systems at elevated pressures and temperatures. According to this review the dual-drop–dual-crystal (DDDC) is more useful technique as compared to the sessile and modified-sessile drop techniques and can be implemented to obtain reproducible water-advancing and receding contact angles to several reservoir studies. Fig. 2.6 shows the various steps involved in the DDDC technique, which are described below:

1. The experiment should be initiated with two separate drops of crude oil on two parallel crystal surfaces immersed in formation brine at reservoir conditions of temperature up to 200 °C and pressure up to 70 MPa. The two-drops-crystal–brine system is then aged for 1–2 days.

2. The lower crystal is then turned over, when one of the three following events can occur: (i) due to strong oil–rock adhesion the entire drop remains attached to the surface; (ii) due to weaker adhesion a small portion of the oil drop remains on the surface while the rest floats away due to buoyancy; and (iii) due to negligible oil–rock adhesion all of the oil drop detaches from the lower surface.

3. Then the upper surface is lowered to mingle the two drops into one and to squeeze the resulting drop between the two surfaces.

4. The lower crystal is then shifted sideways in small steps until the TPCL begins to move on it, thus enabling the water to advance on to a previously oil occupied area of the lower surface. However, on the other side of the oil drop water recedes as the oil advances.

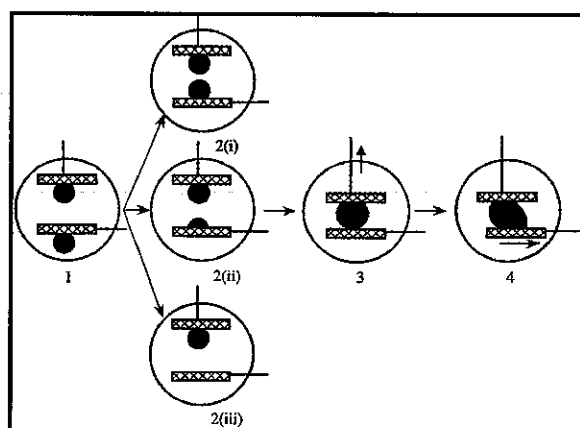


Figure 2.6: Schematic depiction of the dual-drop-dual-crystal contact angle technique [68].

2.1.6 Wettability and Water-advancing Contact Angle Relationship

The DDDC technique has been utilized in several reservoir wettability characterization studies [72]. An oil-wet state wettability is shown in Fig.2.7. All runs were made at respective reservoir pressure and temperature conditions. The highest peaks of contact angle curves represent the maximum angle measured at the initiation of the drop movement and hence are the true water-advancing angles. It can be seen that these peak values are reproducible within 2 - 3°. The DDDC method involves both the upper and lower crystal surfaces in a similar manner to crude oil, hence overcoming the dissimilarity

of the modified sessile drop method as it was. By keeping the drop volume constant throughout the experiment, the problem encountered in the sessile drop technique involving the monotonic increases in contact angle with a decreasing drop volume is resolved. By establishing the adhesion equilibrium on both surfaces, the DDDC technique eliminates the uncertainty of the traditional techniques in advancing water over previously oil occupied area of the solid surface.

An inherent advantage of the DDDC technique is that it accelerates the achievement of the oil–brine–crystal equilibrium during the initial aging of the two drops on the two surfaces because of the destabilizing influence of the buoyancy force on the wetting water film. This result in a considerably shorter run times than the traditional methods. Thus, the DDDC technique resolves the long standing criticisms of the application of the contact angle concept to characterize reservoir wettability, namely, long test duration and poor reproducibility [72].

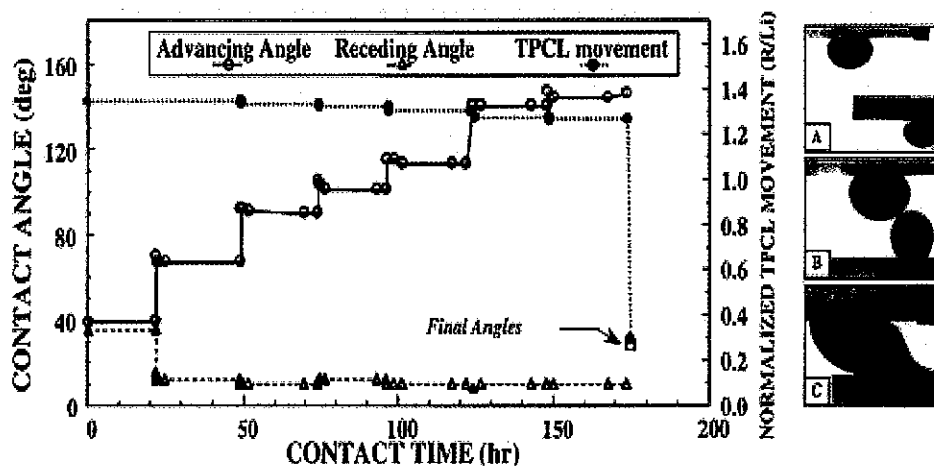


Figure 2.7: Oil-wet case of Beaverhill Lake live oil on calcite under reservoir conditions of 25 MPa, 96 °C and a brine pH of 7.0 [72].

It has been shown in ‘A’ that the measurement was initiated with two separate drops of crude oil on two parallel crystal surfaces, ‘B’ represents when the lower crystal was turned over and ‘C’ depicts when the upper surface was lowered to mingle the two drops into one and to squeeze the resulting drop between the two surfaces, while, TPCL represents three-phase-contact-line as illustrated in steps 1 - 4 previously. Comparison of DDDC results with conventional technique is presented in Table-2.2. Table 2.2 compares

the peak values of advancing angles for the above mentioned cases with those obtained using the modified sessile drop technique. Both the reproducibility of the DDDC results and the contrast with the conventional technique (especially in the intermediate- and oil-wet cases) are quite evident in this table.

Table 2.2: Comparison of DDDC results with conventional technique [72].

Case	DDDC Technique				Conventional Technique
	# 1 (°)	# 2 (°)	# 3 (°)	# 4 (°)	
Water-wet (3600 psi, 205 °F)	50	53	51	50	40
Intermediate-wet (2500 psi, 142 °F)	10	110	108	108	38
Oil-wet (3600 psi, 205 °F)	147	144	144	146	25

2.2 Capillary Pressure

Capillary pressure is an important reservoir property because it directly or indirectly affects other properties such as residual saturations and relative permeabilities. In fluid dynamics, capillary pressure is the difference in pressure across the interface between two immiscible fluids. The pressure difference is proportional to the surface tension, γ , wetting angle of the liquid on the surface of the capillary, θ , and is inversely proportional to the effective radius, r , of the interface as follows:

$$P_c = 2\gamma \cos\theta / r \text{-----} (2.7)$$

The P_c is defined as the capillary pressure:

$$P_c = P_g - P_w \text{-----} (2.8)$$

where, P_g and P_w are the gas and water pressures respectively. The equation for capillary pressure is only valid under capillary equilibrium, which means that there cannot be any flowing phases [77].

Capillary pressure and phase saturation are functions of wettability, pore structure, IFT, rock properties, and saturation history or hysteresis [68]. In oil reservoirs, capillary forces exist because an IFT is present at the interface between two immiscible fluids. It provides a measure of contractile force per unit length. IFT is a function of the attraction of

the molecules across the interface. The curvature of the interface and the pressure difference across the interface can be determined by the minimum in the Gibbs free energy at constant temperature and pressure. This pressure difference is known as the capillary pressure P_c , which can be defined as the difference between the non-wetting phase pressure (P_{nw}) and the wetting phase pressure (P_w). Another commonly used definition in reservoir engineering is the oil pressure minus the water pressure regardless of wettability since wettability is often unknown or poorly known. It is also directly proportional to the IFT, contact angle (θ), and height of rise (h) for the wetting phase in a capillary tube of radius r . Equation 2.7 can be modified as:

$$P_c = P_{nw} - P_w = 2\gamma \cos \theta / r = (\gamma_w - \gamma_{nw}) gh \text{ -----(2.9)}$$

IFT can be reduced by the presence of a suitable surfactant or combination of surfactants. If the IFT becomes zero, the capillary pressure becomes zero and the two fluids become miscible.

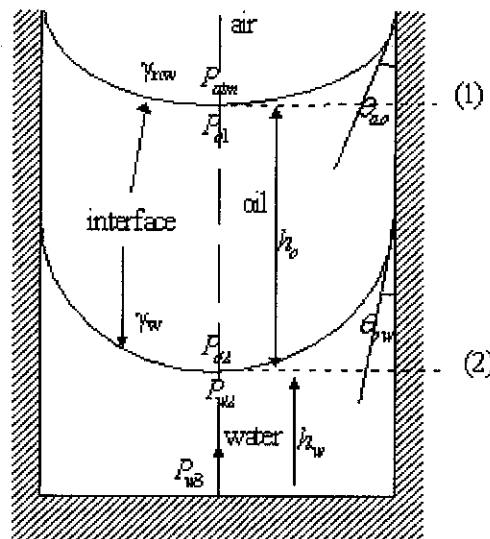


Figure 2.8: Capillary tube containing oil and water exposed to the atmosphere [78].

Fig.2.8 presents the situation of a capillary tube containing oil and water when it was exposed to the atmospheric pressure. Oil and water phases are termed as 1 and 2, where γ_w and γ_{nw} presents IFT at oil-water and air-oil interface respectively. Schematic representation of the role of capillary pores in trapping the oil is explained in Fig.2.9.

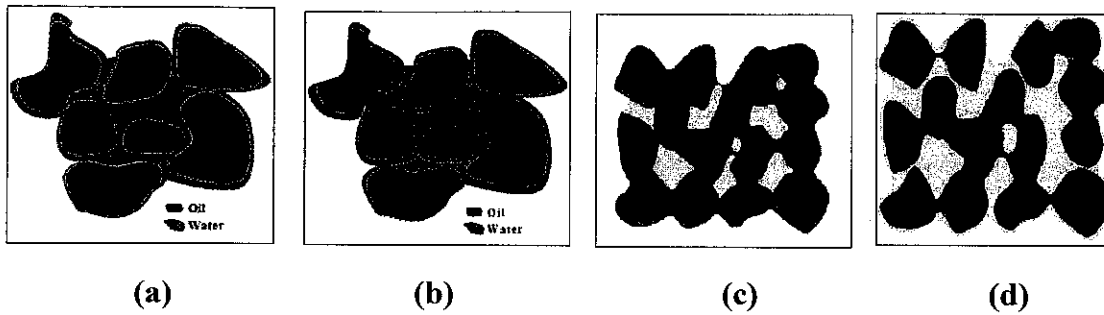


Figure 2.9: (a) Schematic of pore cross-section in a water-wet porous media (grains rocks is surrounded by thin film of brine and are not contacted by oil). (b) Schematic of pore cross-section in an oil-wet porous media (grains are surrounded by thin film of oil and are not contacted by water). (c) In larger pores, the water film ruptures, and oil and rock in direct contact, locally altering wettability to preferentially oil-wet. (d) In smaller pores, the water film covers the grain surfaces completely, thus maintaining those grains water-wet [79].

An oil-wet capillary pressure curve for both drainage and imbibition processes is shown in Figure 2.10 [80]. In a drainage process, the non-wetting phase displaces the wetting phase. In addition, the non-wetting phase pressure must exceed the capillary entry pressure (P_d) in order to displace the wetting phase and enters a pore. During a capillary imbibition, the wetting phase displaces the non-wetting phase. The two capillary pressure curves are different due to hysteresis. The hysteresis is caused by the capillary trapping of the non-wetting phase when it is displaced by the wetting phase [81].

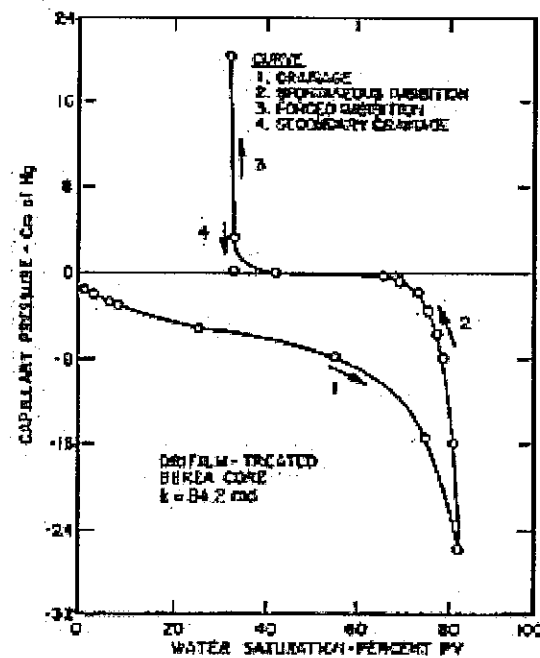


Figure 2.10: Capillary pressure curve for an oil-wet core [80].

2.3 Relative Permeability

Relative permeability is a dimensionless term devised to adapt the Darcy equation to multiphase flow conditions. Relative permeability is the ratio of effective permeability of a particular fluid at a particular saturation to absolute permeability of that fluid at total saturation. If a single fluid is present in a rock, its relative permeability is 1.0. Calculation of relative permeability allows a comparison of the different abilities of fluids to flow in the presence of each other, since the presence of more than one fluid generally inhibits flow. There is evidence that relative permeability may be a function of many more parameters other than fluid saturation [79]. Temperature, flow velocity, saturation history, wettability changes and the mechanical and chemical behaviors of the matrix material may all contribute in changing the functional dependence of the relative permeability on saturation. The best definition of these dependences is the variation of relative permeability with saturation history; Relative Permeability curves show hysteresis between drainage processes (wetting phase decreasing) and imbibition processes (wetting phase increasing).

There are two basic methods of obtaining relative permeability data: steady state and unsteady state. For the steady state method and a two fluid system, the two phases are injected at a certain volumetric ratio until both the pressure drop across the core, and the composition of the effluent, stabilize. The saturations of the two fluids in the core are then determined, typically by weighing the core or by performing mass balance calculations for each phase. The relative permeability can be calculated from the flow equations. The unsteady state method is based on interpreting an immiscible displacement process. For a two phase system, a core, either in the native state (preserved) or restored to the saturation conditions that exist in the reservoir, is flooded with one of the phases. Typically the flood phase is water or gas since in the reservoir one or the other of these phases is expected to displace oil.

Under a single-phase flow at a Reynolds number less than about 1.0, the volumetric flux ' μ ' of a fluid flowing in a permeable medium follows Darcy's law [82]:

$$u = (-k/\mu) \nabla \Phi \text{ ----- (2.10)}$$

where, μ , k , μ , Φ represents volumetric flux, absolute permeability, viscosity and porosity respectively.

For multiphase flow in permeable media, Darcy's law can be modified by adding a relative permeability (k_{rj}) defined in terms of the effective permeability of each phase j :

$$k_j = k_{rj} k \text{ ----- (2.11)}$$

$$u_j = (k_{rj}k/\mu_j) \nabla \Phi_j \text{ ----- (2.12)}$$

Under two-phase flow, the relative permeability of phase j is a function of its own saturation. A typical imbibition relative permeability curve for two-phase flow of oil and water is presented in Figure 2.11. The water relative permeability is zero at the residual water saturation (S_{wr}) and extends until it reaches the residual oil saturation (S_{or}) where it is the only flowing phase. At this point the relative permeability is termed as the endpoint water relative permeability. Similarly, the oil relative permeability is zero at S_{or} and extends to S_{wr} where the endpoint oil relative permeability is reached. The shape of the relative permeability curves depends on the pore morphology, wettability, and IFT (or more generally the ratio of forces defined later as the trapping number).

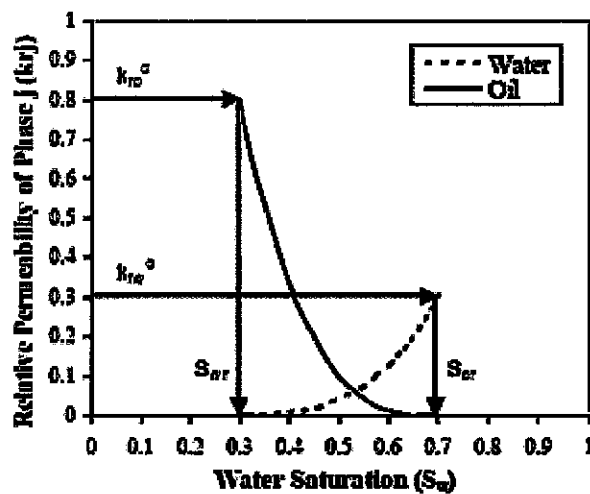


Figure 2.11: Relative permeability curves [69].

2.4 Significance of ASP Flooding

The significance of EOR technologies lie in the promise which they hold for increasing the production from existing oil fields. Generally the increases in reserves from existing fields are considered as less than the resource growth associated with novel successful exploration. Nevertheless, in mature petroleum fields, such as the offshore in particular, the growth of reserves from existing oil fields should contribute more to the industry's continued viability than the discovery of new fields. In other words, thoroughly explored oil fields, better technology, adequate reservoir characterization and effective production from known oil fields should contribute faster than the exploration for new fields.

While several EOR methods have the potential to benefit oil production appreciably, the one that appears to have the greatest potential is ASP flooding. It is one of the most promising economical tertiary recovery methods that can be utilized to obtain additional oil from the domestic reservoirs. It causes the oil to swell, lowering the IFT by reducing the interfacial forces that cause oil to stick to the reservoir rocks initially, lowering oil's viscosity and facilitating its flow towards the production wells. The key criteria for the successful application of the methods using surfactants are minimal loss of surfactants due to adsorption, precipitation elimination, retention by oil the phase and compatibility with the other components. A lot of work has been reported to investigate the chemical flooding methods using conventional polymers and surfactants [3-5,8-21,24,25,28,33-40,48,58,81]. However, very limited work has been carried out using the non-conventional polymers and novel surfactants.

Nowadays ASP has been declared as the most efficient and economical method to recover oil resourcefully [83,84]. Although ASP flooding is an important exception to oil and gas industry to combat the way in which exploration currently dominates towards the new additions to the reserves. However, only the utilization of ASP technology is not an effective way to overcome this difficulty. Designing of an ASP project and conducting the reservoir analyses needed for successful operation requires expertise not only to utilize but also to synthesize the necessary chemicals and materials, computational models, and

laboratory facilities at indigenous level. Small producers face special problems in this regard, because they do not have ready access to the expertise needed for reservoir characterization and proper project design.

In order to set the context for the proper evaluation and implementation of technology, it is crucial to know about the work reported by the researchers previously. Prior to the development of experimental portion for this project the relevant literature was searched and critically reviewed.

2.5 Synergism and Antagonism

Synergism is known as an interaction of two or more elements where the total effect of the elements is greater than the sum of their individual effects and antagonism is the involvement of multiple agents to reduce their overall effect. Regarding a mixture, synergism implies that a property of a mixture is more pronounced than that attainable with any component of the mixture individually. For example, the volume of a mixture may be greater than the sum of the individual volumes that comprise it. Synergism may take place when two or more surfactants are mixed, resulting in a reduced surface tension. Synergism between different surfactant species is usually observed in the formation of mixed micelles.

Zhongkui *et al.* [85] have reported the Dynamic Interfacial Tension (DIFT) behavior of the novel surfactant solutions and Daqing crude oil. According to their findings the added surfactant, ionized and unionized acid can be adsorbed simultaneously onto the interface, causing a reduction in DIFT values. Addition of sodium chloride has an effect on DIFT behavior of crude oil and surfactant flooding systems by affecting surface-active species' absorption behavior onto interface and the distribution between oil and water phases. With the increase of salinity, the required optimum surfactant concentrations were found to be increased. They have concluded that both synergism and antagonism exist between the added surfactant and inorganic salt (also between surfactant and alkali) in lowering DIFT. Towards the stronger lipophilic surfactant, antagonism is dominant, but synergism is the dominant status if lipophilicity is weak. DIFT curves between Alkyl Methyl naphthalene Sulfonate Surfactant (AMNS) solutions and Daqing crude oil have

been reported to take on a “V-shape” as presented in Fig. 2.12. The effects of salinity on the DIT between Dec-MNS surfactant flooding solutions and Daqing crude oil at the 0.6 mass% of alkalinity and various surfactant concentrations have been shown in Fig. 2.12. DIT can reach ultralow at the 2.0–5.0 mass% of NaCl ranges and the three surfactant concentrations. There exists an optimum salinity range of 2.0–5.0 mass%, at which DIT_{min} is the lowest. Especially the 4.0–5.0 mass% of salinity, the DIT can maintain very low value in a long time. It can also be seen that with increases of time, DIT decreases first, and reach the lowest DIT at t_{min} , and then increases [85]. The significance of V shape curve lies in the fact that it provides the solid information about the optimization parameters (alkalinity, salinity, time, etc) required for all the three regions of the curve namely pre, optimal and post. Although various oilfields have diverse nature but through changing the parameters flooding systems like surfactant concentration, alkalinity and salinity, the shape of the “V” curves can be changed according to the particular requirements. Therefore by varying the parameters of flooding systems the demands of minimum DIFT for crude oil in different oil fields can be achieved.

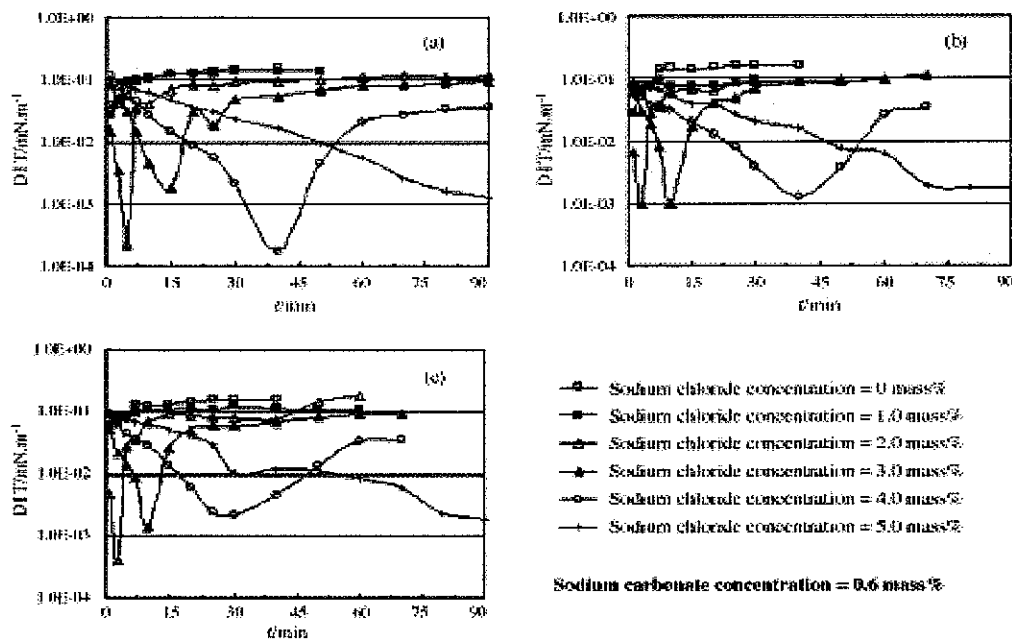


Figure 2.12: Effect of salinity on DIT behaviors (a, b and c are for 0.004, 0.006 and 0.008 mass% of surfactant concentrations, respectively) [85].

Zhongkui *et al.* [86] have also investigated that Alkyl Methylnaphthalene Sulfonate Surfactants (AMNS) can be utilized for EOR applications. The surface tensions of various

surfactant aqueous solutions and the DIFT between the crude oil from Shengli oil field of China and the solution of surfactants, a series of single-component AMNS including various lengths of alkyl chains (hexyl, octyl, decyl, dodecyl and tetradecyl) were estimated. It was observed that the tested surfactant possess great capability and efficiency in lowering the solution surface tension. The CMCs were: $6.1 - 0.018 \times 10^{-3} \text{ mol L}^{-1}$, and the surface tensions at CMC, γ_{CMC} were: $28.27 - 35.06 \text{ mNm}^{-1}$. It was also found that the added surfactants are greatly effective in reducing the IFTs and can reduce the tensions of oil–water interface to ultra-low, even 10^{-6} mNm^{-1} at very low surfactant concentration without alkali. However, the addition of sodium chloride results in an increased effectiveness of surfactant in reducing IFT and shows that there exists both synergism and antagonism effects between the surfactant and inorganic salts. All of the surfactants, except for hexyl methylnaphthalene sulfonate, can reduce the IFT to ultra-low at an optimum surfactant concentration and salinity. Especially Tetradec-MNS surfactant was most efficient in lowering IFT between oil and water without alkaline and the other additives at a 0.002 mass % of surfactant concentration. Both chromatogram separation of flooding and breakage of stratum were avoided effectively, in addition to the less expensive cost for EOR, and therefore they were declared as a good candidate for EOR applications.

Rosen *et al* [4] have reported the effectiveness of synergism between surfactant mixtures. IFT between alkanes and several individual surfactants and their mixtures using three kinds of alkyl hydrocarbons: decane, dodecane, and tetradecane. For individual and mixed surfactant systems, CMCs and areas per molecule at the hydrocarbon-aqueous solution interface were calculated. Ultra-low IFT in the range of 10^{-3} mN/m can be obtained at surfactant concentrations below 0.05 wt % and even at concentrations below 0.01 wt %, when mixtures of certain surfactants are used at proper ratios. Surfactants with branched-chain alkyl groups show a much better IFT reduction effectiveness than those with straight chain alkyl groups. Fig.2.13 presents IFT versus surfactant concentration (wt %) for the Aerosol TR/OT mixtures at various weight ratios. From the data, it is apparent that the Aerosol TR/OT mixtures, due to synergism, can reach ultralow values at surfactant concentrations below 0.06% [4]. By utilizing the concept of synergism between various

surfactant systems their required quantities for EOR applications can be decreased to a large extent making the process economically feasible.

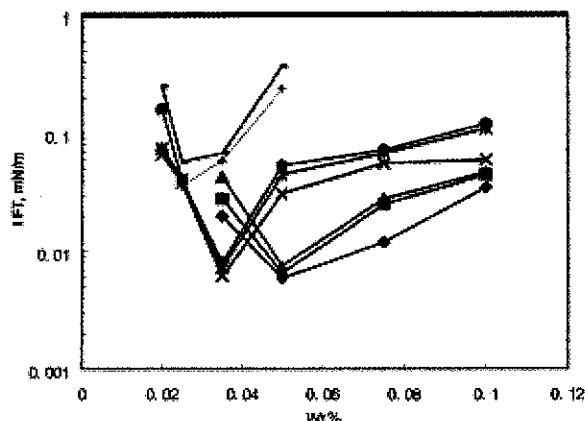


Figure 2.13: IFT vs. wt% of the mixtures of Aerosol TR and Aerosol OT in formation water at 45 °C at various TR/OT weight ratios: (◆) 1:4-decane; (■) 1:4-dodecane; (2) 1:4-tetradecane; (▲) 1:8-decane; (*) 1:8-dodecane; (●) 1:8-tetradecane; (+) 1:20-decane; (-) 1:20-tetradecane [4].

El-Batanoney, *et al* [87] depicted the effect of mixed surfactants on enhancing oil recovery. They have reported that mixed surfactants can lead to the formation of micelles with different structures (mixed micelles). It was pertained to maximize IFT reduction *via* surfactant pairs. In this respect, four types of fatty acid amides based on lauric, myristic, palmitic, and stearic acids were blended with dodecyl benzene sulfonic acid at a molar ratio of 4:1 and designated as A₁, A₂, A₃, and A₄, respectively. The IFT was measured for each blend at different concentrations using Badri crude oil. The most potent formula (A₄) was evaluated for EOR applications. The IFT was monitored in the presence of different electrolyte concentrations with different crude oils at different temperatures. Finally several runs were devoted to study the displacement of Badri crude oil by A₄ surfactant solution using different slug sizes of 10, 20, and 40% of pore volume (PV). The obtained results have revealed that Badri crude oil gave ultra-low IFT at lowest surfactant concentration and 0.5% of NaCl. The enhanced recovery factor at a slug size of 20% PV was 83% of OOIP compared with 59% in case of conventional waterflood.

Qiang *et al.* [88] has reported the surfactant enhanced alkaline flooding for Western Canadian heavy oil recovery. For heavy oil reservoirs (with oil viscosities ranging from 1000 to more than 10,000 mPa s), primary production and waterflooding can only recover

5–10% of Initial Oil in Place (IOIP) due to the unfavorable mobility ratio between water phase and oil phase. If heavy oil is dispersed in formation brine by a chemical injection, the mobility of oil can be greatly improved. In this study, sandpack flood tests were conducted for a heavy oil sample with a viscosity of 1800mPas at 22 °C. The heavy oil was emulsified and entrained in formation brine by AS flooding and then produced out of the core. The results of sandpack flood tests showed that the tertiary oil recovery could reach 24% IOIP by injecting a 0.5 pore volume (PV) of a chemical slug. The tertiary oil recovery did not decrease with the sandpack length. The experimental results showed that the formation of an oil-in-water (O/W) emulsion and an oil bank was necessary to improve the heavy oil recovery in sandpack flood tests. This is viable by injecting a chemical slug containing Na_2CO_3 , NaOH, and a very dilute surfactant. Na_2CO_3 /surfactant had a synergistic enhancement in lowering IFT, leading to the formation of O/W emulsion. The addition of NaOH can accelerate the neutralization of organic acids in oil in sandpack flood tests so that the emulsified oil accumulated to produce an oil bank. When an oil bank was generated, the pressure drop along the sandpack was found to be responding significantly.

Qiang *et al.* [16] has also concluded that the emulsification and entrainment of crude oil into displacing water is one of the mechanisms of alkaline flooding for conventional oil. If this mechanism is applied in heavy oil reservoirs, the flow of viscous oils and subsequently the oil recovery can be greatly improved. The formation brine of heavy oil reservoirs usually has a high salinity and high content of multiple cations, making the in-situ emulsification of heavy oil a great challenge. A heavy oil of 14° API was used to study the mechanism of emulsification of heavy oils in brine under slight interfacial disturbance. Emulsification tests and interfacial measurements were carried out to screen alkalis and surfactant additives for emulsifying the oil in the diluted formation brine. The obtained results indicated that if only alkali or only surfactant is added into the brine, emulsification of the oil in brine cannot be triggered. When alkali (Na_2CO_3) and a very dilute surfactant are used together, the oil can be easily emulsified. The synergy between alkali and surfactant in emulsifying the heavy oil in brine was investigated by measuring the DIFT and zeta-potential of emulsions. Zeta-potential of emulsion refers to the electrostatic potential generated by the accumulation of ions at the surface of a colloidal

particle. It was found that the interaction of added surfactant and in-situ surfactant from the reaction of alkali and organic acids in oil can significantly reduce the IFT between oil and water and increase the surface charge density of emulsions. The synergistic enhancement between alkali and surfactant is the key mechanism of emulsifying heavy oils in brine under slight interfacial disturbance.

2.6 Significance of Ethoxylation Degree

Fabiola *et al.* [89] studied the adsorption of surfactants from aqueous solutions in porous media. Loss of surfactants due to adsorption on the reservoir rocks is expected to impair the effectiveness of the injected chemical slurry which was intended to reduce oil-water IFT. Two nonionic surfactants with different ethoxylation degrees were investigated, ENP95 with an ethoxylation degree 9.5 and ENP150 with an ethoxylation degree 15. The experiments were carried out in a surfactant flooding apparatus, with a pressure gradient of 30 psi. The concentrations of the injected solutions were 30% above the critical micelle concentration, to assure micelle formation. The results from the flow experiments of surfactant solutions in porous media showed that the adsorption extent was higher for ENP95 than for ENP150 because the former surfactant has a smaller ethoxylation degree, and hence, a smaller polar part. The variation of surface tension with surfactant concentration, for ENP95 and ENP150, is shown in Fig 2.14. The break in the curves corresponds to the CMC. It can be seen that ENP150 has a higher CMC than ENP95, because it has a larger polar chain, i.e. higher ethoxylation degree and, consequently, higher solubility in the aqueous phase. Therefore, a higher concentration of ENP150 than ENP95 is required in order to form micelles [84]. Generally, for nonionic surfactants, polyoxyethylene (POE) polar chains possessing a typical size well above the alkyl chain dimensions can fill an extended polar corona. An average volume of interaction per polar chain must replace the average surface per ionic head during the transfer of a POE chain inside this polar corona. In EOR applications the concentration of surfactants must be below the CMCs so it is of great significance to ascertain the degree of ethoxylation.

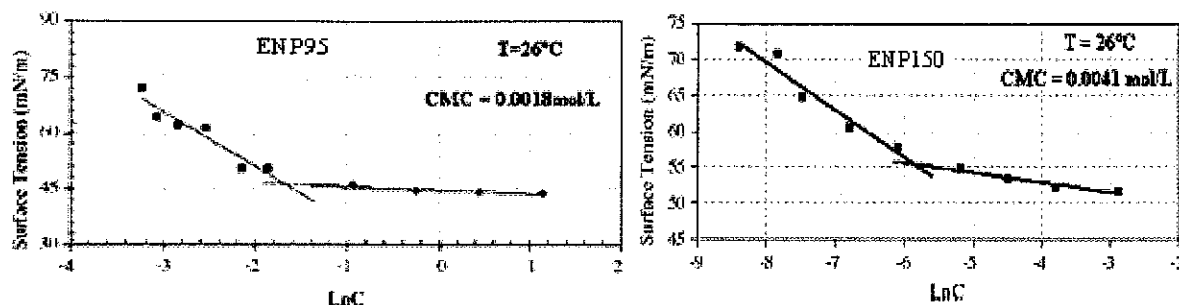


Figure 2.14: Determination of the CMC for surfactant ENP95 and ENP150 [88].

Nedjhioui *et al.* [90] carried out the determination of micellar system behavior in the presence of salt and water-soluble polymers using the phase diagram technique. The use of micellar systems has been growing rapidly during the last few years because of their important and multifarious applications in practical situations. The principal economic interest of microemulsions is focused on EOR but they have also significant applications in pharmaceutical preparations, cosmetics, painting and products for engine lubrication. The effect of varying the compositions of anionic surfactants (α -olefin sulfonates) and the presence of a water-soluble charged polymer (Xanthan gum) and an uncharged polymer [poly (ethylene glycol)] on the phase behavior of pseudo- ternary systems of water-oil surfactants were investigated. Several domains were observed when the composition of surfactants and cosurfactants (e.g., pentanol) in a mixture was varied. The appearance of these domains in the phase diagram has been attributed to the formation of different Winsor systems. Winsor systems depend upon a well-known classification of microemulsions given by Winsor [91] as follows: **Type I:** the surfactant is preferentially soluble in water and oil-in-water (o/w) microemulsions form (Winsor I). The surfactant-rich water phase coexists with the oil phase where surfactant is only present as monomers at small concentration. **Type II:** the surfactant is mainly in the oil phase and water-in-oil (w/o) microemulsions form. The surfactant-rich oil phase coexists with the surfactant-poor aqueous phase (Winsor II). **Type III:** a three-phase system where a surfactant-rich middle-phase coexists with both excess water and oil surfactant-poor phases (Winsor III or middle-phase microemulsion). **Type IV:** a single-phase (isotropic) micellar solution, that forms upon addition of a sufficient quantity of amphiphile (surfactant plus alcohol). Winsor types of phase behavior for surfactant-oil-water emulsions are explained in Fig 2.15.

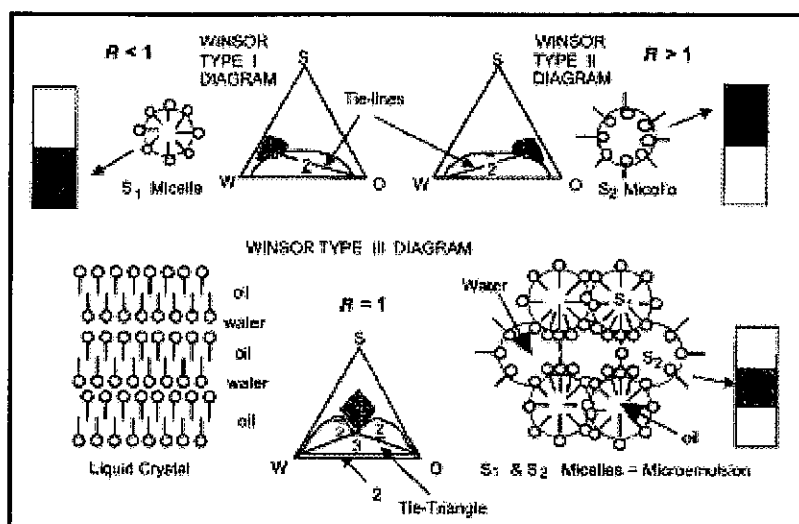


Figure 2.15: The three types of phase behavior for surfactant (S)–oil (O)–water (W) systems according to Winsor: shading indicates the surfactant-rich phase [91].

To interpret the different cases of phase behavior, Winsor has introduced the following ratio of interactions (R) between the surfactant, oil, and water phases:

$$R = A_{CO}/A_{CW} \text{ ----- (2.13)}$$

where, A_{CO} indicates the interaction between the surfactant adsorbed at the interface and the oil phase per unit area of interface, and where A_{CW} does likewise for the water phase. In the simplified form, the Winsor R ratio is a handy tool to interpret the phase behavior changes. By definition, $R = 1$ when a middle-phase microemulsion contains equal volumes of oil and water (the tie triangle shown in Fig. 2.15). When the physicochemical formulation changes, either because of a change in the nature of one of the three components or because of a change in temperature, salinity, or pressure, at least one of the interactions is likely to change. For instance, if the aqueous-phase salinity (electrolyte concentration) increases, the interaction A_{CW} will decrease and R will increase, resulting in an uptake of oil by the middle phase. Hence, a change in R from $R < 1$ to $R > 1$, or vice versa, will produce a change in diagram type, which is easily detectable through a change in the phase behavior.

Zhang *et al.* [92] has highlighted the wettability alteration and spontaneous imbibition in oil-wet carbonate formations. In their study AS flooding was widely tested for its ability to improve oil recovery. The effect of electrolyte-, surfactant concentration and water/oil ratio on wettability, phase behavior, and displacement from a narrow gap was elaborated. It was reported that the wettability of calcite can be altered from about intermediate-wet to preferentially water-wet with alkaline/surfactant systems. The adsorption of anionic surfactant can be significantly reduced in the presence of sodium carbonate.

Somasundaran P. and L. Zhang [10] have shown the adsorption of surfactants on minerals for wettability control in improved oil recovery processes. Chemical-flooding schemes for recovering residual oil have been in general less than satisfactory due to loss of chemicals by adsorption on reservoir rocks, precipitation, and resultant changes in rock wettability. Adsorption and wettability changes can be determined mainly by the chemical structure and mixture of the surfactants, surface properties of the rock, composition of the oil and reservoir fluids, nature of the polymers added and solution conditions such as salinity, pH and temperature. The mineralogical composition of reservoir rocks plays an important role in determining interactions between reservoir minerals and externally added reagents (surfactants/polymers) and their effects on solid-liquid interfacial properties such as surface charge and wettability. Some of the reservoir minerals can be sparingly soluble causing precipitation and changes in wettability as well as drastic depletion of surfactants/polymers. Most importantly, the effect of surfactants on wettability depends not only how much is adsorbed but also on how they adsorb. A water-wet rock surface that is beneficial for displacement of oil can be obtained by manipulating the orientation of the adsorbed layers. New surfactants are promising for EOR applications because they are not only capable of tolerating harsh conditions created by extremes of pH, temperature or inorganics but can also interact favorably with inorganics and polymers. In this regard, sugar based surfactants and pyrrolidones are getting attention, as they are also biodegradable. In many cases, mixed surfactants perform much better than single surfactants due to synergetic effects and ability to alleviate precipitation. Also, addition of inorganics such as silicates, phosphates and carbonates and polymers such as lignins can be

used to control the adsorption and the wettability. In this study, use of specialty surfactants and their mixtures was discussed along with the explanation of involved mechanisms.

Rui Zhang and P. Somasundaran [93] have also reviewed the adsorption of surfactants and their mixtures at solid/solution interfaces. Surfactants and their mixtures can drastically change the interfacial properties and hence are used in many industrial processes such as dispersion/flocculation, flotation, emulsification, corrosion inhibition, cosmetics, drug delivery, chemical, mechanical polishing, EOR and nanolithography. A review of studies on adsorption of single surfactant as well as mixtures of various types (anionic–cationic, anionic–nonionic, cationic–nonionic, cationic–zwitterionic and nonionic–nonionic) was presented along with the description of involved mechanisms. Obtained results using various techniques like zeta potential, flotation, AFM, specular neutron reflectivity, small angle neutron scattering, fluorescence, ESR, Raman spectroscopy, ellipsometry, HPLC and ATR-IR were reviewed along with those from traditional techniques to elucidate the mechanisms of adsorption and particularly to understand synergistic/antagonistic interactions at solution/liquid interfaces and nanostructures of surface aggregates. In addition, adsorption of several mixed surfactant systems was considered due to their industrial relevance. Finally an attempt was presented to derive structure–property relationships to provide a solid foundation for the design and use of surfactant formulations for particular industrial applications.

Wei *et al.* [94] has developed a theoretical model for the understanding of foam flow in a uniform fracture which was verified by experimental data as well. The apparent viscosity was found to be the sum of contributions arising from liquid between bubbles and the resistance to deformation of the interfaces of bubbles passing through the fracture. Apparent viscosity increases with gas fractional flow and is greater for thicker fractures (for a given bubble size), indicating that foam can divert flow from thicker to thinner fractures. This diversion effect was confirmed experimentally and modeled using the above theory for each individual fracture. The amount of surfactant solution required to sweep a heterogeneous fracture system was decreasing greatly with increasing gas fractional flow owing to the diversion effect and to the need for less liquid to occupy a given volume when foam was used.

Tayfun Babadagli [95] has evaluated the critical parameters in oil recovery from fractured chalks by surfactant injection. Parameters affecting the oil recovery by surfactant injection such as IFT, surfactant type, concentration and CMC, solubility characteristics of surfactants and initial water in naturally fractured chalky reservoirs were examined. Both viscous (forced imbibition) and capillary displacement (spontaneous imbibition) experiments have been reported, as they could be possible recovery mechanisms. To identify the importance of existing water phase, some surfactant injection experiments were performed after a total waterflood. In primary surfactant recovery (forced imbibition into a virgin core), IFT plays a major role. For the secondary surfactant injection (forced imbibition after a total waterflood), surfactant type, possibly adsorption and IFT are critical. It is worthwhile noting that the assessment of the adsorption effect is speculative however; no measurement and analyses were done in this regard. The effect of the CMC on oil recovery can be pronounced for cationic surfactants especially for the forced imbibition cases. In case of capillary imbibition recovery, the IFT change was not significant for non-ionic surfactants if there is no initial water in the rock. When there is initial water, however, no significant imbibition recovery was observed. This could be attributed to the high solubility of non-ionics in oleic phase. The analyses and observations presented in this study provide surfactant selection criteria for highly or partly fractured chalky oil reservoirs.

2.7 Surfactant's Structure Effects

Jie *et al.* [96] has explained the effects of branching in hexadecylbenzene sulfonate isomers on IFT behavior in oil/alkali systems. Their investigation was concerned with the study of the effect of the molecular structure of surfactant on the reduction of IFT for EOR techniques. The IFT behavior of nonane and crude oil with three hexadecylbenzene sulfonate isomers (with benzene rings located at different positions along the alkyl chains) were investigated. It was found that the IFTs could be reduced to ultra-low values at low alkali concentrations by using a surfactant molecule with a phenyl group located near the center of the alkyl chain. Molecular structures of this kind were considered to be the most ideal for surfactant flooding. Moreover, it was concluded that the transient low IFTs in crude oil/alkali system were caused by the synergistic effects between surfactant and the

active species generated at interface, but surfactant molecules are responsible to play the dominant role at equilibrium.

Shubiao, *et al* [97] presented the IFTs of phenyltetradecane sulfonates for EOR upon the addition of fatty acids. Producing ultra-low IFT is one of the most important mechanisms relating to surfactant flooding for EOR. Most of the crude oils contain organic acids, so it is of great significance to study the effects of fatty acids on the IFT of surfactant systems. The DIFT behavior of three surfactant systems, 1-phenyltetradecane sulfonate (1-PTDS), 3-phenyltetradecane sulfonate (3-PTDS) and 5-phenyltetradecane sulfonate (PTDS), were researched upon the addition of fatty acids to oil phase, *n*-octane. It has shown that the interfacial activity of surfactants and their ability of adsorption into interface control the dynamic interfacial tensions between aqueous and oil phases. The IFTs of 1-phenyltetradecane sulfonate decrease upon the addition of fatty acids, while of 3-phenyltetradecane sulfonate increase or do not change and that of 5-phenyltetradecane sulfonate increase. When mixed at appropriate concentrations and ratios, phenyltetradecane sulfonates and fatty acids could produce synergism for obtaining lower IFTs. These findings may be helpful in accounting for the cause of producing ultra-low IFTs and for preparing formulations of practical application.

2.8 Significance of Hydrophobically Associating Polymers

Taylor K.C and Nasr-el-Din H.A [98] have reviewed the water-soluble hydrophobically associating polymers with particular emphasis on their utilization in IOR. Water-soluble polymers are used in many oilfield operations including drilling, polymer-augmented waterflooding, chemical flooding and profile modification. The role of the polymers in most EOR applications is to increase the viscosity of the aqueous phase. This increase in viscosity can improve sweep efficiency during EOR processes. In drilling fluids, the solution rheology is very important. Shear thinning fluids are desired that can suspend cutting at low shear rates, but offer little resistance to flow at high shear rates. It was reported that these polymers are very similar to conventional polymers used in EOR, except that they have a small number of hydrophobic groups incorporated into the polymer backbone. However, at levels of less than 1mol%, these hydrophobic groups can

significantly change and enhance the polymer performance. These polymers have potential for use in mobility control, drilling fluids and profile modification. This review includes synthesis, characterization, stability, rheology and flow in porous media of associating polymers.

Taylor K.C and Nasr-el-Din H.A [99] have also presented the effect of synthetic surfactants on the interfacial behavior of crude oil/alkali/polymer systems. The effect of synthetic surfactants on the interfacial properties of an alkali/polymer/crude oil system was examined. This system consisted of crude oil, sodium carbonate (a buffered alkali), either of two synthetic surfactants with high salt tolerance (Neodol 25-3S), an anionic surfactant, or Triton X-100, a nonionic surfactant) and a partially hydrolyzed polyacrylamide (Allied Colloids Alcoflood 1175L). The partitioning of the synthetic surfactant Neodol 25-3S into crude oil was greatly enhanced by sodium carbonate. Increasing the oil volume fraction in the presence of sodium carbonate enhances the amount of partitioning, the effect of the surfactant depending on the sodium carbonate concentration. Low (0.1 mass%), intermediate (0.2 mass%) and high (0.5 - 5 mass%) sodium carbonate concentration regions were examined. A linear relationship was reported between IFT and $t^{-1/2}$, where t is interfacial age, both before and after the minimum IFT was reached. This suggests that the dynamic IFT process is diffusion controlled. With decreasing IFT (before the minimum), the slope of IFT versus $t^{-1/2}$ varies linearly with the low-shear Newtonian viscosity of the polymer solutions. From this it can be conclude that the rate controlling step of the diffusion process occurs in the aqueous phase. Diffusion was found to be inversely proportional to the square of the low-shear Newtonian viscosity, μ_n^2 , indicating a stronger effect of viscosity on diffusion than predicted by the Stokes-Einstein equation. With increasing IFT (after the minimum), the slope of IFT versus $t^{-1/2}$ does not vary linearly with the low-shear Newtonian viscosity of the polymer solutions, suggesting that the rate limiting diffusion process occurs in the oil phase.

Chandra S. V and Dandina N. R [100] have described the compositional effects of fluids on spreading, adhesion and wettability in porous media. The interfacial phenomena of spreading and adhesion of fluids on rock surfaces have serious implications because of their impact on production strategy and oil recovery. The effect of brine dilution and

surfactant addition on spreading and adhesion behavior of Yates crude oil on dolomite surfaces has been evaluated. Spreading and adhesion have been characterized through the measurements of oil–water IFT and dynamic (water-advancing and receding) contact angles. The DDDC technique and the Wilhelmy plate technique were used to measure dynamic contact angles. In order to study the effect of brine dilution, Yates reservoir brine was mixed with deionized water (DIW) in various proportions. According to their findings the oil–water IFT initially decreased as the volume percent of brine in the mixture decreased but IFT increased with further dilution of reservoir brine with DIW. A decreasing trend was observed in the behavior of water-advancing contact angle with brine dilution. However, a strange behavior of spreading of crude oil drop against brine on the dolomite surface (with large water-receding contact angles) was reported at certain brine dilutions. The use of surfactants to enhance oil recovery through reduction in IFT is well known in the industry. However, in this study the capability of certain surfactants to alter wettability in addition to reducing IFT was examined. For the Yates reservoir rock-fluids system, an ethoxy alcohol surfactant altered the strongly oil-wet nature (advancing angle of 158°) to water-wet (advancing angle of 39°) at a concentration of 3500 ppm. While the DDDC technique yielded significant changes in wettability due to surfactant addition, the Wilhelmy Plate technique remained insensitive throughout the range of surfactant concentrations. The practical significance of this study is that it has identified two simple modes through surfactant addition and brine dilution to alter wettability to minimize capillary trapping of oil.

2.9 Transportation through Porous Medium

Ma *et al* [101] have evaluated the effectiveness of chemical flooding using heterogeneous sandpack flood test. According to them alkaline flooding appears to be a promising process for enhancing heavy oil recovery after primary or secondary production from the reservoirs where thermal processes are not applicable. However, due to the heterogeneity of the reservoirs, the injected chemical solutions may flow to the producing wells through the high permeable channels and bypass the residual oil, resulting in poor volumetric sweep efficiency. Thus, evaluation of the chemical blends and the injection strategies through laboratory tests with proper heterogeneous physical models can

substantially reduce the risks of field applications. Channelled-sandpack flooding test was designed to simulate the channeling phenomenon of actual heavy oil reservoirs during the chemical flooding process. The channelled-sandpacks were used to re-evaluate the effectiveness of chemical blends screened through the homogeneous sandpack flood tests. It was found that the effectiveness of the best blend obtained through homogeneous sandpack flood tests is significantly reduced in the channelled-sandpack flood tests. It can be demonstrated that use of heterogeneous physical model, rather than the conventional homogeneous sandpack flood tests, to screen the chemical blends is necessary for designing the chemical flooding process in heterogeneous heavy oil reservoirs. Further experiments carried out for the modified blends with the channelled-sandpack flood tests. An optimal chemical blend was determined for certain heterogeneous reservoirs. The optimal chemical blend can selectively block the high permeability zones and improve the sweep efficiency for a particular heterogeneous sandpack, thereby significantly enhancing the tertiary oil recovery. The developed channelled-sandpack flood test facilitates the optimization, design and implementation of chemical flooding and other enhanced heavy oil recovery processes.

Andrea C and Teamrat A.G. [102] have reported on the transport of emulsion in porous media. Emulsions appear in many subsurface applications including bioremediation, surfactant-enhanced remediation and EOR. Modeling emulsion transport in porous media is particularly challenging because the rheological and physical properties of emulsions are different from averages of the components. Current modeling approaches are based on filtration theories, which are not suited to adequately address the pore-scale permeability fluctuations and reduction of absolute permeability that are often encountered during emulsion transport. Continuous time random walk based alternative approach was introduced in this study that captures unique features of emulsion transport. Calculations based on the proposed approach resulted in excellent match with experimental observations of emulsion breakthrough from the literature. Specifically, the new approach explains the slow late-time tailing behavior that could not be fitted using the standard approach. The presented theory also provides an important stepping stone toward a generalized self-consistent modeling of multiphase flow.

Ying Li *et al* [103] have explained the effect of equilibrium and dynamic surface activity of surfactant on foam transport in porous medium. An apparatus containing a visual porous medium plate model and digital video recorder was employed to investigate the transportation of foam stabilized by sodium polyoxyethylene alkyl ether sulfate (AES), sodium dodecyl benzene sulfonate (SDBS) and TritonX-100 in porous medium. The obtained results have indicated that transfiguration and fracture were the main transport manners for foam in the porous medium at high gas and liquid transfusion rate. The increase in probability of transfiguration in foam transport process corresponded to the higher flow impedance. A simple U-shape device was designed to investigate the rigidity of surfactant layer at the gas/liquid interface, and the equilibrium surface tension was assigned to be the key parameter which manifests the rigidity of surfactant interface layer. The dynamic surface tension of different surfactant system has also been measured, and the parameters given by Rosen model might be the measurement of dynamic elasticity of surfactant interface layer. Consanguineous relationship is expected between the equilibrium surface activity or dynamic activity of the surfactants and the transport of the foam in the porous medium.

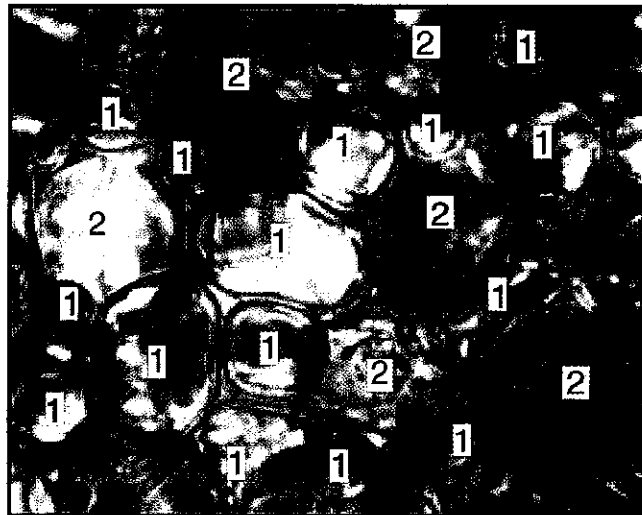


Figure 2.16: The picture of the foam in porous medium. The points labeled 1 represent foam bubble and 2 represent medium [103].

Fig. 2.16 shows a picture of foam in porous medium. Traditional foam production and transportation mechanisms were testified in the long-time investigation, especially in

the process of low gas transfusion rate. The experimental results showed that foam film transfiguration and fracture which consists of membrane disjunction and constrict separation are the main manners for foam transport in the porous medium in the process of high gas and liquid transfusion rate, which might happen more frequently in practical processes.

2.10 Role of Viscoelasticity in EOR

Jirui *et al* [104] have performed the studies in order to treat alkali scale related problems encountered in the ASP flooding pilot area of Daqing Oilfield. The IFT of ASP solutions and the effect of alkalis and surfactants on the viscoelasticity of ASP solutions were measured using tensiometer and rheometer respectively. Macro-coreflood tests were performed using natural cores, 2-D vertically-heterogeneous artificial cores without restraining barriers, and 2-D vertically-heterogeneous artificial cores with restraining barriers. Blind ends' residual oil sweeping tests were performed with simplified blind-end models. The obtained results have indicated that alkali has adverse effect on the viscoelasticity of an ASP solution. A high concentration of alkali can cause the HPAM molecular chains curl up, and can form alkali scales, although it is beneficial to achieve an ultralow IFT. Ultralow IFT has a pronounced effect on the oil recovery of a homogeneous reservoir, while the viscoelasticity of an ASP solution contributes more to the oil recovery of a heterogeneous reservoir. The stronger the homogeneity is, the greater the effect of IFT on the oil recovery; on the contrary, the stronger the heterogeneity is, the greater the effect of viscoelasticity on the oil recovery. Laboratory "co-injection and separated-layer production" experiment also depicted that a reasonable (for example 0.6%) rather than too high an alkali concentration is more beneficial to starting-up layers with medium and low permeability, and washing out the residual oil in the swept layers, and a relatively high viscoelasticity is more beneficial to sweeping the residual oil in blind ends. As far as a heterogeneous reservoir is concerned, ultralow IFT is not a condition for enhancing oil recovery, while the viscoelasticity of an ASP solution is more important to effectively sweeping oil. The capillary number theory is of great practical importance for homogeneous reservoirs, but it has limitations and cannot be readily applied in heterogeneous reservoirs. For example, the trend of capillary numbers versus IFTs

(corresponding to different alkali concentrations), which are based on the theory, does not match with the trend of oil recovery efficiencies. Therefore, for a heterogeneous reservoir, without an ultralow IFT (for example with an IFT of 10^{-2} mN/m), i.e. with a reasonably lower alkali concentration, a satisfying oil recovery can still be achieved as long as the viscoelasticity is high enough. This not only can solve the problems caused by alkali scales, but also can enlarge the selecting range of surfactants and reduce the cost of ASP flooding.

Moran *et al* [105] have discussed the viscoplastic properties of crude oil–water interfaces. The breaking of water-in-crude oil emulsions is a major challenge in the conventional petroleum industry, while oil-in-water emulsions present similar issues in commercial extraction processes. The stability of these emulsions can be attributed to complex rheological properties of the crude oil–water interface. Novel micromechanical techniques were developed for direct measurements of interfacial behavior of emulsion drops. In these techniques, individual emulsion drops were elongated using micropipettes, where one micropipette is shaped into a cantilever for force measurements. As such, the surface behavior of a drop is recorded in stress–strain experiments. In an alternative technique, the extended drop was released from a micropipette, and its natural, tension-driven relaxation was monitored. The surface behavior of bitumen (a heavy crude oil) emulsion drops in aqueous environments, which include dissolved calcium ions and suspended montmorillonite clays, was studied. The plasticity and other surface properties of these bitumen drops were discussed. A simple, lumped-parameter model was proposed to describe the recovery of a bitumen drops to their final non-spherical shapes.

2.11 Effects of Divalent Ions in Surfactant Flooding

Agharazi *et al* [106] have explained the effect of divalent ions on the oil recovery efficacy of petroleum sulfonate based surfactants. The oil recovery tests were conducted in unconsolidated model porous media composed of fine glass particles. It was reported that tertiary recoveries effected by surfactant injection were consistently higher when the brine in the porous medium contained divalent ions. The results were explained by complete or partial pore blockage by precipitates formed when the petroleum sulfonate encounters divalent ions, which results in increased sweep efficiency. This conclusion is corroborated

by the results of the experiments in which a non-surfactant precipitate was formed in the porous medium during the flood.

Qiang, *et al* [107] have evaluated the wettability alteration by magnesium ion binding in heavy oil/brine/chemical/sand systems and analyzed the role of electrostatic forces. Laboratory scale coreflood tests for enhanced heavy oil recovery by alkaline flooding were carried out and it was found that oil recovery was greatly affected by wettability alteration of sand. A heavy oil of 14°API was used to study the effect of the composition of the water phase on wettability alteration in the heavy oil/water/sand system. In micro-slide and micro-model tests, wettability change was observed. The presence of either Na_2CO_3 or Mg^{2+} alone in the water phase was not found to induce wettability alteration. When the water phase contained both Na_2CO_3 and Mg^{2+} , the water-wet sand became preferentially oil-wet by magnesium ion binding. The reduction in zeta-potential value due to the addition of Mg^{2+} into the heavy oil/ Na_2CO_3 solution/sand system confirmed the combination of Mg^{2+} and ionized organic acids at the oil/water interface. In addition, the zeta-potential value of sand in the water phase suggested that Mg^{2+} is also susceptible to be adsorbed on sand surfaces, weakening the electrostatic forces. It can be concluded that the reduction of repulsive electrostatic forces between oil drops and sand surfaces have contributed to the wettability change of the sand from water-wet to more oil-wet.

Peimao, *et al* [108] have reported the wettability alteration and improved oil recovery by spontaneous imbibition of seawater into chalk and evaluated the impact of the potential determining ions Ca^{2+} , Mg^{2+} , and SO_4^{2-} . According to their investigation carbonate wettability is dictated by the surface chemistry related to stability of the water film between the oil phase and the rock surface. It has been verified, both in the field and laboratory, that seawater is an excellent injection fluid to enhance the oil recovery from fractured chalk. The objective of this work was to understand the chemistry involved in improved spontaneous imbibition of seawater into low permeable chalk with poor water wetness. Improved spontaneous imbibition of water will be effective if the wettability of chalk will be altered from oil to water-wet during the production phase. The potential determining ions present in seawater, Mg^{2+} , Ca^{2+} and SO_4^{2-} , have great influence on the

surface charge of chalk, which can modify the wettability during water injection. At higher temperatures, Mg^{2+} can even substitute Ca^{2+} from the chalk surface, and the degree of substitution can be increased with the temperature increase. The interplay between the three potential determining ions: Ca^{2+} , Mg^{2+} and SO_4^{2-} and the chalk surface with the aim to improve the water wetness of biogenic chalk, was investigated from a spontaneous imbibition point of view. To improve water wetness, SO_4^{2-} must act together with either Ca^{2+} or Mg^{2+} . In both cases, the efficiency was found to be increased as the temperature increased. The water wetness of chalk can be improved if some of the carboxylic material previously adsorbed onto the chalk surface is displaced. A chemical mechanism discussing the mutual interaction between the potential determining ions and the chalk surface is presented in Fig. 2.17.

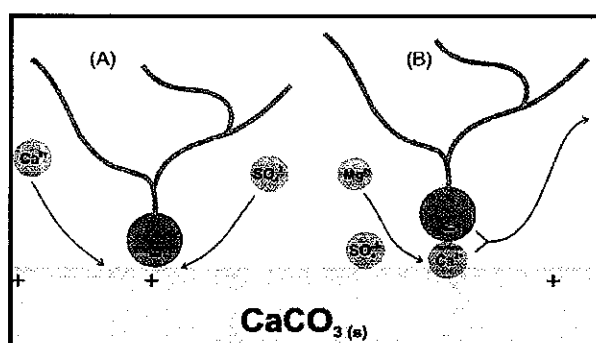


Figure 2.17: Schematic model of the suggested mechanism for the wettability alteration induced by seawater. (A) Proposed mechanism when Ca^{2+} and SO_4^{2-} are active at lower and high temperature. (B) Proposed mechanism when Mg^{2+} and SO_4^{2-} are active at higher temperatures [108].

According to the suggested chemical mechanism for the wettability modification as illustrated in Fig. 2.17, at low and high temperature Ca^{2+} may react with the adsorbed carboxylic group and release it from the surface, Fig. 2.17A. But at high temperature, Mg^{2+} may displace the Ca^{2+} -carboxylate complex, Fig. 2.17B. The fact that the wettability modification using Mg^{2+} and SO_4^{2-} is only active at high temperatures strongly supports the suggested mechanism. It is hard to believe that the small and strongly solvated Mg^{2+} is able to substitute Ca^{2+} in a Ca^{2+} -carboxylate complex by a similar mechanism as suggested in Fig. 2.17A. The Ca^{2+} -carboxylate bond is normally stronger than the Mg^{2+} -carboxylate bond. The suggested mechanisms illustrated in Fig. 2.17, are based on access of injected

water close to the bonding between the carboxylic group and the chalk surface. The active potential determining ions in seawater can only be active through the aqueous phase. However, the carboxylic group, $-\text{COO}-$, being a strong hydrophilic group, can create some water saturation close to the bonding sites at the chalk surface. It is also important to point out that reactivity of the surface of biogenic chalk is much higher than for recrystallized limestone. It is therefore difficult to extend the results obtained for chalk to limestone reservoirs.

2.12 Optimization of a Surfactant Flooding Process

Arne *et al* [109] have presented an optimization study of a surfactant flooding process. As a part of the preparation for a surfactant flooding pilot in a North Sea oil reservoir, several hundred core flood experiments were performed. This paper summarizes the experience obtained from these core floods. The experiments were carried out at temperature of 90 °C, using seawater as the brine, and modified reservoir crude as the oil phase. The purpose of these experiments was to define the surfactant slug design for obtaining a maximum oil recovery per unit surfactant. The core-flood experiments involved variations of critical parameters like surfactant concentration, slug size and microemulsion phase behavior. The core floods are compared not only by the optimum defined as the maximum in the volumetric oil recovery per volume of surfactant injected, but also by several other requirements like: early oil breakthrough, high fractional flow of oil, low pressure buildup and low surfactant retention.

Porzucek *et al* [110] studied the optimal injection strategies (OIS) for surfactant flooding in EOR using an improved phase behavior model and an improved definition of effective salinity. OIS for surfactant/polymer flooding have been calculated using an improved version of a one-dimensional and compositional simulator. This investigation has provided more realistic optimal control policies as compared to previously reported using older version of the simulator. In current simulator a more realistic phase behavior model and an improved definition of the effective salinity variable was utilized. Obtained results have indicated that previous optimization studies consistently overestimated the profit from the process. It was also concluded that previous studies consistently

underestimated the optimal amount of surfactant to inject and overestimated the amount of alcohol needed. However, the trends in optimal surfactant and alcohol control policies are shown to be consistent with the physical property models within the simulator. Also, the improved version of the simulator resulted in an increased sensitivity for anions and calcium controls.

Luis *et al* [111] optimized a methodology of alkaline–surfactant–polymer flooding processes using field scale numerical simulation and multiple surrogates. They have reported that after conventional waterflood processes the residual oil in the reservoir remains as a discontinuous phase in the form of oil drops trapped by capillary forces and is likely to be around 70% of the OOIP. The EOR method so-called ASP flooding has proved to be effective in reducing the oil residual saturation in laboratory experiments and field projects through the reduction of IFT and mobility ratio between oil and water phases. A critical step to make ASP floodings more effective is to find the optimal values of design variables that will maximize a given performance measure (e.g., net present value, cumulative oil recovery) considering a heterogeneous and multiphase petroleum reservoir. Previously reported works using reservoir numerical simulation have been limited to sensitivity analyses at core and field scale levels because the formal optimization problem includes computationally expensive objective function evaluations (field scale numerical simulations). In this work new approach has been proposed which estimates the optimal values for a set of design variables (e.g. slug size and concentration of the chemical agents) to maximize the cumulative oil recovery from a heterogeneous and multiphase petroleum reservoir subject to an ASP flooding. This surrogate-based optimization approach has been shown to be useful in the optimization of computationally expensive simulation-based models in the aerospace, automotive, and oil industries. The existing approach was improved considering two directions: (i) using multiple surrogates for optimization, and (ii) incorporating an adaptive weighted average model of the individual surrogates. The cited approach involves the coupled execution of a global optimization algorithm and fast surrogates (i.e., based on Polynomial Regression, Kriging, Radial Basis Functions and a Weighted Average Model) were constructed from field scale numerical simulation data.

The effectiveness and efficiency of the proposed methodology was demonstrated using a field scale case study.

2.13 Effect of Hydrophilic Polymer on Surfactant Flooding

Svante *et al* [112] have found that the addition of hydrophilic polymers in the range 0 - 10,000 ppm has little effect on surfactant bulk properties. In some cases, added hydrophilic polymer can reduce the saturation value for surfactant adsorption due to competitive adsorption. Surfactant-polymer interactions, for non-associating systems, have little effect on surfactant/polymer core floods. On a larger scale, polymer will of course provide mobility control and a somewhat higher capillary number due to the increased viscosity. It was concluded that the observed effects of polymer on laboratory scale surfactant core floods is due to secondary effects that have little relevance at the reservoir scale. This means that in field applications there is a freedom in the choice of surfactant-polymer combination.

Tor *et al* [113] have presented the effects of polymer on the adsorption of surfactant at the solid/liquid interface related to low tension polymer waterflood (LTPWF) of sandstone oil reservoirs by means of dynamic laboratory experiments. An alkylpropoxyethoxy sulfate was used as surfactant, xanthan and a copolymer of acrylamide and sodium 2-acrylamido-2-methylpropane sulfonate (AN-125) were used as polymers, crude oil and n-heptane were the oils, and synthetic seawater was used for brine. All experiments were conducted at 50°C and 1atm. Long-term adsorption experiments were performed by circulating the chemical solution through clay-containing reservoir cores for several weeks and short-term experiments were conducted by injecting chemical slugs of constant concentration, but different size, through model sandstone cores. Various adsorption regimes of the surfactant were detected at different contact times between the reservoir core material and the circulated chemical solution, and it was observed that xanthan behaves as a sacrificial adsorbate towards the surfactant by decreasing the surfactant adsorption. In the slug experiments, using model cores, xanthan appeared to decrease the surfactant adsorption when using small surfactant slug sizes, but no measurable effect of xanthan or AN-125 on surfactant adsorption was observed for large

sizes. A dynamic reversible adsorption model appeared to predict the propagation of the surfactant slug through the porous medium, but the adsorption level was not fitted.

Alveskoga *et al* [114] have highlighted the influence of surfactant concentration, surfactant adsorption and IFT between oil and aqueous phase on the Amott wettability index and the residual oil saturation during waterflooding. The flooding experiment and Amott wettability tests were performed on 60 core plugs at a temperature of 50°C, with *n*-heptane and 1.5 wt.% NaCl brine with 12 different concentrations of surfactant. The anionic surfactant used in the experiments was *n*-dodecyl-*o*-xylene-sulfonate with a well-known IFT vs. concentration relationship. The core material was Berea Sandstone with an average porosity of 19% and an average permeability of 104 mD. Wettability indices were determined by the standard Amott test involving spontaneous uptake of fluids and forced displacement steps. The Amott wettability index and residual oil saturation vs. surfactant concentration and an adsorption isotherm of the surfactant on Berea sandstone were the main quantities determined. The obtained results have shown that increased surfactant concentration results in a change in wettability from strongly water-wet to weakly oil-wet. The residual oil saturation decreases with increasing surfactant concentration. A dramatic change in wettability from water-wet to neutral and over to oil-wet occurs in a narrow range of low concentrations which coincide with the CMC. In this range the measured adsorption was only approximately 10 % of the maximum value of the adsorption isotherm. However, the higher surfactant adsorption at higher concentrations did not have significant effect on the observed wettability.

Gan-Zuo *et al* [115] have presented an experimental investigation on ASP flooding systems using nature mixed carboxylate. The orthogonal-test-design method was used to determine the optimal formula by phase behavior and transient IFT studies, respectively. The results indicate the major components are cheap, naturally mixed carboxylate SDC (0.5%), alkaline NaHCO₃/Na₂CO₃ weight ratio of 1 (1.0%), and HAPM (1000 mg dm⁻³). In the coreflood experiment, oil recovery was found to be increased by a factor of 25.2 and 26.8% of the OOIP.

Fernando *et al* [116] have reported the modeling of microemulsion phase diagrams from excess Gibbs energy models. Projects on tertiary oil recovery by means of microemulsions have been mainly concerned with, first, the ability of a microemulsion to dissolve oil and water simultaneously and, second, the attainment of very low IFT. Therefore, the design and analyses of chemical flooding processes for EOR must be based on calculations of phase equilibria for these systems, which are composed of water (brine), oil, surfactant and co-previous surfactant term (usually an alcohol). Consequently, the understanding of phase behavior of these systems is of fundamental importance to the development of any surfactant-based chemical flooding process. The purpose of this work was to give a thermodynamic analytical representation of the phase diagram of microemulsion systems similar to those used in EOR. The algorithms presented for the calculation of multiphase liquid equilibria and the methods for the estimation of the excess Gibbs energy model interaction parameters were successfully tested for the representation of experimental multiphase liquid equilibrium data of an oil–brine–surfactant–alcohol model system. In addition, to represent effectively the phase diagram of this system, an empirical expression was introduced into the selected excess Gibbs energy model to account for the specific role of the surfactant in these complex systems. Fig. 2.18 presents the phase diagram of brine–oil–surfactant system.

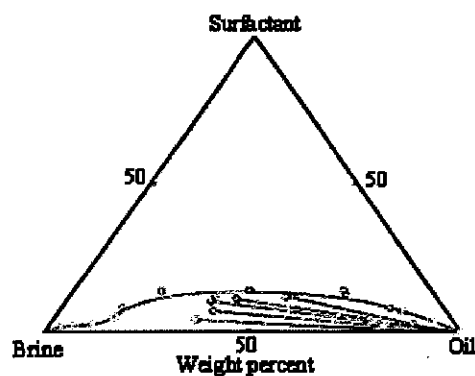


Figure 2.18: Experimental liquid–liquid equilibria phase diagram of the system brine–oil–surfactant at 25 °C. The circles are the experimental results obtained by turbidity titration, which are connected by a full line. The squares are the experimental end points of the tie lines (solid lines) [116].

Shubo *et al* [117] have depicted the effects of ASP on the stability of oil droplets in produced water from ASP flooding. ASP flooding technology has been used successfully in the Daqing oilfield, but the produced water is more difficult to treat than that from waterflooding and polymer flooding. Simulation experiments were conducted to investigate the effects of ASP on the stability of oil droplets in the produced water. Settling experimental results showed that polymer favored oil–water separation when its concentration was less than 1000 mgL^{-1} . Oil concentrations in the water after settling separation was found to be increased with the increase of surfactant concentration, and increased with the increase of NaOH concentration up to 200 mgL^{-1} and then decreased with the further increase of alkaline concentrations. The interfacial properties of oil–water were investigated to find the mechanisms for the stability of oil droplets in produced water from ASP flooding. The synergetic action of surfactant ORS-41 and NaOH was found to greatly influence the IFT of oil and water. ORS-41 and polymer can increase the density of negative electrical charges on the surface of oil droplets and the interfacial elasticity of oil and water. Alkali however can increase the density of negative electrical charges of oil droplets and the interfacial elasticity of oil and water in lower alkaline concentrations, but the effect is reversed in higher alkaline concentrations. On the other hand, the flocculating ability of the polymer also helps small oil droplets to coalesce and form big ones which can be visualized using microscope.

Oslen *et al* [118] declared that ASP flooding can be applied successfully in an oil-wet carbonate reservoir. They have reported the ASP formulations of sodium tripolyphosphate and sodium carbonate along with a low concentration of petroleum sulfonate in order to maintain interfacial activity upon extensive dilution with reservoir brine. According to their findings significant oil recovery was achieved by ASP formulation as compared to alkaline-polymer or polymer formulation. The rock wettability was also altered to less oil-wet surface.

Shawn and Lorenz [119] have investigated mineral-alkaline reactions under dynamic conditions. They have reported that the presence of CO_2 in the reservoir and acid capacity must be neutralized by the injected alkali. It was also observed that alkalis are

responsible to reduce the divalent content of brine which leads to a reduction in degradation of co-injected surfactant.

The effects of the matrix shape factor, wettability, gravity, rock type, oil viscosity, and IFT on the rate of capillary imbibition and development of residual non-wetting phase saturation were studied by Hatiboglua and Babadagli [120]. They have performed the experiments using Berea sandstone and Indiana limestone samples. Cylindrical samples with different shape factors were prepared by cutting the plugs 1/2, 1 and 2 in. in diameter and 2, 4, and 6 in. in length. All sides of the cores were coated with epoxy except one end to ensure counter-current interaction. Static imbibition experiments were conducted on vertically and laterally situated samples to incorporate the effect of gravity where the imbibition took place upward and lateral directions, respectively. Brine-kerosene, brine-mineral oil and surfactant solution-mineral oil pairs were used as fluids. The rate of imbibition was evaluated for different matrix size, shape factor, wetting/non-wetting phase types and IFT. Conditions at which the shape factor controls the residual oil development were reported. It was observed that the residual oil after capillary imbibition can be influenced by the matrix shape factor for the vertically positioned samples (unlike horizontal samples). In the low IFT experiments, surfactant was found to play a strong role on the rate of imbibition and the development of residual oil saturation.

Tayfun Babadagli and Yaman Boluk [121] have elaborated the oil recovery performances of surfactant solutions by capillary imbibition. They have reported the role of critical parameters in oil recovery by capillary imbibition of surfactant solutions. Experiments were conducted on sandstone and carbonate samples using different oil and various surfactants. During the evaluation IFT, surfactant type, solubility characteristics of surfactants, rock type, initial water (pre-wet rock), and surfactant concentration were considered. In addition to these, a new technique was adopted to facilitate the surfactant screening process. This technique is based on assigning inorganic and organic property values and plotting organic conception diagrams (OCD) for surfactants. OCD defines the property of a compound in terms of physical chemistry in such a way that the property that depends much on the Vander Waals force is called "organic" and the one that depends much on electric affinity is called as "inorganic." Correlations between the capillary

imbibition recovery performance and the properties of surfactant and oil (organic value (OV), inorganic value (IV), and IFT of surfactant solutions, oil viscosity, and surfactant type) were obtained. The summarized correlations may be useful in selecting the proper surfactant for IOR as well as identifying the effects of surfactant properties on the capillary imbibition performance.

Wang *et al* [122] highlighted the application of polymeric systems in CEOR. Water breakthrough is a common technical problem during the course of waterflooding in an oil field. Polymer solutions are widely applied to resolve the water-channeling problem in a deep formation. In practice, polymers being used in deep formation treatment either to form a gel blockage and plug high permeability zones in-situ, or to act as mobility control agents and increase the viscosity of injected fluids. However, for an in-depth profile modification operation, a polymer solution has to be injected at a relatively high concentration so as to maximize its penetration. Thus such a treatment may become uneconomical. On the other hand, a traditional polymer flooding may become ineffective mainly due to the viscosity loss caused by mechanical and chemical degradations. In this study a novel polymer solution, weak gelling system, has been evaluated for CEOR applications. The weak gel system has relatively low strength but can still be cross-linked in the reservoir formation. In comparison with a conventional conformance control agent, this weak gel can form a blockage in a deeper formation due to its mobile feature. The EOR mechanisms of the weak gel system were described in detail. In addition to the effects of temperature, concentration, and pH value on gelation time, the rheological property, gelation range, and gel strength are also reported. The core-flood test results not only provide experimental evidence that the weak gel improves injection profile and increases sweep efficiency but also show enhancement in oil recovery. Furthermore, the pilot tests have been performed in Gudong and Gudao oil fields in China since 1992. It has been found that this weak gel system can significantly enhance oil recovery and effectively reduce water-cut.

Islam, M. R. [123] has discussed about the emerging technologies in EOR. Due to low oil prices, many of the conventional EOR techniques have become unattractive. The biggest challenge for any novel recovery technique is to be able to produce under attractive

economic conditions. Also, any novel EOR technique should be able to address marginal reservoirs, such as heavy oil reservoirs, reservoirs with bottom water, and others, because these reservoirs contain the most proven reserves. In this article economically attractive EOR techniques were discussed. Many of these techniques are in the areas of heavy oil and tar sand reservoirs. Studies have also been presented for some of the most promising emerging technologies, such as electromagnetic oil recovery, co-surfactant enhanced chemical processes, microbial EOR, low pressure gas foam injection, and others. The use of horizontal wells is also elaborated in order to improve the effectiveness of various EOR schemes.

Ayirala *et al* [124] has evaluated the beneficial effects of wettability altering surfactants in oil-wet fractured reservoirs. In fractured reservoirs, an effective matrix-fracture mass transfer is required for oil recovery. Surfactants have long been considered for EOR schemes, mainly in terms of their ability to reduce oil–water IFT and wettability alteration. These surfactants are more effective when the fractured formations are water-wet, where capillary imbibition of surfactants from the fracture into the matrix contributes to oil recovery. However, the ability of surfactants to alter wettability remains to be explored and is not fully exploited. In order to explain the wettability alteration DDDC contact angle experiments have been conducted using fractured Yates dolomite reservoir fluids, two types of surfactants (nonionic and anionic) and dolomite rock substrates. A new experimental procedure was developed in which crude oil was equilibrated with reservoir brine and exposed to surfactant to simulate the matrix-fracture interactions in fractured reservoirs. This procedure enabled the measurements of dynamic contact angles and oil–water IFTs, in addition to providing the visual observations of the dynamic behavior of crude oil trapped in the rock matrix as it encounters the diffusing surfactants from the fractures. Both the measurements and visual observations indicate wettability alterations of the matrix surface from more oil-wet to less oil-wet or intermediate wet by the surfactants. This study is of practical importance to oil-wet fractured formations where surfactants-induced wettability alterations can result in significant oil recovery enhancements.

Dag C. Standnes and Tor Austad [125] premeditated the wettability alteration in carbonates using low-cost ammonium surfactants based on bio-derivatives from the coconut palm. Fractured oil-wet carbonate reservoirs are often located at low temperatures and pressures, and oil recovery by pure pressure depletion is usually low. IOR is having tremendous potential. An IOR method is to change the wettability of the reservoir towards more water-wet conditions so that water can spontaneously imbibe into the matrix blocks and expel the oil. This research was focused on cheap commercial available surfactants of the type $R-N(CH_3)_3Cl$ prepared from fatty acids from the coconut palm. These surfactants are able to modify the carbonates from oil-wet to water-wet when added to the injection water. Two products that were tested include: Arquad MC-50 (Arquad) containing a mixture with R-/C12 and C14, and Dodigen 5462 (Dodigen) with the composition R-C12, C14, C16, and C18. Imbibition experiments using low-permeability (3 mD) outcrop chalk cores and 100 -/350 mD dolomite reservoir cores at 40 and 70 °C were performed, both with and without initial water. In general, Arquad was found to be more efficient than Dodigen regarding imbibition rate. Very high oil recovery rates were observed, approximately 70 % OOIP for the chalk cores and 90 % of OOIP for the dolomite cores. The imbibition mechanism was discussed in relation to the influence of capillary and gravity forces, and the difference in behavior of the two surfactant systems was discussed in terms of CMC and oil-water IFT.

Prior to the use of CEOR techniques due attention should be given to the fines migration which otherwise can cause the permeability damage due to clay swelling, disintegration and migration into the oil producing formations. Generally, non-ionic partially hydrolysable PAM based polymers are capable of stabilizing clays by orienting themselves on the reservoir clays in a substantially monomolecular layer in such a manner that it will continue to stabilize the reservoir clays but will not substantially react with the injected chemicals to form permeability damaging precipitates or to decompose thereby reducing its clay stabilization effectiveness. Under controlled fines migration and wettability alteration induced by the surfactants, the oleic phase will be expelled by the aqueous phase from the large pores which will not re-enter the small pores due to capillary forces and oil flow will be facilitated [69].

2.14 Summary

From the literature review it can be concluded that ASP flooding process has captured a tremendous interest. The remarkable potential has been generated through a wide range of research efforts directed to develop appropriate formulations and to understand the mechanisms involved to mobilize waterflood residual oil. The studies were however limited to the use of pure hydrocarbons (methanol, ethanol, hexanol) as oils instead of the original crude. Most of the studies were carried out under ambient conditions of temperature and pressure instead of the real reservoir conditions.

Lot of work has been extensively reported as far as the conventional surfactants are concerned. In most of the cases reported concentrations of the surfactants ranged from 3,000 – 4,000 ppm. However, limited literature is available for non-conventional surfactants, particularly their mixtures in ultralow concentrations. Some of the studies are purely focused on IFT reduction and wettability alteration by the surfactants. The others are related to the spontaneous imbibition supported by the simulation studies. Limited literature is available as far as the synergistic effects and mutual compatibility of alkaline-surfactant-polymer formulations are concerned. Moreover, there is a lack of information regarding the residual additives in produced oil which can be generated either as a result of the mutual interactions between alkali and acidic components of the crude or due to the retention of surfactants by hydrocarbon phase itself.

The complex nature of oil fields with different heterogeneity, high temperature and harsh salinity and availability of modified chemical agents requires a lot of work to be conducted for a successful implementation of the process a particular reservoir.

This study was proposed to overcome these ambiguities and challenges to minimize the chances for mismatch between lab and field trials. Comprehensive experimental investigations including the screening of appropriate chemicals, IFT reduction, wettability alteration, core characterization, spontaneous and forced imbibition experiments will be carried out. Comparative detailed and critical discussions will be carried out throughout the study to elaborate the involved mechanisms properly.

CHAPTER 3

3. EXPERIMENTAL

This chapter has been organized into various sections to elucidate the experimental procedures, theoretical background and working principle of the utilized equipments. Sections 3.1 and section 3.2 are related to the characterization of brine solution and explains the sensitivity and tolerance levels of ASP towards ions, salts and solvents present in the Angsi Sea and formation waters. Section 3.3 is concerned about the materials coding. Use of rotary viscometer for the analyses of viscosity and shear thinning of HPAM has been elaborated in section 3.4. Utilization of TGA of surfactants and polymers for the elaboration of thermal stability, structure-property relationship is given in section 3.5 to elucidate the limits of stability and applicability. In order to explain the role of molecular interactions involved in the combination of various chemicals FTIR-ATR spectroscopy has been explained in section 3.6. Available IFT measurement techniques are presented in section 3.7. Partition functions of surfactants in aqueous and organic phases are discussed in section 3.8. Role of atomic force microscopy to appraise oil-water emulsion stability is given in section 3.9. Efficacy of surfactants in wettability alteration has been described through contact angle measurements in section 3.10. Characterization of sandstone cores for porosity, permeability, surface area, pore structure, elemental profile and internal structure measurements has been explained with the help of helium porosimeter, BET, SEM, EDX techniques in sections 3.11, 3.13 and 3.14. Spontaneous and forced imbibition studies are discussed in sections 3.12 and 3.15 respectively. Surfactants adsorption mechanism and kinetics behaviour is discussed in section 3.16.

3.1 Water Analyses

Waterflooding involves injecting of water into a petroleum reservoir causing the crude oil to flow. Water under high pressure is pumped into the wells and it is forced through the petroleum-bearing formations usually porous rocks. However, if the level of salinity, alkalinity and other intervening factors are not within their controlled limits then

waterflooding may cause operational problems such as precipitation and scaling, hence restricting oil flow instead of increasing. It is of fundamental importance to carry out water analyses in order to ascertain the content of dissolved metal ions and avoid related discrepancies.

3.1.1 pH Measurement

Measurement of pH is one of the most important and frequently used tests in water chemistry. Practically every phase of water supply and wastewater treatment, e.g., acid-base neutralization, water softening, precipitation, coagulation, disinfection, scale and corrosion control, is pH-dependent.

At a given temperature, the intensity of the acidic or basic character of a solution is indicated by pH or hydrogen ion activity. Alkalinity and acidity are the acid- and base-neutralizing capacities of water respectively and are usually expressed as milligrams CaCO_3 per liter.

pH as defined by Sorenson [126] is $-\log [\text{H}^+]$; it is the “intensity” factor of acidity. Pure water is only slightly ionized and at equilibrium the ion product is

$$\left. \begin{aligned} [\text{H}^+][\text{OH}^-] &= K_w = 1.01 \times 10^{-14} \text{ at } 25^\circ \text{C} \\ \text{and } [\text{H}^+] &= [\text{OH}^-] = 1.005 \times 10^{-7} \\ \text{or } \text{pH} + \text{pOH} &= \text{p}K_w \end{aligned} \right\} \text{----- (3.1)}$$

where, $[\text{H}^+]$ = activity of hydrogen ions, moles/L

$[\text{OH}^-]$ = activity of hydroxyl ions, moles/L and

K_w = ion product of water and $\text{pH} = \log_{10} a\text{H}^+$ and $\text{pOH} = \log_{10} a\text{OH}^-$

As pH increases, pOH decreases correspondingly and vice versa because $\text{p}K_w$ is a constant for a given temperature. At 25°C , pH 7 is neutral, the activities of the hydrogen and hydroxyl ions are equal, and each corresponds to an approximate activity of 10^{-7} moles/L. The neutral point is temperature-dependent, at 0°C pH is 7.5 and at 60°C pH is 6.5 [127].

For pH measurements of the samples a digital pH meter, (HANNA 8519N of Hanna Instruments) with a range of 0.0 to 14, resolution of 0.01, equipped with a temperature-compensation adjustment, was used. Electrode and temperature control probe of the pH meter were immersed in the test solution. When desired temperature value was reached, pH values were recorded with the help of digital display. All the samples were analyzed at 25 °C.

3.1.2 Conductivity (Salinity/Total Dissolved Solids) Measurement

Conductance is a measure of the ability of water to conduct an electric current. Pure water is highly resistant to electric current. When mineral salts, acids, or alkalis are added to pure water they dissociate into positive and negative ions which in turn increases the conductivity value in proportion to the number of ions present. Therefore conductivity can be used as a test to determine the amount of dissolved solids in water. Seawater has a much higher concentration of ionic substances content, and consequently is expected to possess a higher conductivity than inland waters. Conductivity measurement performs many useful jobs to estimate total dissolved solids (TDS) and salinity in water/wastewater.

According to Ohm's law the current, I (amperes), flowing through a conductor is directly proportional to the applied electromotive force, E (volts), and inversely proportional to the resistance, R (ohms) of the conductor [128].

$$\left. \begin{array}{l} I = E/R \\ \text{or } R = E/I \\ \text{and } 1/R = I/E = C \end{array} \right\} \text{----- (3.2)}$$

C , is the reciprocal of resistance R , and is termed as conductance. It is measured in reciprocal ohms (ohm^{-1}), also called "mhos" or "siemens" (S).

By multiplying conductivity with an empirical factor (which is obtained from samples of known dissolved solid concentration and conductivities), the total dissolved solids can be estimated. The empirical factor may have a value in the range of 0.55 to 0.9,

depending upon the conductivity and temperature of the given water sample. For seawaters the factor has values close to the 0.85 and for normal inland waters this factor has values close to 0.65 [127]. For the measurement of conductivity the multi meter, (HI9033 auto temperature control conductivity meter of HANNA Instruments) with a range of 0 to 3999 $\mu\text{S}/\text{cm}$ and resolution $1\mu\text{S}/\text{cm}$, equipped with a temperature-compensation adjustment was used. All the samples were analyzed at 25°C .

3.1.3 Total Hardness- EDTA Titration Method

The total hardness is determined by titration with a standard solution of ethylenediamine tetra acetic acid (EDTA) using eriochrome black T, an organic dye, as an indicator. The eriochrome black T indicator forms a wine-red complex even when slight traces of calcium and magnesium salts are present in the sample water. If no calcium or magnesium, the eriochrome black T will have a blue color. EDTA also forms colorless complexes with calcium and magnesium. These EDTA complexes are more stable than eriochrome black T complexes. When sufficient EDTA is added to combine with all the calcium and magnesium in the water sample containing eriochrome black T, the solution will change color from wine red to blue indicating the equivalence point of titration [127,129].

Preparation of Reagents

NH_4Cl - NH_4OH buffer solution:

Firstly 16.9 grams of NH_4Cl was dissolved in 143 mL concentrated NH_4OH and finally the volume of the resultant solution was adjusted to 250 mL with the help of deionized water.

Indicator: Eriochrome Black T (EBT)

EBT indicator was prepared by dissolving dye 0.5 grams of eriochrome black T dye in 100 mL of triethanolamine.

Standard EDTA Titrant (0.01M)

Standard EDTA solution was prepared by dissolving 3.723 grams of di-sodium salt of EDTA in 100 mL deionized water and the final volume was adjusted to 1000 mL using deionized water. EDTA being a strong complexing agent is capable of extracting metal ions such as silica, zinc, etc. from glass containers. The prepared EDTA solution was kept in polyethylene containers for subsequent use.

3.1.4 Estimation of Total Hardness, ppm as CaCO₃

Aliquots of 10 mL sample solution were placed in a conical flask. One mL of the NH₄Cl- NH₄OH buffer solution was added in order to maintain the pH of the sample at 10.0±0.1 units during titration. Few drops of the eriochrome black T indicator solution was added in the conical flask and titrated against the standard EDTA solution. The end point was identified by the appearance of a blue color solution and the disappearance of the reddish tinge. The parts per million of total hardness, expressed in terms of CaCO₃, was calculated as follows [127]:

$$\left(\frac{\text{Volume of EDTA titrating solution used in mL}}{\text{Volume of the sample taken in mL}} \right) \times 1000$$

As the volume of the sample solution taken was 10 mL, this relation can be written as:

$$\text{Total hardness (ppm as CaCO}_3\text{)} = \text{Volume of EDTA solution used in mL} \times 100$$

3.1.5 Calcium Hardness- EDTA Titration

Calcium hardness was estimated by titration with a standard solution of EDTA (as mentioned in 3.1.4) using ammonium purpurate (also called murexide) and an organic dye, as an indicator. At pH 12 the ammonium purpurate indicator is sensitive to calcium ions and insensitive to magnesium ions. This indicator will form a pink color even with just a trace of calcium in water. If no calcium is present, the indicator will be purple. As in the test for total hardness, if sufficient EDTA is added to combine with all the calcium in the water sample containing ammonium purpurate, the solution will change color from pink to purple [127].

Preparation of Reagents

Standard EDTA titrant (0.01M)

Standard EDTA solution was prepared as previously mentioned in 3.1.3.

Indicator: - Ammonium Purpurate

Ammonium purpurate indicator solution was prepared by dissolving 0.2 grams of ammonium purpurate in 100 mL of glycerin to get a homogenous solution.

Sodium Hydroxide Solution (0.2 N)

Sodium hydroxide solution was prepared by dissolving 0.8 grams of NaOH in a little water initially and finally making up the volume to 100 mL with deionized water.

3.1.6 Estimation of Calcium Hardness, ppm as CaCO₃

10 mL of water was placed in a conical flask. 1 mL of 0.2N sodium hydroxide solution was added to the sample and stirred for a while using a magnetic stirrer. The pinkish color solution was titrated against standard solution of EDTA until the color has changed from pink to purple. The parts per million of calcium hardness, expressed in terms of CaCO₃ was calculated as mentioned previously in 3.1.3.

3.1.7 Magnesium Hardness (Calculation method)

Magnesium hardness was estimated as the difference between total hardness and calcium hardness as CaCO₃ by ignoring other trace interfering metals.

Mg/L as CaCO₃ = [Total hardness (as mg CaCO₃/L) – Calcium hardness (as mg CaCO₃/L)]

3.1.8 Chlorides– Mohr Titration Method

The amount of chloride ions was determined by titration with a standard silver nitrate solution. Potassium chromate was used as an indicator. The chloride ions are preferentially precipitated by silver nitrate as silver chloride. When all the soluble chlorides are precipitated, the silver nitrate reacts with the chromate indicator. Red silver

chromate is then precipitated out. The permanent appearance of this red color marks the end point of titration [127, 129,130].

3.1.9 Testing Procedure, Chlorides (ppm as Cl)

Sample solution, 10 mL, was placed in a conical flask. Two drops of phenolphthalein indicator was added to it in order to check the neutrality. Samples giving color to the indicator was neutralized by the addition of 0.02N solution of sulfuric acid. Potassium chromate indicator solution, 1 mL was added to the neutralized sample solution. The color of the solution changed to bright yellow. It was titrated against a standard silver nitrate solution until a permanent dark brown color was achieved.

Preparation of Reagents

Silver nitrate, 0.028N

Standard silver nitrate solution, 1 mL = 1 mg Cl, 0.028N, was prepared by initially dissolving 4.792 grams of silver nitrate in 100 mL of deionized water and finally making up the volume to 1000 mL by the addition of deionized water.

Potassium Chromate Indicator, 5%

Standard silver nitrate solution was prepared by dissolving five grams of $K_2Cr_2O_4$ in 100 mL of distilled water. A slight precipitation was observed. The solution was allowed to stay overnight and filtered to remove the precipitates. The amount of chloride present in parts per million was calculated as follows:

$$\left(\frac{\text{Volume of EDTA titrating solution used in mL}}{\text{Volume of the sample taken in mL}} \right) \times 1000$$

As the volume of sample solution taken was 10 mL, the above equation can be written as follows:

$$\text{Chlorides (ppm as Cl)} = \text{Vol of AgNO}_3 \text{ used in mL} \times 100$$

3.1.10 Sulfates

The principal problem associated with sulfate ions in water is the possibility of calcium scale formation. Precipitation of calcium sulfate can occur when high concentrations of both calcium and sulfate exist simultaneously. In EOR applications, calcium sulfate scale formation can cause an adverse cementing problem by blocking the pore channels.

3.1.11 Titration Test for Sulfate (ppm as SO₄) Using THQ

The sulfate was analyzed by titrating with a standard solution of barium chloride in alcoholic solution using tetrahydroxyquinone (THQ) dye as an indicator. The barium chloride reacts with sulfate to precipitate out the barium sulfate. When there is no excess of barium ions, the color of the indicator in solution is yellow. But as soon as there is an excess of soluble barium ions the yellow color changes to pink. Soluble phosphates do interfere with the test. When soluble phosphates are known to be present then the test procedure must be modified as given below [127,130].

3.1.12 Procedure (Phosphate Absent)

Sample solution, 10 mL, was placed in an Erlenmeyer flask. Two to three drops of phenolphthalein indicator was added to it. Samples giving pinkish shade were neutralized by means of dilute hydrochloric acid (0.1N). The samples that did not produce pinkish shade i.e. neutral samples were initially treated by dilute solution of sodium hydroxide (0.01%) until the appearance of a pinkish shade and then finally neutralized by means of 0.1N hydrochloric acid solution. Ethyl alcohol, 25 mL, was mixed in the neutral sample along with the addition of 0.2 grams of THQ indicator. A yellow solution was produced. It was titrated against 0.025N barium chloride solution with constant stirring until the color of solution changes to red.

The amount of sulfates present in parts per million as SO₄ equals:

$$\left(\frac{\text{Volume of barium chloride used in mL}}{\text{Volume of the sample taken in mL}} \right) \times 1200$$

As 10 mL of sample was utilized the above relation can be written as:

$$\text{Sulfate (ppm as SO}_4\text{)} = \text{Volume of BaCl}_2 \text{ used in mL} \times 120$$

3.1.13 Procedure (Phosphate Present)

A 10 mL sample solution was placed in an Erlenmeyer flask. Four drops of bromocresol green indicator was added. A green solution was produced. This was titrated against a 0.1N hydrochloric acid solution until the color changed from green to straw. Then by following the same procedure as previously provided using THQ titration the concentration of sulfate can be determined.

Preparation of Reagents

Barium chloride, 0.025N

Dissolved 3.05 grams of $\text{BaCl}_2 \cdot 2\text{H}_2\text{O}$ in 100 mL of deionized water, added enough water to make up a total volume of one liter.

Hydrochloric acid, 0.1N

The molarity of the hydrochloric acid was calculated with the help of following relationship:

$$\begin{aligned} \text{Molarity} &= \left(\frac{\text{Density}}{\text{Molecular weight}} \times \frac{\text{Percentage purity}}{100} \right) \times 1000 \\ &= 1.19/36.5 \times 37 \times 10 \\ &= 12.06 \text{ M} \end{aligned}$$

Using the relationship of $M_1V_1 = M_2V_2$

$$V_1 = M_2V_2 / M_1$$

where, M_1 is the molarity of concentrated hydrochloric acid, V_1 is required volume of concentrated hydrochloric acid to prepare the desired molarity M_2 in requisite volume V_2 .

$$\begin{aligned} &= 0.1 \times 1000 / 12.06 \\ &= 8.29 \text{ mL} \end{aligned}$$

8.29 mL of concentrated hydrochloric acid was diluted in distilled water and made up a total volume of one liter to obtain 0.1N HCl.

Bromocresol-green indicator solution

A small amount (0.1 g) of bromocresol-green was dissolved in 14.3 mL of 0.01N sodium hydroxide solution. It was later diluted to 250 mL with deionized water.

3.1.14 Estimation of Carbonate and Bicarbonates

Two-Indicator Methods were utilized for the analyses of carbonate and bicarbonates. In this procedure, the amount of carbonate present is taken as the amount of hydrochloric acid required for titration to the phenolphthalein end point. The total amount of the two analytes equals the amount of hydrochloric acid required to continue the titration to the methyl orange end point [127]. The amount of bicarbonate is the difference between two values.

10 mL sample solution was placed in an Erlenmeyer flask. Two drops of phenolphthalein indicator was added to it. Solution turned pink. This was titrated against a 0.1N hydrochloric acid solution until the color changed from pink to colorless. Two drops of methyl orange was added to the same solution and continued the titration with hydrochloric acid until the end point is reached. Using the relationship $M_1V_1 = M_2V_2$, parts per million concentrations for both carbonate and bicarbonate were calculated. Densities of the water samples at various temperatures were calculated using the specific gravity bottle by following the relationship $D = M/V$.

3.2 Analyses of Sodium, Potassium, Iron, Barium and Strontium

Angsi formation water was analyzed for Sodium, Potassium, Iron, Barium and Strontium using an atomic absorption spectrometer (AAS). Alan Walsh [131] was the originator and developer of the atomic absorption method of chemical analyses, which revolutionized quantitative analyses in 1960's. AAS provided a quick, easy, accurate and highly sensitive method of determining the concentrations of elements at trace levels. The method has found multifarious applications in areas as diverse as medicine, agriculture, mineral exploration, metallurgy, food, biochemistry and environmental control, and has been described as 'the most significant advancement in chemical

analyses' in the twentieth century as far as the quantitative analyses of the metals is concerned.

3.2.1 Atomic Absorption Spectroscopy (AAS)

AAS is the measurement of absorption of optical radiations by the atoms of an analyte in the gaseous state. Since samples are usually liquids or solids, the analyte atoms or ions must be vaporized in a flame or graphite furnace. Electrons exist in specified energy levels within an atom. These levels have well defined energies. During atomization process in AAS the atoms absorb ultraviolet or visible light and make the transitions to higher electronic energy levels as presented in Fig. 3.1.

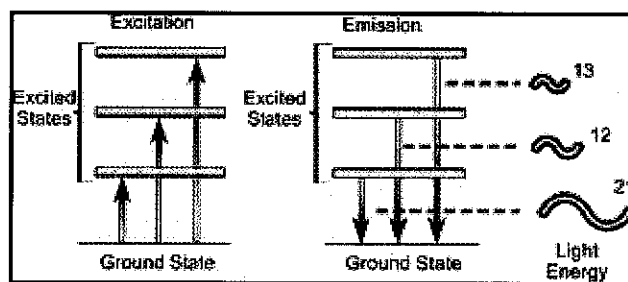


Figure 3.1: Energy transitions during atomic absorption spectroscopy [132].

The science of atomic spectroscopy has yielded three techniques for analytical use, namely: atomic absorption, atomic emission and atomic fluorescence. The processes of excitation and decay are responsible for all the three techniques of atomic spectroscopy. Either the energy absorbed in the excitation process, or the energy emitted in the decay process is measured and used for analytical purposes. AAS technique uses the wavelengths of light specifically absorbed by an element which correspond to the energies needed to promote electrons from a lower energy level to another, of a higher energy level. The wavelength of the emitted radiant energy is directly related to the electronic transition. Since every element has a unique electronic structure, the wavelength of light emitted is a unique property of each individual element. The analyte concentration is determined from the amount of absorption using the Beer-Lambert law [133], more commonly known as Beer's Law, which is the linear relationship between

absorbance and concentration of an absorbing species. Beer-Lambert law is usually written as:

$$A = \epsilon cl \text{ ----- (3.3)}$$

where, A represents the measured absorbance, ϵ is a molar extinction coefficient, c is the analyte concentration and l , is the path length. Concentration measurements are usually determined from a calibration curve after calibrating the instrument with standards of known concentrations.

3.2.2 Instrumentation of Atomic Absorption Spectrometer

An AAS is presented as in Fig. 3.2. It consists of a light source, sample cell, atomizer, nebulizer, monochromator and a detector.

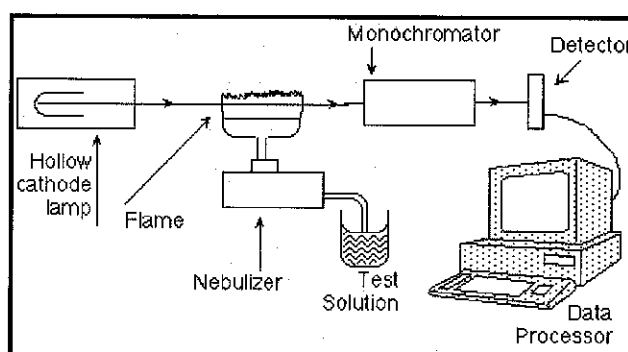


Figure 3.2: Schematic of an atomic absorption spectrometer [134].

Light Source

The light source is usually a hollow-cathode lamp of the element that is being measured. It is designed to emit the atomic spectrum of a particular element. Specific lamps are selected according to the element to be determined. The disadvantage of these narrow-band light sources is that only one element is measurable at a time.

Sample Cell

In the sample cell, vapors are generated in the light beam from the source. This is usually done by introducing the sample into a burner system (Flame AAS) or electrically heated graphite furnace, aligned in the optical path of the spectrophotometer.

Atomizer

AA spectroscopy requires the analyte atoms to be in the gaseous phase. Ions or atoms in a sample must undergo vaporization in a high-temperature source such as a flame or graphite furnace. Flame AA uses a slot type burner to increase the path length, and therefore increase the total absorbance. Sample solutions are usually aspirated/atomized with the gas flow into a nebulizing/mixing chamber to form small droplets before entering the flame. The graphite furnace has several advantages over a flame. It is a much more efficient atomizer than a flame and it can directly accept very small absolute quantities of sample. It also provides a reducing environment for easily oxidized elements. Samples are placed directly in the graphite furnace and the furnace is electrically heated in several steps to dry the sample, ash the organic matter, and vaporize the analyte atoms.

Light Separation and Detection

AA spectrometers use monochromators to disperse several wavelengths of lights that are emitted from the light source to isolate a particular wavelength of interest. Detectors (photomultiplier tubes) for UV and visible light to produce an electrical current that is dependent on the light intensity are employed. The main purpose of the monochromator is to isolate the absorption line from the background light due to interferences. The electrical current is amplified and processed by the instrument electronics to produce a signal, which is a measure of the light attenuation occurring in the sample cell. This signal is further processed to generate instrument readout in concentration units. Standard atomic absorption conditions for the analyzed elements are presented in Table 3.1.

Table 3.1: Standard atomic absorption conditions for Na, K, Fe, Ba and Sr

Element	Wavelength (nm)	Flame type	Slit width (nm)
Na	330.2	Air-Acetylene	0.7
K	766.5	Air-Acetylene	0.7
Fe	248.3	Air-Acetylene	0.2
Ba	553.6	Nitrous oxide-Acetylene	0.2
Sr	460.7	Nitrous oxide-Acetylene	0.4

Angsi formation water was analyzed using the specified hollow cathode lamps for Na, K, Fe, Ba and Sr in AAS (Hitachi AA 6800, shown in Fig 3.3). Initially a calibration curve for each element was plotted using three standard solutions of known concentrations and finally the concentrations in the samples were determined by estimating the absorption through aspirating the sample solution using the mentioned flame.

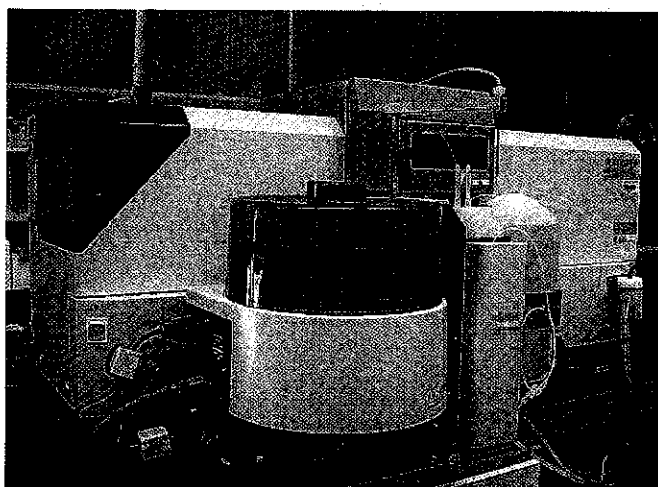
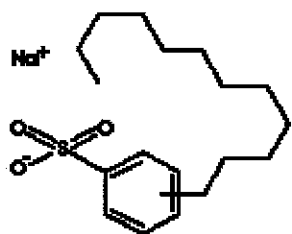


Figure 3.3: Hitachi AA 6800 atomic absorption spectrometer.

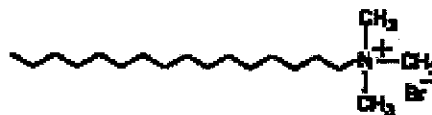
3.3 Materials Coding

The entire chemicals utilized for water analyses including ethylenediamine tetra acetic acid, ammonium chloride, ammonium hydroxide, eriochrome black T, ammonium purpurate, potassium chromate, silver nitrate, hydrochloric acid, barium chloride, bromocresol green, sodium nitrate, potassium nitrate, ferric nitrate, barium nitrate, and strontium nitrate were of analytical reagent (AR) grades which were purchased from Merck and used as received. The utilized conventional surfactants, dodecylbenzene sulfonic acid (DBSA), cetyltrimethyl ammonium bromide (CTAB), sodium dodecyl sulfate (SDS) and alkali sodium carbonate, potassium chloride were also of AR grade and supplied by Merck which were used without further purification. Non-conventional surfactants Aerosol OT-85AE (AOT) and Aerosol TR-70 (ATR) were used as received from Cytec Industries. The polymers Hybomax-4785 and Hybomax-6417, commercial products of HYBO industries, hereafter named as Polymer-1 and Polymer-2 respectively

were purchased from HYBO industries and used as received. Deionized water was used throughout the study for the preparation of solutions, whereas Angsi formation water was utilized for imbibition and core flooding studies, if not specified otherwise. Chemical structures of the utilized surfactants are presented below:

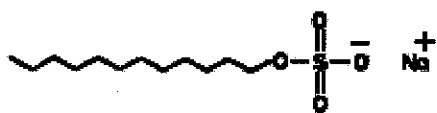


(A) Dodecyl benzene sulfonic acid sodium salt

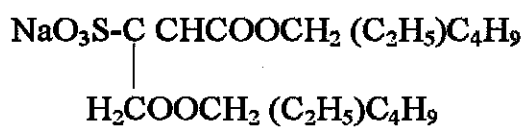


(B) Cetyltrimethyl ammonium bromide

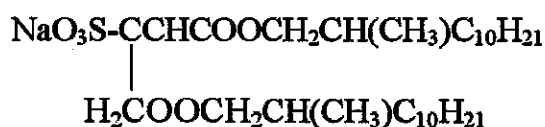
Sodium dodecyl sulfate



(C) Sodium dodecyl sulfate



(D) Aerosol OT



(E) Aerosol TR

3.4 Viscosity and Shear Thinning of High Molecular Weight PAM

Viscosity is the resistance caused by the internal friction of a liquid to its flow. The absolute viscosity (η) of a fluid is defined as the ratio of the shear stress (τ) to the shear rate ($\dot{\gamma}$), as shown in Equation 3.4 [135].

$$\eta = \tau / \dot{\gamma} \text{-----} (3.4)$$

On the basis of shear rate the fluids can be categorized into two of classes Newtonian and non-Newtonian fluids. A Newtonian fluid is the one in which the ratio of

shear stress to the rate of shear is constant, whereas, a non-Newtonian fluid is one in which the viscosity is not a constant parameter, it depends on the shear rate [136]. The Newtonian model is accurate over a large range for most low molecular weight fluids, including water and aqueous solutions, liquid metals, organic compounds, and silicones. Other non-Newtonian fluids such as suspensions obey various more complex models. A large number of such models have been proposed, for example Casson [136], the Bingham [137] and power law fluid [138] models.

There are several types of non-Newtonian flow behavior, characterized by the way a fluid viscosity changes in response to variations in shear rates. The most common types of non-Newtonian fluids include: *Pseudoplastics*, fluid displays a decreasing viscosity with an increasing shear rate. Probably the most common of the non-Newtonian fluids, pseudo-plastics include paints, polymeric solutions, emulsions, and dispersions of many types. This behavior is also called as shear-thinning sometimes. *Dilatants* are fluid in which their viscosity increases with an increase in shear rate. Rarer than pseudoplasticity, dilatancy is frequently observed in fluids containing high levels of deflocculated solids, such as clay slurries, corn starch in water and sand/water mixtures. Dilatancy is also referred to as shear-thickening flow behavior. *Plastics*, fluid behaves as a solid under static conditions. A certain amount of force must be applied to the fluid before any flow is induced; this force is called the yield value. Tomato ketchup is a good example of this type; it refuses to pour from the bottle until the bottle is shaken or struck. Once the yield value is exceeded and flow begins, plastic fluids may display Newtonian, pseudoplastic or dilatant flow characteristics.

Viscosity is a principal parameter when flow measurements of fluids, such as liquids, gelling agents, semi-solids, gases and even solids are made. The viscosity of the polymeric materials varies with shear rate. With the increase in shear rate, pseudoplastic or shear thinning materials exhibit a decrease in the viscosity. At high temperature and shear rates polyacrylamide solution exhibit shear thinning; i.e., the viscosity η reduces with an increase in temperature and shear rate. Measurement of viscosity in fluids and particularly the polymeric materials being utilized for EOR applications is a critical parameter in determining not only the flow properties but also to control the process

efficiency. In oil and gas industry viscosity measurement is a crucial part from exploration to the finished products. Viscosity measurements are often the quickest, most precise and most reliable way to analyze some of the most important factors affecting product performance.

There are different techniques for measuring viscosity, each suitable to specific circumstances and materials. The two main types of viscometers can be categorized as the tube and rotational instruments [136]. Tube type viscometers observe the rate of flow through tubes due to a known pressure difference and are associated with some discrepancies. The rotational viscometers can be further categorized into two classes: those where two concentric cylinders rotate relative to one another around a common axis; and those consisting of a cone of large vertical angle (approaching 180 degrees), and plate whose plane is through the apex of the cone. Many variations on this theme are possible, but in all types the test fluid is always sheared between the rotating parts. In water, high molecular weight polyacrylamide forms viscous homogeneous solutions, their viscosity increases with increase in the polymer concentration but is highly dependant on temperature, salinity and pH, etc. In some cases polyacrylamide is partially hydrolyzed to give greater viscosity. Polyacrylamide molecules are very flexible and very long, with a relatively small diameter. This makes the polymer susceptible to shear degradation or mechanical breakage. On the other hand, polyacrylamide is relatively immune to bacterial attack.

Brookfield LVDV-14 digital viscometer, shown in Fig 3.4, was utilized to measure the viscosity of aqueous solutions of polyacrylamide at various concentrations, temperatures, salinity contents and pH. Initially the concentration of each polymer 1 and 2 were varied to evaluate the effect of polymer concentration on viscosity in brine solution of 10,000 ppm salinity at constant temperature of 90 ± 2 °C. Finally 1500 ppm concentration of each polymer 1 and 2 was selected and effect of temperature was investigated in the range of 70 – 120 °C. Cylinder of the rotary viscometer was immersed in the test solution and gradually rotated till the rotational speed reached to 4,000 rpm. Viscosities were estimated with the help of digital display. Viscosities of

alkali plus polymer and alkali plus polymer plus surfactants were also evaluated in the similar fashion.

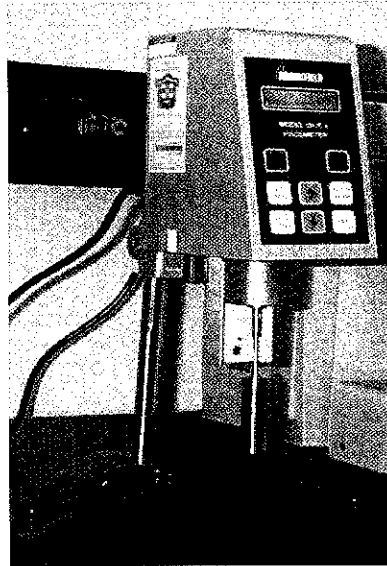


Figure 3.4: Brookfield LVDV-14 digital viscometer.

3.4.1 Working Principle of Rotary Viscometer

A rotary viscometer consists of an inner and an outer cylinder. The liquid to be investigated is placed between them. The principal of operation for Brookfield viscometer is to drive an elongated, radially balanced straight spindle made of a suitably stiff material, immersed in the test fluid to contact and interface with it yielding a drag through a calibrated spring. The viscous drag of the fluid against the spindle is measured by the spring deflection and calculated with a rotary transducer. If the liquid is placed between the two plates and a force F acts along the plate in the direction of the x axis, the plate moves with velocity v . The corresponding component of the shearing stress can be written as presented in Eq. 3.5 below [136].

$$\tau = F / A \text{-----} (3.5)$$

where, F represents force in x -direction and A is the area of contact between the plate and the liquid. This can be linked with the velocity gradient dv/dx as follows:

$$\tau = \eta \left(\frac{dv}{dx} \right) \text{-----} (3.6)$$

where, η is the viscosity of the liquid and dv/dx is the velocity gradient describing the change of velocity between the layers in x-direction.

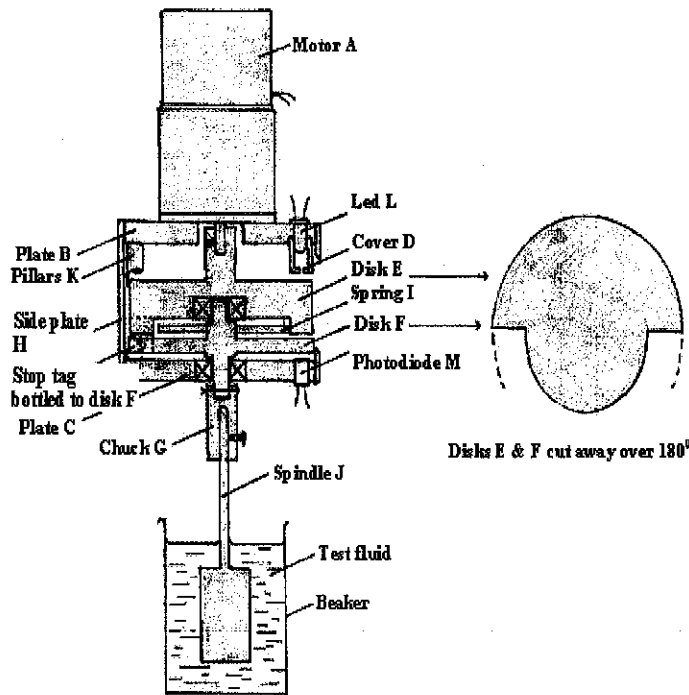


Figure 3.5: Major components of a rotary viscometer [139].

The major components of a rotary viscometer are shown in Fig 3.5. A small DC motor (A) drives the disk (E), the outer edge of which is removed over 180 degrees, as shown in the detail. Disk (F) is also cut in a similar way. Disks (E) and (F) may rotate independently about the same axis, due to the bearings in (E) and lower plate (C). The outer end of a spiral hair spring (I) is bolted to (E), while the inner end slots into part (F). Therefore the lower disk (F) is indirectly driven by the upper disk (E), via the torque spring (I) connected to (F) by means of a pinned push-fit joint chuck (G). Screws in this component clamp the glass stirring rod (J) securely.

The dimensions of the cylindrical and the stirring end (J) restrict the utility of the instrument to a certain range of viscosity. Different ranges can easily be obtained by altering the size of this stirring cylinder. During its operation, an infra-red light beam is

being emitted by the LED (L), and passes through the mechanism before detection by the photo diode (M). The LED cover (D) ensures that the beam is sufficiently narrow so that reflections from parts of the mechanism do not disrupt readings. The mounting plates (B) and (C) are supported by four corner pillars, (K). Side plates (H) not only increase the rigidity of the structure, they also exclude dirt, and prevent ambient light from corrupting the infra-red beam measurements. In its operation, the motor rotates at variable speeds, adjusted by the control electronics. The stirrer is turned via the spiral spring (I), which provides a torque proportional to its angular extension. The relative angular displacement between disks (E) and (F) depends directly on the viscosity of the fluid and rotation rate. As described earlier, parts (E) and (F) are cut away over 180 degrees; which causes the beam to be interrupted once per revolution. The viscous drag of the fluid against the immersed spindle (J) is measured by the spring (I) deflection and calculated with a rotary transducer [139].

3.5 Temperature Stability of Used Chemicals

The temperature of oil reservoirs may exceed 120 °C in some cases. Chemical-flooding schemes for recovering residual oil have been in general less than satisfactory due to multifarious factors including loss of chemicals by adsorption, precipitation, and instability of the injected chemicals towards temperature, etc. For a successful implementation of CEOR process the injected chemicals must be capable of tolerating harsh conditions created by extremes of temperature, pH, salinity and capable of interacting favorably with the inorganics. Evaluation of temperature stability of the surfactants, polymers, etc using appropriate thermal analyses techniques is one of the important parameters to evaluate the efficacy of the CEOR process.

Thermal analyses generally cover three different experimental techniques: Thermogravimetric Analyses (TGA), Differential Thermal Analyses (DTA) and Differential Scanning Calorimetry (DSC). These techniques are used in many sectors, from pharmacy and foods to polymer science, materials and glasses; in fact any field where changes in sample behavior are observed under controlled heating or controlled cooling conditions. The wide range of measurements possibly provides fundamental

information on the material basic properties. However, TGA is the most common and reliable technique to investigate a material's thermal stability and its fraction of volatile components by monitoring the weight change that occurs as the specimen is heated. It can be used for diverse materials including polymers, composites, surfactants, plastics, etc. The measurement is normally carried out in air or in an inert atmosphere, such as Helium or Argon, and the change in mass is recorded as a function of increasing temperature. Sometimes, the measurements are also performed in a lean oxygen atmosphere (1 to 5% O₂ in N₂ or He) to slow down oxidation.

3.5.1 Thermogravimetric Analyses (TGA)

TGA is a technique in which changes in weight of a specimen are recorded as a function of temperature by heating the specimen in air or in a controlled atmosphere such as nitrogen. Thermogravimetric curves (thermograms) provide information regarding polymerization reactions, the efficiencies of stabilizers and activators, the thermal stability of the materials and direct analyses. TGA involves heating a known mass of sample in an inert or oxidizing atmosphere and measuring the mass. The mass change over specific temperature ranges provides indications of the composition of the sample and thermal stability. General applications include: assessment of moisture and volatile contents, assessment of composition, thermal, oxidative stability and decomposition kinetics [140]. In order to evaluate the temperature stability of the polyacrylamide polymers and surfactants, Perkin Elmer TGA7 model, presented in Fig 3.6, was utilized.

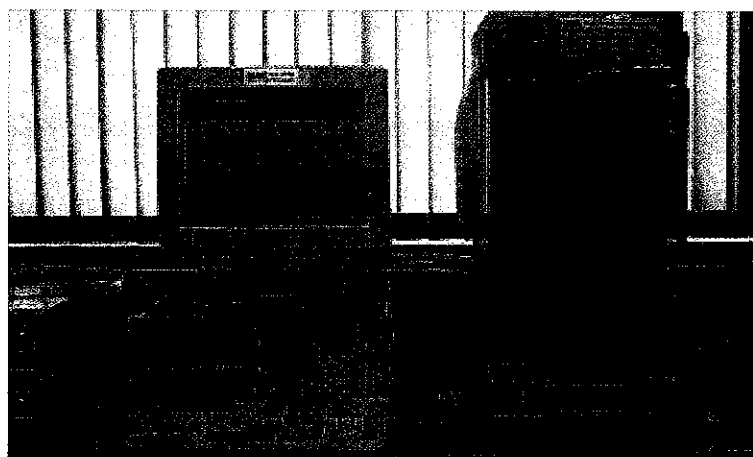


Figure 3.6: Perkin Elmer TGA7 Bench Model Thermogravimetric Analyzer.

3.5.2 TGA-Principle of Operation

A sample of the test material is placed into an alumina cup that is supported on, or suspended from an analytical balance located outside the furnace chamber. The balance is zeroed, and the sample cup is heated according to a predetermined thermal program. The balance sends the weight signal to the computer for storage, along with the sample temperature and the elapsed time. The TGA curve plots the TGA signal, converted to percent weight change on the Y-axis against the reference material temperature on the X-axis.

3.5.3 Instrumentation of TGA

The essential major components of a TGA includes a sample holder, recording balance, furnace, temperature programmer, an enclosure for establishing the required atmosphere, and a transducer for recording and displaying the data as presented in Fig. 3.7. Balance sensitivity is usually around one microgram, with a total capacity of a few hundred milligrams. A typical operating range for the furnace is normally from ambient to 1000°C, with heating rates from 10 to 100°C min⁻¹. The quality of the furnace atmosphere deserves careful attention, particularly the ability to establish an inert (oxygen-free) atmosphere, and it is useful to be able to quickly change the nature of the atmosphere. Compatibility between the materials of construction, sample, its decomposition products, and the gaseous atmosphere is of great importance and must be considered before analyzing the samples. Commonly available sample holder materials include aluminum, platinum, silica, alumina, etc.

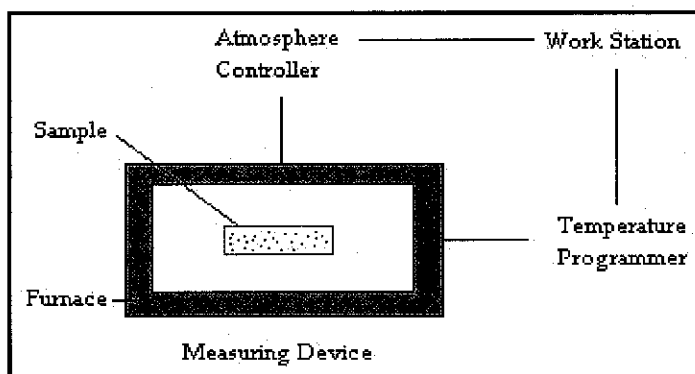


Figure 3.7: Major components of thermogravimetric analyzer.

3.5.4 Factors Affecting the TGA Curve

Many factors influence the form of the TGA curve, both sample- and instrument-related, some of which are interactive. The primary factors are heating rate and sample size, an increase in either of which tends to increase the temperature at which sample decomposition occurs, and to decrease the resolution between successive mass losses. The particle size of the sample material, the way in which it is packed, the crucible shape, and the gas flow rate can also affect the progress of the reaction. Careful attention is required in order to obtain consistent results with good repeatability.

3.5.5 Procedure for Thermogravimetric Analyses

Prior to analyses, the instrument was calibrated to ensure accurate weight and temperature measurement, TGA furnace was purged with N₂ for at least 10 minutes to eliminate the moisture from the system. About 10 mg of sample, each for polymers and surfactants individually, was placed into platinum crucible inside a temperature programmable furnace, hold for 1 minute at 50 °C with continuous purging of N₂. TGA was carried out with increasing temperature (20 °C/min) in a controlled, flowing N₂ atmosphere by heating the polymer samples from 50 – 700 °C, SDS, from 50 – 500 °C, AOT and ATR from 50 °C – 400 °C respectively.

3.6 Molecular Interactions between Various Chemicals

When polymers and surfactants are mixed together, they might self-assemble into ordered complexes under suitable conditions of temperature, pH, etc. In EOR applications this phenomenon is of specific importance in terms of thermodynamics associated with polymer-surfactant interactions, the morphological sensitivity to surfactant concentration, and the overall effect of ionic strength on the aggregation process. Molecular interactions such as hydrogen bondings are considered to play a key role in the compatibility of various surfactants and polymers. It is of great technological importance to understand and elaborate the molecular and electrostatic interactions involved between the aqueous solution of polyacrylamide and various surfactants. Infrared spectroscopy, particularly Fourier Transform Infrared Spectroscopy (FTIR) is a

widely used technique that for many years has been an important tool for investigating chemical processes and structures. The combination of infrared spectroscopy with the theories of reflection has made advances in surface analyses possible. Specific IR reflectance techniques may be divided into the areas of specular reflectance, diffuse reflectance, and internal reflectance. The latter is often termed as attenuated total reflectance (ATR). In order to gain an insight into the complex interactions existing between the various chemicals being proposed for EOR applications, FTIR-ATR spectroscopy was implemented. FTIR-ATR spectra of the individual polymers, surfactants and crude oil were recorded using the Perkin Elmer-2000 FTIR-ATR spectrometer as shown in Fig 3.8. Later on when these chemicals were in combination with each other, again FTIR-ATR spectra are recorded and changes in various functional groups are elaborated by comparing the spectra with originally recorded spectra.

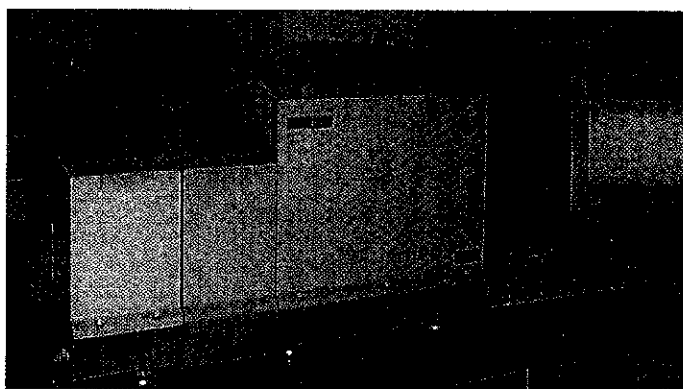


Figure 3.8: Perkin Elmer-2000 FTIR-ATR spectrometer.

3.6.1 FTIR-ATR Spectroscopy

Infrared Spectroscopy exists since the 1930's. The first commercially available infrared spectrometers were of the dispersive nature, in which the light coming from a broad band source is split into separate wavelengths through a grating or a prism. Spectral resolution of such spectrometers was limited by the grating spacing. Another related disadvantage of dispersive spectrometers was the duration of the measurement. The scanning of the whole spectral range was obtained by changing the position of the detector or the prism. Thus, the collection of the whole spectrum requires a long time. A turning point for infrared spectroscopy was the development of FTIR spectrometer, in which the spectral resolution can be obtained through modulation of the light, occurring

in the Michelson-Interferometer. In this way the information about the whole spectrum can be collected within single measurement. However, a further Inverse Fourier Transform of the collected signal is also necessary. For years this calculation represented the most serious problem of the FTIR measurement. The discovery of Fast Fourier Transform algorithm, by Cooley and Tukey in 1965 [141], has changed the entire situation. Presently, FTIR spectroscopy is a very well established method for chemical analyses [142-148]. Major components of FTIR spectrometer include Michelson Interferometer, light source, mirrors, probe, detector, etc, and are presented in below mentioned Fig 3.9. The working principle of a FTIR spectrometer depends upon the Michelson-Interferometer. The structure of the Michelson-Interferometer with beam splitter of 50% efficiency is shown in Fig 3.10, where I represent the intensity of light.

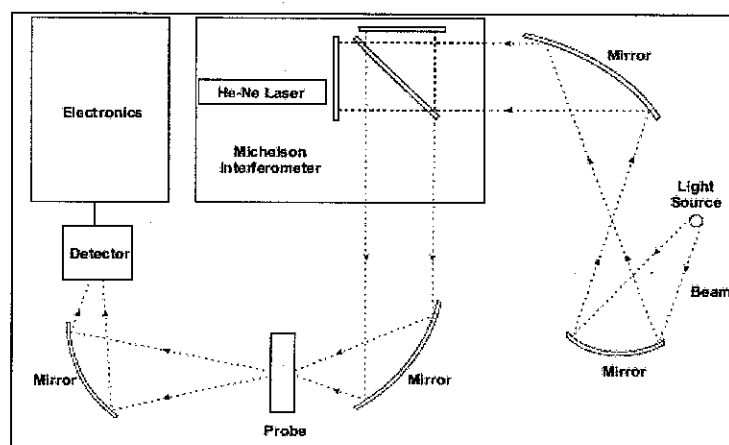


Figure 3.9: Schematic of the FTIR spectrometer [131].

The main objective of FTIR-ATR spectroscopic analyses is to determine the chemical functional groups present in the sample. Different functional groups are susceptible to absorb characteristic frequencies of IR radiation. Using various sampling accessories, FTIR-ATR spectrometers can analyze a wide range of sample types such as gases, liquids, and solids. Thus, FTIR-ATR spectroscopy is an important and popular tool for structural elucidation and the identification of various compounds.

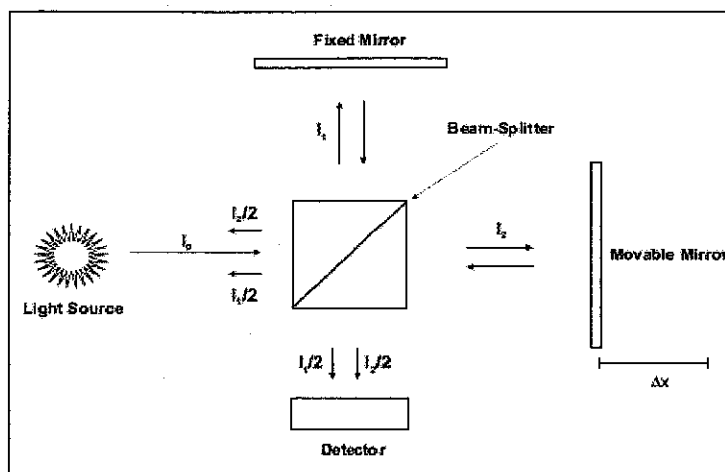


Figure 3.10: Schematic diagram of Michelson-Interferometer [149].

3.6.2 Sample Preparation and Analyses

FTIR-ATR spectrums of liquid surfactants, Aerosol OT, Aerosol TR, blend of Aerosol OT and TR, pure Angsi crude, Angsi crude in combination with individual surfactants, Aerosol OT, Aerosol TR, SDS, CTAB and blend of Aerosol OT and TR were recorded by inserting a droplet of the respective liquid in-between diamond-composite FTIR-ATR sample holding plates. The sample holding plates were equipped with a load to spread the sample uniformly and tightly against the diamond surface. FTIR-ATR spectra were obtained by averaging 10 scans from 350 to 6000 cm^{-1} wavelength at a resolution of 2 cm^{-1} . A spectrum from the diamond-composite plates was recorded as a background. FTIR-ATR spectra of the solid samples, SDS, CTAB and polymers 1,2 were recorded by preparing the transmission KBr disk of the relevant solid. Approximately 0.5 g of the respective solid sample was thoroughly mixed with 1.5 g of analytical reagent grade KBr. A small quantity of the resulting mixture was placed in-between two stainless steel discs and pressed applying high load (10 tons) to generate uniform transmission KBr thin films. Thin films of ASP combinations were prepared between the diamond-composite plates by evaporating the samples at low temperatures to obtain thin films for FTIR-ATR analyses.

3.7 Interfacial Tension (IFT)

The distinguishing feature of surfactants is that they lower the surface tension of a pure liquid by adsorbing at the surface strongly at relatively lower bulk concentrations. The IFT of immiscible liquids is an important thermophysical property that is useful to elaborate the behavior of liquids both in microgravity and in EOR processes under normal gravity [150]. Many techniques are available for the measurement of IFT, such as the ring method, powder contact angle method, dynamic Wilhelmy method, drop volume method, Wilhelmy plate method, sessile drop method, bubble pressure method, drop weight method, spinning drop method, and capillary rise method [151,152]. According to Kani and Mathur [153], many of these techniques use equations that contain a density difference term and are inappropriate for the liquids having similar density. Since surface tension is a measurable quantity, there are many existing methods for measuring the surface or interfacial tension of a liquid. The more accurate methods measure the pressure difference on the two sides of a curved surface, which possess surface or interfacial tension. They include the capillary rise, maximum bubble pressure, and drop-weight methods. However, less accurate methods are also used sometime because they are convenient and fast. Methods in this category include the ring and the Wilhelmy method. These methods measure the force needed to extend and detach a liquid film by means of a support (either a ring or a plate). Generally, the surface tension measuring techniques can be categorized into static and dynamic methods. Static methods, capillary rise method, Du Noüy Ring method, Pendant drop method, etc, involve the measurement of the tension of a stationary surface that has been formed over an appreciable time. Whereas, dynamic methods, drop weight, maximum bubble pressure, and oscillating jet methods involve the measurement of the surface tension of a freshly formed surface [154]. When the surface area of a solution is increased by stretching, a part of the bulk liquid is forced to enter the surface layer by convection. The fresh surface is called zero age and its surface concentration is supposed to be same as the bulk concentration. The surface tension of a surface of zero age is known as pure dynamic surface tension. As time increases, the surface concentration of the adsorbed molecules increases and the surface tension decreases with time during the aging of the surface. This surface tension

is known as dynamic surface tension. As time approaches infinity, the surface tension of the solution approaches an asymptote. This surface tension is equilibrium surface tension or static surface tension of the solution. Static (equilibrium) surface tension has significance alone, but the dynamic surface tension has no significance unless related directly to surface age. When the liquid is pure, the only change at the surface with age will be the orientation of the surface molecules which happens instantaneously. When one or more components of a system are preferentially adsorbed at the surface, the solute molecules diffuse to the subsurface until an equilibrium adsorbed layer is established. Therefore, the surface tension of the system changes from a value almost equal to that of the solvent to the equilibrium value of the solution.

3.7.1 Techniques for Measuring Surface Tension

Various techniques which are being used to study the surface tension and IFT are briefly described here.

3.7.2 Capillary Rise Method

The Capillary Rise Method is the easiest static method for measuring surface tension. When a capillary tube is wetted by a liquid, the liquid rises in the capillary because this change is in the direction of reducing surface area. When the liquid reaches equilibrium, as presented in Figure 3.11, the force of gravity pulling downward must be equal and opposite to the force of capillary rise [155]. At the equilibrium position, the weight of liquid between line A and line A' is equal to the surface tension of the liquid. Therefore, surface tension can be calculated using the following equation:

$$\sigma = (1/2)h r \rho g \text{ ----- (3.7)}$$

where, σ is surface tension (dynes/cm), h is height difference between menisci (cm), r is radius of capillary (cm), ρ is density of liquid (g/cm^3) and g is acceleration due to gravity (cm/sec^2).

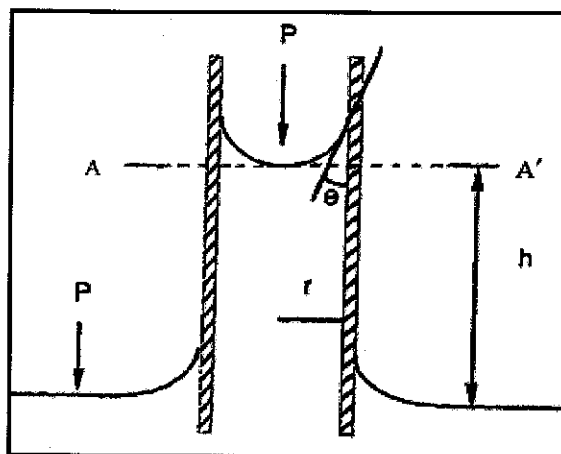


Figure 3.11: Capillary rise method [155].

The advantage of this method is that it is easy to perform and inexpensive. However, in order to obtain sufficient accuracy using this method, the diameter of capillary tube must be small (< 0.1 cm), the inside wall of capillary must be neat and clean (e.g. cleaned thoroughly with chromic acid) so that contact angle (θ) is zero. This method is not suitable for measuring the surface tension of a surfactant solution because the surfactant molecule adsorbs on the glass surface and make it repellent, thereby increasing the contact angle to a value above zero.

3.7.3 Du Noüy Ring Method

Du Noüy was not the first to measure the surface tension using ring method, but he is the one who has described this method in a convenient form of apparatus and his name has become inseparable from this method. The ring method depends upon the determination of the maximum pulling force necessary to detach a circular ring of round wire from the surface of a liquid with a zero contact angle. The ring is submerged below the interface and subsequently raised upwards. As the ring moves upwards it raises a meniscus of the liquid. Eventually this meniscus tears from the ring and returns to its original position. Prior to this, the volume, and the force exerted, of the meniscus passes through a maximum value and begins to diminish prior to the actual tearing. The apparatus designed by him utilizes a torsion balance to measure the tension instead of measuring it by means of weights. The torsion of the wire is being utilized to counteract the tension of the liquid film and to break it [156]. The process is shown in Fig. 3.12.

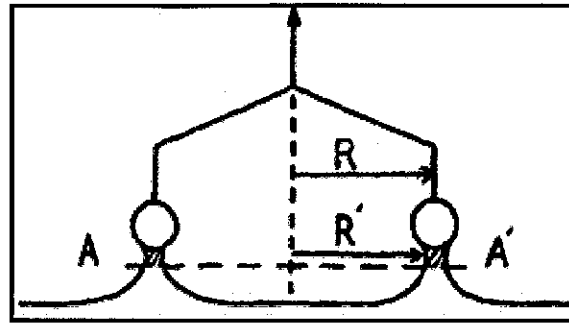


Figure 3.12: The position of Du Noüy ring right before the film rupture [156].

The elementary theory of ring method is that the maximum force required to detach the ring from the surface is equal to the total perimeter of the wire times the liquid surface tension.

$$mg = \sigma 4\pi r \text{ ----- (3.8)}$$

where, 'm' is mass of the ring (g), ' σ ' is the liquid surface tension (dynes/cm), 'g' is gravity of acceleration (cm/ sec²) and 'r' is the radius of the ring (cm).

However, Harkins and Jorden [157], Freund and Freund [158] have elaborated that the Eq. 3.8 is incorrect and modified it by including a correction factor 'f' which is as follows:

$$\sigma = (mg / 4 \pi r) f \text{ ----- (3.9)}$$

The physical significance of the correction factor 'f' can be understood by referring to Figure 3.12. In the position of maximum pull, it can be seen that the rupture of the surface occurs at plane AA' and leaves behind a small but significant volume of the liquid attached to the ring. Therefore, the force applied to raise the ring to the breaking point is actually equal to the weight of the ring plus the weight of the liquid lifted. The correction factor takes account of both the extra volume effect and the discrepancy between the measured radius, R, and the radius, R', of the meniscus in the plane of rupture. Ring method's advantage is that it is extremely rapid, very simple and does not need to be calibrated using solutions of known surface tension. However, it is less accurate than capillary rise method. Nevertheless, when properly applied to pure liquids,

the accuracy can be as high as $\pm 0.25\%$. The following outlines are important if higher accuracy is demanded: The plane of the ring must be horizontal to the liquid surface, the ratio between the measuring vessel and the ring radius should not be too small, the ring must be completely wet with the liquid and vibrations must be avoided. The major disadvantage of this method is that it is inappropriate for the determination of surface tensions of surfactant solutions and reproducibility of results is always difficult to achieve.

3.7.4 Pendant Drop Shape Analyses

The shape of a drop of liquid hanging from a syringe tip can be determined from the balance of forces which include the surface tension of that liquid. The surface or IFT at the liquid interface, presented in Fig. 3.13, can be related to the drop shape through the following equation [159]:

$$\gamma = (\rho \Delta g R_0^2) / \beta \text{ ----- (3.10)}$$

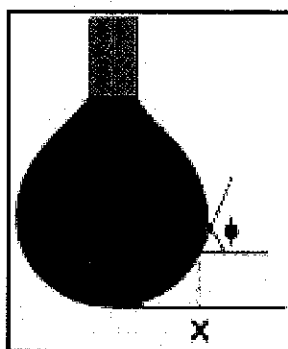


Figure 3.13: The liquid interface of pendant drop.

β , the shape factor, can be defined by the Young-Laplace equation expressed in three dimensionless first order equations as given below in Eqs. 3.11 – 3.13 [160].

$$dX / dS = \text{Cos}\Phi \text{ ----- (3.11)}$$

$$dZ / dS = \text{Sin}\Phi \text{ ----- (3.12)}$$

$$d\Phi/dS = 2 + \beta Z - \text{Sin}(\Phi / X) \text{ ---- (3.13)}$$

Modern computational methods using iterative approximations are being utilized to solve the Young-Laplace equation for ' β '. For any pendant drop where the densities

of the two fluids in contact are known, the IFT can be measured based upon the Young-Laplace equation. This method requires small amounts of liquids for analyses; measure ultra-low IFT and can also analyze molten materials easily.

3.7.5 Drop Weight or Drop Volume Method

The drop weight or drop volume method is one of the dynamic surface tension measurement methods. The drop weight method originally owes Harkins and Brown (HB) [161], is an accurate, simple, and low-cost technique for determining the surface tension. It relies on dripping a liquid at a low flow rate from a capillary of radius 'R' and measuring the combined volume 'V' of the primary and satellite drops that are formed. Surface tension is then inferred from an empirical correlation due to HB which only requires information about 'V' and 'R'. Although it is a very simple method but it requires an empirical correction (fudge factor) for the wetted diameter of the dispense tip. Normally many drops are dispensed into a weighing boat and taken to a sensitive balance. The drop volume method is preferred when it is difficult to form a pendant drop with sufficient stability to use the Laplace-Young method. This can happen, for example, with paints which tend to skim over, and it often happens in liquid/liquid measurements when the IFT is having ultra-low values. As mentioned earlier, dynamic surface tension is function of time, as well as composition. Therefore, unlike static methods, the dynamic methods are good for studying aging effects and adsorption kinetics of solutions.

The first person to notice that a drop is not a definite quantity was Tate [162]. Later, Lahnstein [162] found that the weight of a liquid drop hanging on an orifice was supported by liquid surface tension. When this force was exceeded, the drop falls away from the orifice. The relationship is known as "Tate's law" which can be mathematically expressed as follows [162]:

$$W = 2 \pi r \sigma \text{ ----- (3.14)}$$

where, r is the radius of the orifice.

This equation is having discrepancies due to the following two reasons: It is assumed that the breakaway drop possesses a perfect hemispherical shape and the weight of hanging drop is equal to the weight of falling drop. The erroneous assumption can be discovered by observing Fig. 3.14. In Figure 3.14(c), the breakaway drop can be divided to three parts: main drop, satellite drop, and residual drop. The satellite drops arise from the mechanical instability of the thin cylindrical neck. In any event, it is clear that only a portion of the drop (main drop) that has reached the point of instability actually falls. As much as 40% of the liquid may remain attached to the tip (residual drop). Therefore, the radius of the main drop that was collected and weighted is not equal to the radius of tip. In fact, it is a function of V/V , where 'V' is the volume of the perfect drop. The weight of a drop is a function of (r/a) , where 'a' is square root of the capillary constant. The surface tension measured by drop weight method is given in equations below.

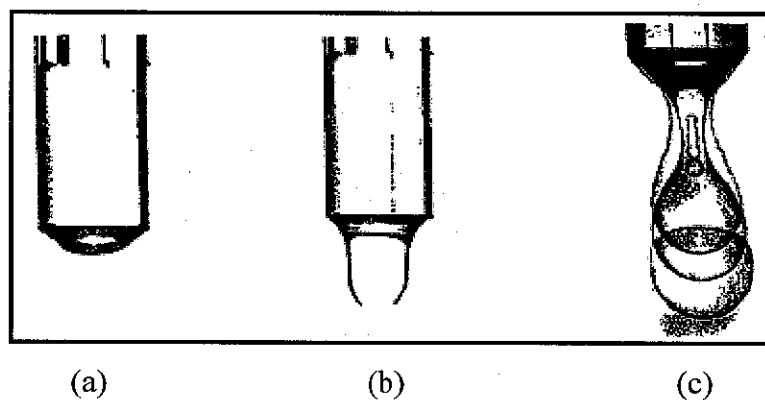


Figure 3.14: A drop breakaway process [163].

$$\sigma = (mg/2 \pi r) \psi (r/V^{1/3}) \text{ ----- (3.15)}$$

or

$$\sigma = (mg/2 \pi r) \Phi (r/a) \text{ ----- (3.16)}$$

where, 'a' is a capillary constant, which is defined as:

$$a^2 = rh = 2 \sigma / \{g(D - d)\} \text{ ----- (3.17)}$$

where, 'r' is radius of capillary, 'h' is height of liquid rises, ' σ ' is surface tension, 'g' is acceleration of gravity, 'D' is density of denser phase and 'd' is density of lighter phase.

The drop weight method can be called as drop volume method if the surface is calculated by the volume of drops instead of the weight of drops. The drop weight method has been extensively used over the drop volume method because of the accuracy in which measurements can be made. However, with the increased accuracy of micro-burettes, it has become equally advantageous to use the drop volume technique as well. The method itself is convenient for studying aging effects but unfortunately it is not suitable for measuring the surface or interfacial tension of liquids or solutions that reach equilibrium slowly.

3.7.6 Maximum Bubble Pressure Method (MBPM)

This MBPM is very old but an easy-to-use method for measuring surface tension which was proposed by Simon [164] in 1851. In this method the surface tension of a liquid can be determined from the maximum pressure in a bubble being formed in fine circular capillary tube that is immersed in a liquid. Gas bubbles are produced in the sample liquid at an exactly defined bubble generation rate. The gas bubbles enter the liquid through a capillary whose radius is already known. During this process the pressure passes through a maximum value which can be recorded.

Since the tube is a fine capillary, due to capillary rise phenomena, the liquid will rise to a height in the capillary so that the pressure at the liquid surface (meniscus) is zero. As the meniscus is pushed down to the bottom of capillary by a linearly increasing pressure, it remains in the same shape. The increasing pressure finally forces the meniscus to change to a bubble. This bubble, emerging at the end of a capillary, is stable and continuously expands with increasing gas pressure until its shape is hemisphere. At this moment, the pressure inside the bubble is the maximum pressure before it becomes unstable. The time of pressure increase from zero to maximum is known as calm stage. The time elapsed is called effective bubble age. As soon as the bubble size grows larger than hemisphere, it becomes unstable because the equilibrium pressure within it decreases as the bubble grows and the bubble escapes. This process is called as explosive stage and it happens within negligible time. The following illustration shows the pressure curve during bubble formation plotted as a function of time [165]:

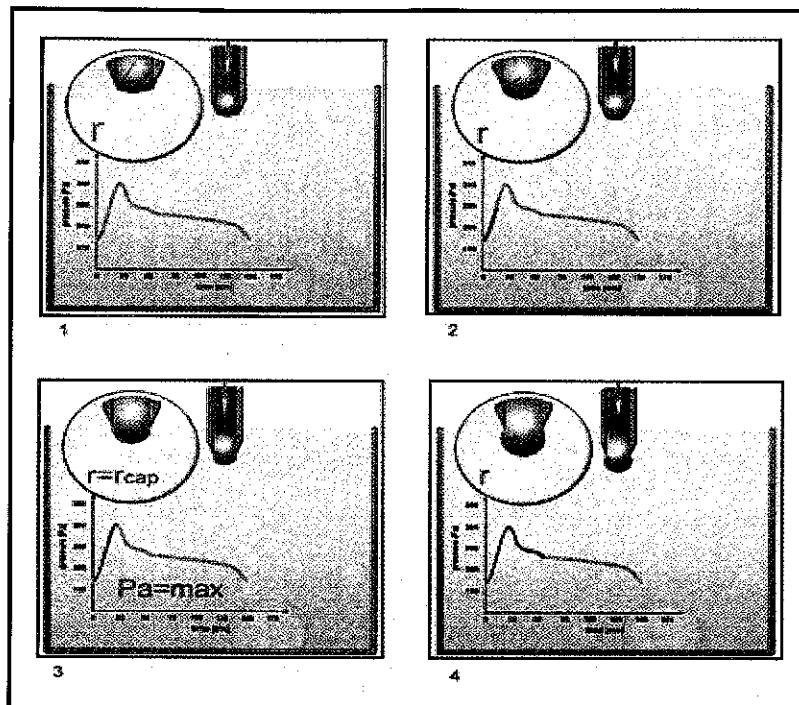


Figure 3.15: Pressure curves during bubble formation as a function of time [164].

1: The bubble is formed. Initially the pressure is below the maximum pressure; the radius of curvature of the air bubble is larger than the radius of the capillary.

2: The pressure curve passes through a maximum. At this point the air bubble radius is the same as that of the capillary; the air bubble forms an exact hemisphere. The following relationship exists between the maximum pressure P_{\max} , the hydro-static pressure in the capillary P_0 , the inner radius r of the capillary and the surface tension:

$$\sigma = (P_{\max} \cdot P_0 \cdot r) / 2 \text{ ----- (3.18)}$$

3: After the maximum the “dead time” of the measurement starts. The pressure decreases again, the radius of the air bubble becomes larger.

4: The bubble finally escapes from the capillary and rises. The cycle begins again with the formation of the next bubble. However, this type of bubble pressure experiments is not suitable for concentrated surfactant solutions.

3.7.7 Selection of an Appropriate Method

There are many existing techniques for surface tension and IFT measurements. However, the selection of the best method requires a compromise between accuracy and simplicity of operation. Moreover, the economical factors and the nature of the liquid also need to be considered. Generally speaking, the static methods are not suitable if the formation of new surface is involved. In contrast, the dynamic methods are considered as appropriate to measure the surface tension and IFT change versus surface life. Just like other analytical methods, each dynamic method has detection limitations in terms of surface life, especially for very short surface life like the generation of unstable oil-water emulsions. In order to determine the wide range of low IFTs for alkaline/surfactant/polymer solutions in crude oils, use of spinning drop tensiometer is considered as most appropriate [88, 166].

3.7.8 Spinning Drop Tensiometer

SVT 20, spinning drop video tensiometer of Dataphysics, Germany presented in Fig. 3.16 has been utilized to measure the IFTs between Angsi crude oil and various water phases containing alkali, surfactants and polymers. Spinning drop tensiometer is an improved instrument for the precise measurement of IFT between two fluid phases by means of a drop of the less dense fluid surrounded by the more dense fluid, both fluids spinning together in gyrostatic equilibrium. This technique eliminates departures from gyrostatic equilibrium which went unrecognized in the prior art. Operation of the instrument comprises the combined use of air bearings and sample-holder mountings which reduce vibrations and eccentricities, eliminate temperature gradients within the sample, and assure that the interfering hydrodynamic flows are suppressed.



Figure 3.16: SVT 20 spinning drop video tensiometer.

Spinning drop geometry can be described by considering the Fig. 3.17, in which the rotation takes place around axis “x”, and axis “y” denotes the distance from the rotation axis. The drop shape exhibits symmetry around axis “x”. The centrifugal acceleration is $\omega^2 y$ (ω is the rotational velocity), and it increases with the distance from the axis in such a way that the natural gravity effects are negligible. Hence the influence of the density difference between the two fluids increases with the distance from the axis and produces a pull of the interface toward the axis. It results in the elongation of the drop along the “x” axis, which is opposed by the IFT that tends to minimize the surface area, i.e. to make the drop shape more spherical. The principle of measurement of IFT with a spinning drop tensiometer can be discussed in the so-called Vonegut’s case [167] of an elongated drop in which the central part of the drop is essentially cylindrical, i.e. the radius of curvature at equator point E in the plane of Fig. 3.17 (R_m) is much larger than the radius of the slice cut (R_m), so that the curvature at point E may be approximated by the inverse of the radius of the cylinder ($1/R_m$). This approximation is valid whenever the length of the drop is at least 4 times compared to its diameter [168].

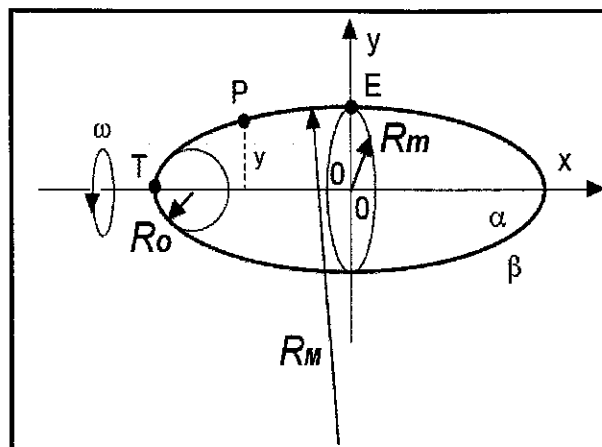


Figure 3.17: Geometry of a spinning drop of denser liquid α in less dense liquid β [168].

Prior to the IFT measurements densities and refractive indices (RI) of both of the phases should be known. Densities of both (oil and water) phases were measured using specific gravity bottles, whereas, the refractive indices were measured using ATAGO RX-5000 model digital refractometer presented in Fig. 3.18.

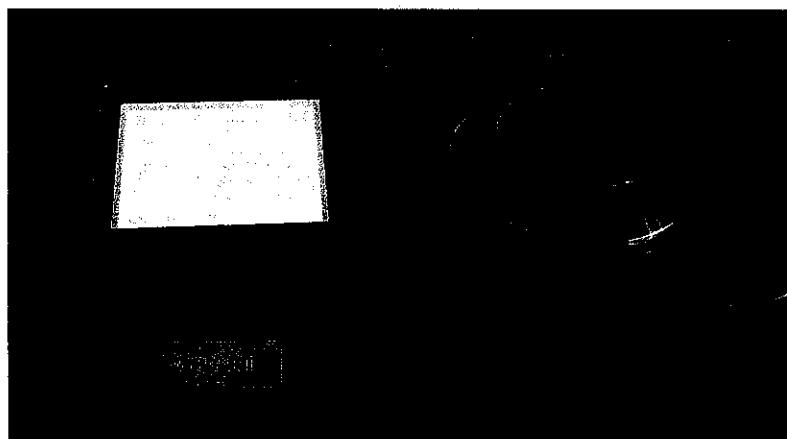


Figure 3.18: ATAGO RX-5000 model digital refractometer.

In the spinning drop method, the capillary tube was filled with water phase (dense phase) and an oil drop (light phase) was injected during rotation about its longitudinal axis at a high speed. In most cases in which surfactants were used, the rotation speed was maintained sufficiently high so that the length of the oil drop is greater than four times its diameter. The oil/water IFTs were calculated with a built-in software system according to the following equation:

$$\sigma = 3.42694 \times 10^{-7} (\rho_h - \rho_d) \omega^2 D^3, L/D \geq 4 \text{ ----- (3.19)}$$

where, σ is interfacial tension (dyne/cm), ρ_h the density of dense (outer) phase (g/cm^3), ρ_d the density of the light (drop) phase (g/cm^3), ω the rotational velocity (rpm), D the measured drop width (diameter) (mm), and L is the length of the oil drop (mm).

When measuring the interfacial tension, the oil droplet must be measured in equilibrium with any colloidal dispersion present within the aqueous phase containing alkali, polymer and surfactants. If the aqueous phase turbidity is too great, then no contrast may be obtained between the oil droplet and the aqueous phase. Furthermore, for an accurate measurement, it was ensured that the oil droplet and the aqueous phase achieve equilibrium. Spinning speed was gradually increased from 500 rpm to 6000 rpm in order to ensure that the radius of oil droplet remains constant for a given rotation speed. In this way, IFTs between various Angsi crude oil and aqueous phases were calculated.

3.8 Calculation of Partition Coefficients

Partition functions of surfactants between oil and water phases were estimated by measuring refractive index using ATAGO RX-5000 model digital refractometer. Known concentrations of the various surfactants were dissolved in Angsi crude oil and aqueous phases individually. Calibration curves between surfactant concentrations and refractive indices were plotted both for aqueous and hydrocarbon phases respectively. Later on known volume of aqueous surfactant solution, V_w of a known concentration, M_1 was mixed with a known volume of hydrocarbon, V_{hyd} phase. These oil and water phases were mixed together using magnetic stirrer at 30 °C for half an hour, allowed to stay overnight in order to ensure the achievement of equilibrium. Both the phases were separated from each other using the separating funnel and refractive indices were measured. Concentration of surfactant in each phase was estimated by comparing the obtained RI values with initially plotted calibration curves. Partition coefficients were calculated using the relationship given in Eq. 3.20 [4].

$$K = (M_{\text{hyd}} V_w) / (M_1 - M_{\text{hyd}}) \cdot V_{\text{hyd}} \text{-----} \quad (3.20)$$

3.9 Characterization of Oil-in-Water Emulsions

Sorption of surfactants from aqueous phase to hydrocarbon phase may lead to produce oil in water emulsion at oil-water interface during alkaline, polymer and ASP flooding process. Such kind of new surfaces cause the variations in interparticle forces and change the stability of the system. Electrostatic interactions between surfactants, polymers and reservoir rocks modify the nature of the surface from oil-wet to water-wet, amend the surface charge, and the electrical potential between various surfaces. Even though, the ASP flooding is expected to increase the oil production compared to the waterflooding techniques, it is faced with multifarious problems. One of these associated problems is production fluids which form stable oil-in-water emulsions and the separation of crude oil and water becomes difficult. Production of large amounts of oil-in-water emulsions of alkali, crude oil, water, polymer and surfactants may cause the oil recovery initially and finally needs additional cost to be separated into a surfactant-polymer-water layer and an oil-rich layer. In order to separate the water layer from the oil-rich, a demulsifier is required which can separate the aqueous and hydrocarbon phases. It is believed that the alkali added in the surfactant solution is the reason which causes this problem. The alkali added reacts with the acidic components in crude oil and form interfacially active components that accumulate at the oil/water interface and facilitates the formation of oil-in-water emulsion. However, the stability of this emulsion depends on the concentration of the reservoir formed alkali-oil surfactant at the interface. This again depends on the concentration of the potential acidic components from crude oil that form interfacially active soap components [5].

3.9.1 Atomic Force Microscopy (AFM)

Developments in the microscopy field, as in control, manipulation and measurement devices on a nanoscopic scale, led to the invention of the Scanning Tunneling Microscope (STM) by Binnig and Rohrer in 1982 [169]. Shortly afterwards, in 1986, Binnig, Quate and Gerber invented the Atomic Force Microscope (AFM) [170]. STM relies on measurement of exponentially decaying tunneling current between a metal

tip and a conducting substrate. While, not being restricted to conductive materials, AFM is a much more versatile technique than STM, and more adopted in studies applied to colloidal systems and soft matter. These days AFM is being applied in several fields of research, such as materials science and engineering, biochemistry and biology, in studies of the most varied phenomena, such as colloidal stability and emulsification [171], characterization of nanostructures and molecules [172], adhesion and delamination [173], surface elasticity [174], corrosion, etching, friction [175] and lubrication. The materials which are being widely investigated using AFM include emulsions, thin and thick film coatings, ceramics, composites, glasses, synthetic and biological membranes, metals, polymers, and semiconductors. The AFM is being applied to study various phenomena such as abrasion, adhesion, cleaning, corrosion, etching, friction, emulsification, lubrication, plating, and polishing. Various Angsi crude oil-water emulsions were prepared, in combination with SDS, CTAB, AOT and ATR surfactants in the presence and absence of Na_2CO_3 . In order to explain the emulsification phenomenon AFM micrographs of these emulsions were recorded using atomic force microscope, Agilent 4500, presented in Fig 3.19.

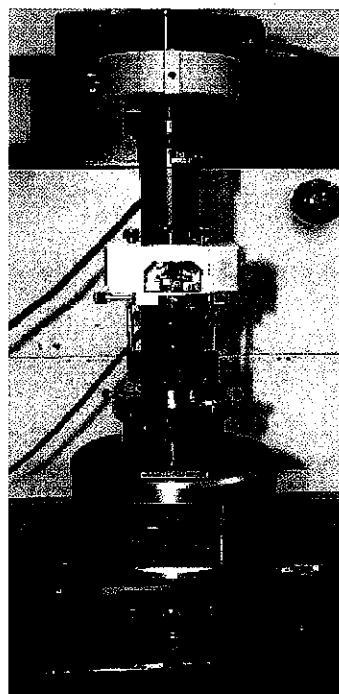


Figure 3.19: Agilent series 4500 AFM.

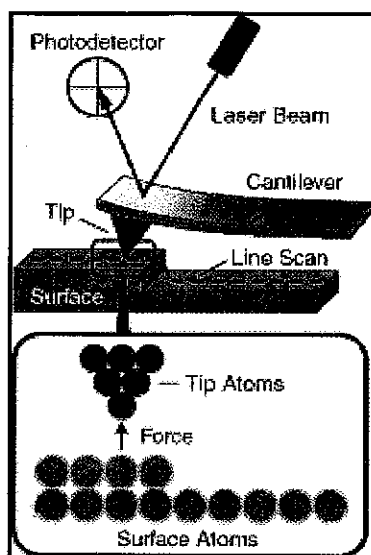


Figure 3.20: Schematic of AFM [176].

Schematic of AFM is given in Fig. 3.20. AFM works by bringing a cantilever tip in contact with the surface to be imaged. The sample surface is scanned by a sharp tip (radius 1-10 nm), which is integrated at the end of a very flexible cantilever on which a laser beam is directed to be deflected in a detector, consisting of a split diode. As the tip encounters height differences at the surface, it moves up and down, which in turn causes the cantilever to deflect up and down. This deflection is monitored, through the laser beam, by the detector. In this way, a profile of the scanned surface can be obtained depending on the sample. In fact an ionic repulsive force from the surface applied to the tip bends the cantilever upwards. The amount of bending, measured by a laser spot reflected on to a split photo detector, can be used to calculate the force. By keeping the force constant while scanning the tip across the surface, the vertical movement of the tip follows the surface profile and is recorded by the AFM. AFM has much broader potential and applications because it can be used for imaging the conducting or non-conducting surfaces.

3.9.2 Emulsion Stability

The emulsions stability was evaluated by analyzing the Angsi crude oil water emulsions volumetrically. Specified concentrations of SDS, 2000 ppm, AOT, ATR and mixture of ATR and AOT, 1500 ppm each, surfactants were used in combination with

0.1%, Na_2CO_3 to prepare 5% oil-in-water emulsions using brine solution of 10,000 ppm. The prepared emulsions were stored overnight to attain the equilibrium and the relative volumes of hydrocarbon phases being separated from emulsions were estimated [6].

3.10 Wettability through Contact Angle Measurements

Contact angle measurement is a well-known technique for investigating and controlling adhesion, wettability alteration, surface treatments, cleaning, and polymer film modification. The wetting of solid substrates is a basic feature of many natural and industrial processes and contact angle is a simple, rapid, and sensitive method of characterizing the wettability of a solid surface. It has been elaborated in sections 2.1.5 and 2.1.6 that the dynamic contact angle measurement is the suitable and preferred technique to elaborate the wettability alteration for oil recovery and other related processes. The contact angles of brine water containing various surfactants on sandstone substrates was measured by contact angle analyzer, Phoenix-300, SEO, Korea, presented in Fig. 3.21.

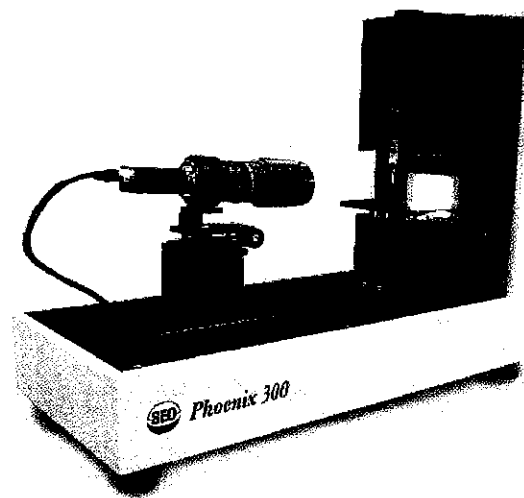


Figure 3.21: Contact angle analyzer Phoenix300.

Previously oil saturated sandstones from Angsi field were used as substrates to measure the contact angle of water with and without alkaline-surfactant-polymer formulations. Initially a pure water droplet was placed on the surface of oil-wet sandstone and respective contact angle was measured. Later on droplets from brine water in combination with SDS, AOT, ATR, mixture of ATR and AOT in the presence of

Na_2CO_3 were also placed on oil-wet sandstone and the respective contact angles were recorded.

3.11 Characterization of Sandstone Cores

Sandstone core samples were collected from Angsi field and characterized for weight, length, area, air permeability, bulk density, bulk volume, grain volume, grain density, pore volume and porosity. Weight of the cores was noted using analytical balance, whereas the length was measured using Vernier calliper. Air permeability, bulk density, bulk volume, grain volume, grain density, pore volume and porosity were measured with the help of helium porosimeter and air permeability meter of core labs Dallas, Texas as presented in Figs 3.22 and 3.23 respectively.

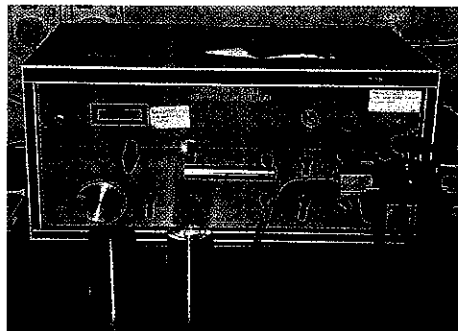


Figure 3.22: Extended range helium porosimeter.

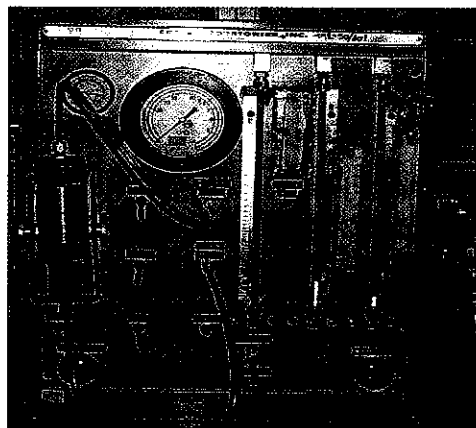


Figure 3.23: Air permeability meter.

3.12 Spontaneous Imbibition Studies

Laboratory scale spontaneous imbibition experiments were developed and conducted to measure accurately Angsi water imbibition in the presence and absence of surfactants and polymers. Actual and self designed imbibition cells are presented in Fig. 3.24. Angsi sea water was utilized for all the studies until unless specified otherwise. Previously characterized and cleaned sandstone core samples were initially saturated with synthetic brine solution containing 8% NaCl, 1% CaCl₂ and 1% KCl. The total uptake of water was checked against independent weighing of the sample before and after each experiment. These water-wet cores were treated with dodecane to convert them to oil-wet and saturated with Angsi crude oil, with 3.0 cp viscosity and 0.8238 g/cm³ density, under ambient conditions till the weight of core samples gained the constant value at least for 24 hrs. The volumes of crude oil saturated in the individual core samples were calculated on the basis of mass difference and volume of brine solution that was displaced as a result of spontaneous imbibition with crude oil. Further spontaneous imbibition studies were conducted under ambient temperatures and pressures using self designed imbibition cell, with and without alkali, surfactants and polymers. From the obtained results selected concentrations of alkali, surfactants and polymers were utilized for further core flooding experiments.

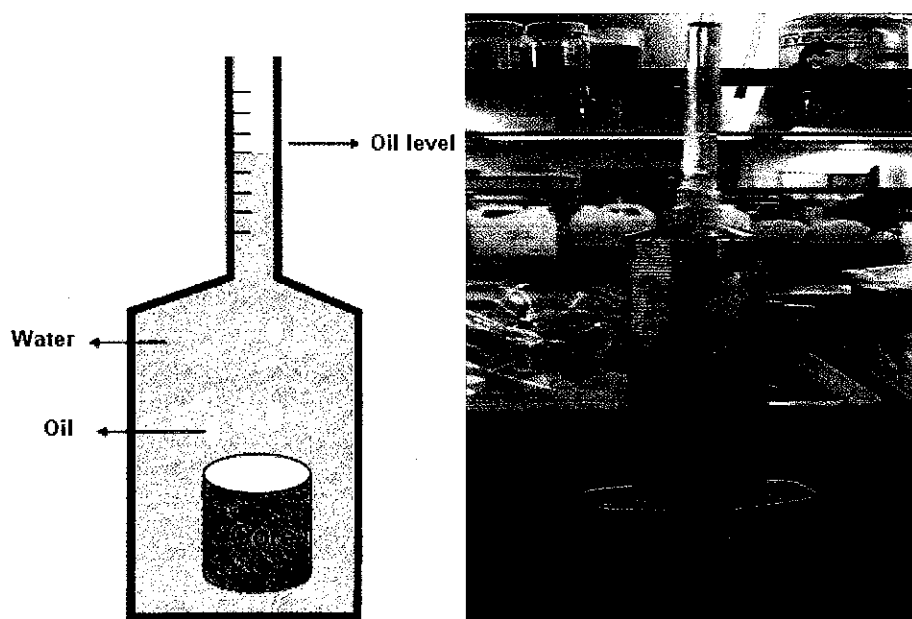


Figure 3.24: Actual (L) and self designed (R) imbibition cells.

3.13 BET Surface Area and Pore Structure Measurements

Surface area and porosity are important characteristics in EOR processes, capable of affecting the quality and utility of various chemicals being utilized to the enhancement of trapped oil. For this reason it is important to determine and monitor them accurately during chemical flooding. The most widely used technique for estimating surface area is the BET method (Brunauer, Emmett and Teller) [177].

The Micrometrics ASAP 2000 model, shown in Fig. 3.25, was used to measure surface area and pore size of the sandstone core samples before and after imbibition and core flooding experiments. This equipment utilizes the gas (nitrogen) adsorption function of materials to estimate both the surface area and pore size.

In order to understand the theoretical background about BET method let suppose that the surface of the substrate is an array with N_s identical adsorption sites. No more than one atom can occupy one site and the atoms do not interact between each other. In the grand canonical ensemble, each site's grand partition function can be written as:

$$\Sigma_s = 1 + z \exp \{ \beta (\mu - E_0) \} \text{ ----- (3.21)}$$

E_0 is the surface binding energy; z is the partition function associated with possible internal degrees of freedom at every site (sometimes may be taken as unity); β is the inversed temperature and μ is the chemical potential of the film.

where, $\beta = 1/K_B T$ and the grand canonical free energy is:

$$\Omega = - (1/\beta) \ln \Sigma_s = - (N_s/\beta) \ln \Sigma_s \text{ ----- (3.22)}$$

Since the mean number of particles in the ensemble satisfies:

$$N = - (\partial \Omega / \partial \mu)_\beta \text{ ----- (3.23)}$$

The fractional occupation can be written in terms of Langmuir adsorption isotherm as follows:

$$\theta = N/N_s = p/(p + p_L) \text{ ----- (3.24)}$$

The characteristic scale of pressure is:

$$p_L = (g/z\beta\lambda^3) \exp(\beta E_0) \text{ ----- (3.25)}$$

Here $\lambda = \sqrt{2\pi\beta\hbar^2/m}$ is the de Broglie thermal wavelength and g is the spin degeneracy of the atom. The Langmuir isotherm shows the coverage grows linearly at low p according to Henry's law and saturates at $p \gg p_L$.

Brunauer, Emmett & Teller have extended this lattice gas model to the case of multi-layer films. Their model allows the particles to occupy a 3D array of sites above the surface. The interactions between the sites are neglected, but the sites closest to the substrate experience additional attraction V_1 . The relative probability, exactly N sites above a given surface to be occupied, is proportional to the corresponding term in the grand partition function for this site:

$$\Sigma_s = 1 + c \sum_{N=1}^{\infty} Z^N \exp(N\beta\mu) \text{ ----- (3.26)}$$

Here $c = \exp(-\beta V_1)$ and z is the internal partition function per site of the bulk adsorbate. Thus, analogously to the Langmuir isotherm one obtains the BET isotherm:

$$\frac{p}{p_L} \frac{N_s}{\left(1 - \frac{p}{p_L}\right)^N} = \frac{1 + \frac{p}{p_L}(c-1)}{c} \text{ ----- (3.27)}$$

On the basis of this isotherm, by measuring the number of gas molecules adsorbed in the first layer, specific surface area of the substrate can be calculated [178,179].

The samples were degassed at 120 °C overnight and then nitrogen gas was inserted, in steps, into the evacuated sample chamber. Gas molecules that stick to the surface of the adsorbent are said to be adsorbed and tend to form a thin layer that covers

the entire adsorbent surface. The number of molecules required to cover the adsorbent surface with a monolayer of adsorbed molecules can be estimated, and the surface area was calculated with the help of built in software that use the BET method. By continuing the addition of gas beyond the monolayer formation, the equilibrium adsorbate pressures approach saturation producing an adsorption isotherm. By measuring the volume of gas absorbed by the test material across a range of pressures, the data was analyzed by the built in software and the pore sizes were computed from equilibrium gas pressures. As the equilibrium adsorbate pressures approach saturation, the pores become completely filled with adsorbate. Knowing the density of the adsorbate, the volume can be calculated which the gas occupies and hence the total pore volume of the sample can be calculated.



Figure 3.25: Micrometrics ASAP 2000 surface area and pore size analyzer.

3.14 Scanning Electron Microscopy/Energy Dispersive X-ray Analyses

Scanning electron microscopy and energy dispersive analyses (SEM/EDX) can be used to determine the elemental composition and observe structural and surface morphology for various substances. Understanding of the elemental composition, surface and morphological properties of the rock samples is rapidly becoming an essential requirement for EOR processes. Using the SEM/EDX analyses technique it is possible to measure the chemical and physical composition of any solid material. Particularly considering the complexity of the mechanisms involved in CEOR processes SEM/EDX is being utilized to understand and control the surface and morphological properties of the oil wells [180].

3.14.1 Principle of SEM

SEM is a type of electron microscope capable of producing high-resolution images of a sample surface. In a typical SEM, electrons are thermionically emitted from a tungsten or lanthanum hexaboride (LaB_6) cathode and are accelerated towards an anode; alternatively, these electrons can be emitted via field emission (FE). Tungsten is used because it has the highest melting point and lowest vapor pressure among all the metals, thereby allowing it to be heated for electron emission. The electron beam, which typically has an energy ranging from 100 eV to 100 keV, is focused by one or two condenser lenses into a beam with a very fine focal spot of 1 nm to 5 nm size. The beam passes through pairs of scanning coils in the objective lens, which deflect the beam horizontally and vertically so that it can scan the sample in a raster fashion over a rectangular area of the sample surface. When the primary electron beam interacts with the sample, the electrons lose energy by repeated scattering and absorption within a teardrop-shaped volume of the specimen known as the interaction volume, which extends from less than 100 nm to around 5 μm into the surface. The energy exchange between the electron beam and the sample results in the emission of electrons and electromagnetic radiation which can be detected to produce SEM image. Two sorts of electrons are produced from the interaction of the electron beam with the sample surface, secondary electrons and backscatter electrons. Secondary electrons are the result of the high-energy

electron beam displacing loosely held surface electrons that are then recorded using a secondary electron detector to produce an image of the surface. Secondary electrons are more dependent upon the surface area within a given area of intersection of the beam and therefore relate to topographic features. Backscatter electrons are high-energy electrons from the primary beam that are scattered back out of the sample by the atomic nuclei. The intensity of the signal is dependant upon the mean atomic number of the area of interaction [181,182]. Simple schematic diagram of SEM showing its major components is presented in Fig. 3.26.

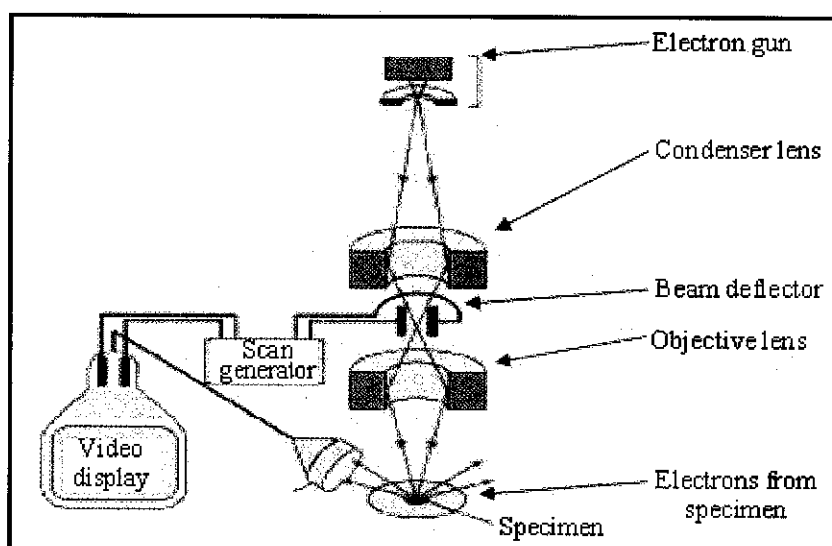


Figure 3.26: Schematic of scanning electron microscope [181].

3.14.2 Principle of EDX

An energy-dispersive x-ray analyzer (EDX) is a common accessory which gives the scanning electron microscope (SEM) a very valuable capability for elemental analyses. EDX uses a solid-state cooled detector system to detect and measure individual X-ray pulses from the point of interaction that takes place between the primary electron beam and the sample electrons. As a result of these interactions electrons are knocked out of orbits within the atom. Vacancies are filled by electrons from higher energy outer electron shells with a consequent loss of energy. The energy photon is emitted as an X-ray. The energy (or wavelength) of the X-ray is characteristic of both the element and the energy level transition and provides a direct means of elemental identification at the point of electron beam interaction. Segregation of the X-rays is conducted by either

wavelength dispersive means that measures the intensity of a single wavelength peak, or by energy dispersive techniques that give a wide spectrum of energies but with poorer resolution. A single spectrum will detect elements from carbon upwards in the periodic table, although some significant peak overlaps may occur as well. Quantification is based on real standards and mathematical models of the interactions and secondary fluorescence and absorbance processes. Figure 3.27 illustrates the interaction of an electron beam (in red) with a specimen (shaded blue). The electron beam in an SEM has energy typically between 5,000 and 20,000 electron volts (eV). The energy holding electrons in atoms (the binding energy) ranges from a few eV up to many kilovolts. Many of these atomic electrons are dislodged as the incident electrons pass through the specimen, thus ionizing atoms of the specimen. This process is illustrated schematically in the inset box of the figure. Ejection of an atomic electron by an electron in the beam ionizes the atom, which is then quickly neutralized by other electrons. In the neutralization process an x-ray with an energy characteristic of the parent atom is emitted. By collecting and analyzing the energy of these x-rays, the constituent elements of the specimen can be determined [183].

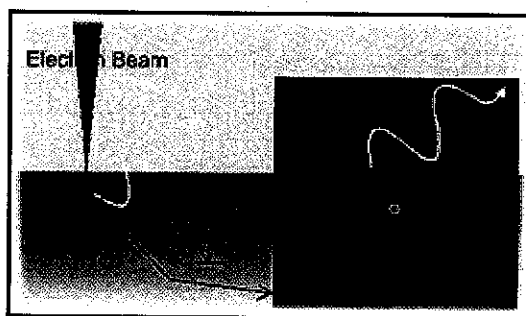


Figure 3.27: Interaction of an electron beam with specimen in EDX [183].

SEM/EDX analyses of the core samples were carried out using Zeiss DSM-950 model electron microscope from Germany as presented in Fig. 3.28. Small chips containing freshly broken dried rock samples were glued and mounted to an aluminum sample stub for gold-palladium coating prior to be exposed to the electron beam and SEM images, EDX patterns were recorded respectively.

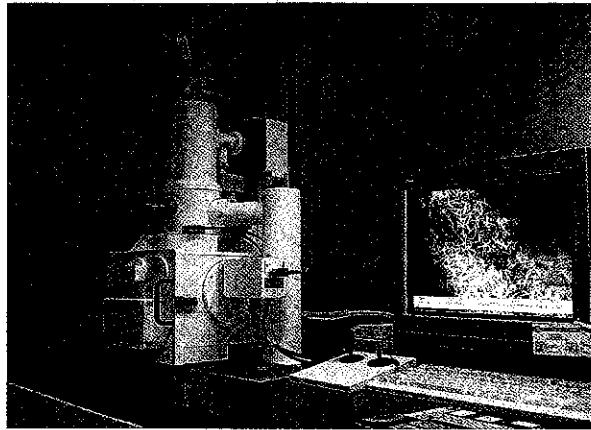


Figure 3.28: Zeiss DSM-950 SEM/EDX electron microscope.

3.15 Core Flooding Studies

Core-flooding experiments are important to perform the flow experiments according to the actual reservoir conditions regarding temperature and pressure. The performance of the injected chemicals like polymer, surfactants and alkalis can be analyzed by considering the selective effects on water/oil or water/gas permeability and mobility/permeability reduction can be determined in a broad range of injection rates. Cores and crude oil samples were collected from Angsi field and characterized prior to core-flooding experiments. Core-flood apparatus, Fig. 3.29, manufactured by TEMCO, Inc., Tulsa, USA that can withstand pressures upto 10,000 psi was utilized for the chemical flooding experiments.

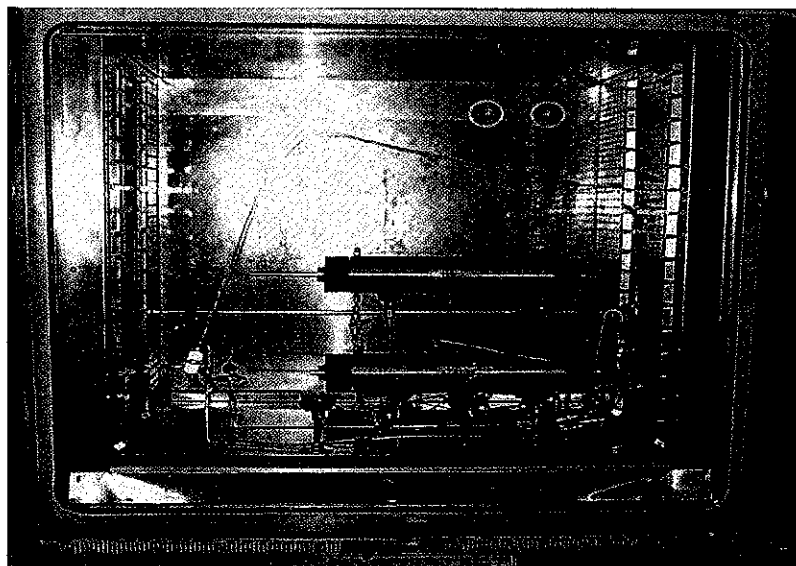


Figure 3.29: Coreflooding system by Temco, USA.

Schematic diagram of the experimental setup used in this study is presented in Fig. 3.30. It consists of a core holder, pumps for fluid injection, pressure gauges to control and measure the pressure during flooding experiments, fraction collector and read out devices.

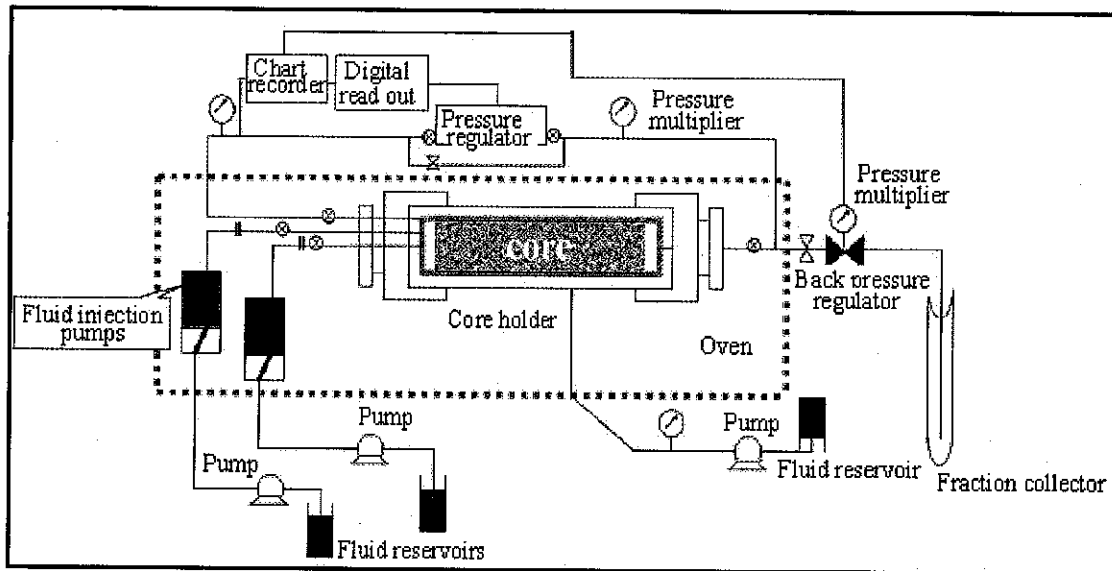
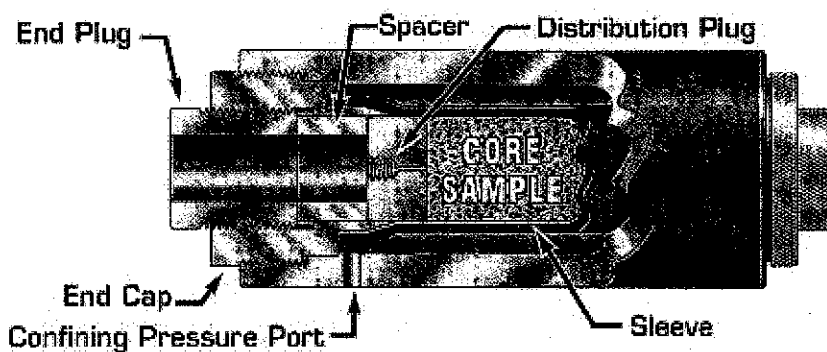
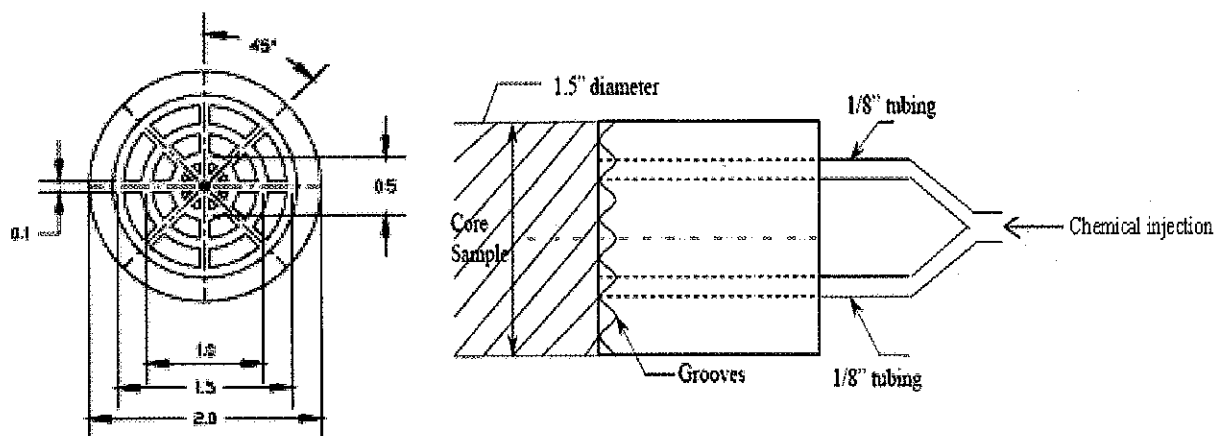
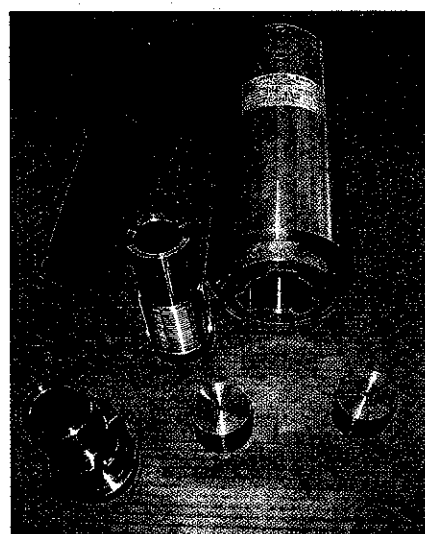
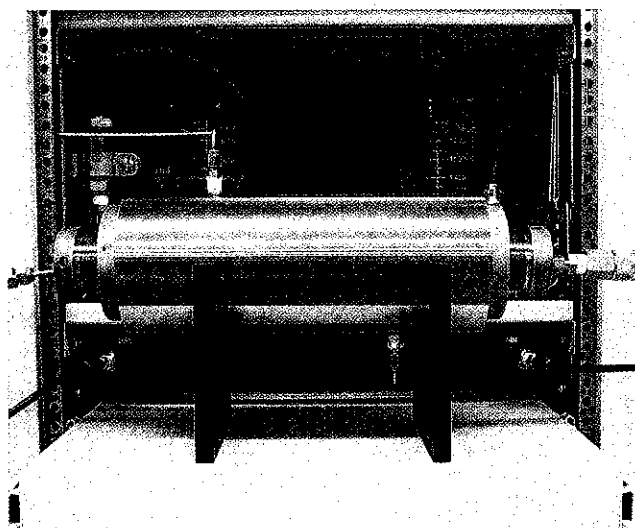


Figure 3.30: Schematic diagram of coreflooding system.

Dried and cleaned sandstone cores from Angsi field were characterized following the procedures as mentioned in 3.11. These characterized sandstone core samples were saturated with synthetic brine solution containing 8% NaCl, 1% CaCl₂ and 1% KCl at 2,000 psi. The saturation was performed by loading the core samples in the heat resistant rubber sleeve. This assembly was then placed in the core holder with the end pieces clamped over the sleeve and caps were fixed. A Hassler type, stainless steel core holder model HCH-1.5 designed for consolidated core samples up to 12 inches in length was used. The holder was also manufactured by TEMCO, Inc., Tulsa, USA and can withstand pressures upto 10,000 psi. A cross sectional, sectional and photographs of the core holder are shown in Fig. 3.31. A confining pressure of 2,000 psi was applied to the core holder. Vacuum was then applied to the core samples for 12 hours. A known amount of brine solution was then injected to saturate the core, while the evacuation was continuing. After the appearance of brine solution at the outlet, vacuum was stopped immediately while flooding was continued long enough to ensure 100% saturation.



(A) Cross sectional (L) and sectional (R) view of inlet end plug of core holder (C)



(B) Photographs of core holder.

Figure 3.31: Specifications and views of core holder.

The total uptake of brine solution was monitored against independent weighing of the sample before and after each experiment and the obtained experimental pore volumes were compared with the calculated pore volumes which were initially recorded.

The core sample was housed inside a viton rubber sleeve, which is held in place by two ferrules. Each ferrule rests on one end of the core holder body where an 'O' ring which is placed in a groove around the rim of the body. These ferrules are pressed against the holder's body by two screw-on end caps. An end plug made of stainless steel was inserted into each end of the sleeve and is pressed against the core sample by a retaining screw, which threads through the end cap. Both end plugs have circular grooves to ensure fluid injection into and production from the entire cross-section of the core as shown in Fig. 3.31 a (R). The annular space between the sleeve and the core holder body is filled with a confining fluid and is pressurized up to the desired pressure. This pressure prevents fluid by-pass around the core and ensures good sealing between the ferrules and sleeve. Later on the core samples were individually placed in core holder assembly, placed in the oven containing the separate reservoirs for crude oil and injected fluid, to attain the required temperature. The system was left overnight for temperature equilibrium to be attained and flushed with Angsi crude at 90 °C and confining pressure of 2,000 psi. Volumes of the crude saturated inside the cores were estimated on the basis of the volumes of brine solution that were displaced as a result of forced imbibition by Angsi crude oil. The dead volumes of all the flow lines were measured and accounted for in all the material balance calculations.

These crude oil saturated cores were individually flushed with brine solution and fractional recoveries of oil were recorded. Chemical flooding run for each core was started with polymer flooding by injecting the Hybomax polymer at concentrations of 1500 ppm with flow rate of 0.5 ml/min. The fractional enhanced oil recoveries from each core sample were recorded. In order to assure that no more remaining oil can be squeezed out, the core was flushed with another extra 200 ml of the polymer solution. After that 2000 ppm of conventional surfactant SDS and 1500 ppm of each AOT, ATR and ATR:AOT (1:9) was separately added into the brine solution containing polymer which was initially utilized for flushing from cores 1 – 4 respectively. This brine solution

containing polymer and respective surfactant was incorporated to flush the core sample with flow rate of 2 ml/min. The additional fractional enhanced oil recoveries from each core sample were recorded independently. Again when no more oil was recoverable, each core was flushed with another extra 200 ml of the brine solution containing polymer and respective surfactant. At the last stage, 0.1 and 0.05 % of Na_2CO_3 for conventional and non-conventional surfactants respectively, were added into the same brine solution containing polymer and respective surfactant that was utilized for flushing to the respective core samples. Each core was flushed by the respective brine solution, with a flow rate of 3 ml/min, having alkali, surfactant and polymer which is generally known as ASP flooding. During each flood, pressure drop, oil and brine production were continuously monitored. The flushing was kept in process for each core till no more oil recovery was observed. Further enhanced oil recoveries as a result of polymer, surfactant and alkaline flooding were carefully estimated.

3.16 Surfactants Adsorption and Kinetics Studies

Adsorption of surfactants from aqueous solutions in porous media is having tremendous technical important in EOR because surfactant loss due to adsorption on the reservoir rocks not only impairs the effectiveness of the chemical slurry injected to reduce the oil–water IFT but also renders the process economically unfeasible. Generally, adsorption can be categorized in three classes i.e. ion exchange adsorption, physical adsorption and chemical adsorption. Exchange adsorption is the result of electrostatic interactions, having the ion charge as the principal determining factor of the strength of the attraction to a site of opposite charge. Physical adsorption results from Vander Waals forces. The adsorbed molecule is not affixed to a specific site at the surface but is free to undergo translational movement within the interface. It is predominantly a low temperature phenomenon, characterized by a relatively low energy of adsorption. Physical adsorption is usually a reversible process; an increase in temperature causes a decrease in adsorption efficiency and capacity. Chemical adsorption is a chemical interaction between the surfactant and surface mineral. This bonding leads to a change in the chemical form of the adsorbed compound, and is not reversible. Adsorption of surfactants at the solid/liquid interface is strongly influenced by the type and specific

properties of the surfactant's molecule, the solvent conditions, such as pH, salinity (Na^+ , Cl^- , Ca^{2+} , Mg^{2+} , etc), surface type and nature of adsorbing subsurface like surface area, etc and environment of the aqueous phase such as temperature and flow rate, etc [184].

3.16.1 Langmuir and Freundlich Adsorption Isotherms

A number of adsorption isotherms are available in literature that can be implemented to elaborate the adsorption mechanism. However, in this study Langmuir and Freundlich adsorption isotherms were used to explain the adsorption of various surfactants on sandstone cores. Effects of temperature, salinity, pH and polymer concentration on adsorption intensity have been investigated using Langmuir and Freundlich isotherm models. The linearized forms of Langmuir and Freundlich isotherm models are given in Eqs. 3.27 and 3.28 respectively [7,185].

$$C_e/q_e = C_e/q_{\max} + 1/b.q_{\max} \text{-----} (3.28)$$

$$\ln q_e = \ln K_F + (1/n) \ln C_e \text{-----} (3.29)$$

where, q_e and C_e are the amount of surfactant adsorbed per gram of the sandstone core and concentration of surfactant in adsorbate solution at equilibrium, respectively. q_{\max} is the maximum adsorption at monolayer coverage, b the adsorption equilibrium constant related to the energy of adsorption, K_F is the Freundlich constant representing the adsorption capacity and n is a constant related to surface heterogeneity.

The amount of surfactant adsorbed per unit mass of the sandstone cores at equilibrium, q_e , was calculated by Eq. 3.29:

$$q_e = V(C_0 - C_e)/m \text{-----} (3.30)$$

where, V is the volume of the solution of surfactant (L), C_0 and C_e are the initial and equilibrium concentrations, respectively (mM) and m is the mass of respective sandstone core (g). Eq. (3.29) provides q_e in mM surfactant adsorbed per gram of sandstone core.

Circulation experiment, were carried out by following the schematic presented in Fig. 3.32, to study the adsorption behavior of various surfactants on previously characterized and brine (8% NaCl, 1% KCl, 1% CaCl₂) saturated sandstone samples from Angsi field. Schematic of the circulation apparatus consists of a flask with a surfactant solution of known weight and concentration, a core of known pore volume (PV) and weight. A known concentration of respective surfactant solution was circulated through the sandstone cores. The total volume of circulated fluid was 200 cm³, including the volumes in the flask, tube and pore volume of core.

Initially the surfactant's solutions i.e. 2000 mg/L for SDS, 1500 mg/L for AOT, ATR and ATR:AOT (1:9) respectively were prepared in the brine solution and circulated at constant temperature (90 °C) and injection rate (1 cm³/min) until the adsorption equilibrium was achieved. During circulation at regular time interval of five minutes the remaining concentration of the respective surfactant was estimated by measuring the refractive index as mentioned in 3.8. Similar procedure was repeated to evaluate the adsorption in the presence of alkali. Surfactant's solutions were prepared in brine solution along with alkali and circulated in the core sample at constant temperature, 90 °C with injection rate of 1 cm³/min. Refractive indices of the surfactants solutions in the presence of alkali with known concentrations were initially recorded and later on remaining concentration of the surfactant was estimated by refractive index measurements whereas the remaining concentrations of alkali were estimated by acid base titration using phenolphthalein as an indicator.

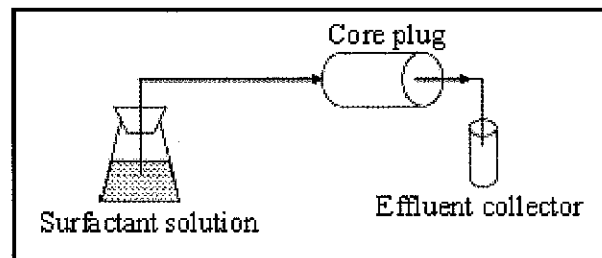


Figure 3.32: Schematic of circulation process.

The obtained data for the adsorption of SDS, ATR, AOT and ATR:AOT (1:9) in the presence and absence of alkali was analyzed using Langmuir and Freundlich

adsorption isotherms. Values for q_{\max} , maximum adsorption at monolayer coverage, b the adsorption equilibrium constant, K_F , the Freundlich constant and n , surface heterogeneity were obtained from the slope and intercept of the obtained isotherms.

3.16.2 Adsorption Kinetics

The prediction of adsorption kinetics is necessary for the design of a process because it can explain how fast or slow the rate of adsorption will be. As it is already mentioned that the nature of adsorption process mainly depends on physicochemical characteristics of the adsorbent and system conditions like temperature, salinity, pH, etc. Measurement of adsorption rate constants can be an important physico-chemical parameter to evaluate the basic qualities of a reservoir suitable for chemical flooding. In appropriate chemical flooding processes the adsorbate molecules diffuse into the interior of the porous rocks to reach mille pores and micro pores level. In order to observe the adsorption kinetics of various surfactants (SDS, ATR, AOT and ATR:AOT) on sandstone cores three kinetic models were implemented, including pseudo-first-order, pseudo-second-order and intra-particle diffusion model. Batch studies were performed with known mass of the sandstone samples in the presence of 0.1% Na_2CO_3 and 2000 ppm, SDS and 1500 ppm each of ATR, AOT and ATR:AOT (1:9).

3.16.3 Pseudo-first-order Model

The pseudo-first-order equation can be written as [7,185]:

$$dq_t/dt = k_f(q_e - q_t) \text{-----} (3.31)$$

where, q_t (mg/g) is the amount of surfactant absorbed at time t , q_e (mg/g) the adsorption capacity in equilibrium, $k_f = K_1^{\text{st}}$ (min^{-1}) the rate constant for pseudo-first-order model and t (min) is the time. After definite integration by applying the initial conditions i.e. $q_t = 0$ at $t = 0$ and $q_t = q_t$ at $t = t$, the Eq. 3.30 becomes:

$$\log(q_e - q_t) = \log q_e - k_f \cdot t / 2.303 \text{ ---} (3.32)$$

Adsorption rate constants (K_1^{st}) for the adsorption of various surfactants by sandstone cores in the presence of alkali were calculated from the slope and intercept of the plots of $\log (q_e - q_t)$ vs. t .

3.16.4 Pseudo-second-order Model

The pseudo-second-order model can be presented in the following form [7,185]:

$$dq_t/dt = k_s (q_e - q_t)^2 \text{ ----- (3.33)}$$

where, $k_s = K_2^{nd}$ (min^{-1}) is the rate constant of pseudo-second-order model. Definite integration of Eq. 3.32 for boundary conditions $q_t = 0$ when $t = 0$ and $q_t = q_t$ at $t = t$, the following form of equation can be obtained:

$$t/q_t = 1/(k_s q_e^2) + (1/q_e)t \text{ ---- (3.34)}$$

The initial adsorption rate constant, h (mg/g.min), at $t = 0$ can be defined as:

$$h = k_s q_e^2 \text{ ----- (3.35)}$$

Pseudo-second-order rate constants K_2^{nd} (min^{-1}) for the adsorption of various surfactants on sandstone cores in the presence of alkali were obtained from the slope and intercept of the plots of t/q_t vs. t for various surfactant's systems.

3.16.5 Intra-particle-diffusion Model

An empirically functional relationship, common to the most adsorption processes, is that the uptake by various adsorbents varies almost proportionally with $t^{1/2}$, the Webere Morris plot, rather than with the contact time, t [186]:

$$q_t = k_{id} t^{1/2} + C \text{ ----- (3.36)}$$

where, k_{id} is the intra-particle-diffusion rate constant. According to Eq. 3.35, a plot of q_t vs. $t^{1/2}$ should be a straight line with a slope K_{id} and intercept C when adsorption

mechanism follows the intra-particle diffusion process. Values of intercept provide an idea about the thickness of boundary layer, i.e., the larger the intercept the greater will be the boundary layer effect. However, the deviation of straight lines from the origin can be attributed to the difference in rate of mass transfer in the initial and final stages of adsorption [7]. The values of K_{id} for the adsorption of various surfactants on sandstone cores in the presence of alkali were obtained from the slopes of straight line plots for q_t vs. $t^{1/2}$.

3.17 Summary

Various techniques and methods that were utilized for the analyses have been elaborated by explaining the theoretical background and involved mechanisms. Volumetric and atomic absorption spectroscopic methods which were implemented for water analyses have been elucidated. Viscosity measurement and shear thinning behavior of polyacrylamide has been enlightened. TGA and its importance to explain the temperature stability of various chemicals including polymers and surfactants has also been presented. FTIR-ATR spectroscopy has been implemented to elaborate the interactions between various components that have been proposed for ASP flooding. Available methods for the measurement of IFT have been discussed, generally and spinning drop tensiometer has been explained particularly. Calculation of partition functions of surfactants in oil-water systems has also been described. Atomic force microscopy and contact angle measurements were applied to understand the emulsification and wettability phenomenon respectively. Characterization methods for sandstone cores including permeability, porosity, surface area, pore size, pore volume, etc were elaborated as well. Spontaneous and forced imbibition has been explained using imbibition cell and coreflooding equipment respectively. Scanning electron microscopy has also been explained with reference to the morphology of the core samples. Langmuir and Freundlich adsorption isotherms, pseudo-first-order, pseudo-second-order and intra-particle diffusion models have been elaborated to understand the adsorption mechanism and kinetics involved in chemical flooding processes.

CHAPTER 4

4. RESULTS AND DISCUSSION

This chapter has been organized into various sections. General characteristics of the Angsi field, Angsi crude assay and Angsi Sea and formation water analyses are reported and critically analyzed in section 4.1. Viscosity measurements of polyacrylamide solutions as a function of polymer concentration and roles of temperature, alkali and surfactants towards viscosity will be presented in section 4.2. Thermal stabilities of the polymers and surfactants will be reported and evaluated in terms of structure-property relationship and applicability for EOR activity in section 4.3. FTIR-ATR spectra of the individual components and proposed formulations will be reported and compared in section 4.4 to analyze the synergistic effects and compatibility. Time dependency of IFT reduction at crude oil-water interfaces will be assessed and examined in section 4.5. Atomic force micrographs of oil-water emulsions and emulsion stability will be analyzed in section 4.6. Partition functions of various surfactants in aqueous and organic phases will be presented and related to the respective molecular structures in section 4.7.

Wettability alteration from oil-wet to water-wet will be evaluated and reviewed in section 4.8. The initial characterization parameters for sandstone core samples are provided in section 4.9. Laboratory scale spontaneous imbibition studied will be reported and analyzed in section 4.10 to elaborate the role of ASP for screening and evaluation of chemicals. BET surface area, pore structure, SEM and EDX analyses of cores, prior and later to imbibition studies will be reported and discussed in sections 4.11 and 4.12 respectively. The results of spontaneous imbibition studies will be compared with ASP and LASP formulations using industry accepted core flooding protocol and will be shown in section 4.13. Surfactants adsorption, kinetics on sandstone cores and role of alkali in minimizing the adsorption capacity will be reported in section 4.14.

4.1 Characteristics of Angsi Field

The Angsi field, a deepwater site, is located in the Malay Basin, about 106 miles off the East Coast of Peninsular Malaysia, the coast of Terengganu in a water depth of 6,339m. It is the largest integrated oil and gas development project in Malaysia which was undertaken by Petronas Carigali and ExxonMobil Exploration and Production Malaysia in 1997. It consists of four drilling platforms and one production platform. The major oil bearing reservoirs are the I-35 and I-68 sands, while the major gas bearing reservoirs are the I-1, I-85, I-100 and the tight K-group sands. This field is a testimony of Petronas commitment towards enhancing indigenous exploration, production processes and technologies in efforts to augment Malaysia's oil and gas reserves for the future. The field began its oil production on 21st December 2001 with an initial flow of 15,000 barrels per day (BPD), while its gas production started at about 60 million standard cubic feet per day (SCFD) [187]. As a result of ever increasing demands and declining recoveries, efforts are on the way to enhance the oil production from existing reserves. A protocol is now presented to evaluate and then recommend a production enhancement strategy using combination of chemicals.

General characteristics of Angsi field are presented in Table-4.1. Its lithology is sandstone in nature with an average porosity, permeability and current pressure of 22%, 200 mD and 2199.93 psi respectively. A huge amount of remaining recoverable reserves is still there that can be recovered. Oil viscosity and density are 3 cp under reservoir conditions and 0.827 g/cm³ respectively. Depending upon the presence of light crude, reasonable porosity and permeability values, this oil field can be considered as a suitable candidate for the implementation of chemical flooding to enhance oil production. However, the presence of a high salinity value of 10,000 ppm (formation water) and 20,000 ppm (injection water) are impediments against chemicals-fluid compatibility (Table 4.1).

Table 4.1: Characteristics of Angsi Field*

Parameters	Quantity	Units
Carbonate Contents	7	ppm (IW)
	110	ppm (FW)
Formation Thickness	31	meters
Average Porosity	22	%
Permeability	200	mD
Oil Viscosity (Reservoir Conditions)	3	cp
Oil Density (at 20 °C)	0.827	g/cm ³
Formation Temperature	119	°C
Clay contents	4 - 29	%
Salinity of Brine	20,000	ppm (IW)
	10,000	ppm (FW)
Saturation Pressure	2514.95	psi
Current Pressure	2199.93	psi
Reservoir Depth	1730 - 1761	meters
Initial OIP	26,757,600	m ³
Cumulative Produced Oil	19,0785	m ³
Remaining Recoverable Reserves	102,07000	m ³
Total Recoverable Reserves	103,97785	m ³
Lithology	Sandstone	-

* By the courtesy of Petronas Research and Scientific Services (PRSS)

4.1.1 Angsi Crude Assay

Each crude oil has unique molecular characteristics which are important to be considered and understood prior to the implementation of an oil recovery method. Angsi crude assay is presented in Table-4.2. It can be observed that wax content, asphaltenes and total acid number are 14.1 wt%, <0.50 wt% and 0.478 mgKOH/g respectively. The concentrations of trace elements like Na, K, Cu, Pb, Fe, V and As are less than 1 ppm by wt, whereas the concentration of Ni is 2 ppm by wt. Crude oils with asphaltenes of less than its wax contents and are slightly acidic in nature are considered as suitable candidate for ASP flooding. As a result of the interactions between acidic components of the crude (naphthene) and the extraneously injected alkali the chances for sponification are less compared to emulsification implying that there is a reduced risk of the precipitation of trace metals. The concentration of the surfactant retained by the hydrocarbon phase is beneficial in solubilizing the asphaltene and keeps the tendency of wax formation in check. Kinematic viscosity is expected to decrease as the fluids behave like a pour point depressant. The problems of flow retardation, deposit formation as caused by the

presence of asphaltenes and wax formation in crude oils are likely to be suppressed in the presence of ultralow concentrations of surfactants. At lower temperatures, the asphaltenes and wax crystallize gradually in the form of needles and thin plates. As crystallization progresses, these needles and thin plates turn into 3-D networks causing solidification of the crude; particularly if the crude is very waxy.

Table 4.2: Angsi Crude Assay*

Test	Method	Units	Results
API gravity	ASTM D1298	degree	40.17
Water content	ASTM D4006	vol. %	<0.025
Flash point	IP 170	°C	<25
Pour point	ASTM D97	°C	+ 30
ASTM color	ASTM D1500	-	>8.0
Total acid number	ASTM D664	mg KOH/g	0.478
Total sulfur	ASTM D4294	wt %	0.0392
Salt content	IP 265	lb/1000 bbls	11.5
Nitrogen content	ASTM 4629	ppm wt	170
Ash content	ASTM D482	wt %	0.002
Gross calorific value	ASTM D240	MJ/kg	45.85
Wax content	DIN 52015	wt %	14.1
Asphaltenes	ASTM D3279	wt %	<0.50
Refractive index @ 20 °C	ASTM D1218	-	1.4436
Cetane index	ASTM D976	-	51.7
Mercury (Hg)	UOP 938	ppb wt	8
Sodium (Na)	IP 501 (modified)	ppm wt	<1
Potassium (K)	IP 501 (modified)	ppm wt	<1
Copper (Cu)	IP 501 (modified)	ppm wt	<1
Lead (Pb)	IP 501 (modified)	ppm wt	<1
Iron (Fe)	IP 501 (modified)	ppm wt	<1
Nickel (Ni)	IP 501 (modified)	ppm wt	2
Vanadium (V)	IP 501 (modified)	ppm wt	<1
Arsenic (As)	IP 501 (modified)	ppm wt	<1

* By the courtesy of Petronas Research and Scientific Services (PRSS)

Surfactants have the ability to prevent the formation of 3-D networks by retarding the agglomeration and growth of waxy crystals by producing numerous tiny crystals. Change in crystal shape diminishes the ability of waxy aggregates to intergrow and interlock, resulting in a lowered pour point of the crude and an improved oil flow. The underlying mechanism involves the formation of a monolayer coating on the surface of the asphaltene and wax crystal by adsorption; keeping the entire system dispersed. The

other benefits of surfactants involve the enhanced lubrication, extreme stability to oxidation and corrosion inhibition.

4.1.2 Angsi Sea Water Analyses

Sea water from Angsi field has been analyzed for total hardness, calcium hardness, magnesium hardness, chlorides, carbonates, bicarbonates, density, pH and sulfates. Total dissolved solids and resistivity were estimated conductometrically and the concentrations of Na^+ , K^+ , Fe^{2+} , Sr^{2+} and Ba^{2+} were analyzed by atomic absorption spectrometer. The obtained results are presented in Table-4.3. It can be observed that there are high concentrations of chlorides, sulfates and hardness constituting species. During waterflooding such higher concentrations of undesired minerals (divalent metals) would have caused severe precipitation and cementing problems which will ultimately block the open channels and hinder oil flow.

Table 4.3: Angsi sea water analyses.

Analyzed Parameters	Quantity	Units
Total hardness (TH as CaCO_3)	19,15.0	ppm
Calcium hardness (Ca^{+2} as CaCO_3)	450.0	ppm
Magnesium hardness (Mg^{+2} as CaCO_3)	13,63.0	ppm
Carbonates (CO_3^{2-} as CaCO_3)	7	ppm
Bicarbonates (HCO_3^- as CaCO_3)	107.0	ppm
pH	8.138	-
Sodium (Na^+)	9,731.0	ppm
Potassium (K^+)	3,90.0	ppm
Chlorides (Cl)	19,940.0	ppm
Total Dissolved Solids (TDS)	39,354.0	ppm
Sulfates (SO_4^{2-})	2,823.0	ppm
Iron ($\text{Fe}^{+2}/\text{Fe}^{+3}$)	<5	ppm
Resistivity at 25 °C	0.195	ohm-m
Barium (Ba^{+2})	<5	ppm
Strontium (Sr^{+2})	<5	ppm
Density at 119 °C	0.9810	g/cm^3

Stringent care must be taken to inject the water because it is always expected that the injected water can also dissolve more mineral constituents present in reservoir rocks. In order to precisely evaluate the compatibility of the utilized chemicals towards salinity, brine solution with 10,000 ppm salinity was synthesized using 8% NaCl and 1% each

KCl, CaCl₂. No compounds of magnesium and sulfates were deliberately added in the brine solution to accurately appraise the wettability alteration as a result of injected chemicals. This synthetic brine solution was utilized for further studies until unless specified otherwise.

4.2 Viscosity Measurements of Polyacrylamide

Aqueous solutions of partially hydrolyzed polyacrylamide are commonly used in oil recovery processes. Most of the polymers and surfactants which are suitable for oil recovery operations at lower temperatures and less saline waters are either ineffective in high salinity or high hardness waters. They do not possess high temperature tolerance as is encountered in many formations. Viscosities of the selected polymers Hybomax-1 and Hybomax-2 were recorded in 10,000 ppm synthetic brine solution. The effects of polymer concentration, salinity, alkalinity, temperature and various surfactants on the viscosity of HPAM have been reported in detail to look out for any synergistic and antagonistic effects these may have on the performance of polyacrylamide.

4.2.1 Effect of Polymer Concentration

Various concentrations of the polymers were prepared in the synthetic brine solution. The viscosities of the brine solutions of these polymers were measured by means of a Brookfield LVDV-14 digital viscometer.

Temperatures were controlled to 90 ± 2 °C and all the measurements were made at a constant rotational speed. The average of three concordant values was recorded. Fig. 4.1 represents the viscosities of polymer 1 and 2 in synthetic brine solution as a function of polymer concentration at 90 ± 2 °C. Increase in the polymers concentrations from 300 – 2100 ppm resulted in the enhancement of viscosities from 4.97 cp to 65.21 cp and 3.91 – 59.28 cp for polymers 1 and 2 respectively. Comparatively, polymer 1 was found to acquire more viscosity elevation in brine solution and is more expected to be resistant towards high temperatures.

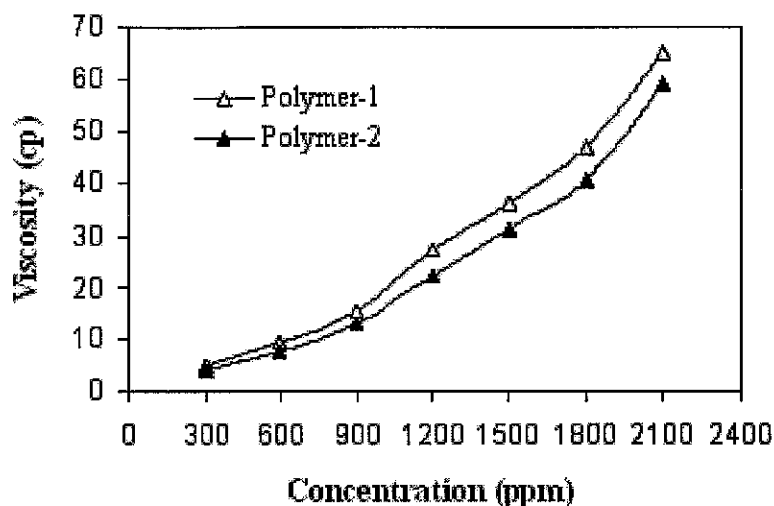


Figure 4.1: Viscosities of polymer 1 and 2 in brine Vs. concentration at 90 °C.

In EOR applications dilute concentrations of the polymers are highly desired not only due to economical factors but also in dilute regime, the ionic and hydrophobic groups contained in HPAM have a far great influence on the polymer conformation. Initially the viscosity of the polymers should be high enough to decrease viscous fingering and thereby beneficially increase the displacing phase viscosity. This enhances sweep efficiency thereby upto a certain limit, they must be capable of viscosity thinning together with surfactants and alkali, to reach the micro and mille pores of the reservoir to squeeze out maximum oil.

Low concentrations of the polymers are also responsible for reduction in hydraulic conductivity of higher-permeability zones which will promote cross-flow into lower- permeability zones as well, thereby masking the detrimental influence of heterogeneity. Medium concentrations, 1500 ppm, of Polymers 1 and 2 have been selected for further investigation.

4.2.2 Effect of Temperature

Polyacrylamides are generally more susceptible to degradation than other polymers. This degradation tendency is accelerated at comparatively higher temperatures, and in extreme cases, the polymer solution becomes useless for the intended application. The effect of temperature on the viscosity behavior of the brine

solutions with 1500 ppm of polymer 1 and 2 was studied in the temperature range of 70 – 120 °C. The reported values are the average of three concordant measurements. It was observed that the viscosities of both of the polymer solutions decreased with increase in temperature.

Fig. 4.2 shows that the viscosities decreased from 40.12 cp to 20.19 cp and 36.68 cp to 17.38 cp when the temperature is increased from 70 °C to 120 °C for polymers 1 and 2 respectively. Generally, with the increase of temperature the polymer mobility is increased as the interchain polymer Vander Waals forces become progressively weakened. The 3D-network built up by the associative polymer molecules is progressively destroyed and the degree of dissociation of the water molecules also increases as more ions are dissolved in solution. The latter is detrimental to the intermolecular hydrophobic association and consequently it leads to a rapid decrease of the thickening efficiency of the polymers [188].

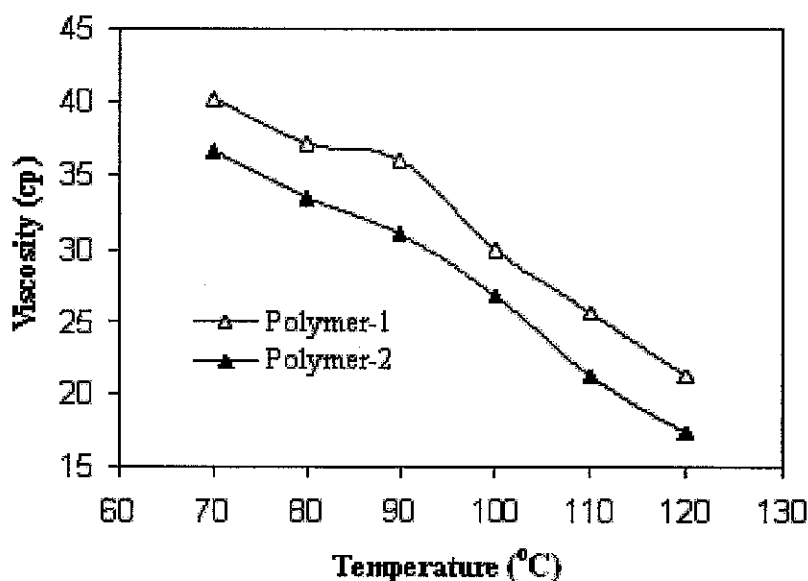


Figure 4.2: Temperature Vs. viscosities of polymers 1 and 2 with 1500 ppm in brine.

4.2.3 Effect of Alkalinity and Surfactants

The data for the stability of polymeric solutions in combination with the various solvents in brine solution at 90 ± 2 °C in the presence of 0.1 % Na_2CO_3 is presented in Table 4.4. The chemicals remained stable under the alkaline conditions in the presence of alkali except for those which have DBSA, CTAB, SDS and ATR surfactants

incorporation. The precipitation in the presence of DBSA is associated with the presence of sulfonic acid possessing severe incompatibility with the saline and alkaline conditions. CTAB is cationic in nature and the formation of precipitates is due to its strong electrostatic interactive forces and affinity with the mildly anionic polymers. SDS and ATR are pretty stable in saline, alkaline plus polymer solutions when salinity is not exceeding 10,000 ppm. However, slight precipitation was observed when the salinity exceeds 10,000 ppm. The alkaline solutions and the alkaline plus surfactant plus polymer solutions in the presence of AOT and ATR:AOT (1:9) demonstrated solution stability and there is no jeopardy regarding the precipitation.

Table 4.4: Stability of Alkaline-Surfactant-Polymer Formulations.

Polymers	Surfactant	Alkali	Salinity	Solution stability
Polymer-1	SDS, 2000 ppm	Na ₂ CO ₃ , 0.1 %	Brine, 10,000 ppm	Stable
	CTAB, 2000 ppm			Precipitation
	DBSA, 2000 ppm			Precipitation
	ATR, 2000 ppm			Stable
	AOT, 2000 ppm			Stable
	ATR:AOT (1:9), 2000 ppm			Stable
Polymer-2	SDS, 2000 ppm			Stable
	ATR, 2000 ppm			Stable
	AOT, 2000 ppm			Stable
	ATR:AOT (1:9), 2000 ppm			Stable
Polymer-1	SDS, 2000 ppm			Slight precipitation
	ATR, 2000 ppm			Slight precipitation
	AOT, 2000 ppm		Stable	
	ATR:AOT (1:9), 2000 ppm		Stable	
Polymer-2	SDS, 2000 ppm		Slight precipitation	
	ATR, 2000 ppm		Slight precipitation	
	AOT, 2000 ppm		Stable	
	ATR:AOT (1:9), 2000 ppm		Stable	
Polymer-1	SDS, 2000 ppm		Precipitation	
	ATR, 2000 ppm		Slight precipitation	
	AOT, 2000 ppm		Stable	
	ATR:AOT (1:9), 2000 ppm		Stable	
Polymer-2	SDS, 2000 ppm		Slight precipitation	
	ATR, 2000 ppm		Slight precipitation	
	AOT, 2000 ppm	Stable		
	ATR:AOT (1:9), 2000 ppm	Stable		
Polymer-1	SDS, 2000 ppm	0.1 %	Brine, 20,000 ppm	Slight precipitation
				Slight precipitation
				Stable
				Stable
				Slight precipitation
				Slight precipitation
			Brine, 30,000 ppm	Precipitation
				Slight precipitation
				Stable
				Stable
				Slight precipitation
				Slight precipitation

Subsequent solution viscosity analyses here not performed on the systems incorporating DBSA and CTAB because of precipitation. Instead the focus is now directed towards the effect of blending 0.1 % Na_2CO_3 alkali with SDS, AOT and ATR:AOT (1:9) surfactants in a 10,000 ppm synthetic brine solution using polymers 1 and 2 at 90 °C. A total of 2000 ppm (0.2 %) of each surfactant is used in all blending formulations.

The viscosities of alkaline plus polymer and alkaline plus surfactant plus polymer formulations are reported in Table 4.5. The viscosities of the polymeric solutions decreased with the addition of alkali for each of the two polymeric solutions consisting 1500 ppm of polyacrylamide. Sodium carbonate acts as a retarder and decrease the degree of hydrolysis of the polyacrylamide. This helps in arresting viscosity reduction [189]. The addition of SDS on the other hand resulted in slight increase in the viscosities of the polymeric solutions. The formulations on the other incorporating surfactants AOT, ATR and their mixture, ATR:AOT possessed reduced viscosities. This increase and decrease in viscosities of alkaline-polymer-surfactants solutions may be attributed to the surfactant type and structure making, structure breaking effects. Structure-making ions (sulfates, phosphate and sodium) enhance the hydrogen bond strength while structure-breaking (nitrate and potassium) ones are responsible to weaken the hydrogen bonds in aqueous solution.

Table 4.5: Viscosities of alkaline-polymer and alkaline-surfactant-polymer formulations.

Polymers	Viscosity (cp) with 0.1% Na_2CO_3	Viscosity (cp) with surfactant
Polymer-1	26.49	SDS, 33.22
		ATR, 24.15
		AOT, 21.79
		ATR:AOT, 20.08
Polymer-2	23.54	SDS, 29.47
		ATR, 20.28
		AOT, 19.26
		ATR: AOT, 16.37

4.3 Thermogravimetric Analyses

The degradation phenomenon of polyacrylamide based polymers is more complicated as compared to other polymeric materials. Thermal degradation of polymers 1 and 2, surfactants SDS, CTAB, ATR and AOT was examined by thermogravimetric analyses (TGA) between 50 and 700 °C in a nitrogenous atmosphere. The thermal behavior of the polymers and surfactants were compared with each other. TGA is commonly employed to determine the degradation temperatures, absorbed moisture content of materials, level of various components and to elaborate decomposition kinetics. The decomposition of the polymers and surfactants depend on the nature of various functional groups attached to them. Every material is unique in nature and possesses exceptional chemical and thermal stability.

4.3.1 Thermal Stability of Polymers

Known amounts of polymers 1 and 2 were independently placed in the sample holder, retained at 50 °C for 1 min and the temperature was gradually increased, 20 °C per minute, from 50 – 700 °C in nitrogenous atmosphere using Perkin Elmer TGA7 bench model thermogravimetric analyzer. The obtained TGA curves for polymers 1 and 2 are presented in Figs. 4.3 and 4.4 respectively.

TGA curves of both of the polymers have shown similar trends with distinguished degradation regions. The first region near 110 °C is due to the loss of bound water. The second region from 230 – 450 °C corresponds to the degradation of amide group. Ammonia is produced by the degradation of polyacrylamide and polyacrylonitrile. The third region from 450 – 580 °C represents a complex degradation process which may result from the condensation of residual amide groups and cyclic amide rings [190].

The region beyond 600 °C represents char residue. As the formation temperature of Angsi is 119 °C (Table 4.1) both polymers 1 and 2 retain up to as much as 90% and 87% of their structure and mass. It can be concluded that these polymers are thermally stable under reservoir conditions; however, polymer-1 is slightly better than polymer-2.

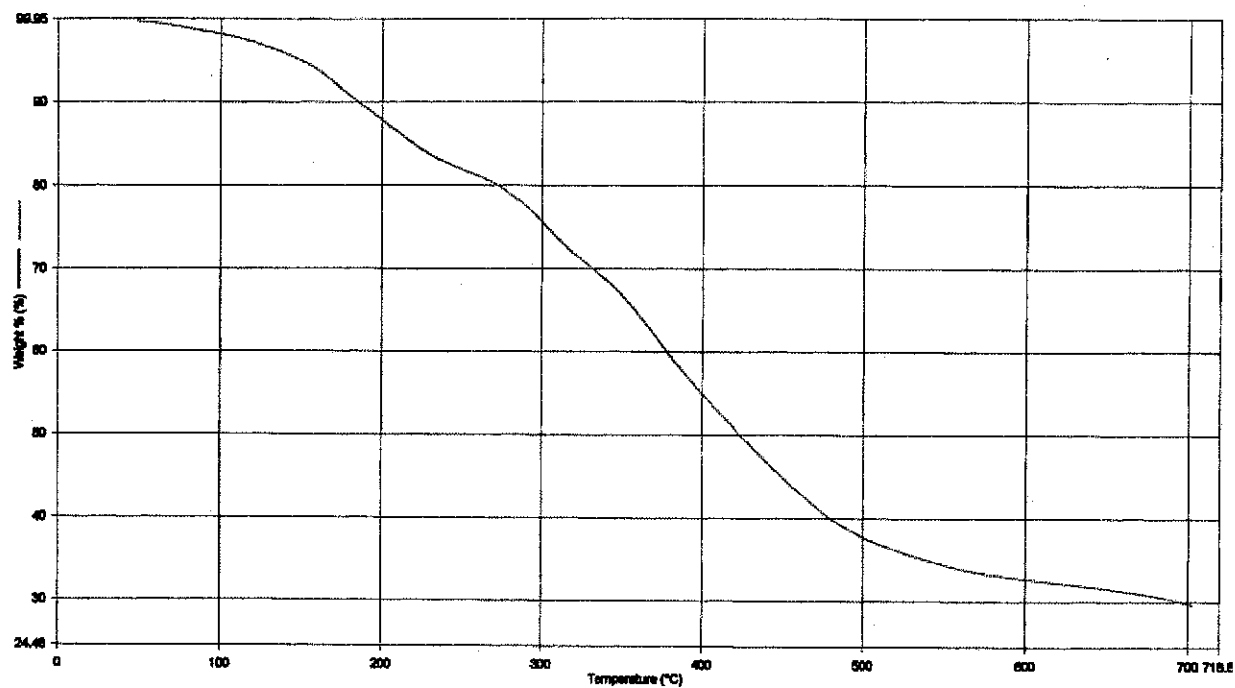


Figure 4.3: TGA curve for polymer-1.

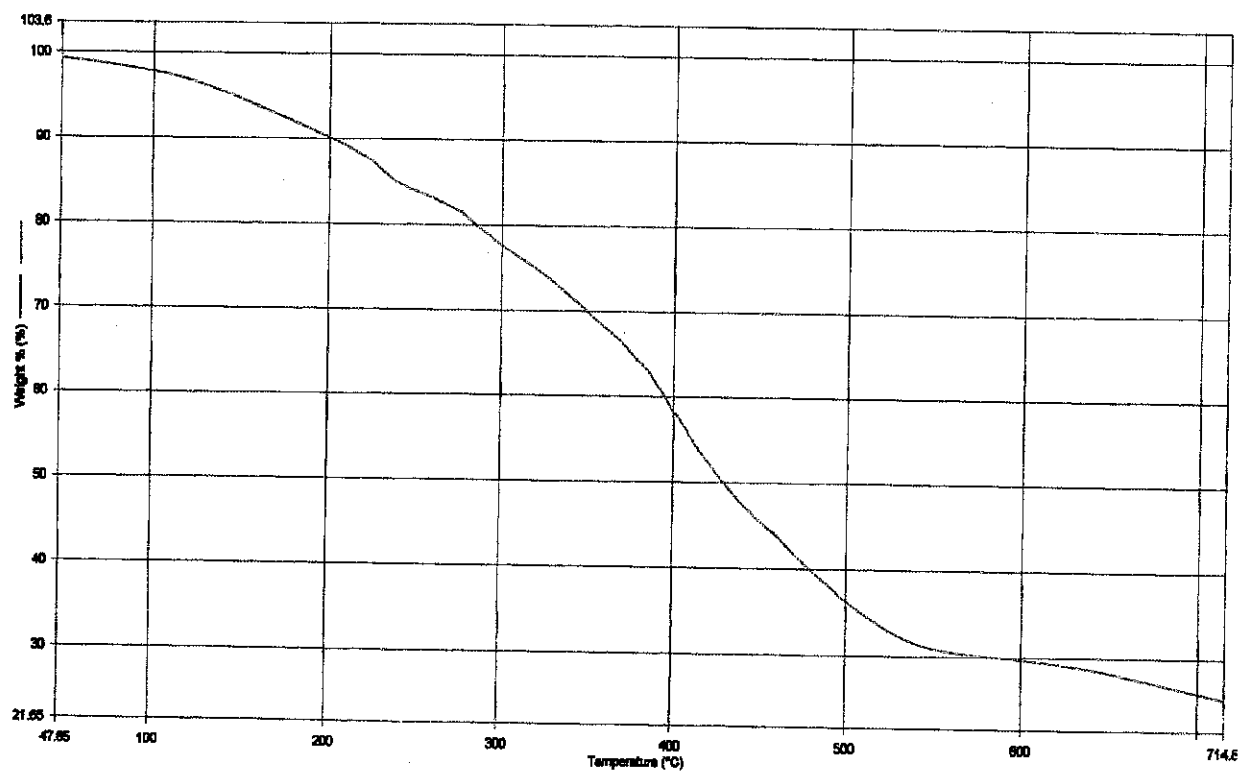


Figure 4.4: TGA curve for polymer-2.

4.3.2 Thermal Stability of Surfactants

In order to evaluate the thermal stabilities of SDS, CTAB, AOT and ATR, TGA curves of the respective surfactant were recorded using Perkin Elmer TGA7 bench model thermogravimetric analyzer.

Known amounts of SDS, CTAB, AOT and ATR were independently placed in sample holder, retained at 50 °C for 1 min and the temperature was gradually increased, 20 °C per minute, from 50 – 500 °C for SDS, CTAB and from 50 – 400 °C for AOT and ATR respectively in nitrogenous atmosphere.

The obtained TGA profiles for SDS, CTAB, AOT and ATR are presented in Figs. 4.5 – 4.8 respectively. The TGA profile for SDS shows that the weight loss occurs in four steps.

First thermal degradation started around 130 °C and the weight loss from 130 °C – 215 °C was less than 4 %.

The second and third degradations were recorded from 215 – 275 °C and 275 °C – 375 °C respectively, where approximately 70 % weight loss was recorded. The remaining weight beyond 375 °C represents char residue.

In the case of CTAB, approximately less than 2 % weight loss was observed till 220 °C, but about 95 % weight loss occurred sharply from 220 °C – 350 °C, revealing that CTAB molecules were decomposed thermally within this temperature range. These chemicals are also stable under reservoir conditions because there is no danger of thermal decomposition between 100 °C and 120 °C.

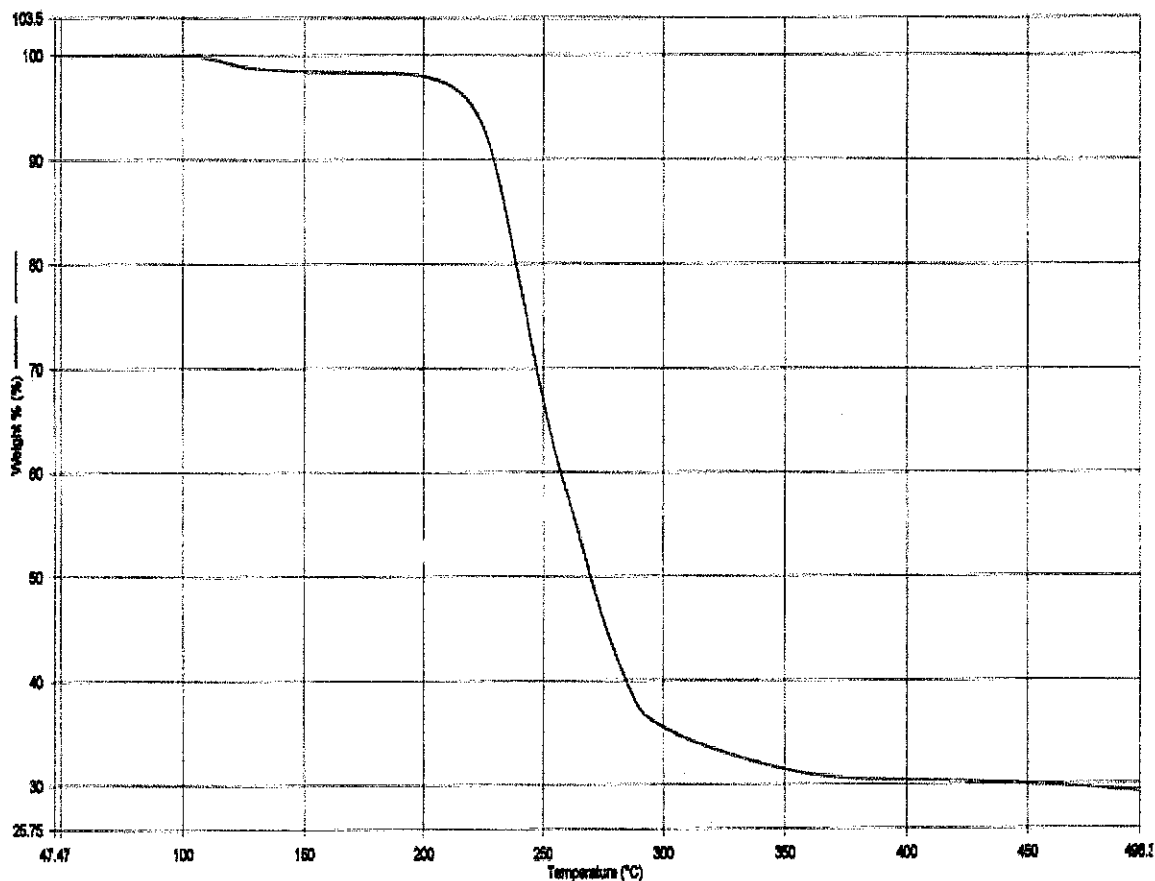


Figure 4.5: TGA curve for SDS.

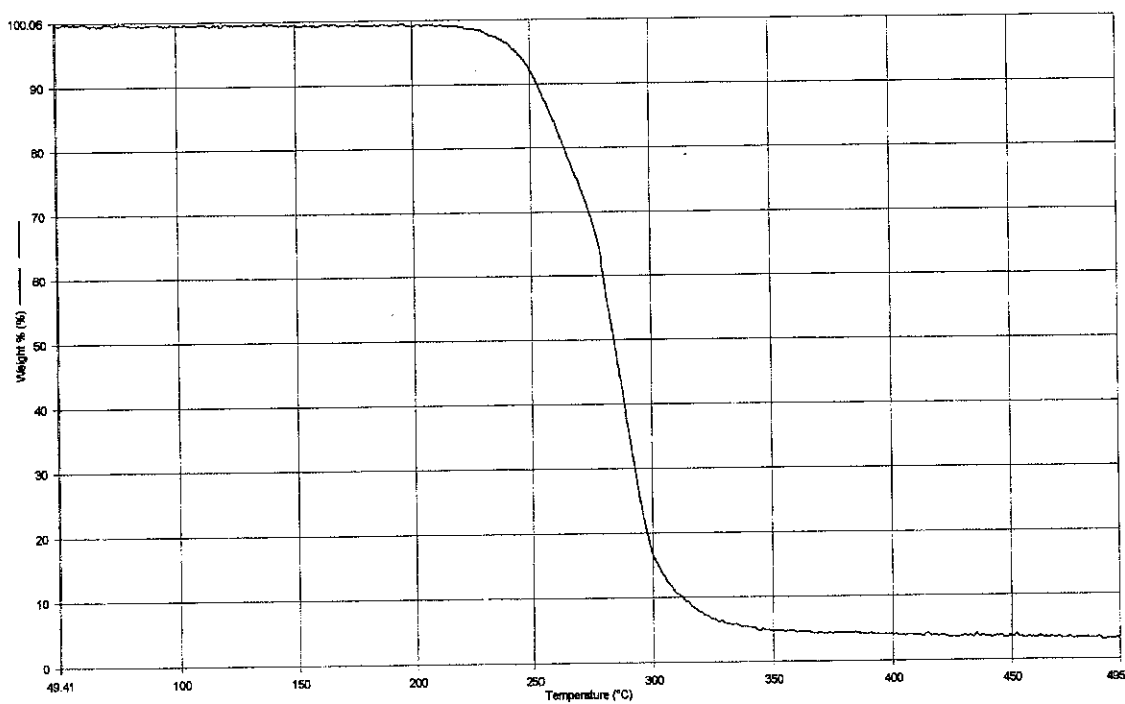


Figure 4.6: TGA curve for CTAB.

The percentage purities of AOT and ATR are 85 and 70 % respectively. The remaining portion is based on solvents which are likely to be low boiling point alcohols. The obtained TGA profiles (Figs. 4.7 and 4.8) for AOT and ATR have showed that approximately 15 and 30 % contents were decomposed up to 120 °C and 130 °C. Beyond this region the weight losses were retarded with approximately 80 and 66 % remaining contents from 120 – 275 °C and 130 – 250 °C for AOT and ATR correspondingly. AOT and ATR are completely decomposed at temperatures exceeding 275 °C and 250 °C respectively. It is concluded that both the surfactants AOT and ATR are suitable for EOR applications. Presence of short chain alcohols is indicated by the low degradation components which originate from the low boiling point solvents or co-surfactants. Co-surfactants are intentionally incorporated along with primary surfactants to facilitate the formation of stable oil-water emulsions.

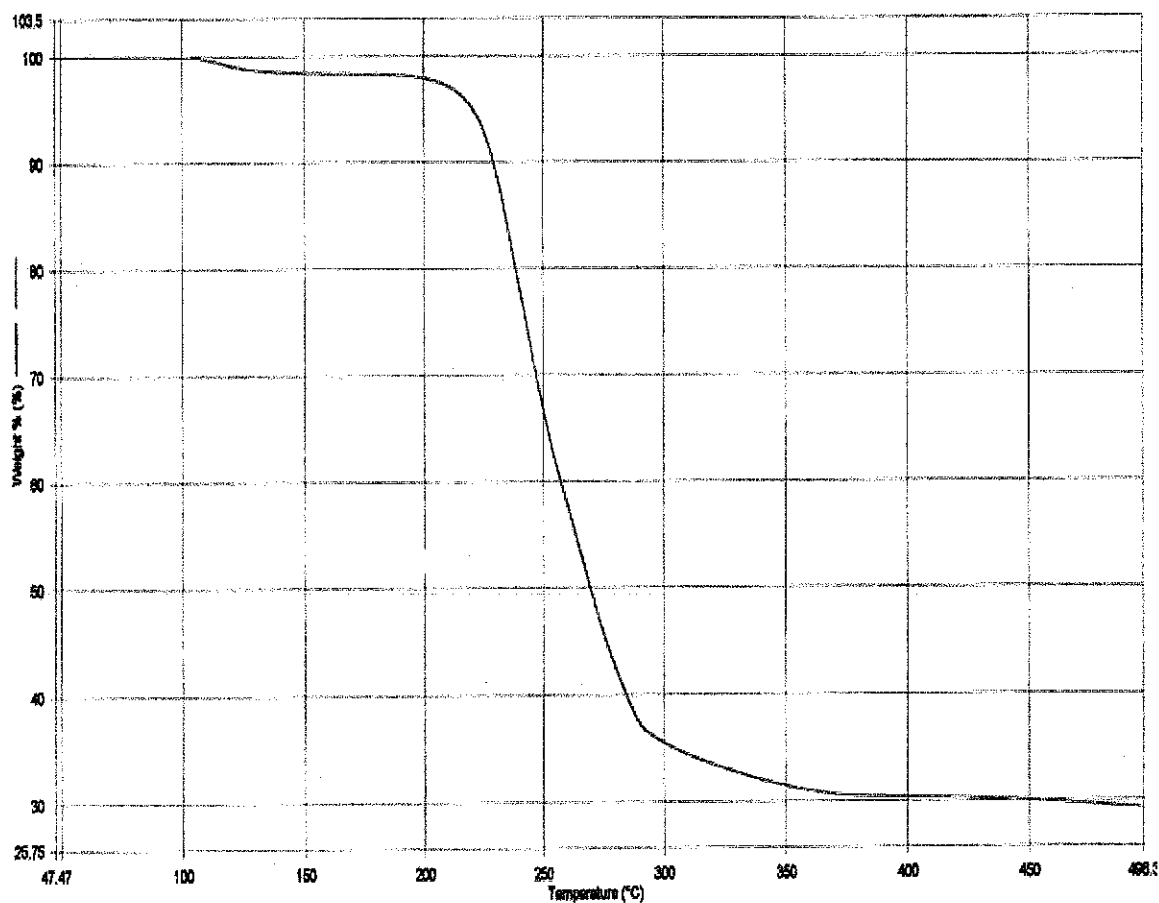


Figure 4.7: TGA curve for AOT.

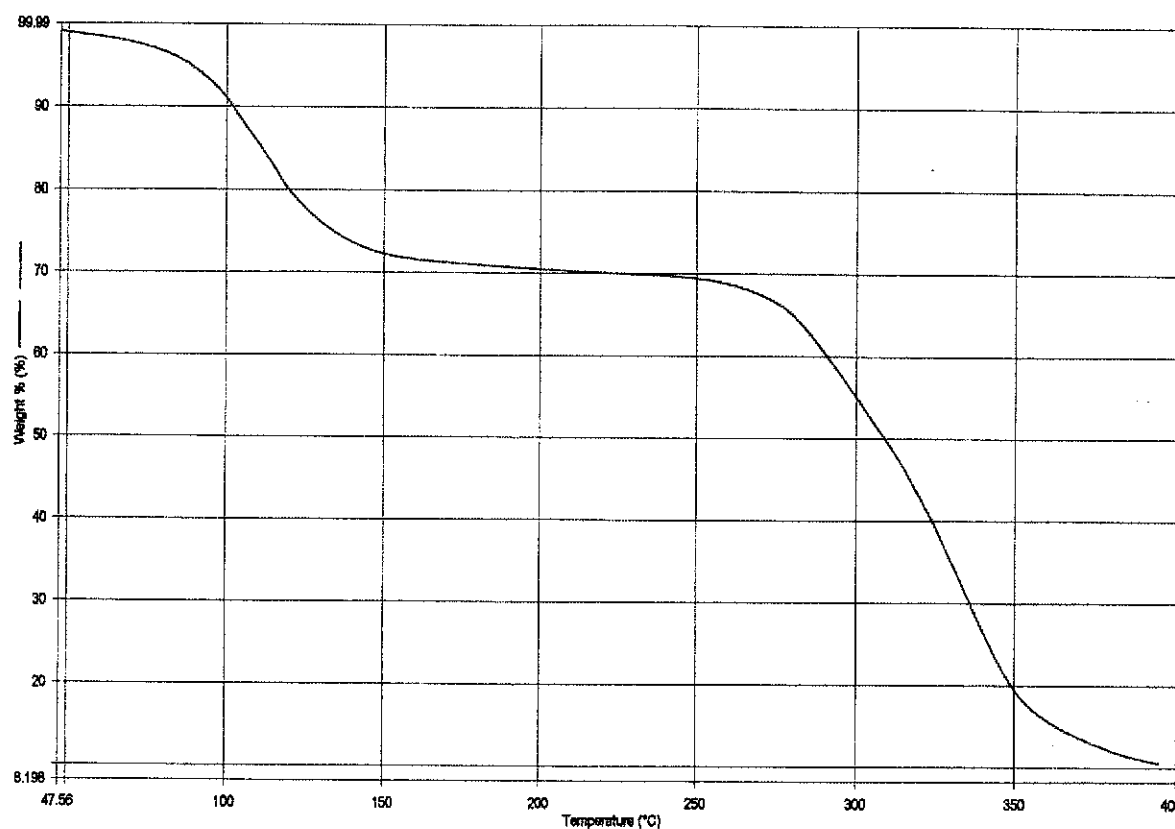


Figure 4.8: TGA curve for ATR.

4.4 FTIR-ATR Spectroscopic Analyses

FTIR-ATR spectroscopy was utilized to examine the possible interactions which may be induced between various components as a result of synergistic and antagonistic effects. FTIR-ATR spectra of the various proposed formulations were recorded using Perkin Elmer-2000 model FTIR-ATR spectrometer, which were compared with the initially recorded spectra of pure polymers, surfactants and Angsi crude oil.

4.4.1 FTIR-ATR Spectroscopy of Polymers

FTIR-ATR spectrums of 1500 ppm concentration of each polymer 1 and 2 are presented in Fig. 4.9. Similar spectra were obtained but the percentage transmission was different associated with the variation in their molecular weights. The existence of the carboxylate and amide functionalities in both of the polymers was confirmed by the presence of absorption peaks at 1635, 1638 and 3305, 3306 cm^{-1} , respectively [191].

Chemical assignments for the obtained absorption bands from IR spectroscopy are represented in Table 4.6.

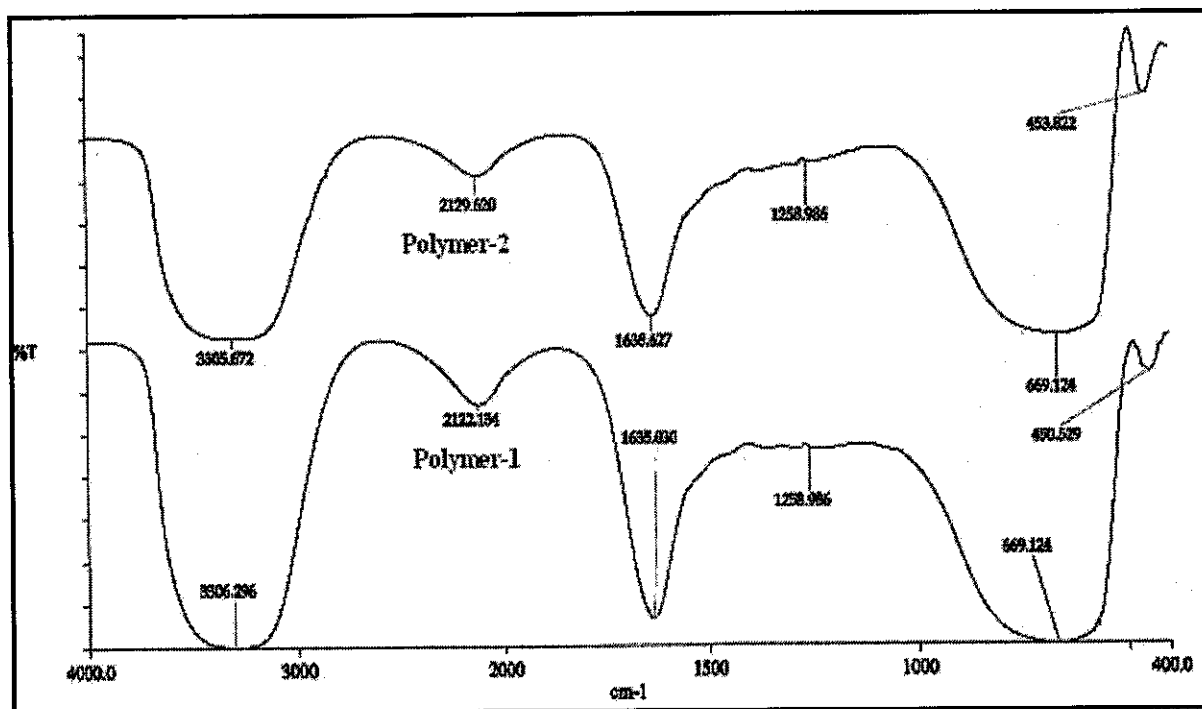


Figure 4.9: FTIR-ATR spectrums of polymers 1 and 2.

Table 4.6: Chemical assignments for absorption bands for polymer 1 and 2.

Chemical assignments	Polymer-1 and 2, wavelength/cm ⁻¹
N-H and O-H stretching	3305, 3306 (b), (b)
C-H stretching	2122, 2129 (m), (m)
C=O stretching	1635, 1638 (sh), (sh)
O-C-O stretching	1535 (w), (w)
-CH ₂ - bending	1258 (w), (w)
-C-H bending	1404 (m), (w)

(s)- strong peak, (m)- medium peak, (b)- broad peak, (w)- weak peak, (sh)- sharp peak

4.4.2 FTIR-ATR Spectroscopic Analyses of Angsi Crude Oil

FTIR-ATR spectrum of pure Angsi crude is presented in Fig. 4.10. The presence of a mixture of compounds was assessed from the library which was provided with the equipment by the Perkin Elmer. The detected compounds which may be present comprise decane, dodecane, nonane, heptane, hexane, 2-methylnonane, dimethylcyclohexane, methyloctane, paraffin oil, olefin free tetradecane,

chlorohexadecane, 3-methylpentane, hexacosanol, 1,1,3-trimethylcyclohexane, 1-decanethiol, 1-octanethiol, toluene-4-sulfonic acid, 2-methyl-1,3-cyclopentanedione, 2,5-diaminotoluene sulfate, pyrazole-3,5-dicarboxylic acid, pyridyl ethanesulfonic acid, nicotinic acid, toluene-4-sulfonic acid, dichloroisocyanuric acid sodium salt, 2-hydroxytetradecanoic acid and 5,6-dimethylbenzimidazole.

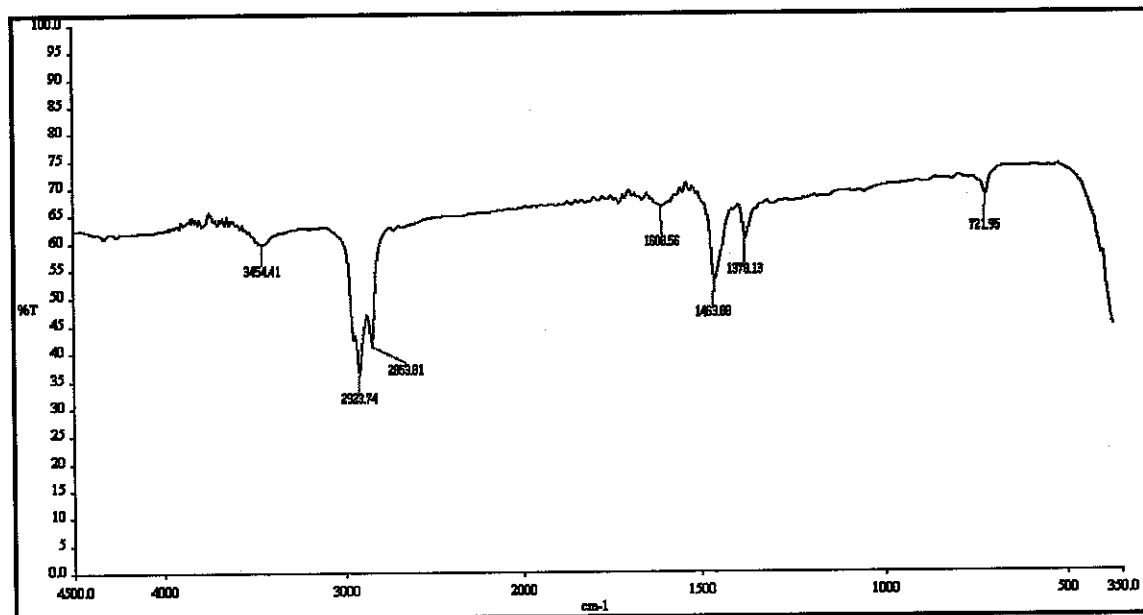


Figure 4.10: FTIR-ATR spectrum of pure Angsi crude oil.

4.4.3 FTIR-ATR Spectroscopic Analyses of Surfactants

FTIR-ATR spectrum of surfactants SDS, CTAB, ATR, AOT and ATR:AOT are presented in Figs. 4.11 – 4.15 respectively. Again with the help of library identification of the various compounds was carried out individually for each of the mentioned surfactants.

The detected compounds that are present in FTIR spectra of SDS (Fig. 4.11) surfactant in the range of 350.0 – 4500 cm^{-1} consists of methyl-octyldimethoxysilane, octadecyl-trimethoxysilane, tert-butyl methyl ether, 2-tert-butylamino ethanol, 5-thio-D-glucose, trans-2-hexen-1-ol, alpha-humulene, D1-beta-dipalmitoyl-N,N-dimethyl-alpha-cephalin, tert-butylamine, dimethyloctylchlorosilane, L-alfa-glycerol-phosphorycholine cadmiumchloride complex, acetate mixture of isomers, pentylamine, 4-

hydroxypiperidine, farnesol mixture of stereoisomers, N-hydroxysuccinimide, crotyl alcohol, 2,6-dimethoxy-phenol, tetrabutylphosphonium chloride, 1,6-diaminohexane, methyltrimethoxysilane, tert-butylamine, 1,12-dibromododecane, 4-chlorophenol, 4-nonylphenol, methyl 2,5-dimethylfuran-3-carboxylate and trichloroacetic acid.

Whereas, the specified components present in case of CTAB surfactant in the range of $350.0 - 4500 \text{ cm}^{-1}$ (Fig. 4.11) are benzalkonium bromide, hexatriacontane, octadecylamine, dotriacontane, tetraoctadecylammonium Bromide, octacosane, 1-bromoheptadecane, hexadecylamine, tetradodecylammonium Bromide, 1,2-hexadecanediol, 1,2-octadecanediol, 1-hexacosanol, 1-tridecanol, 1,6-diaminohexane, dodecylamine, 1,2,1-docosadiene, 1,1,2-dibromododecane, N,O-dimethylhydroxylamine hydrochloride, 1,4-diaminobutane, tridodecylamine, nonadecanoic acid, 2,4-dichloroaniline, 1-chlorohexadecane, sulfonazo III, 4-nonene (cis+trans), batyl alcohol, 1-decanol and 5,6-dimethylbenzimidazole.

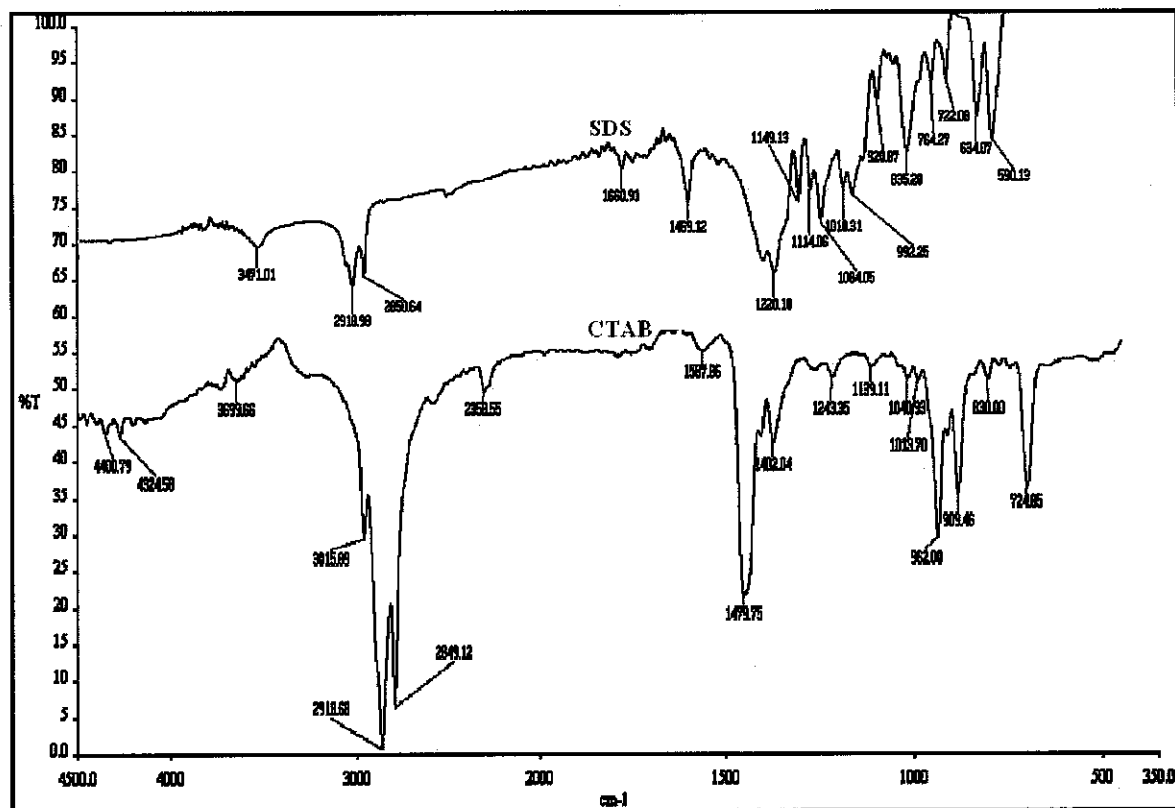


Figure 4.11: FTIR spectra of pure SDS and CTAB.

hydroxypiperidine, farnesol mixture of stereoisomers, N-hydroxysuccinimide, crotyl alcohol, 2,6-dimethoxy-phenol, tetrabutylphosphonium chloride, 1,6-diaminohexane, methyltrimethoxysilane, tert-butylamine, 1,12-dibromododecane, 4-chlorophenol, 4-nonylphenol, methyl 2,5-dimethylfuran-3-carboxylate and trichloroacetic acid.

Whereas, the specified components present in case of CTAB surfactant in the range of $350.0 - 4500 \text{ cm}^{-1}$ (Fig. 4.11) are benzalkonium bromide, hexatriacontane, octadecylamine, dotriacontane, tetraoctadecylammonium Bromide, octacosane, 1-bromoheptadecane, hexadecylamine, tetradodecylammonium Bromide, 1,2-hexadecanediol, 1,2-octadecanediol, 1-hexacosanol, 1-tridecanol, 1,6-diaminohexane, dodecylamine, 1,2,1-docosadiene, 1,1,2-dibromododecane, N,O-dimethylhydroxylamine hydrochloride, 1,4-diaminobutane, tridodecylamine, nonadecanoic acid, 2,4-dichloroaniline, 1-chlorohexadecane, sulfonazo III, 4-nonene (cis+trans), butyl alcohol, 1-decanol and 5,6-dimethylbenzimidazole.

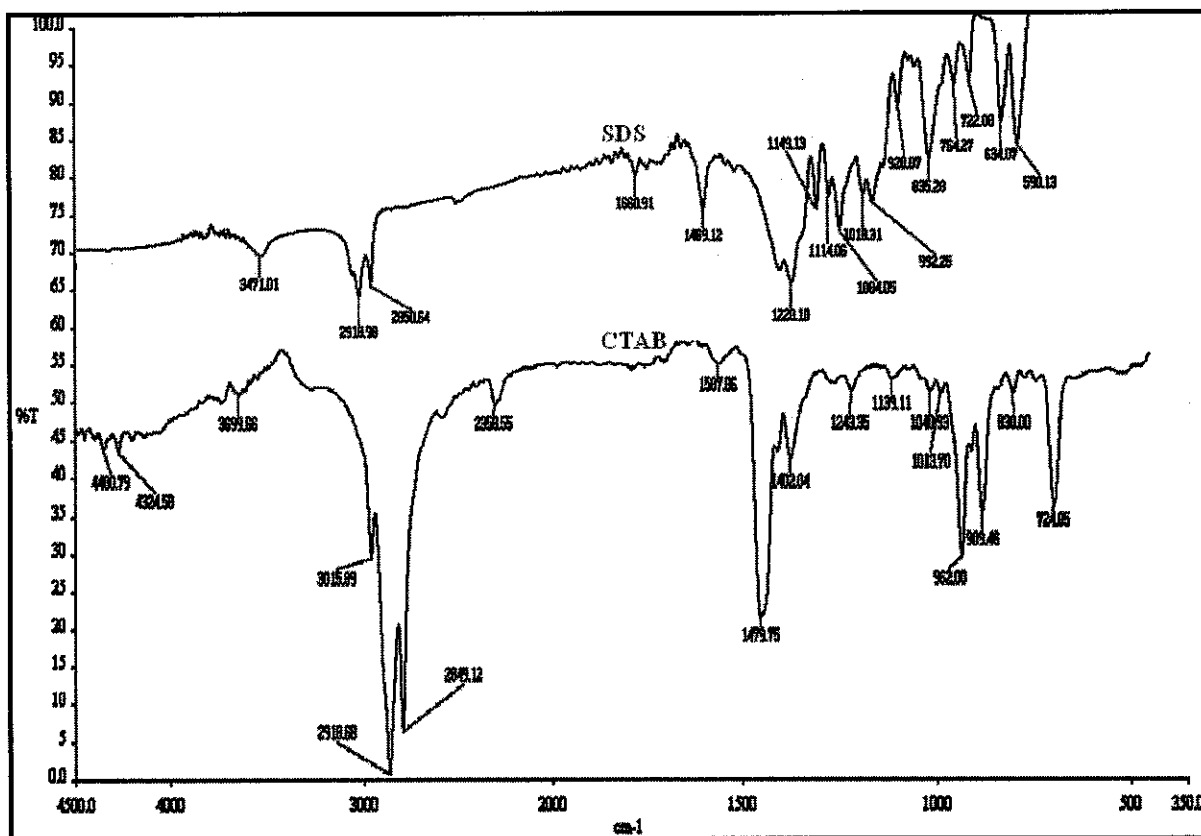


Figure 4.11: FTIR spectra of pure SDS and CTAB.

The particular constituents detected in the FTIR spectra of ATR (Fig. 4.12A), AOT (B) and mixture of ATR:AOT (C) in the range of 350.0 – 4500 cm^{-1} include dimethyl cyclohexane-1,4-dicarboxylate, methyl linoleate, 2-methylpentanal, delta-valerolactone, bis(1-butyphenyl) adipate, ethyl 2-hydroxycapronate, citronellal, butyl stearate, cis-androsterone, ethyl palmitate, 2-ethylbutyraldehyde, methyl elaidate, ethyl myristate, 3-chloroperbenzoic acid, ethyl 4-bromobutyrate, diethylenetriamine pentaacetic acid, butyl 2-methylbutyrate, trichloroacetic acid, deoxycholic acid, 3 beta-acetoxy-5-etienc acid, bis(2-ethylhexyl) sebacate, diethyl oxalpropionate, (+)-camphor-10-sulfonyl chloride, bis(2-ethylhexyl) sulfosuccinate sodium, propionic acid, quabain, ethyl 5-bromovalerate, and ethyl butyrate. In case of AOT (Fig. 4.12B) the promising ingredients are bis(2-ethylhexyl) sebacate, butyl stearate, ethyl linoleate, diethylenetriamine pentaacetic acid, ethyl palmitate, ethyl myristate, bis(2-ethylhexyl) sulfosuccinate sodium, (+)-camphor-10-sulfonyl chloride, sulfonazo III, decane, nonane, olefin free tetradecane, bis(1-butyphenyl) adipate, dodecane, 2-hydroxytetradecanoic acid, 2-methyloctane, 2-methylnonane, heptane, 1-hexacosanol, 1-bromoheptane, 3-methyloctane, 1,1,3-trimethylcyclohexane and N-acetylneuraminic acid.

FTIR-ATR spectrum of ATR:AOT (1:9), Fig. 4.12C, has revealed the occurrence of nonane, decane, olefin free tetradecane, bis(2-ethylhexyl) sebacate, dodecane, 3-methyloctane, 2-methylnonane, 2-hydroxytetradecanoic acid, diethylenetriamine pentaacetic acid, 1-hexacosanol, heptane, hexane, sulfonazo III, 3-methylnonane, 2-methyloctane, 1,1,3-trimethylcyclohexane, 3-methylheptane, docosane, N-acetylneuraminic acid, 1-bromoheptane, 2-methyl-1,3-cyclopentanedione and olefin free octadecane.

Both ATR and AOT surfactants are comprised of similar components with small differences due to the presence of higher and shorter hydrophobic chains respectively. However, in the mixture, slight wavelength shift suggests the change of different hydrogen bonding as compared to the pure surfactants.

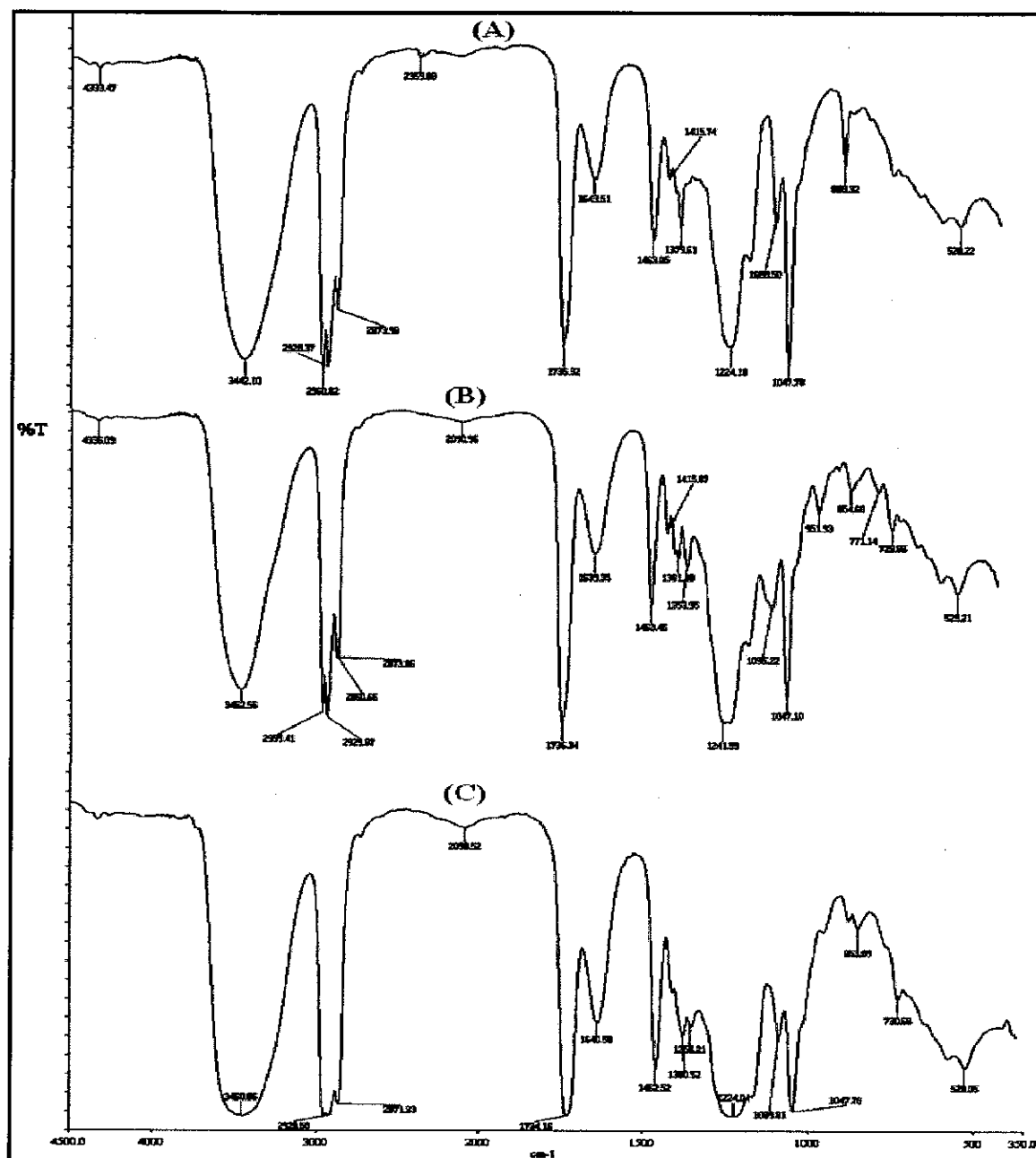


Figure 4.12: FTIR-ATR spectra of ATR (A), AOT (B) and mixture of ATR:AOT (C).

4.4.4 FTIR-ATR Spectroscopic Analyses of Various Combinations

FTIR-ATR spectra of mixture of pure Angsi crude with SDS, CTAB, with 2000 ppm concentration, ATR, AOT, ATR:AOT, with 1500 ppm concentration, and the Angsi

crude recovered after ASP flooding using SDS, and ATR:AOT surfactants are presented in Figs. 4.13 – 4.16 respectively.

The obtained spectrum for the mixture of Angsi crude with SDS, Fig. 4.13, has revealed the existence of, petroleum fraction, dodecane, paraffin oil, 4-nitroaniline, dichloroisocyanuric acid sodium salt, 2-(4-pyridyl) ethanesulfonic acid, pentadecylamine, nicotinic acid, 1-octanethiol, 2-hydroxytetradecanoic acid, nonane, pyrazole-3,5-dicarboxylic acid, decane, 1-chlorohexadecane, 3-methylheptane, 1,1,3-trimethylcyclohexane, olefin free tetradecane, 1,1-dimethylcyclohexane, toluene-4-sulfonic acid sodium salt, 1-hexacosanol, methylcyclopentane, 3-methylnonane, 5,6-dimethylbenzimidazole, 1-bromooctane, isopropylcyclohexane and 1-decanethiol.

The appearance of new compounds, particularly dichloroisocyanuric acid sodium salt and toluene-4-sulfonic acid sodium salt, which were not initially present in the spectrums of pure Angsi crude and SDS, have revealed that sodium content of SDS can interact with the acidic fractions of crude resulting in the formation of soap like materials which can further lower down the IFT resulting in enhanced mobility of trapped oil.

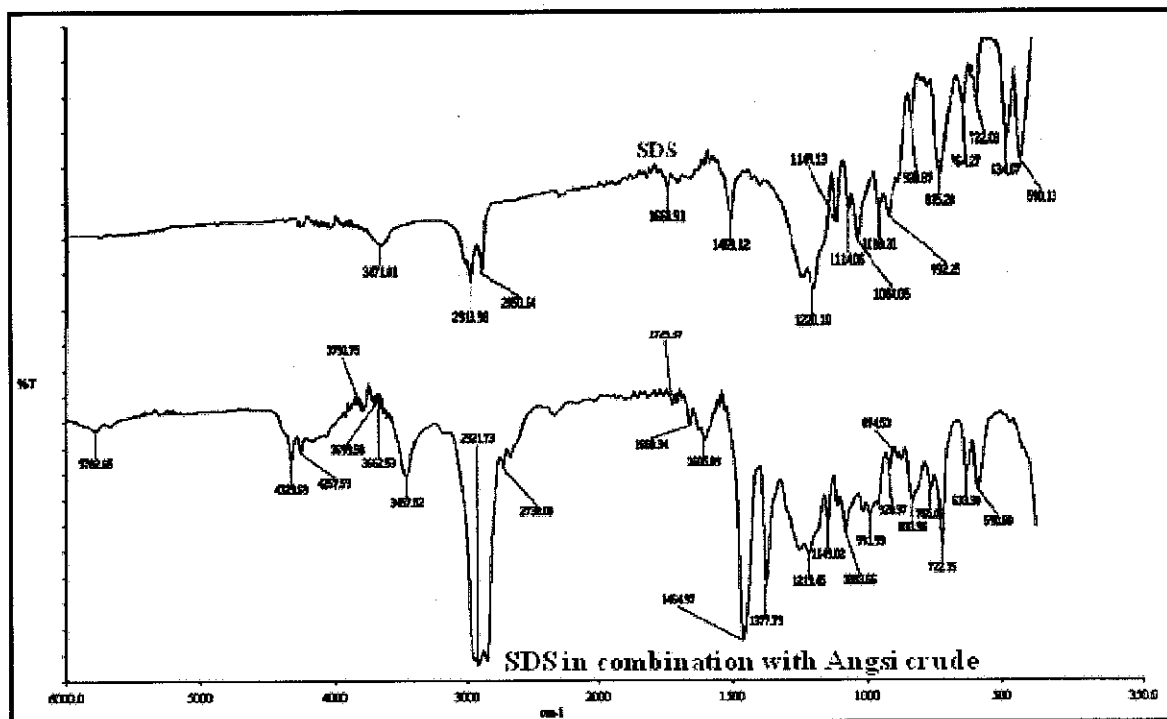


Figure 4.13: FTIR-ATR spectrum of SDS and Angsi crude in combination with SDS.

Fig. 4.14 represents the FTIR-ATR spectrum of Angsi crude in combination with CTAB. Major compounds which were detected are nonane, decane, olefin free tetradecane, 1-hexacosanol, paraffin oil, dodecane, 4-nitroaniline, 1-chlorohexadecane, dichloroisocyanuric acid sodium salt, 1-octanethiol, tetradodecylammonium bromide, 3-methyloctane, hexane, 1-decanethiol, petroleum fraction, 2-methylnonane, 3-methylnonane, 3-methylheptane, 1,1,3-trimethylcyclohexane, heptane, dotriacontane, docosane, nicotinic acid, hexatriacontane, 2-methyloctane, 2-hydroxytetradecanoic acid and pyrazole-3,5-dicarboxylic acid.

Again the indication of new compounds, that were not initially present in the spectra of pure Angsi crude and CTAB (Fig. 4.10 and 4.11), have revealed that CTAB can also interact with the acidic fractions of crude leading to the generation of new soap like materials (Fig. 4.14).

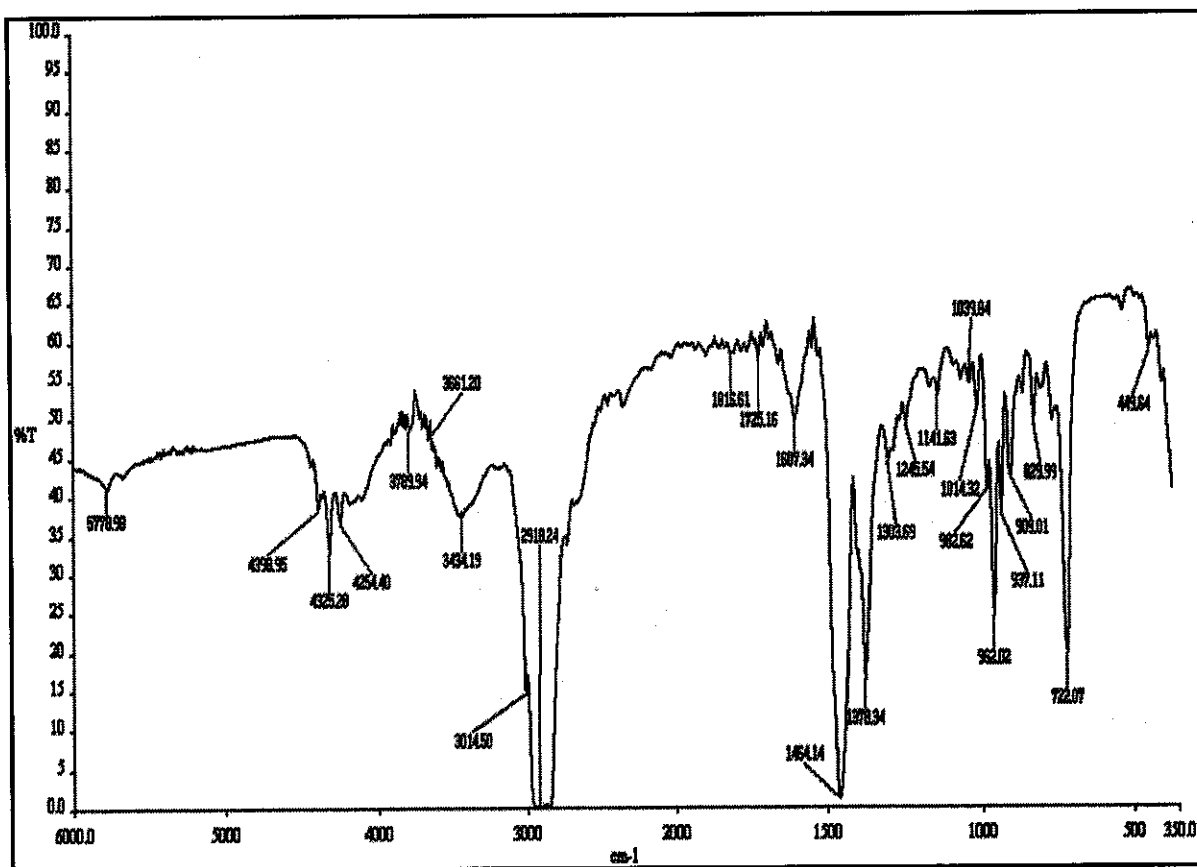


Figure 4.14: FTIR-ATR spectrum of Angsi crude in combination with CTAB.

FTIR-ATR spectra of Angsi crude in combination with ATR, AOT and ATR:AOT are shown in Fig. 4.15. Most important compounds which are present in the spectra of ATR in combination with Angsi crude (Fig. 4.15 C) include nonane, decane, olefin free tetradecane, 1-hexacosanol, paraffin oil, dodecane, hexane, heptane, bis(2-ethylhexyl) sulfosuccinate sodium, bis(2-ethylhexyl) sebacate, ethyl linoleate, diethylenetriamine pentaacetic acid, petroleum fraction, (+)-camphor-10-sulfonyl chloride, sulfonazo III, bis(1-butyphenyl) adipate, 2-ethylbutyraldehyde, N-acetylneuraminic acid, 2-hydroxytetradecanoic acid, butyl stearate, ethyl myristate, paraffin oil, ethyl palmitate, nicotinic acid, 2-methylpentanal, 1-octanethiol, 1-hexacosanol, diethyl adipate and 1-hexanol.

Compounds which were reported in the spectrum of Angsi crude with AOT (Fig. 4.15 B) surfactant include hexane, decane, dodecane, nonane, petroleum fraction, paraffin oil, heptane, olefin free tetradecane, bis(2-ethylhexyl) sulfosuccinate sodium, bis(1-butyphenyl) adipate, menthyl acetate, bis(2-ethylhexyl) sebacate, ethyl 2-hydroxycapronate, 2-methylpentanal, neomenthyl acetate, 2-ethylbutyraldehyde, beta-acetoxy-5-etiencic acid, ethyl linoleate, deoxycholic acid, quabain, diethyl adipate, dimethyl cyclohexane-1,4-dicarbonxylate, butyl stearate, hydrocortisone acetate, 2-ethyl-1-hexylamine and ethyl myristate.

FTIR-ATR spectrum of the mixture of ATR and AOT in combination with Angsi crude is given in Fig. 4.15 A which indicates the presence of decane, dodecane, hexane, heptane, petroleum fraction, paraffin oil, nonane, olefin free tetradecane, bis(2-ethylhexyl) sebacate, 3-methyloctane, 2-methylnonane, 2-hydroxytetradecanoic acid, diethylenetriamine pentaacetic acid, 1-hexacosanol, sulfonazo III, 3-methylnonane, methyloctane, 1,1,3-trimethylcyclohexane, 3-methylheptane, docosane, 2-methyl-1,3-cyclopentanedione and 2,5-diaminotoluene sulfate.

In terms of interactions in between Angsi crude and AOT, ATR, ATR:AOT (1:9) surfactants similar trend was observed. Most of the compounds are hydrocarbon in nature and were initially recorded in the spectra of ATR, AOT, ATR:AOT (Fig. 4.12) and Angsi crude (Fig. 4.10). In terms of compatibility towards hydrocarbon phase these non-

conventional surfactants are found to be better than the conventional surfactants due to the presence of larger hydrophobic tails. It can be concluded that the presence of more hydrocarbon fractions than the spectra of Angsi crude in combination with SDS and CTAB depend upon the hydrophobic portion of non-conventional surfactants which is having dimeric homologous chains in the presence of short chain alcohols as indicated in Fig. 4.12 in the pure spectra of ATR, AOT and ATR:AOT (1:9). As the extent of hydrophobic portion is more in these surfactants than the conventional surfactants with single chain, due to which ATR, AOT and their mixture possess more affinity towards the hydrocarbon phase than SDS and CTAB which is obvious from the obtained components shown in Fig. 4.15.

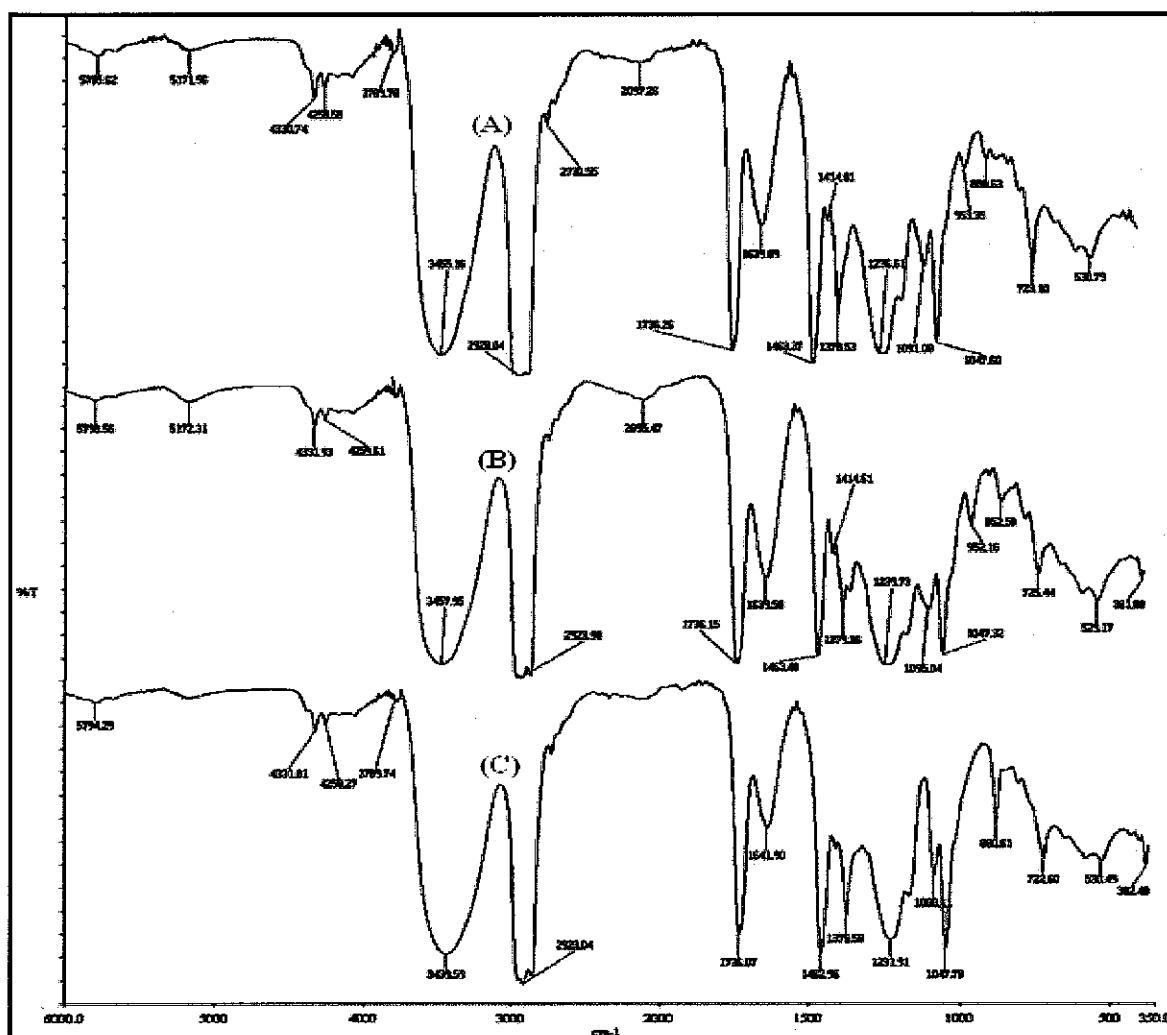


Figure 4.15: FTIR-ATR spectra of Angsi crude in combination with ATR (C), AOT (B) and ATR:AOT (A, 1:9) surfactants.

FTIR-ATR spectra of Angsi crude recovered by ASP flooding using SDS and mixture of ATR and AOT surfactants is presented in Fig. 4.16. Most important detected compounds in case of ASP flooding with SDS (Fig. 4.16 A) include decane, dodecane, nonane, heptane, hexane, 2-methylnonane, dimethylcyclohexane, methyloctane, paraffin oil, olefin free tetradecane, chlorohexadecane, 3-methylpentane, hexacosanol, 1,1,3-trimethylcyclohexane, 2-methyl-1,3-cyclopentanedione, 2,5-diaminotoluene sulfate, 4-nitroaniline, 3-methylheptane, 1,1,3-trimethylcyclohexane, methylcyclopentane, 3-methylnonane, taurocholic acid sodium salt and isopropylcyclohexane.

FTIR-ATR spectrum of Angsi crude recovered by ASP flooding using mixture of ATR and AOT is presented in Fig. 4.16 B. Detected compounds indicated by the spectrum are closer to those one which were initially detected in the spectra of pure Angsi crude and Angsi crude in combination with mixture of ATR and AOT. The identified compounds are decane, dodecane, nonane, heptane, hexane, paraffin oil, olefin free tetradecane, 2-methylnonane, dimethylcyclohexane, methyloctane, 3-methylpentane, hexacosanol, 1,1,3-trimethylcyclohexane, 2-methyl-1,3-cyclopentanedione, 4-nitroaniline, chlorohexadecane, 3-methylheptane, 1,1,3-trimethylcyclohexane, methylcyclopentane, 3-methylnonane, taurocholic acid sodium salt, isopropylcyclohexane and hexacosanol.

It can be concluded that most of the components, except acidic fractions, are similar to those of pure Angsi crude. Acidic fractions might have been consumed for the formation of soap like materials. While, few of the components also have the similarity as reported in the combination of SDS, ATR:AOT and Angsi crude earlier but the peaks intensities are too low that is because of the presence of ultra-low concentrations. Small amounts of the SDS and mixture of ATR and AOT surfactants have been retained by the hydrocarbon phase and no more acidic fractions are there. The portion of surfactant that has been retained by the hydrocarbon phase is consumed to produce the chemicals which are not only compatible with the crude itself but also offer multifarious additional benefits in terms of pour point depression and enhanced lubrication which are fundamental properties of surfactants [6,8,9,18].

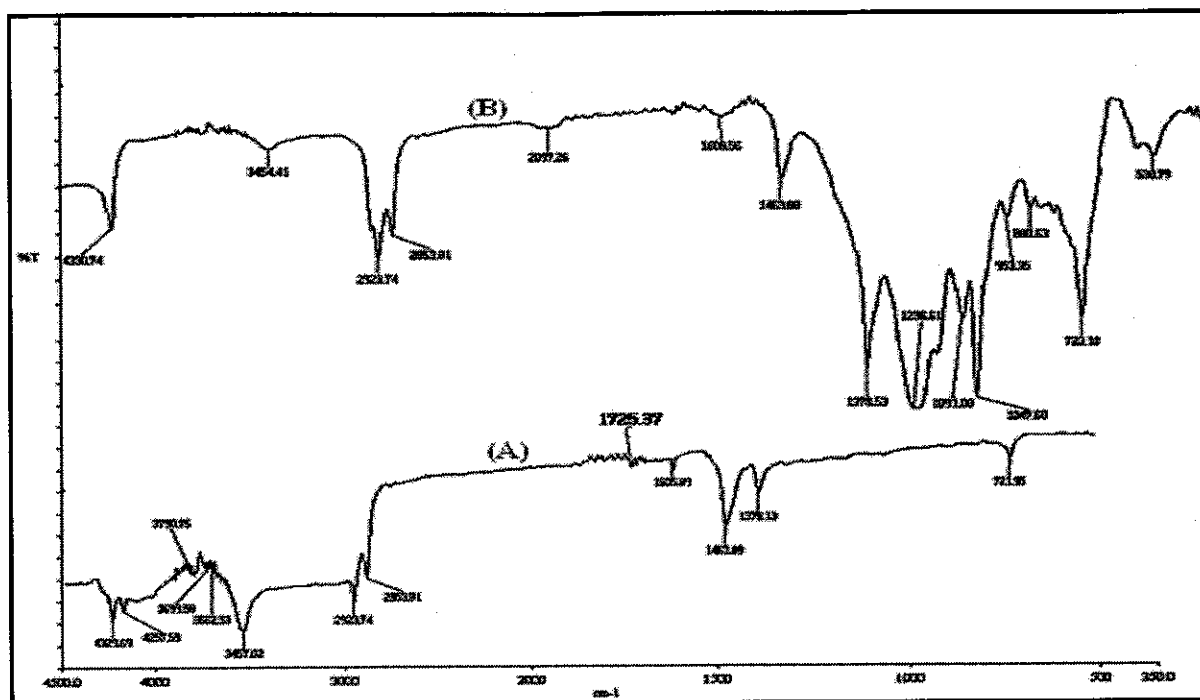


Figure 4.16: FTIR-ATR spectra of Angsi crude recovered by ASP flooding with SDS (A) and ATR:AOT (B).

4.5 IFT Measurements

IFT measurements at various Angsi crude oil and water interfaces in the presence and absence of alkali, surfactants and polymers have been performed using the SVT 20, spinning drop video tensiometer of Dataphysics, Germany.

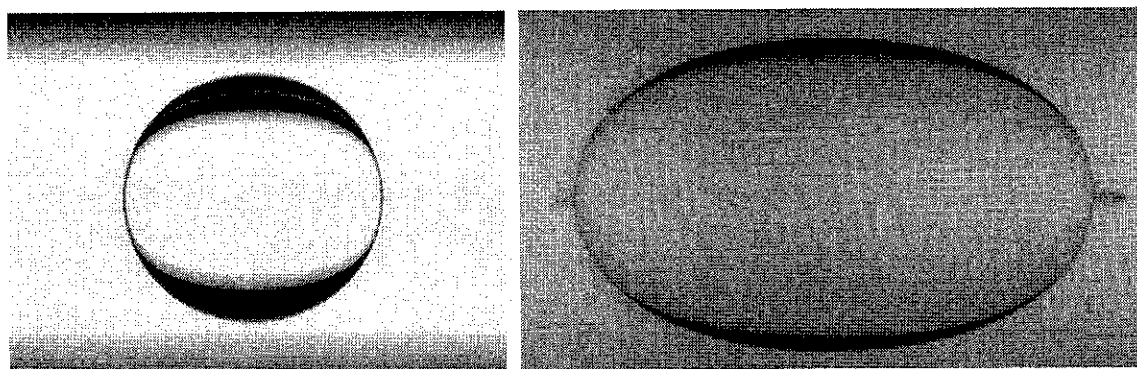


Figure 4.17: Normal (L) and elongated (R) oil droplet.

Oil droplet was inserted inside the capillary which was previously filled with the desired aqueous phase. Appropriate spinning speed was adjusted so that the oil droplet can be suitably elongated. The positions of normal and elongated oil droplet inside the

capillary of spinning drop tensiometer are depicted in Fig. 4.17. The IFT values of Angsi crude in contact with 10,000 ppm pure synthetic brine solution was found to vary from 21.5 mN/m to 18.9 mN/m at 45 °C as contact time increases from 5 to 40 minutes. By comparison, the IFTs of synthetic brine solution of 10,000 ppm in combination with 2000 ppm each of DBSA, CTAB, SDS and 1500 ppm each of ATR, AOT, mixture of ATR and AOT, 1500 ppm of each are shown in Fig. 4.18. The reported values are the average of three concordant measurements.

Fig. 4.18 presents the attainment of low IFT value over time duration. Combination of ATR:AOT (1:9) offers the least IFT followed by AOT and ATR and after this conventional surfactants SDS, CTAB and DBSA respectively. Except for CTAB and DBSA, IFT reduction accomplished by the SDS, AOT, ATR and ATR:AOT surfactants are time independent. The non-conventional surfactants produce an IFT reduction of 1.5 mN/m to 2 mN/m lower than the conventional surfactants. Synergistic combination of ATR and AOT provide an improved IFT reduction (as lower as 0.06 mN/m) compared to the individual surfactants (1.57 mN/m in DBSA) which is 26 times fold benefit in IFT reduction. The outstanding feature is that of its non-dependency on time. This has a major significance on its in service utilization on a protracted basis, providing an ultralow IFT reduction immediately on application and sustaining the effect on a prolong basis. From the obtained IFTs it can be concluded that non-conventional surfactants are not only economical but more prominent as compared to the conventional surfactants as far as the IFT reduction at oil-water interface is concerned.

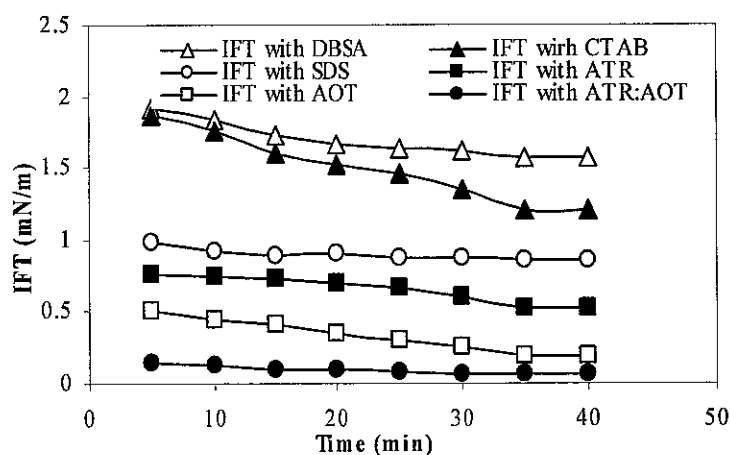


Figure 4.18: IFTs at crude oil-water interface in combination with various surfactants.

IFTs of Angsi crude in combination with ASP formulations having 1500 ppm of polymer-1, 0.1% Na_2CO_3 , 2000 ppm, SDS, 1500 ppm of each ATR, AOT and mixture of ATR:AOT (1:9) are given in Fig. 4.20. Due to severe precipitation DBSA and CTAB were not compatible with the other constituting chemicals so they were not further processed for IFT measurements. Measured IFT values were found to be further reduced from 0.099 – 0.036, 0.064 – 0.031, 0.047 – 0.018 and 0.099 – 0.0064 mN/m for ASP formulations containing SDS, ATR, AOT, mixture of ATR and AOT at 45 °C with increase in contact time from 5 to 40 minutes. In case of conventional surfactant alkalinity has performed a pronounced effect in further lowering the IFT, whereas in case of non-conventional surfactant this effect is not as prominent. The results have also exhibited that synergism is the important mechanism than the antagonism which exists between the added surfactant and alkali. Moreover, the longer the alkyl chain length is, the less alkalinity is needed. The appropriate IFT reduction required for EOR applications is attainable using the mixture of proper surfactants in precise ratio. It has been reported in Fig. 4.20 by Nasr-El-Din [15], that IFT values at crude oil-water interface from 10^{-2} – 10^{-3} mN/m are suitable for maximum oil mobility and recovery.

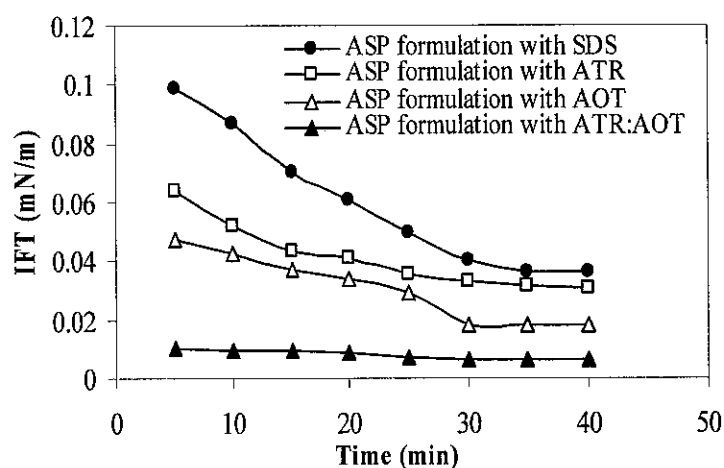


Figure 4.19: IFTs at crude oil-water interface in combination with ASP formulations.

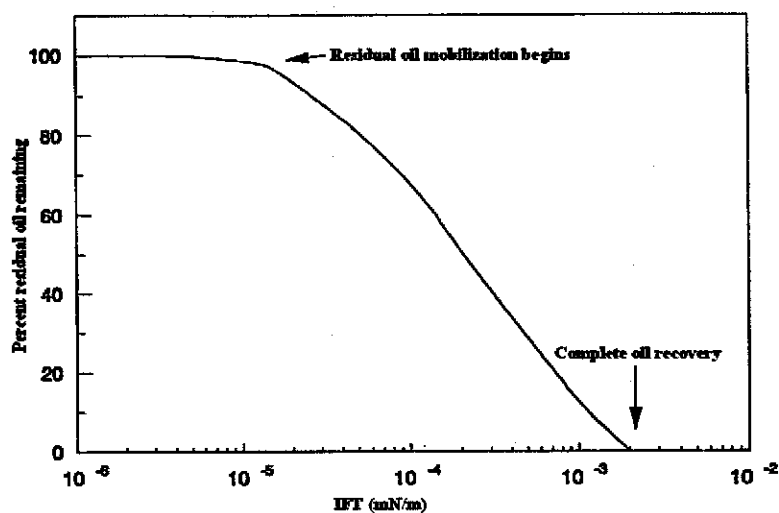


Figure 4.20: Oil recovery and IFT correlation [15].

4.6 Atomic Force Microscopy of Oil-Water Emulsions

AFM has been used to provide an image of the oil-in-water emulsions using Agilent series 4500 Atomic Force Microscope. Oil-water emulsions have been initially prepared using 5% Angsi crude in combination with 95% brine solution consisting of 10,000 ppm salinity and 0.1% Na_2CO_3 . Surfactants, 2000 ppm SDS, 1500 ppm each of ATR, AOT, mixture of ATR:AOT (1:9) were then added to the oil-brine emulsions respectively.

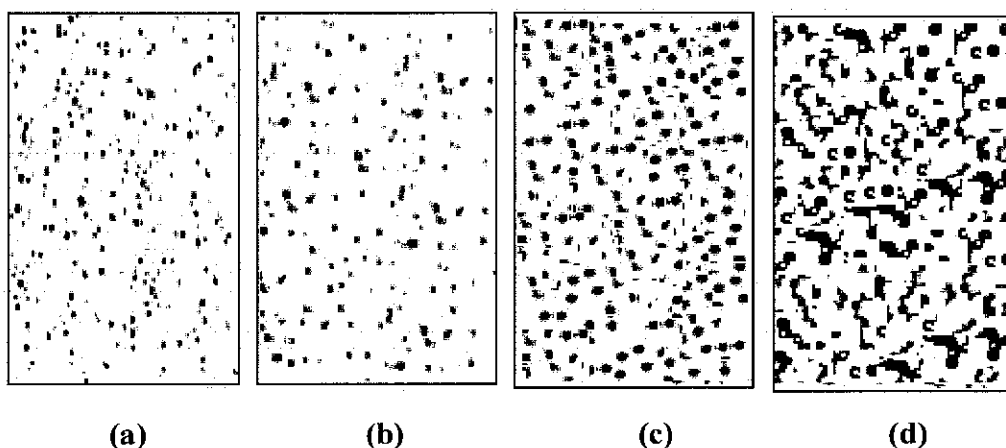


Figure 4.21: AFM micrographs of oil-water emulsions: (a) emulsion with SDS (b) emulsion with AOT (c) emulsion with ATR (d) emulsion with mixture of ATR and AOT.

It is obvious from AFM micrographs that the emulsion with SDS, Fig. 4.21 (a),

provides finely dispersed droplets of oil-in-water, whereas the emulsions with AOT, ATR and particularly with the mixture of ATR and AOT, Fig. 4.21 (b), (c) and (d) generated more pronounced oil droplet dispersion. Finely dispersed droplets favor emulsion stability, whereas more heavily dispersed oil droplet, pseudo emulsions are desirable for EOR activity. The propensity of larger oil droplet dispersion is dependant upon the chain length that is in contact with the hydrocarbon phase. Conventional, straight chain surfactants like SDS can be easily accommodated even if the hydrocarbon phase is low but the surfactants with branched structures such as in ATR and AOT require bulky hydrocarbon cage to be accommodated. If the situation is reverse then they can wash out the hydrocarbon phase but the emulsion will be instable leading to a rapid phase separation. But in case of water-in-oil emulsions containing branched chain and dimeric surfactants are crucial to accomplish the stable emulsion as compared to conventional surfactants as it is depicted in Fig. 1.6 previously [6]. The involved mechanism in phase separation phenomenon in oil-water emulsions can be demonstrated considering Fig. 4.22. In case of unstable oil-water emulsions, heavily dispersed oil droplets are bridged together by coagulation, flocculation and creaming processes as shown in Fig. 4.22. This produced an enhanced phase coalescence hence achieving a high degree of phase separation.

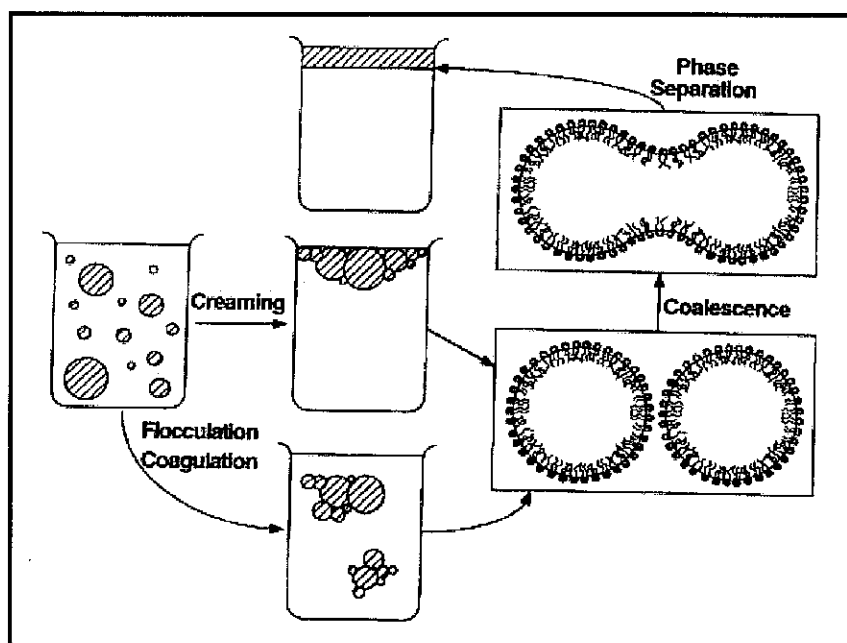


Figure 4.22: Phase separation in oil-water emulsions [60].

In case of EOR applications it is vital that there is a production of stable emulsions that are associated with multifarious diverse factors like oil separation and hindrances in pipeline transportation due to fluids of contrasting viscosities. It can be concluded that branched chain surfactants can act as a better substitute compared to the conventional surfactants not only to enhance oil production but also to facilitate pipeline transportation to refinery by maintaining a low effective viscosity and drag.

4.6.1 Stability of O/W Emulsions

Previously equilibrated oil-water emulsions containing 5 mL of oil and 95 mL of brine solution in combination with alkali and surfactants were separated. Obtained volumes of the crude following separation are reported as in Table 4.7. In the presence of low concentrations of alkali, simultaneous processes involving emulsification and sponification provide the stability of oil-water emulsion. However, it is observed that the prepared emulsions are not stable and various fractions have a tendency to drop out of solution. On the other hand, the non-conventional surfactants, particularly the mixture of AOT and ATR in specified proportions has proved two distinct behaviors and is expected to be more prominent due to synergistic and antagonistic effects than the individual surfactants. More than 98% oil the original hydrocarbon phase was separated in case of the mixture of ATR and AOT which is also supporting the results obtained by the AFM micrographs and confirming that if the volume of hydrocarbon phase is less than the aqueous phase the surfactants will tend to adsorb on the oil-water interface instead of staying in the bulk solution.

Table 4.7: Volumes of hydrocarbon phase separated from O/W emulsions

Emulsions	Volume of the crude separated/mL	Percentage
Emulsion with SDS	4.60	92
Emulsion with ATR	4.72	94
Emulsion with AOT	4.80	96
Emulsion with mixture of ATR and AOT	4.91	98.2

4.7 Estimation of Partition Coefficients

The calculated partition coefficients of various oil-water ratios are presented as in

Table 4.8. If the partition function is 1, it means that same concentrations of the surfactant are present in both hydrocarbon and aqueous phases. Partition coefficients having values > 1 indicate that the surfactant has a strong affinity towards hydrocarbon phase. The reverse is true for partition coefficients having values < 1 . With reference to Table 4.8 in 1:1 O/W emulsion system partition coefficient for non-conventional surfactants is higher than the conventional surfactant by a factor of 2. The partition coefficient values increase appreciably when the oil phase content is increased. The contrast is more pronounced for the non-conventional as compared to the conventional surfactants. A differential of 2 fold is observed in the partition coefficients between aqueous rich to oil rich.

The partitioning coefficient of a surfactant between oil and water is related to the free energy of transfer from one phase to the other. The variation of the partition coefficient with volumetric variables of each phase can be used as a benchmark for the concept of generalized formulation. Emulsions are usually stabilized with a mixture of surfactants with different hydrophilicity. The initial partitioning of surfactants between the dispersed phase and continuous phase, and how these phases are brought into contact, can significantly affect the emulsification processes and associated oil recoveries. The concept of hydrophilic-lipophilic balance (HLB), which is an indication of the relative strength of the hydrophilic and hydrophobic portions of the surfactant molecules, can be used to characterize the relative affinity of surfactants for aqueous and organic phases. Generally, non-conventional surfactants have high HLB values than conventional surfactants which indicate good surfactant solubility in water, while a low HLB number indicates a high relative affinity for the organic phase. As a result, surfactants with a high HLB tend to stabilize oil-in-water (O/W) emulsions whereas surfactants with low HLB tend to stabilize W/O emulsions. Usually depending on the crude oil properties HLB number within 10–16 are appropriate for oil recovery applications [6]. However, in case of O/W emulsions with mixture of surfactants HLB values should not be much different, as the emulsion stability is greatly affected when a wide HLB difference exists and reverse is true for W/O emulsion. Non-conventional surfactants may lead to a transitional-phase inversion (TPI) to the opposite emulsion. This is also associated with

an ultra-low interfacial tension at the inversion point. TPI may also occur by variation in disperse-phase ratio as a result of favored partitioning of surfactant into oil and water phase. As a matter of fact, mixing that involves addition of a phase into another phase with a different surfactant HLB is associated with variations in the dispersed-phase ratio as well as HLB [9,18].

In oil reservoirs oil is trapped inside the pores and it is not present as a continuous phase particularly in near depleted reservoirs. During a chemical flooding exercise if the conditions of ultralow IFT and suitable wettability alteration are favorable, the surfactants are able to reach to micro and mille pores of the reservoir and interact with the hydrocarbon phase. The surfactant will be distributed in oil and aqueous phases. As a result trapped oil will be emulsified and mobilized in the form of tiny droplets suspended in the aqueous phase. Non-conventional surfactants will tend to orient themselves at the oil-water interfaces and will continue to do so until the formation of a pseudo-emulsion which will lead to TPI, further facilitating the oil recovery process. The conventional surfactants on the other hand trapped and retained by the hydrocarbon phase can impede oil flow due to the formation of stable emulsion of high viscosity and rendering the process impracticable.

Table 4.8: Partition coefficients of various surfactants in O/W systems.

Surfactants	Oil/Water Volumes, mL	Partition Coefficients, K
SDS, 2000 ppm	10/10	0.72
	2/18	0.65
ATR, 1500 ppm	10/10	1.97
	2/18	0.85
AOT, 1500 ppm	10/10	1.64
	2/18	0.78
ATR:AOT, 1500 ppm	10/10	1.73
	2/18	0.81

4.8 Wettability through Contact Angle Measurements

For the evaluation of wettability alteration, initially the contact angle between brine water droplet on oil-wet substrate was measured using a contact angle analyzer, Phoenix-300, SEO, Korea. Contact angle between brine water and oil-wet substrate was found to be $65 \pm 1^\circ$. The reported values are the average of three concordant measurements. Fig. 4.23 represents the relationship between surfactant concentration and contact angles. Contact angles of brine solution droplet containing alkali in the presence of surfactants gradually increased with an increase in surfactant concentrations. The contact angles were found to be increasing from 78° to 154° , 79° to 168° , 81° to 175° and 84° to 178° in the presence of SDS, AOT, ATR, mixture of ATR and AOT for a set up concentrations of 500 – 2000 ppm respectively. As the contact angles approached to 180 degrees, complete spreading of the saline droplet is expected which is an indication that the wettability of the substrate has been altered from oil-wet to water-wet. The same mechanism of wettability alteration and advancement in contact angles has also been reported by Subhash *et al* [124].

Fig. 4.24 explains the detailed mechanism regarding the surfactant's orientation involved in wettability alteration. Initially the hydrophobic tails of the surfactants orient towards the oil-wet surface and the hydrophilic heads will be oriented outwards. Water molecules become attracted towards oil-wet surface. It is suspected that the alkali and polymer solution can deeply penetrate deep within the pores of the rocks to reach the previously unswept areas.

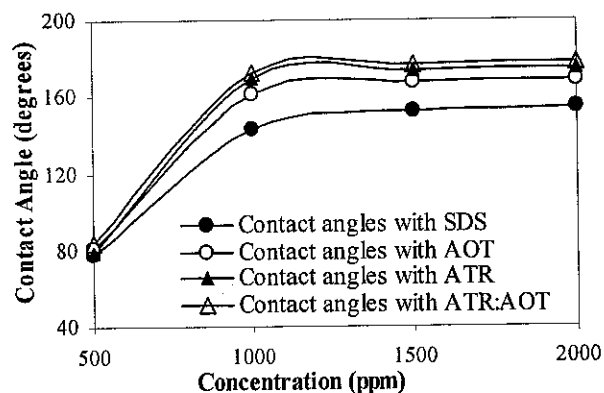


Figure 4.23: Surfactant's concentration and contact angles of brine solution droplet.

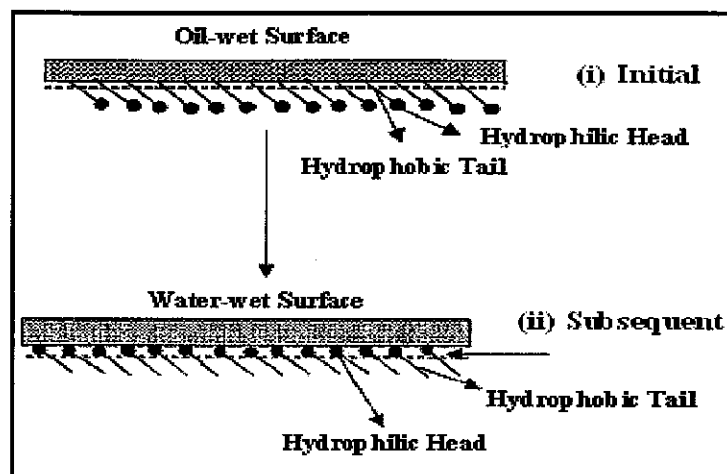


Figure 4.24: Wettability alteration mechanism by surfactants.

4.9 Characterization of Sandstone Cores

Basic properties of the sandstone core samples that were used for spontaneous and forced imbibition studies are reported in Table 4.9. Core samples, 1 – 5 were utilized for spontaneous imbibition studies, whereas 6 – 9 were used for core flooding experiments. Although all the samples were collected from the same reservoir each core sample possess a different set of property compared to each other. However all the selected samples were possess porosities values ranging 21 – 28 %. The average porosity of Angsi field is 22 %.

Table 4.9: Basic properties of sandstone core samples.

Serial No. Properties	1	2	3	4	5	6	7	8	9
Length (cm)	3.10	3.28	3.10	3.25	3.61	4.92	6.53	4.07	4.89
Weight (g)	70.30	74.81	69.89	73.45	81.85	111.57	138.44	94.12	104.40
Air Perm., K (mD)	154.32	190.54	156.37	165.52	184.23	177.87	157.59	194.78	217.72
Porosity, Φ (%)	23.15	26.28	21.36	24.29	25.74	24.12	28.37	23.62	26.88
Bulk Volume (cm ³)	26.27	29.15	25.68	30.57	36.13	46.15	53.99	54.91	57.92
Bulk Density (g/cm ³)	1.87	1.92	1.97	2.01	1.85	1.96	1.89	1.93	2.02
Grain Volume (cm ³)	33.25	34.16	29.38	31.77	36.10	39.47	41.66	35.25	42.77
Grain Density (g/cm ³)	2.68	2.66	2.67	2.64	2.53	2.68	2.66	2.67	2.64
Pore Volume (cm ³)	7.54	8.67	7.32	8.19	7.34	10.90	13.24	12.62	14.51
OOIP (mL)	4.8	5.1	4.7	4.9	4.3	7.7	8.7	7.1	10.5

4.10 Spontaneous Imbibition Studies

Spontaneous imbibition studies were performed to provide an initial screening of the chemicals. This screening provides a guide assessment of the compatibility of the chemicals with the target reservoir rock and fluids. It also indicates the selected concentration of the chemicals required to achieve desirable oil recovery factor.

4.10.1 Oil Recovery from Low and High Permeability Cores

In order to evaluate the suitabilities of the core porosity and permeability of for the chemical flooding, two core samples were chosen: sample A, $\Phi = 22.15^\circ$, $k = 70$ mD and sample B, $\Phi = 22.35^\circ$, $k = 150$ mD. The cores were initially saturated with Angsi crude oil and finally imbibed with the combination of brine solution, TDS = 10,000 ppm and 0.5 % alkali. The obtained results are shown in Fig. 4.25.

It can be observed that oil recovery from the core sample with low permeability started earlier than the core with high permeability. The cores were saturated with crude without the implementation of pressure. In the case of the core with permeability = 70 mD, the penetration of the crude is lower than the core of permeability = 150 mD. After 1000 minutes time interval, in terms of PV% more recovery was observed from the core with high permeability than the lower.

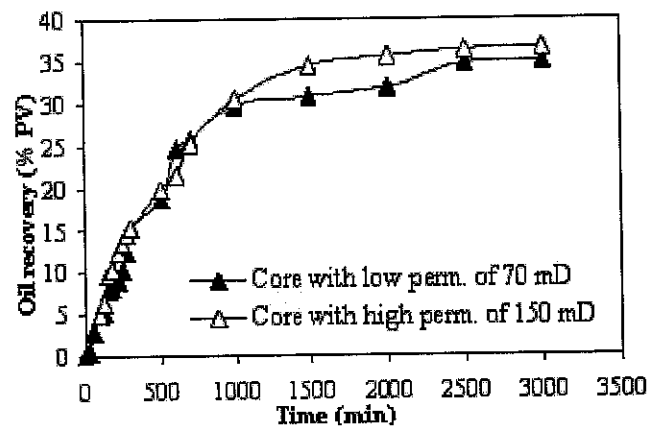


Figure 4.25: Oil recovery from the cores with low and high permeability.

4.10.2 Oil Recovery by ASP Imbibition with SDS

Core sample 1 was investigated for imbibition studies by ASP flooding using SDS. It was imbibed with synthetic brine solution, TDS = 10,000 ppm, to a point where no more oil recovery was observed. Imbibition was carried out further with the addition of 1500 ppm, polymer 1, 2000 ppm SDS, and 0.1 % Na₂CO₃, sequentially. The obtained results are presented in Fig. 4.26.

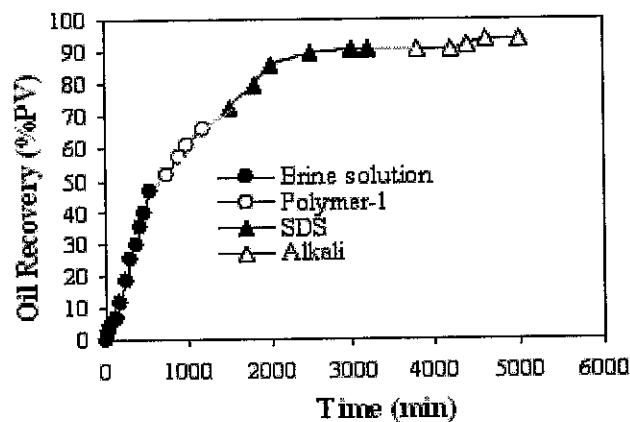


Figure 4.26: Oil recoveries by spontaneous imbibition with ASP by SDS.

It is obvious from the Fig. 4.26 that 46.65 % of OOIP was displaced by the brine solution leaving behind 53.35 %. Injection of polymer, surfactant and alkali has further enhanced the recoveries in terms of PV to 65.7, 90.68 and 94 % respectively.

4.10.3 Oil Recovery by ASP Imbibition with ATR

Core sample 2 was examined for imbibition studies by ASP flooding using ATR. It was imbibed with synthetic brine solution, TDS = 10,000 ppm, till no more oil recovery was observed. Imbibition was carried out further with the addition of 1500 ppm, polymer 1, 1500 ppm, ATR and 0.1 % Na₂CO₃ gradually when further oil recovery was ceased in each stage. The obtained results are presented in Fig. 4.27.

Fig. 4.27 implies that 48.7 % of PV was displaced by the brine solution leaving behind 52.3 %. Subsequent injection of polymer, surfactant and alkali has further enhanced the recoveries to 63.98, 81.39 and 85.57 % respectively.

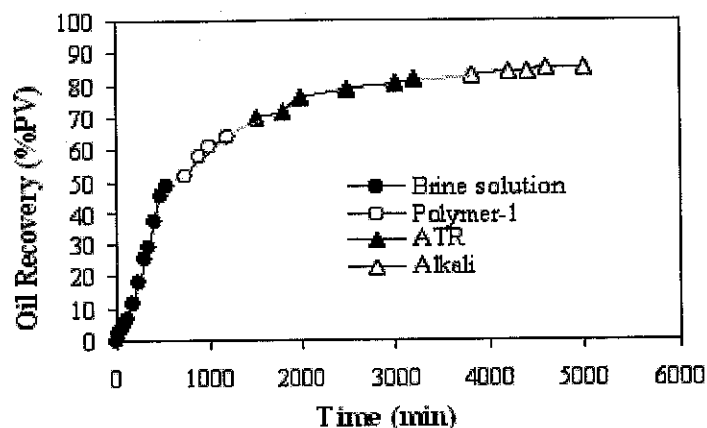


Figure 4.27: Oil recoveries by spontaneous imbibition with ASP by ATR.

4.10.4 Oil Recovery by ASP Imbibition with AOT

Core sample 3 was utilized for imbibition studies by ASP flooding using AOT. Just like the previous core samples, it was also imbibed with synthetic brine solution, 10,000 ppm, till no more oil recovery was observed. Imbibition was carried out further with the addition of 1500 ppm, polymer 1, 1500 ppm, AOT and 0.1 % Na_2CO_3 progressively when further oil recovery was come to an end in each stage. The obtained results are presented in Fig. 4.28.

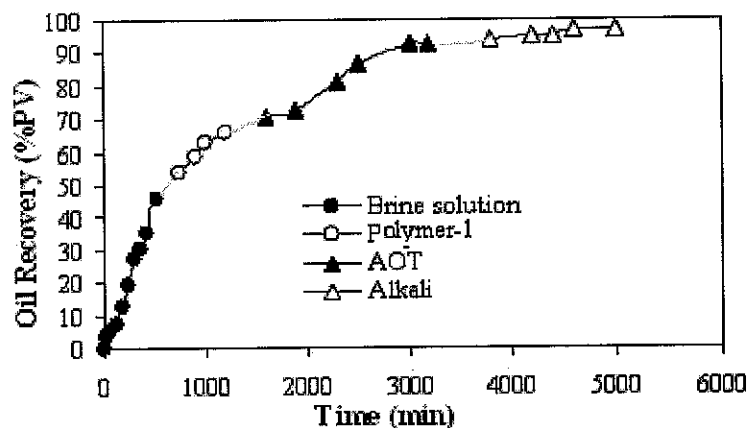


Figure 4.28: Oil recoveries by spontaneous imbibition with ASP by AOT.

It can be accomplished from the Fig. 4.29 that 49.3 % of OOIP was recovered by the brine solution leaving behind 51.7 %. Gradual, injection of polymer, surfactant and alkali has further enhanced the recoveries to 66.88, 92.53 and 96.99 % respectively.

4.10.5 Oil Recovery by ASP Imbibition with ATR and AOT

Core sample 4 was examined for imbibition studies by ASP flooding using mixture of ATR and AOT surfactants in ratio 1:9 correspondingly. Similar procedure as given in 4.10.3 and 4.10.4 was followed for the injection of chemicals. The obtained results are shown in Fig. 4.29.

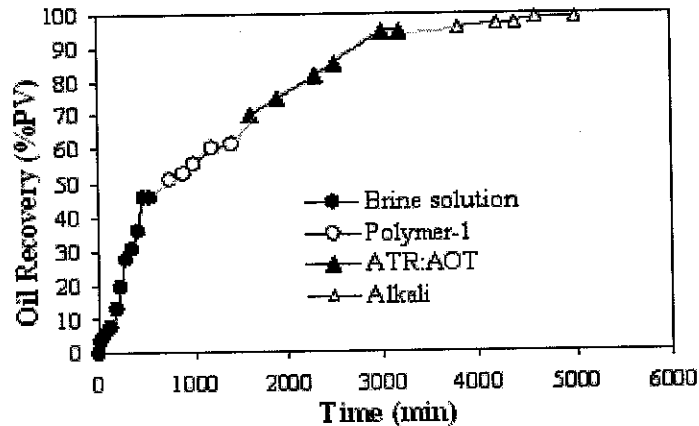


Figure 4.29: Oil recoveries by spontaneous imbibition with ASP by ATR:AOT.

It can be concluded from the Fig. 4.30 that 45.7 % of OOIP was recovered by the brine solution alone leaving behind 54.3 %. Subsequent, injection of polymer, surfactant and alkali in sequence has further enhanced the recoveries to 61.56, 94.79 and 98.56 % respectively.

Figs. 4.26 – 4.29 have indicated that oil recoveries can be significantly enhanced by ASP flooding. Polymer-1 has achieved a consistent performance in all cases. Various surfactants have displayed a variation in their performance. This is attributed to their structural differences. ATR has shown less recoveries compared to SDS and AOT. This is likely due to the hydrocarbon chain in AOT impairing surfactant ability to adsorb and penetrate deep into mille pores. However, the combination of ATR and AOT has been found to be better as compared to the individual surfactants whether conventional or non-conventional. This synergistic effect of alkali with surfactants is more pronounced in the case of SDS than the non-conventional surfactants.

Instead of ASP, it is also likely to use low-alkaline-surfactant-polymer (LASP) flooding by incorporating non-conventional surfactants to further minimize the associated jeopardy of precipitation. LASP offers another exciting approach for an enhanced recovery strategy. LASP will be further investigated in core flooding studies.

4.10.6 Oil Recovery by ASP Imbibition with CTAB

It has been previously concluded that CTAB is not compatible with the other constituting chemicals (section 4.2.3). It has been evaluated further to elaborate the involved mechanism and to understand the importance of selecting a suitable surfactant for EOR applications. Core sample 5 has been studied for imbibition experiments by ASP flooding using CTAB by adopting the similar procedure as reported 4.10.3 – 4.10.5. The obtained results are presented in Fig. 4.36 and discussed here.

It is obvious from Fig. 4.30 that 66 % oil was recovered as result of brine and polymer injection. Addition of CTAB has resulted in a negligible increase i.e. from 66 – 68 %. Subsequent imbibition with alkali did not increase the recovery appreciably. The recovery factor (RF) in terms of PV rise to 68 – 69.28 % only. CTAB did not produce the desired recoveries. This is due to the strong electrostatic interactions between the cationic CTAB, the anionic polymer-1 and negatively charged rock samples. The strong affinity between CTAB, polymer-1 and rock has marked rock surface. As a consequence the pores and open channels are blocked and oil flow becomes restricted. This mechanism will be justified by SEM analyses later on.

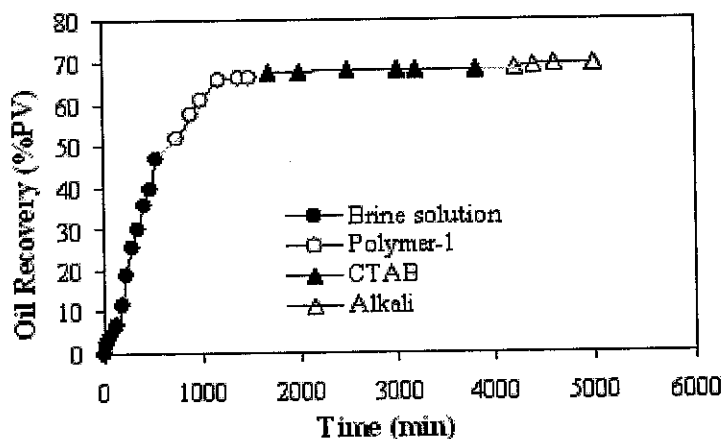


Figure 4.30: Oil recoveries by spontaneous imbibition with ASP by CTAB.

4.11 BET Surface Area and Pore Structure Measurements

BET surface and micropore areas of the selected core samples were measured by using Micrometrics ASAP 2000 model surface area and pore size analyzer. Adsorption-desorption, and BET isotherms of core sample 1 are presented in Figs. 4.31 and 4.32 respectively. BET surface and micropore areas of the analyzed sandstone samples are given as in Table 4.10.

Table 4.10: BET surface and micropore areas of sandstones.

Sample ID	Surface Area (m ² /g)	Micropore area (m ² /g)
Sandstone original	0.7101	0.4846
Sandstone saturated with Angsi crude	0.0727	0.0070
Sandstone after ASP imbibition by ATR:AOT	0.3112	0.0302

It is clear that the available surface and micropore area have been extensively covered during the oil saturation step. However, ASP flooding has resulted in a comprehensive oil recovery leading to the enhancement of surface area again. As much as 44% of the original surface area of sandstone has been recovered following a ASP imbibition by ATR:AOT surfactant mixture.

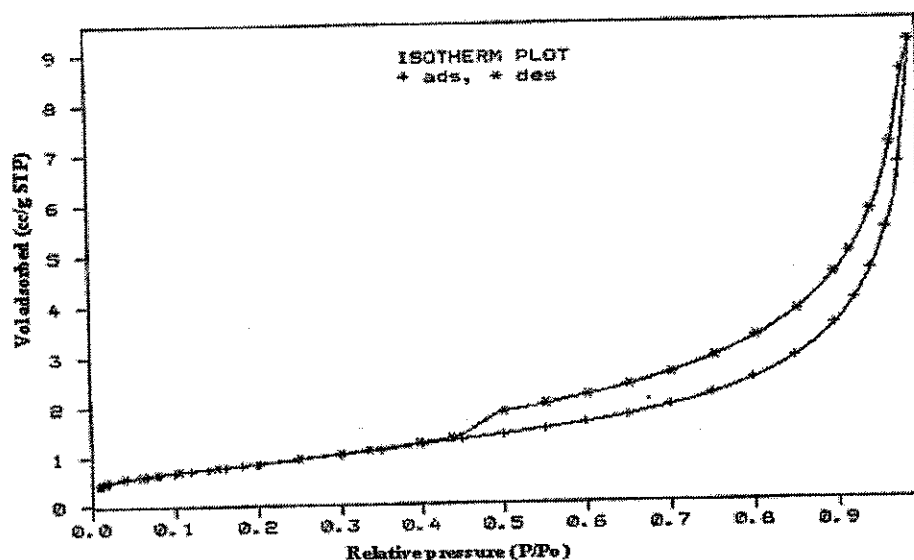


Figure 4.31: Adsorption, desorption isotherms for liquid nitrogen on sandstone.

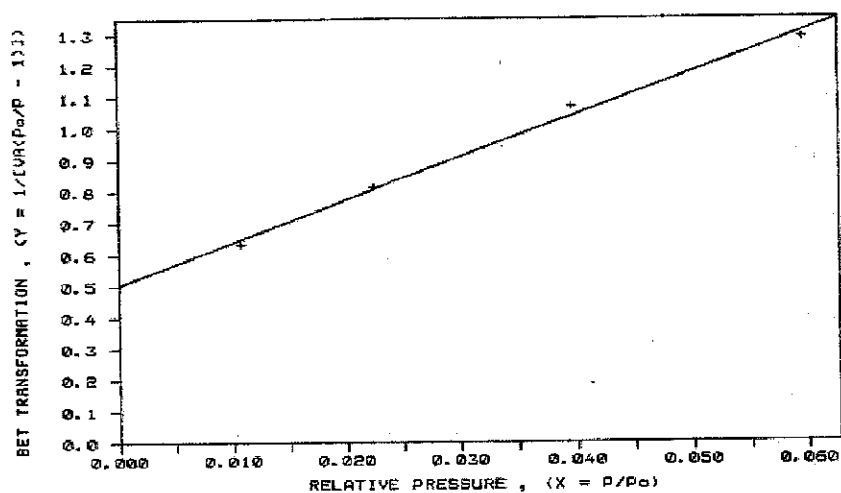


Figure 4.32: BET plot for the adsorption of liquid nitrogen on sandstone.

4.12 SEM/EDX Analyses of Cores

SEM and EDX analyses have been performed on the selected core samples using Zeiss DSM-950 SEM/EDX electron microscope. The obtained SEM images and EDX peaks are presented in Figs. 4.33 – 4.36 respectively.

Figs. 4.33 and 4.34 represent the SEM images of the original and oil saturated sandstone cores. The open pores, Fig. 4.34 have been saturated with oil and are not visible.

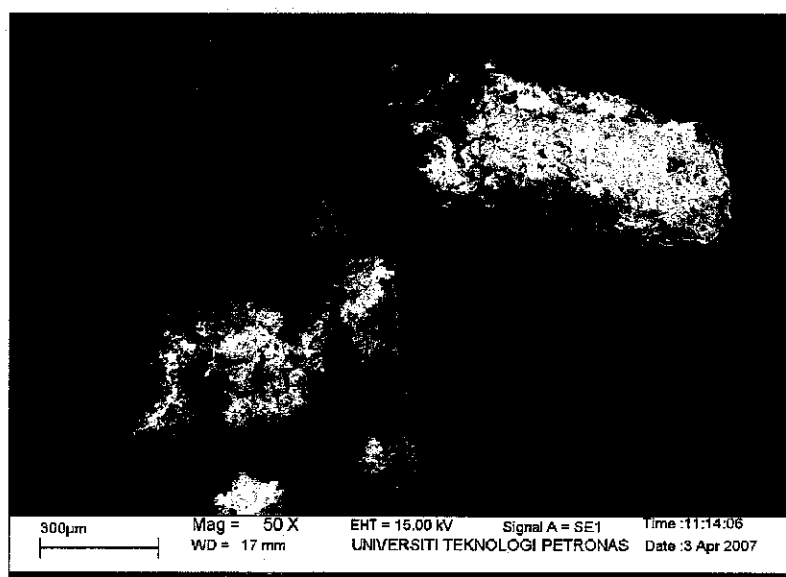


Figure 4.33. SEM image of original sandstone.

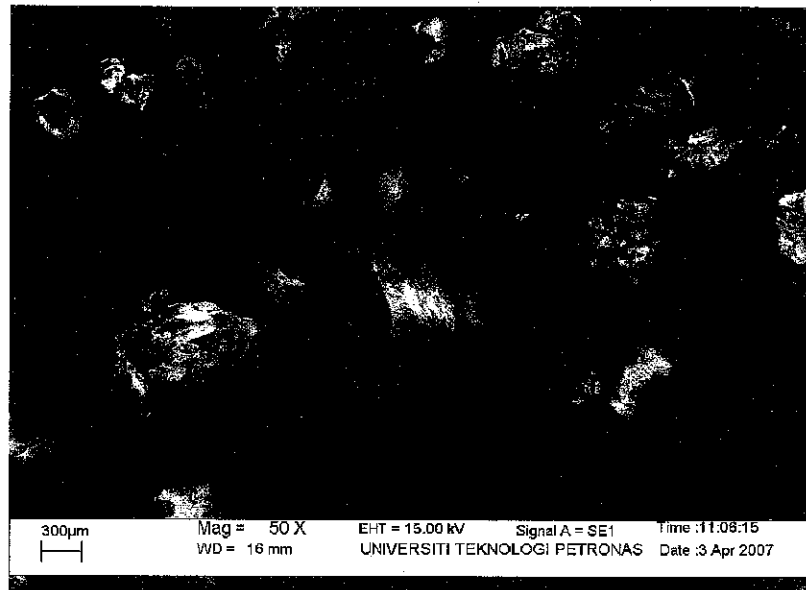


Figure 4.34: SEM image of an oil saturated sandstone.

Fig. 4.35 is SEM image of the sandstone after an ASP flooding with ATR:AOT. There is enough contrast to make out the pore throat opening. The original topography of the surface and micropores which were initially saturated by oil have been restored implying that these areas are completely washed by the ATR:AOT surfactants mixture.

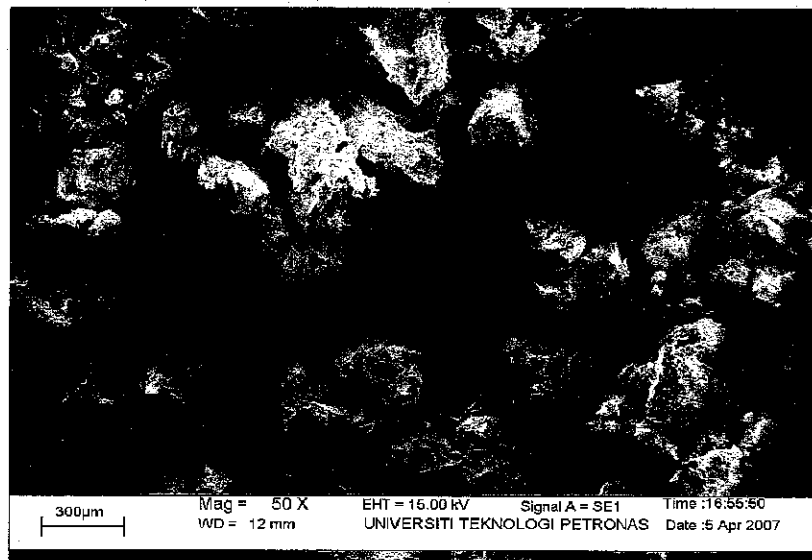


Figure 4.35: SEM image of sandstone after ASP flooding with ATR:AOT.

Fig. 4.36 is SEM image of sandstone core after ASP flooding with CTAB. As discussed earlier in 4.10.6, the strong electrostatic interactions between cationic CTAB surfactant and the anionic polymer-1 caused the surface of core to be blocked. As a result severe adsorption on the core sample is evident with CTAB (Fig. 4.36).

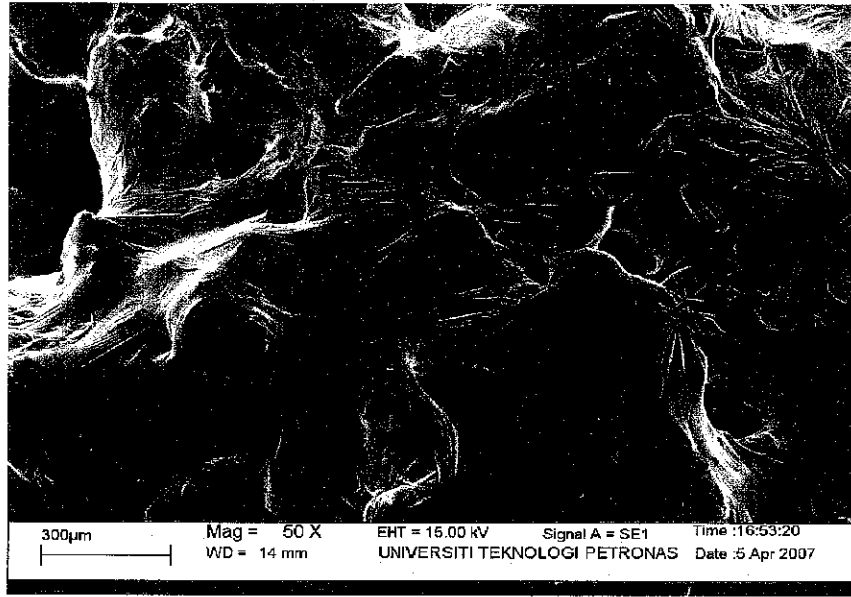


Figure 4.36: SEM image of sandstone after ASP flooding with CTAB.

EDX analyses of the two core samples are presented in Figs. 4.37 and 4.38 respectively. From the peaks it is apparent that Si content of both of the samples is prominent compared with other elements. Although they were collected from the same field, they vary from each other in terms of elemental composition and can behave differently as far as the wettability alteration is concerned. Elemental profiles are given in Table 4.11.

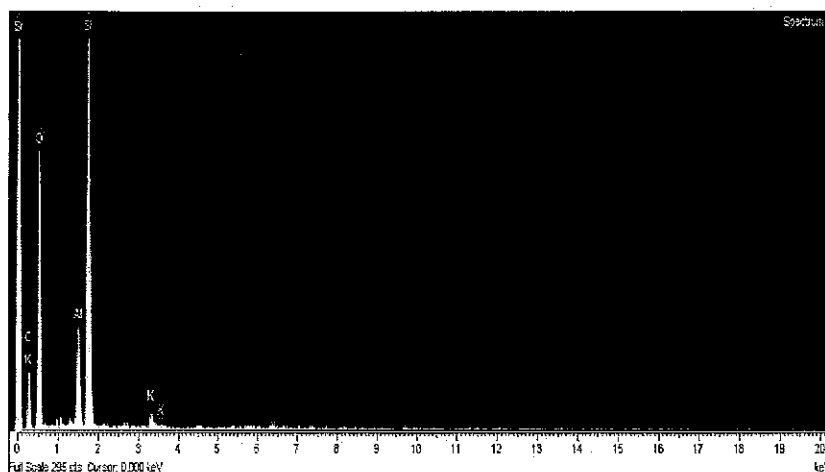


Figure 4.37: EDX analyses of sandstone core sample 1.

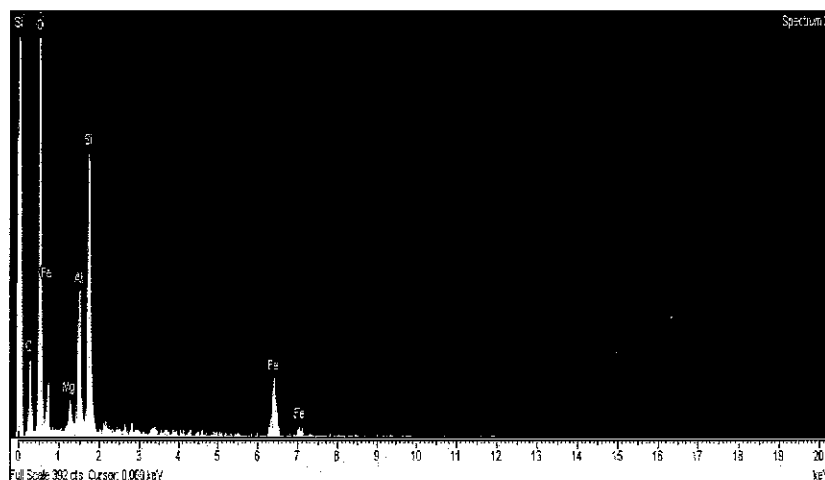


Figure 4.38: EDX analyses of sandstone core sample 7.

Table 4.11: Elemental profiles of core samples 1 and 7.

Core sample-1		Core sample-7	
Elements	Weight %	Elements	Weight %
C	27.62	C	22.65
O	35.51	O	41.03
Al	3.85	Al	4.80
Si	32.16	Si	26.08
K	0.86	Mg	1.04
-	-	Fe	4.40
Total	100.00	Total	100.00

4.13 Core Flooding Studies

Coreflooding studies were performed using core samples 6 – 9 correspondingly for ASP flooding using mixture of ATR and AOT, SDS, ATR and AOT respectively. Confining pressure and temperature were maintained at 2,000 psi and 90 °C. In all the flooding experiments predetermined concentrations of brine, TDS = 10,000 ppm and 1500 ppm of polymer-1 were utilized. The concentrations of alkali were 0.1% with 2000 ppm, SDS surfactant and 1500 ppm for non-conventional surfactants; it was fixed as 0.05%. Similar protocols were adopted as it was for the cores with spontaneous imbibition studies i.e. flushing with brine solution initially, followed by polymer and surfactant flooding and finally flushing with alkali.

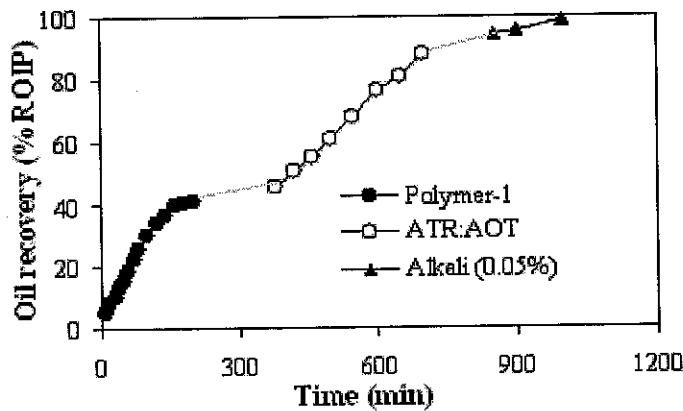


Figure 4.39: Oil recoveries in coreflooding with ASP by ATR:AOT.

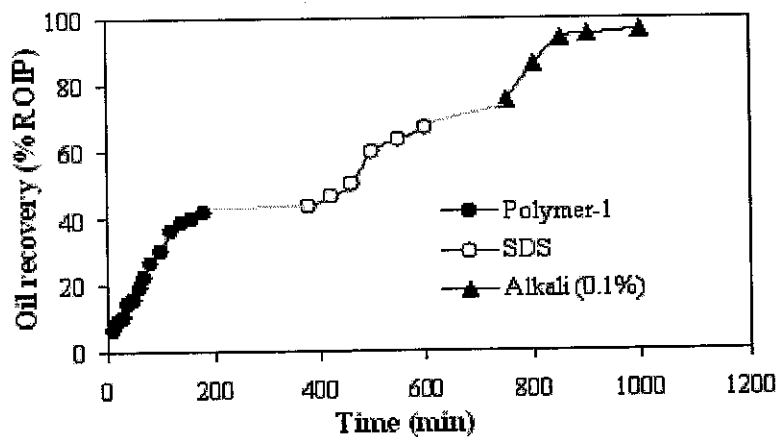


Figure 4.40: Oil recoveries in coreflooding with ASP by SDS.

The results revealed that the brine and polymer flooding results in almost similar fashion in all the core samples as far as the oil recovery is concerned. However, conventional and non-conventional surfactants have resulted in dissimilar performance and have also exposed variations in terms of interactions with alkali. Recoveries of remaining oil in position (ROIP) were approximately found to be 99, 96, 82 and 96% respectively for the mixture of ATR and AOT, SDS, ATR and AOT.

Proportions of oil recovered by various components with respect to ROIP are given in Table 4.12. Recoveries as a result of polymerfloods are attributed to the controlled mobility due to high viscosity and improved sweep efficiency. The similar mechanism was observed again, as it was previously reported, 4.10.5, that SDS and alkali have strong interactions resulting in enhanced IFT reduction than non-conventional surfactants which is one of the mechanisms involved in enhanced recoveries. It was also confirmed that using mixture of non-conventional surfactants LASP is also effective as ASP is. ATR has resulted in less oil recoveries than AOT which is also in accordance to the previously reported results of imbibition studies.

Table 4.12: Chemically enhanced oil recoveries by various components.

Surfactant system	ROIP (mL)	Polymer recovery (mL)	Surfactant's recovery (mL)	Alkali recovery (mL)	Overall recovery (% ROIP)
TR:OT	3.7	1.52	1.7	0.44	99
SDS	2.4	1.0	0.6	0.7	96
ATR	3.5	1.3	0.9	0.7	82
AOT	2.9	1.4	1.0	0.4	96

From the pictures (Fig. 4.43) of cores at various stages of flooding it is apparent that the combination of polymer and surfactants flooding is still leaving behind some oil in place that was progressively recovered after ASP flooding.

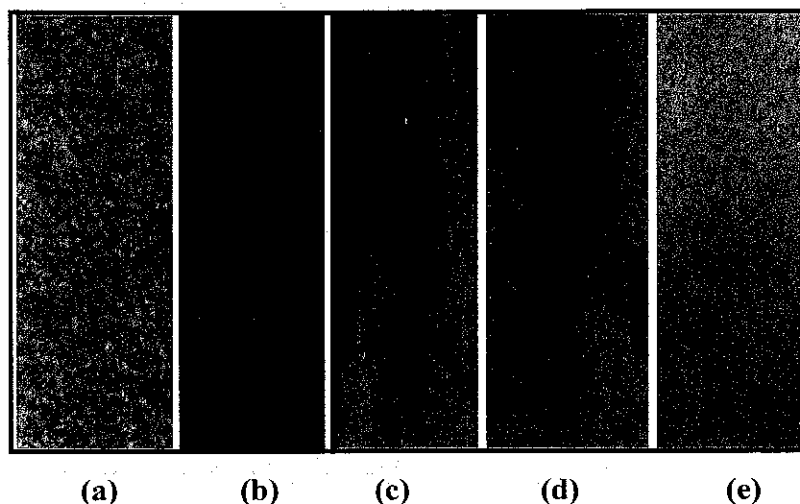


Figure 4.43: Pictures of sandstone core: (a) original sandstone (b) oil saturated sandstone after brine flushing (c) oil saturated sandstone after flooding with polymer-1 (d) oil saturated sandstone after flooding with polymer plus surfactant (e) oil saturated sandstone after flooding with polymer plus surfactant plus alkali.

The major mechanisms involved in CEOR include the IFT reduction and wettability alteration i.e. from oil-wet to water-wet. However, care must be taken as far as the selection of suitable surfactant or combination of surfactants is concerned. DBSA and CTAB were incompatible with the other components and are not suitable in combination with slightly anionic polymer and high salinity and alkalinity. Among the utilized non-conventional surfactants mixture of ATR and AOT has been found to be best not only in terms of oil recoveries but also for stability and compatibility towards polymer, salinity and alkalinity as compared to the individual surfactants. This behavior can be attributed to the synergistic and antagonistic effects. In the mixture of surfactants comprising of long and short chain hydrophobic groups, smaller chains are expected to be adsorbed within the longer chains and will act as co-surfactant which will make the system stable and enhance the overall efficiency. HLB values can also be adjusted using the appropriate ratios of various surfactants according to the specific requirement which can give rise to the controlled emulsification and demulsification. Although the conventional surfactants like SDS also have the potential for EOR applications but higher concentrations are required than the non-conventional surfactants which may lead to precipitation, cementation and other related issues in severe saline and alkaline conditions. Polymer-1 is capable of retaining the viscosity which is not only enough to

enhance the sweep efficiency by reaching the micro and millie pores but also can increase the electrophoretic mobility due to electrostatic repulsive forces between slightly anionic head groups of the polymer and anionic surfactants. The synergetic effect of alkali and mixture of surfactants may bring ultra-low IFT at oil-water interface i.e. 10^{-3} mN/m order of magnitude, and the whole system is a super-low interfacial tension system. Therefore, the flushing efficiency may be increased, thereby resulting in significant enhancement of oil recovery.

From the presented results, it can be concluded that LASP, using low concentration of the combination of non-conventional surfactants, slightly anionic HPAM and alkali can be a suitable and economical choice for CEOR from sandstone reservoirs in general and Angsi field in particular.

4.14 Surfactant Adsorption and Kinetics Studies

The understanding of the surfactant adsorption on sandstone cores is essential for surfactant-enhanced oil recovery system. Centre to this is the mechanism and kinetics of surfactant adsorption as they form the basic prerequisite for designing suitable surfactant formulation. In this regard various adsorption equilibrium isotherms (Langmuir and Freundlich) and kinetic models (Pseudo-first-order, Pseudo-second-order and Intra-particle-diffusion model) were implemented to explain the adsorption and kinetics of surfactants on sandstone cores.

4.14.1 Langmuir and Freundlich Adsorption Isotherms

The kinetics and equilibrium adsorption of surfactants at the solid-liquid interface depend upon the nature of the surfactant and the nature of solid surface. The most appropriate step in designing a surfactant involves the investigation into the adsorption isotherms. Linear regression is utilized to determine the most appropriate fitted isotherm. Linearized forms of Langmuir and Freundlich adsorption isotherms are given in section 3.16.1. Freundlich isotherm model assumes that adsorption takes place on a heterogeneous surface, whereas the reverse is true for Langmuir model. Langmuir and Freundlich adsorption isotherms in the absence and presence of alkali are presented in

Figs. 4.44 and 4.45 respectively whereas, the obtained parameters like adsorption intensity (n), q_{\max} , Freundlich constant, K_f and R^2 values are reported in Tables 4.13 and 4.14.

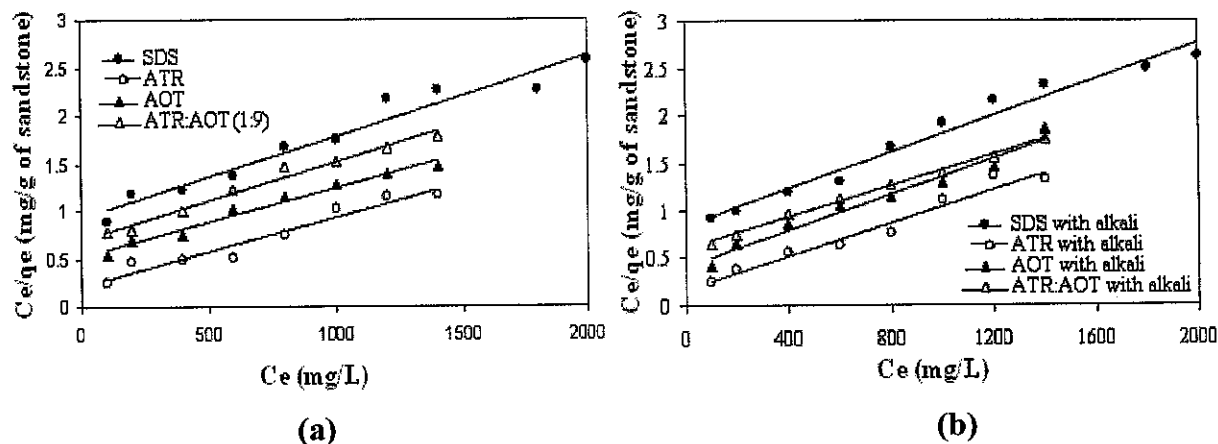


Figure 4.44: Langmuir adsorption isotherms for SDS, ATR, AOT and ATR:AOT in the absence (a) and in the presence (b) of alkali.

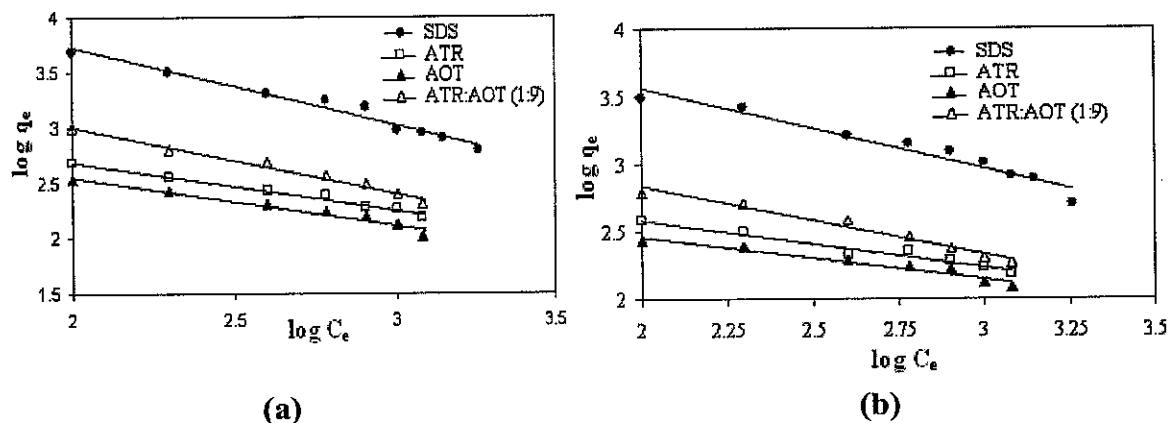


Figure 4.45: Freundlich adsorption isotherms for SDS, ATR, AOT and ATR:AOT in the absence (a) and in the presence (b) of alkali.

Table 4.13: Adsorption constants for Langmuir isotherm.

Surfactants	Langmuir constants in the absence of alkali			Langmuir constants in the presence of alkali		
	q_{\max}	b	R^2	q_{\max}	b	R^2
SDS	1250.00	1167.37	0.9491	1111.10	946.68	0.9728
ATR	1428.57	315.57	0.9433	1111.10	189.22	0.9628
AOT	1428.57	753.99	0.9776	1250.00	513.87	0.9637
ATR:AOT	1250.00	868.63	0.9800	1000.00	599.10	0.9939

Table 4.14: Adsorption constants for Freundlich isotherm.

Surfactants	Freundlich constants in the absence of alkali			Freundlich constants in the presence of alkali		
	K_f	$1/n$	R^2	K_f	$1/n$	R^2
SDS	113.07	-0.05891	0.9475	170.69	-0.7087	0.9687
ATR	26.71	-0.3520	0.9612	35.42	-0.4405	0.9845
AOT	21.98	-0.3148	0.9399	30.49	-0.4388	0.9566
ATR:AOT	45.60	-0.4988	0.970	68.23	-0.6085	0.9811

Based on the correlation coefficients (R^2) values of greater than 0.93 the choice of deciding between the Freundlich and Langmuir isotherms becomes obscure. However, the correlation coefficients of Langmuir isotherm are closer to 1 than Freundlich isotherm coefficients. Negative values of adsorption intensity ($1/n$) for Freundlich isotherm is also one of the indications that the model is not useful in representing the obtained data. Theoretical calculations performed on the remaining concentration of surfactants were found to have a close agreement with the experimentally measured values (within $\pm 5\%$ difference) for Langmuir isotherm compared to Freundlich. It will appear that the Langmuir model is more suitable than Freundlich in describing the adsorption data.

This reinforces a previous observation that Langmuir isotherm is more useful to explain the adsorption from solution when it follows the monolayer mode rather than the multilayer mode. A basic assumption of the Langmuir theory is that the sorption takes place at specific homogenous sites on the adsorbent. When a site is occupied by an adsorbate, no further sorption can take place at this site [192]. A Langmuir type isotherm as was found from the adsorption studies supports that adsorption is accomplished via the formation of a monolayer of surfactant which is an indication that ultralow concentrations of surfactants are adequate to maximize oil recovery.

It is evident from Table 4.13 that the amount of surfactants retained by the sandstone (q_{max}) decreases in the presence of an alkali (20% reduction in the ATR:AOT combination). Percentage reduction in the presence of alkali for Langmuir isotherm was found to be 11, 22, 12 and 20 % for SDS, ATR, AOT and ATR:AOT respectively. The zeta potential on sandstone cores is negative associated with a higher silica content at normal pH, a pore structure that is more heterogeneous and a permeability that is

significantly high. The presence of alkali is thought to have enhanced the negative potential of the sandstones which in turn not only reduces the adsorption of anionic surfactants due to electrostatic repulsive forces but on the contrary increases the electrophoretic mobility.

As one of the biggest challenges involve the excessive loss of surfactants, any steps taken to increase surfactant retention while not undermining its efficiency are highly desirable. As it turns out combination of the appropriate surfactants and alkali work together to overcome the economic tradeoff of excessive surfactant losses.

4.14.2 Adsorption Kinetics of Surfactants

Adsorption is a time-dependent process. It is necessary to determine the rate of adsorption to design and evaluate the adsorbent performance. It is important to investigate the adsorption kinetics and to determine their phenomenological coefficients in order to characterize the transport of sorbate within the sorbents.

In order to investigate the mechanism of adsorption, particularly which involves potential rate controlling step (e.g. chemical reaction, diffusion and mass transfer activities) Pseudo-first-order, Pseudo-second-order and Intra-particle-diffusion models (given in 3.16.2) have been evaluated to validate the adsorption kinetics of surfactants from aqueous solutions in the presence of alkali over 600 min time intervals. These are shown in Fig. 4.46.

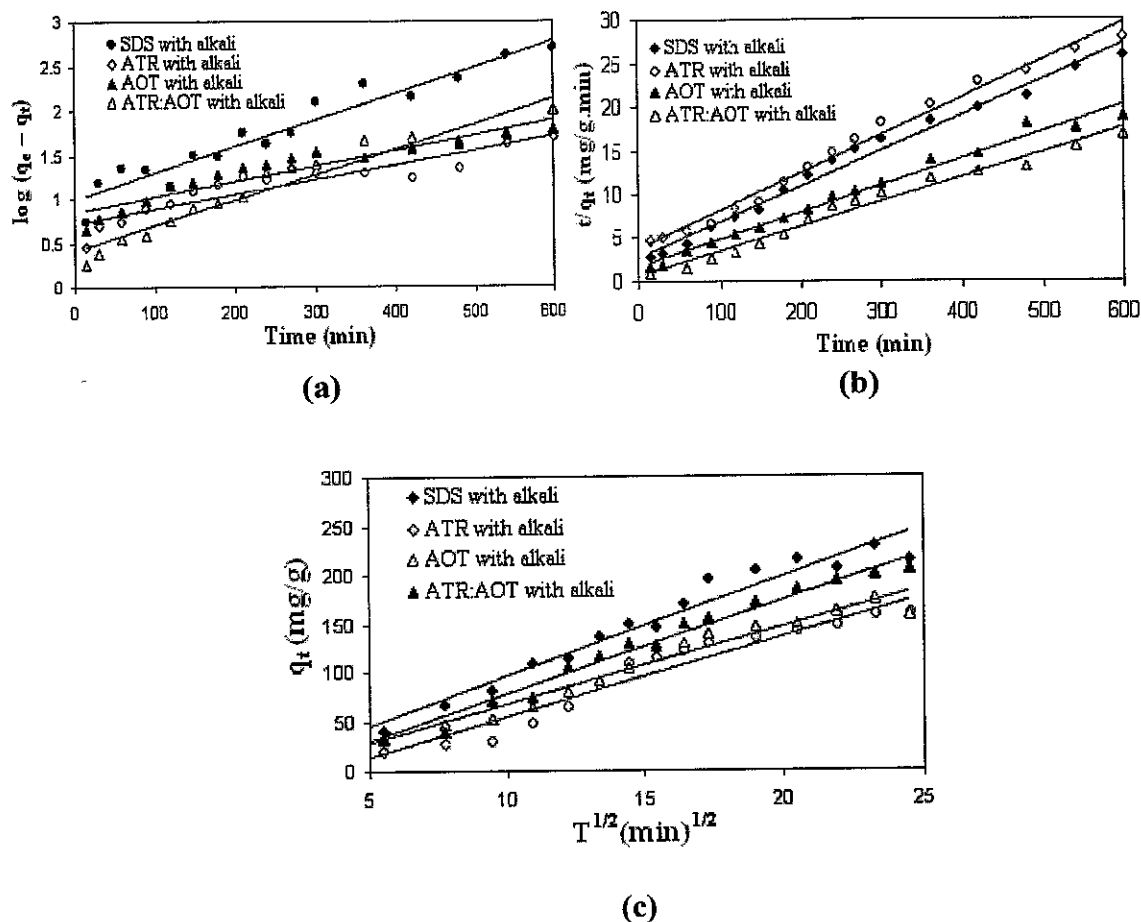


Figure 4.46: Pseudo-first-order (a), Pseudo-second-order (b) and intra-particle diffusion (c) kinetics for the adsorption of surfactants on sandstone.

The obtained rate constants and correlation values are given in Table 4.15. Between the three presented models, the Pseudo-second order model provides the best fit to elaborate the adsorption kinetics. The slowest step is the rate determining step in the reaction mechanism and it governs the overall reaction rate. Lowest rate constants were obtained when Pseudo-second order model was considered. The correlation values (R^2) for Pseudo-second order model supports its suitability as far as the adsorption of surfactants from aqueous solution to sandstones is concerned. It can be concluded that Langmuir adsorption isotherm and Pseudo-second order model appropriately elaborate the surfactant adsorption mechanism and kinetics. It has been reported [193, 194] that pseudo-zero- and pseudo-first-order kinetics are not suitable to ascribe the adsorption of two reactive compounds as the product will interfere with the kinetics. The Pseudo-second-order kinetics provides a better fit. An Intra-particle diffusion model is more

useful where the adsorbent penetrates deeply into the micropores of the adsorbent. In EOR applications deep penetration of the surfactants may lead to the surfactant's protracted retention rendering the process economically unfavorable. Based on the above, the Pseudo-second-order kinetics adequately provides a better fit of the surfactant-alkali adsorption on the sandstone.

Table 4.15: Kinetic parameters for the adsorption of surfactants by sandstone adsorbents.

Pseudo-1st-order rate constants	K_1^{st} (min⁻¹)	R²
SDS in the presence of alkali	0.0030	0.9309
ATR in the presence of alkali	0.0016	0.8311
AOT in the presence of alkali	0.0017	0.8857
ATR:AOT (1:9) in the presence of alkali	0.0028	0.9362
Pseudo-2nd-order rate constants	K_2^{nd} (mg/g.min)	R²
SDS in the presence of alkali	0.000752	0.9846
ATR in the presence of alkali	0.000475	0.9873
AOT in the presence of alkali	0.00055	0.9849
ATR:AOT (1:9) in the presence of alkali	0.000545	0.9777
Intra-particle diffusion rate constants	K_{id} (mg/g.min)	R²
SDS in the presence of alkali	10.098	0.9599
ATR in the presence of alkali	8.207	0.952
AOT in the presence of alkali	7.8124	0.9605
ATR:AOT (1:9) in the presence of alkali	9.554	0.9701

4.15 Summary

In this chapter, the general characteristics of the Angsi field, Angsi crude assay and Angsi sea, formation water analyses are given. Lithology of Angsi field is sandstone in nature with an average porosity of 22%. Oil viscosity and density are 3 cp and 0.287 g/cm³ respectively under reservoir conditions. The presence of light crude and reasonable porosity indicate that the field is a suitable candidate for the implementation of chemical flooding. Sea water from Angsi field has been found to possess high concentrations of

chlorides, sulfates and hardness constituting species. Viscosity measurements of polyacrylamide solutions as a function of polymer concentration and the roles of temperature, alkali and surfactants towards viscosity have been reported. Polymer-1 was found to possess a more viscosity elevation in brine solution compared to polymer-2. Polymer-1 is also more resistant towards high temperatures. Thermal stabilities of the polymers and surfactants have been evaluated. Thermal decomposition profiles of polymers-1,2 and SDS, ATR, AOT surfactants have demonstrated that they possess the needful thermal stabilities under reservoir conditions (excess of 120 °C). There is no jeopardy as far as the thermal decomposition of the polymers and surfactants are concerned. FTIR-ATR spectra of the individual components and their mixtures have confirmed their mutual compatibility along with the creation of beneficial co-components. Time dependency of IFT reduction at crude oil-water interfaces has been reported. Combination of non-conventional anionic surfactants, ATR:AOT (1:9) offers the highest IFT benefits followed by AOT, ATR and the conventional SDS, CTAB and DBSA. Moreover, IFT reduction offered by ATR, AOT and SDS are time independent. The atomic force microscopy of oil-water emulsions has revealed the presence of a more finely dispersed oil-in-water droplets with SDS compared with ATR and AOT surfactants. Emulsion stabilities have indicated that almost 98% oil phase was separated when the emulsion was stabilised using the mixture of ATR and AOT surfactants. Partition functions of surfactants in aqueous and organic phases have established that chances of surfactants to be retained by the oil phase can be minimized using the appropriate mixtures of non-conventional surfactants. Wettability alteration mechanism from oil-wet to water-wet surfaces has been elaborated with the help of contact angle measurements. The increase in the contact angles of brine droplet with oil-wet substrate, with an accompanying increase in surfactant concentrations indicates that the wettability of the substrate has been altered. Essential characterization parameters have shown that the selected cores have more than 20% porosity. Good agreement between an in-house spontaneous imbibition and industry accepted core flooding studies have been observed. EDX analyses have indicated the variations in the mineral profiles of the core samples. BET surface area and SEM analyses of the sandstone cores, prior and post imbibition studies have demonstrated that ASP flooding has resulted in an oil recovery leading to the

pore opening and enhancement of surface area. It was apparent from the micrographs of cores at various stages of flooding that the combination of polymer and surfactants have successively removed most of the remaining oil left behind following a waterflood. The recovery rate is significantly improved with the addition of alkali further. Recoveries of remaining oil in position (ROIP) were approximately found to be 99, 96, 82 and 96% respectively for the mixture of ATR and AOT, SDS, ATR and AOT. Surfactants adsorption from aqueous solution to sandstones, their kinetics and the role of alkali in minimizing the adsorption capacity are explained with the help of appropriate adsorption models. Adsorption mechanism is well elaborated by Langmuir isotherm instead of Freundlich. The adsorption kinetics obeys Pseudo-second-order model. It can be concluded that Angsi field is a good candidate for the implementation of ASP flooding as a tool to maximize the oil recoveries.

CHAPTER 5

5. CONCLUSIONS AND RECOMMENDATIONS

5.1 Conclusions

Chemical enhanced oil recovery, especially ASP flooding is an important technique being used to maximize oil recovery from depleted reservoirs. However, it can not be generalized due to the unique properties of each reservoir. Chemical floods are generally considered as successful for the oil reservoirs, which commonly have light crude. The beneficiaries of CEOR are confined to oil and mixed wet reservoirs.

Through the detailed discussion with the help of available literature about the basic concepts of EOR, ASP flooding, surfactants, CMC, IFT, emulsification, partition coefficient, wettability alteration, viscosity and shear thinning of polymer solution, inaccessible pore volume in polymer flooding and polymer retention in porous medium it was concluded that these factors play vital role in chemical flooding and must be critically analyzed before implementing the CEOR.

Most of the previously reported studies have demonstrated the effect of surfactant-based wettability alteration i.e. from oil-wet to water-wet. The implementation of ASP flooding was previously hindered due to the lack of appropriate technology, economical and environmental factors despite its many potential in an EOR strategy. The present work provides laboratory data to adequately demonstrate the benefits of surfactant molecules engineered to maximize oil recovery. LASP flooding process which was not considered as an economical process in the past due to certain limitations is shown to provide a viable method for EOR applications.

This study presents the detailed work starting from the lithology of the field of interest, crude assay, formation water analyses, characterization of the core samples, stability of the proposed chemicals and formulations towards temperature, alkalinity, salinity, wettability alteration, IFT reduction, partition functions of surfactants and compatibility of the surfactants with crude and other components. Initial screening of the

concentrations of surfactants, polymers and alkali was carried out using an in-house imbibition cell which was later on verified using industry accepted core flooding apparatus.

As this project was focused for Angsi oilfield so the experimental protocols were established according to the reservoir conditions. Non-conventional branched chain anionic surfactants with homologous branching have the ability to reduce IFT more than conventional surfactants. The synergistic effects of employing the non-conventional surfactants in appropriate ratios have resulted in a better and desirable combination possessing suitable partition for EOR applications. Mixed surfactants with larger and smaller hydrophobic chains work together in order to the micropores and to remain at the oil-water interface due to thermodynamic instability as it was observed in the combination of ATR (larger hydrophobic tail) and AOT (smaller hydrophobic tail).

From the thermogravimetric analyses and viscosity measurement it was shown that Hybomax polymers and SDS, ATR and AOT surfactants are not only temperature stable but can also sustain the viscosity for in service temperature, salinity and are also compatible with alkalinity up to a certain extent.

FTIR-ATR spectroscopy has revealed that the components of the proposed formulations are not only compatible with each other but can also enhance the oil recovery drastically.

Atomic force microscopy demonstrated that non-conventional surfactants will lead to an unstable oil-water emulsions which is one of the key parameters for a successful CEOR.

Contact angle measurements demonstrated that the combination of non-conventional surfactants can alter oil-wet to water-wet reservoirs even when they are present in minimum amounts.

BET surface area measurements and scanning electron microscopy have explained the morphology of the core samples prior and post imbibition and it can be

concluded that previously occupied pores remain opened as a result of chemical flooding and a high degree of the core surface is available and more oil becomes accessible for an eventual waterflooding. EDX analyses have verified the heterogeneity of the reservoir showing the variations in the mineral profiles of the core samples.

Spontaneous imbibition results were verified by core flooding studies which is an indication that the former can be utilized for an initial screening prior to the core flooding treatments.

Addition of alkali to the surfactant-polymer solution has not only increased the oil recovery but also reduced the adsorption of surfactants significantly.

Langmuir adsorption isotherm elaborates the adsorption mechanism indicating that adsorption is monolayer in nature. Pseudo-second-order model is suitable to study the adsorption kinetics as compared to the Pseudo-first-order and Intra-particle diffusion models.

These results suggest the need of a combination of surfactants (synergistic and antagonistic effects) not only to maximize the oil recovery but also to control the adsorption process in combination with alkali. To reduce the surfactant's loss due to adsorption on reservoir rock, a relatively weak adsorption of the surfactants is one of the important factors to keep the process cost-effective.

It can be concluded that the challenges and ambiguities involved (temperature stability, brine tolerance, viscosity reduction, imbalance partitioning in single phase, loss due to adsorption and retention by the oil phase) in the use of chemicals which were previously hindering the CEOR can be resolved. CEOR possess a bright future if implemented to the proper reservoir conditions after critically evaluating the required parameters at lab scale prior to field testing.

5.2 Recommendations

World oil resources are limited and declining with the passage of time but fuel consumption is ever increasing. The exploitation of oil new oilfields as well as the recovery from depleted and near depleted reservoirs to a higher degree are desirable. New technologies and methods are required to improve the recovery rates of depleted oilfields to recover the trapped oil found in pores between rock particles.

It has been shown that CEOR using LASP floods in combination with non-conventional anionic surfactants with homologous branching can significantly enhance the oil recovery from sandstones. But every reservoir is unique in its characteristics, due to the complex nature of oil fields with different heterogeneity, high temperature and harsh saline conditions. Phase behaviors of the underlying phases (oil, water and surfactants) have to be investigated. There is a need for phase behavior characterization for the successful implementation of LASP flooding process.

Moreover, other non-conventional surfactants like, branched chain with heterologous chains, gemini, viscoelastic and non-migratory versions can also be evaluated with respect to their temperature stability, IFT reduction, partitioning and other bulk properties are concerned. As no two fields are alike, data from such an extensive program can be utilized to develop a software capable to simulate the reservoir fluid regimes for each ALSP formulation to cater for the each field. As the search for green surfactants intensifies, a synthetic route using indigenous renewable resources such as palm oil derivatives may become the motive of future research.

REFERENCES

- [1] Norman R. and Geoffery M. Recovery of oil by spontaneous imbibition. *Current Opinion in Colloid and Interface Science* 6 (2001) 321-337.
- [2] Raymond L.S. and Paul B. V. Enhanced oil recovery-Current status and future needs. *Chemical Engineering Progress* (1990) 47-59.
- [3] Shah D.O. and Schechter R.S. Improved oil recovery by surfactant and polymer flooding. Academic Press Inc, (1977).
- [4] Milton J.R. Hongzhuang W. Pingping S and Youyi Z. Ultralow interfacial tension for enhanced oil recovery at very low surfactant concentrations. *Langmuir* 21 (2005) 3749-3756.
- [5] Jixiang G. Qing L. Mingyuan L. Zhaoliang W. and Alfred A.C. The effect of alkali on crude oil/water interfacial properties and the stability of crude oil emulsions. *Colloids and Surfaces A: Physicochem. Eng. Aspects* 273 (2006) 213–218.
- [6] Nadeem M. Rangkuti C. Anuar K. Haq M.R.U. Tan I.B. and Shah S.S. Diesel engine performance and emission evaluation using emulsified fuels stabilized by conventional and gemini surfactants. *Fuel* 85 (2006) 2111–2119.
- [7] Nadeem M. Mahmood A. Shahid S.A. Shah S.S. Khalid A.M. and McKaye G. Sorption of lead from aqueous solution by chemically modified carbon adsorbents. *Journal of Hazardous Materials B138* (2006) 604–613.
- [8] Laurier L.S. *Surfactants: Fundamentals and applications in the petroleum industry*. Cambridge university press, (2000).
- [9] Rosen M.J. *Surfactants and interfacial phenomenon*. John Wiley and Sons, Inc, (2004).
- [10] Somasundaran P. Zhang L. Adsorption of surfactants on minerals for wettability control in improved oil recovery processes. *Journal of Petroleum Science and Engineering* 52 (2006) 198–212.
- [11] Somasundaran P. Fuerstenau D.W. Mechanism of alkyl sulfonate adsorption at alumina–water interface. *J. Phys. Chem.* 70 (1966) 90.

- [12] Somasundaran, P., Fuerstenau, D.W., Heat and entropy of adsorption and association of long-chain surfactants at alumina aqueous solution interface. *Trans. SME* 252 (1972a) 275.
- [13] Somasundaran P. Fuerstenau D.W. The heat and entropy of adsorption and association of long-chain surfactants at the alumina-aqueous solution interface. *Trans. AIME* 252 (1972b) 275.
- [14] Somasundaran P. Kunjappu J.T. In-situ investigation of adsorbed surfactants and polymers on solids in solution. *Colloids Surf.* 37 (1989) 245.
- [15] Nasr-El-Din H.A. and Taylor K.C. The role of surfactants in enhanced oil recovery, 'Micelles, Microemulsions and Monolayers, Science and Technology', Marcell-Dekker Inc: New York, (1998).
- [16] Qiang L. Mingzhe D. Xiangnan Y. Jirui H. Synergy of alkali and surfactant in emulsification of heavy oil in brine. *Colloids and Surfaces A: Physicochem. Eng. Aspects* 273 (2006) 219–228.
- [17] Dabros T. Yeung A. Masliyah J. Czarnecki J. Emulsification through Area Contraction. *Journal of Colloid and Interface Science* 210 (1999) 222-224.
- [18] Katarzyna S. and Bronisław J. The wettability of polytetrafluoroethylene by aqueous solution of cetyltrimethylammonium bromide and Triton X-100 mixtures. *Journal of Colloid and Interface Science* 303 (2006) 319–325.
- [19] Krister H. *Handbook of Applied Surface and Colloid Chemistry*. John Wiley and Sons, (2001).
- [20] T.D. Blake. Dynamic contact angles and wetting kinetics. In: J.C. Berg (ed.) *Wettability*, Marcel Dekker, New York (1993) 251–309.
- [21] Cipriano B.H. Raghavan S.R. McGuiggan P.M. Surface tension and contact angle measurements of a hexadecyl imidazolium surfactant adsorbed on a clay surface. *Colloids and Surfaces A: Physicochem. Eng. Aspects* 262 (2005) 8–13.
- [22] Shah D.O. The world of surface science, in *Chemical Engineering Education*, Anderson, T. J. (Ed.), American Society for Engineering Education, p 14–48, (1977).

- [23] Patist A. Jha B. K. Oh S.G. Shah D. O. Importance of micellar relaxation time on detergent properties. *Journal of Surfactants and Detergents*. 2 (1999) 317–324.
- [24] Shupe R.D. Chemical Stability of Polyacrylamide Polymers, *Journal of Petroleum Technology*, August 33 (1981).
- [25] Ezeddin S. Mobility control by polymers under bottom-water conditions, *Experimental Approach*. SPE 64506, October (2000).
- [26] Chang Y. Lochhead R.Y. McCormick C.L. *Macromolecules* 27 (1994) 2145.
- [27] E. Jimenez-Regalado, J. Selb, F. Candau, *Langmuir* 16 (2000) 8611.
- [28] Yan Li, Jan C.T. Kwak. Rheology and binding studies in aqueous systems of hydrophobically modified acrylamide and acrylic acid copolymers and surfactants. *Colloids and Surfaces A: Physicochem. Eng. Aspects* 225 (2003) 169 – 180.
- [29] S. Biggs, J. Selb, F. Candau, *Langmuir* 8 (1992) 838.
- [30] J.J. Effing, I.J. McLennan, J.C.T. Kwak, *J. Phys. Chem.* 98 (1994) 2499.
- [31] B. Magny, I. Iliopoulos, R. Zana, R. Audebert, *Langmuir* 10 (1994) 3180.
- [32] Rapier Dawson and Ronald B. Lantz, *Inaccessible Pore Volume in Polymer Flooding*, *Trans. AIME*, 253, (1972).
- [33] P. Barreau, D. Lasseux, H. Bertin, Ph. Glénat and A. Zaitoun, Polymer adsorption effect on relative permeability and capillary pressure: Investigation of a pore scale scenario, SPE37303, (1997).
- [34] Tim L. Hunning X. Mingzhe D. Tailor-modified starch/cyclodextrin-based polymers for use in tertiary oil recovery. *Journal of Petroleum Science and Engineering*. 46 (2005) 225-232.
- [35] E. Volpert, J. Selb, F. Candau, Influence of the hydrophobe structure on composition, microstructure, and rheology in associating polyacrylamides prepared by micellar copolymerization, *Macromolecules* 29 (1996) 1452–1463.
- [36] F. Candau, J. Selb, Hydrophobically-modified polyacrylamides prepared by micellar polymerization, *Adv. Colloid Interface Sci.* 79 (1999) 149–172.
- [37] Evis K.P. Laura G. Irima J. F. Alejandro J. M. Antonio D. Eduardo A. S. Rheology of aqueous solutions of hydrophobically modified polyacrylamides

- and surfactants. *Colloids and Surfaces A: Physicochem. Eng. Aspects* 295 (2007) 99–106.
- [38] Grattoni C.A., Luckhamb P.F., Jinga X.D., Normanc L., Zimmerman R.W. Polymers as relative permeability modifiers: adsorption and the dynamic formation of thick polyacrylamide layers. *Journal of Petroleum Science and Engineering* 45 (2004) 233–245.
- [39] Liang, J.T., Seright, R.S. Further investigations of why gels reduce k_w more than k_o . *SPE Prod. Facil.* 12, (1997) 225–230.
- [40] Zaitoun, A., Bertin, H. Two-phase flow property modifications by polymer adsorption. SPE 39631, SPE Improved Oil Recovery Symp., Tulsa, (1998).
- [41] Barreau, P., Lasseux, D., Bertin, H., Glenat, P., Zaitoun, A. An experimental and numerical study of polymer action on relative permeability and capillary pressure. *Petrol. Geosci.* 5 (1999) 201–206.
- [42] Dalrymple, E.D., Eoff, L., Reddy, B.R., Botermans, C.W. Relative permeability modifiers for improved oil recovery: a literature review. Proc. 11th International Oil Field Chemicals Symposium, Fagerness, Norway (2000).
- [43] Liang, J.T., Seright, R.S. Wall effect/gel droplet model of disproportionate permeability modification. SPE 59344, SPE/DOE Improved Oil Recovery Symp., Tulsa (2000).
- [44] Al-Sharji, H.H., Grattoni, C.A., Dawe, R.A., Zimmerman, R.W. Flow of oil and water through elastic polymer gels. *Oil and Gas Science and Technology (IFP Revue)* 56 (2001a) 145–152.
- [45] Grattoni, C.A., Al-Sharji, H.H., Dawe, R.A., Zimmerman, R.W. Segregated pathways mechanism for oil and water flow through silica gels formed from an oil-based gelant. *J. Pet. Sci. Eng.* 35 (2002) 183–190.
- [46] Gonglun C. and Daniel T. An experimental study of stability of oil–water emulsion. *Fuel Process Technology* 86 (2005) 499–508.
- [47] M. Dong, P. Liu, L. Zhang, Y. Zhu, in: *The SPE International Meeting on Petroleum Engineering*, Beijing, China, 17–20 March, SPE 14855 (1986).
- [48] K.S. Chan, D.O. Shah, in: D.O. Shah (Ed.), *Surface Phenomena in Enhanced Oil Recovery*, Plenum Press, New York, p. 53–72 (1981).

- [49] F. Verzaro, M. Bourrel, O. Garnier, H.G. Zhou, J.F. Argillier, in: *The SPE International Thermal Operations and Heavy Oil Symposium and the International Horizontal Well Technology*, Calgary, Alberta, Canada, 4–7 November, SPE 78959 (2002).
- [50] DOE Fossil Energy Enhanced Oil Recovery /CO₂ Injection <http://www.fe.doe.gov>.
- [51] M. A. Malana, M. Nadeem, S. S. Naqvi and S. N. Sarwar “Inorganic metal settlement in fuel tanks and their environmental effects for disposal” *Science Technology and Development*: 19 (2): (2000) 32 – 35.
- [52] A. Pina, P. Mougin, E. Béhar. Characterization of Asphaltenes and Modeling of Flocculation – State of the Art. *Oil & Gas Science and Technology – Rev. IFP*, Vol. 61 (3): (2006) 319-343.
- [53] Sheu, E. Y.; Mullins, O. C. *Asphaltenes: Fundamentals and Applications*; Plenum Press: New York, (1995).
- [54] Sheu, E. Y. Petroleum asphaltene-properties, characterization, and issues, *Energy & Fuels* 16 (2002) 74-82.
- [55] Green W., Willhite Paul G.: *Enhanced Oil Recovery*. SPE (1998).
- [56] Giuliano F.A *Introduction to Oil & Gas Technology*, 3rd Ed. Prentice Hall, New Jersey (1989).
- [57] Karel B, Petr B, Karel L. Application of enhanced oil recovery methods to oil deposits. *Wiertnictwo Nafta Gaz Tom 23 (1)*: (2006) 95 – 100.
- [58] D.O Shah, *Fundamental aspects of Surfactant-Polymer Flooding Process*, Cambridge university press, (2000).
- [59] Craig, F.F.: “The Reservoir Engineering Aspects of Waterflooding,” *Monograph Series*, SPE (1971) 3.
- [60] D. Fennell Evans, Håkan Wennerström. *The Colloidal Domain: Where Physics, Chemistry, Biology, and Technology Meet (Advances in Interfacial Engineering)*. Wiley-VCH, (1999).
- [61] Salathiel R.A. Oil recovery by surface film drainage in mixed-wettability rocks. *Journal of Petroleum Technology*, October (1973) 1216 – 1224.

- [62] Jarrell, P.M., Fox, C.E., Stein, M.H., Webb, S.L.: "Practical Aspects of CO₂ Flooding," Johns, R.T. Monograph Series, SPE (2002) 22.
- [63] Carlos D. and Jacob I. Fundamental studies of crude oil–surface water interactions and its relationship to reservoir wettability. *Journal of Petroleum Science and Engineering*, Volume 45 (1-2): (2004) 61-81.
- [64] Skule S. Eli J.H. Tor A. Wettability alteration of carbonates-Effects of potential determining ions (Ca²⁺ and SO₄²⁻) and temperature. *Colloids and Surfaces A: Physicochem. Eng. Aspects* 275 (2006) 1–10.
- [65] Amott E. Observations Relating to the Wettability of Porous Rock. *Trans., AIME* 216 (1959) 156 – 162.
- [66] Anderson, William G. [A]: Wettability Literature Survey – Part 1: Rock/Oil/Brine Interactions and the Effects of Core Handling on Wettability, *Journal of Petroleum Technology*, October (1986) 1125 – 1144.
- [67] Anderson, William G. [B]: Wettability Literature Survey – Part 2 Wettability Measurement, *Journal of Petroleum Technology*, November (1986) 1246 – 1262.
- [68] Anderson, W.G. Wettability Literature Survey – Part 4: Effects of Wettability on Capillary Pressure, *Journal of Petroleum Technology*, October (1987) 1283 – 1300.
- [69] Glen A. A. Simulation of Chemical Flood Enhanced Oil Recovery Processes Including the Effects of Reservoir Wettability. (2006) Master Thesis. University of Texas Austin.
- [70] Graue, A., Bogno, T. Wettability Effects on Oil Recovery Mechanisms in Fractured Reservoirs, SPE56672, SPE Annual Tech. Conf. And Exh. Houston, TX, Oct. 3-6, (1999).
- [71] Donaldson, E.C., Thomas, R.D., and Lorenz, P.B.: Wettability Determination and Its Effect on Recovery Efficiency, *SPEJ*, March (1969) p. 13 – 20.
- [72] Dandina N.R. Measurements of dynamic contact angles in solid–liquid–liquid systems at elevated pressures and temperatures. *Colloids and Surfaces A: Physicochemical and Engineering Aspects* 206 (2002) 203–216.

- [73] Zisman W.A. Relation of equilibrium contact angle to liquid and solid constitution, *Advances in Chemistry Series No. 43*, American Chemical Society, Washington DC, (1964) Chapter 1.
- [74] O.R. Wagner, R.O. Leach, *Journal of Petroleum Technology*, Transactions of AIME 216, April (1959).
- [75] L.E. Treiber, D.L. Archer, W.W. Owens, *Society of Petroleum Engineers Journal*, December (1972).
- [76] Ratner B.D. Hoffman A.S. Schoen F.J. Lemons J.E. *Biomaterials science: An introduction to materials in medicine*. San Diego, CA: Academic Press (1996).
- [77] Kim Kinoshita, *Electrochemical Oxygen Technology*, John Wiley & Sons, Inc. (1992) p.139.
- [78] Slider H.C. *Worldwide Practical Petroleum Reservoir Engineering Methods*, Penwell Books (1983).
- [79] H. Elshahawi, K. Fathy, S. Hiekal. *Capillary Pressure and Rock Wettability Effects on Wireline Formation Tester Measurements*. SPE 56712.
- [80] Killins, C.R., Nielsen, R.F., and Calhoun, J.C.: *Capillary desaturation and imbibition in porous rocks*, *Producers Monthly*, December 18 (2): (1953) 18, 30 - 39.
- [81] Stegemeier, G.L.: *Mechanisms of Entrapment and Mobilization of Oil in Porous Media*. *Improved Oil Recovery by Surfactant and Polymer Flooding*, Shah, D.O. and Schechter, R.S. (eds.), Academic Press, New York City (1977), 59 – 91.
- [82] Mouaouia F. Jean-Luc G. Patric L.Q. *Nonlinear corrections to Darcy's law at low Reynolds numbers*. *Journal of Fluid Mechanics* 343 (1997) 331-350.
- [83] Enrique Carrero, Nestor V. Queipo, Salvador Pintos and Luis E. Zerpa. *Global sensitivity analyses of Alkali-Surfactant-Polymer enhanced oil recovery processes*. *Journal of Petroleum Science and Engineering*, 58 (1-2) 2007, 30-42.
- [84] Luis E. Zerpa, Nestor V. Queipo, Salvador Pintos and Jean-Louis Salager. *An optimization methodology of alkaline-surfactant-polymer flooding processes using field scale numerical simulation and multiple surrogates* *Journal of Petroleum Science and Engineering*, 47 (3-4): (2005) 197-208.

- [85] Zhongkui Z. Chenguang B. Weihong Q. Zongshi L. L'ubo C. Dynamic interfacial tension behavior of the novel surfactant solutions and Daqing crude oil. *Colloids and Surfaces A: Physicochem. Eng. Aspects* 294 (2007) 191–202.
- [86] Zhongkui Z. Fei L. Weihong Q. Zongshi L. Lu'bo C. Novel alkyl methylnaphthalene sulfonate surfactants: A good candidate for enhanced oil recovery. *Fuel* 85 (2006) 1815–1820.
- [87] M. El-Batanoney, Th. Abdel-Moghny and M. Ramzi. The effect of mixed surfactants on enhancing oil recovery. *Journal of Surfactants and Detergents*, 2 (2): (1999) 201-205.
- [88] Qiang L. Mingzhe D. Shanzhou M. Yun T. Surfactant enhanced alkaline flooding for Western Canadian heavy oil recovery. *Colloids and Surfaces A: Physicochem. Eng. Aspects* 293 (2007) 63–71.
- [89] Fab'iola D.S.C. Vanessa C. S. Eduardo L.B. Tarc'ilio V.D. Jr. Tereza N.C.D. Afonso A. Dantas N. Alfredo I.C.G. Adsorption of nonionic surfactants in sandstones. *Colloids and Surfaces A: Physicochem. Eng. Aspects* 293 (2007) 1–4.
- [90] Nedjhiouia M. Canselierb J.P. Moulai-Mostefaa N. Bensmailic A. Skendera A. Determination of micellar system behavior in the presence of salt and water soluble polymers using the phase diagram technique. *Desalination* 206 (2007) 589–593.
- [91] Winsor, P., *Solvent Properties of Amphiphilic Compounds*, Butterworth, London, (1954).
- [92] Zhang D.L. Shunhua L. Maura P. Clarence A.M. George J.H. Wettability alteration and spontaneous imbibition in oil-wet carbonate formations. *Journal of Petroleum Science and Engineering* 52 (2006) 213–226.
- [93] Rui Zhang and P. Somasundaran. Advances in adsorption of surfactants and their mixtures at solid/solution interfaces. *Advances in Colloid and Interface Science* 123–126 (2006) 213–229.
- [94] Wei Y. Clarence A. M. George J. H. Foam sweep in fractures for enhanced oil recovery. *Colloids and Surfaces A: Physicochem. Eng. Aspects* 282–283 (2006) 348–359.

- [95] Tayfun B. Evaluation of the critical parameters in oil recovery from fractured chalks by surfactant injection. *Journal of Petroleum Science and Engineering* 54 (2006) 43–54.
- [96] Jie Y. Weihong Q. Zongshi L. Lvbo C. Effects of branching in hexadecylbenzene sulfonate isomers on interfacial tension behavior in oil/alkali systems. *Fuel* 84 (2005) 1607–1611.
- [97] Shubiao Zhanga, Jie Yanb, Huimian Qia, Jimei Luanc, Weihong Qiaod and Zongshi Li. Interfacial tensions of phenyltetradecane sulfonates for enhanced oil recovery upon the addition of fatty acids. *Journal of Petroleum Science and Engineering* 30 (2005) 117-122.
- [98] Taylor K.C. and Nasr-el-Din H.A. Water-soluble hydrophobically associating polymers for improved oil recovery: A literature review. SPE 29008. SPE International Symposium on Oilfield Chemistry, San Antonio, TX, USA, 14-17 February, (1995).
- [99] Taylor K.C. and Nasr-el-Din H.A. The effect of synthetic surfactants on the interfacial behavior of crude oil/alkali/polymer systems. *Colloids and Surfaces A: Physicochemical and Engineering Aspects* 108 (1, 8): (1996) 49-72.
- [100] Chandra S. Vijapurapu, Dandina N. Rao. Compositional effects of fluids on spreading, adhesion and wettability in porous media. *Colloids and Surfaces A: Physicochem. Eng. Aspects* 241 (2004) 335–342.
- [101] S. Ma, M. Don, Z. Li, E. Shirif. Evaluation of the effectiveness of chemical flooding using heterogeneous sandpack flood test. *Journal of Petroleum Science and Engineering*. 55 (3-4): (2007) 294-300.
- [102] Andrea C and Teamrat A.G. On the transport of emulsions in porous media. *Journal of Colloid and Interface Science*. 313 (1, 1): (2007) 1-4.
- [103] Ying Li, Peng Zhang, Guo-Qing Zhao, Xu-Long Cao, Qi-Wei Wang, Hong-Yan Wang. Effect of equilibrium and dynamic surface activity of surfactant on foam transport in porous medium. *Colloids and Surfaces A: Physicochem. Eng. Aspects* 272 (2006) 124–129.
- [104] Jirui Hou, Zhongchun Liu, Shufen Zhang, Xiang'an Yue and Jinzong Yang. The role of viscoelasticity of alkali/surfactant/polymer solutions in enhanced oil

- recovery. *Journal of Petroleum Science and Engineering*. 47 (3-4): (2005) 219-235.
- [105] K. Moran, A. Yeung, J. Masliyah. The viscoplastic properties of crude oil–water interfaces. *Chemical Engineering Science* 61 (2006) 6016 – 6028.
- [106] N. Agharazi-Dormani, V. Hornof and G. H. Neale. Effects of divalent ions in surfactant flooding. *Journal of Petroleum Science and Engineering* 4 (3): (1990) 189-196.
- [107] Qiang Liua, Mingzhe Donga, Koorosh Asgharia, and Yun Tu. Wettability alteration by magnesium ion binding in heavy oil/brine/chemical/sand systems- Analyses of electrostatic forces, 59 (1-2): (2007) 147-156
- [108] Peimao Zhang, Medad T. Tweheyo, Tor Austad. Wettability alteration and improved oil recovery by spontaneous imbibition of seawater into chalk: Impact of the potential determining ions Ca^{2+} , Mg^{2+} , and SO_4^{2-} , *Colloids and Surfaces A: Physicochem. Eng. Aspects* 301 (2007) 199–208.
- [109] Arne Skauge, Jan Magne Garnes, Ole J. Mørner and Lisa Torske. Optimization of a surfactant flooding process by core-flood experiments. *Journal of Petroleum Science and Engineering*. 7 (1-2): (1992) 117-130.
- [110] C. Porzucek and W. F. Ramirez. Optimal injection strategies for surfactant flooding enhanced oil recovery, Part 2-Studies using an improved phase behavior model and an improved definition of effective salinity. *Journal of Petroleum Science and Engineering* 4 (4): (1990) 335-345.
- [111] Luis E. Zerpa, Nestor V. Queipo, Salvador Pintos and Jean-Louis Salager. An optimization methodology of alkaline–surfactant–polymer flooding processes using field scale numerical simulation and multiple surrogates. *Journal of Petroleum Science and Engineering* 47 (3-4): (2005) 197-208.
- [112] Svante Nilsson, Arild Lohne and Kirsti Veggeland. Effect of polymer on surfactant floodings of oil reservoirs. *Colloids and Surfaces A: Physicochemical and Engineering Aspects*. 127 (1-3): (1997) 241-247.
- [113] Tor Austad, Steinar Ekran, Ingebret Fjelde and Knut Taugbøl. Chemical flooding of oil reservoirs Part 9. Dynamic adsorption of surfactant onto sandstone cores from injection water with and without polymer present.

- Colloids and Surfaces A: Physicochemical and Engineering Aspects. 127 (1-3): (1997) 69-82.
- [114] P. L. Alveskoga, T. Holt and O. Torsæter. The effect of surfactant concentration on the Amott wettability index and residual oil saturation. *Journal of Petroleum Science and Engineering*. 20 (3-4): (1998) 247-252.
- [115] Gan-Zuo Li, Jian-Hai Mu, Ying Li and Shi-Ling Yuan. An experimental study on alkaline/surfactant/ polymer flooding systems using nature mixed carboxylate. *Colloids and Surfaces A: Physicochemical and Engineering Aspects* 173 (1-3): (2000) 219-229.
- [116] Fernando García, Gaudencio Eliosa-Jiménez, Alejandrina Salas-Padrón, Otilio Hernández-Garduza and David Ápam-Martínez Modeling of microemulsion phase diagrams from excess Gibbs energy models. *Chemical Engineering Journal* 84 (3, 15): (2001) 257-274.
- [117] Shubo Deng, Renbi Bai, J. Paul Chen, Gang Yu, Zhanpeng Jiang and Fusheng Zhou. Effects of alkaline/surfactant/polymer on stability of oil droplets in produced water from ASP flooding. *Colloids and Surfaces A: Physicochemical and Engineering Aspects*. 211 (2-3): (2002) 275-284.
- [118] Oslen O.K. Hicks M.D. Hurd B.G. Sinnokrot A.A. and Sweigart C.N. Design of a novel flooding system for an oil-wet central Texas carbonate reservoir. Paper SPE/DOE 20224. Tulsa Oklahoma, (1990).
- [119] Shawn D.T. and Lorenz P.B. Mineral alkali reactions under dynamic conditions. Department of Energy, report no NIPER-340, (1988).
- [120] Can Ulas Hatiboglu and Tayfun Babadagli. Oil recovery by counter-current spontaneous imbibition: Effects of matrix shape factor, gravity, IFT, oil viscosity, wettability, and rock type. *Journal of Petroleum Science and Engineering*, 59 (1-2): (2007) 106-122.
- [121] Tayfun Babadagli, Yaman Boluk. Oil recovery performances of surfactant solutions by capillary imbibition. *Journal of Colloid and Interface Science* 282 (2005) 162–175.

- [122] Wei Wang, Yuzhang Liu, Yongan Gu. Application of a Novel Polymer System in Chemical Enhanced Oil Recovery (EOR). *Colloid & Polymer Science*. 281 (11): (2003) 1046 – 1054.
- [123] M. R. Islam. Emerging Technologies in Enhanced Oil Recovery. *Energy Sources, Part A: Recovery, Utilization, and Environmental Effects*, 21 (1 & 2): (1999) 97 – 111.
- [124] Subhash C. Ayirala, Chandra S. Vijapurapu and Dandina N. Rao. Beneficial effects of wettability altering surfactants in oil-wet fractured reservoirs. *Journal of Petroleum Science and Engineering* 52 (1-4): (2006) 261-274.
- [125] Dag C. Standnes, Tor Austad. Wettability alteration in carbonates Low-cost ammonium surfactants based on bio-derivatives from the coconut palm as active chemicals to change the wettability from oil-wet to water-wet conditions. *Colloids and Surfaces A: Physicochem. Eng. Aspects* 218 (2003) 161-173.
- [126] Sorenson, S. Uber die Messung and die Bedeutung der Wasserstoff ionen Konzentration bei Enzymatischen Prozessen. 1909. *Biochem. Z.*21: 131.
- [127] Arnold E. Greenberg, Lenore S. Clesceri & Andrew D. Eaton, AWWA. *Standard Methods for the Examination of Water and Wastewater*. 18th Edition, (1992).
- [128] Wayne M. Saslow. Chapter 7- Ohm's Law: Electric Current Is Driven by emf, and Limited by Electrical Resistance. *Electricity, Magnetism, and Light* (2002) 281-335.
- [129] W.J. Ryan. *Water Treatment and Purification Technology*. AGROBIOS (India), (2000).
- [130] Minoru Okazaki. *Kurita Hand Book of Water Treatment*. Kurita Water Industries, Tokyo, Japan, (1985).
- [131] A. Walsh and B. M. Gatehouse. Analyses of metallic samples by atomic absorption spectroscopy *Spectrochimica Acta*, 16 (5): (1960) 602-604.
- [132] <http://www.andor.com/chemistry/?app=91>
- [133] Zhu Changjiang, Griffiths Peter R. Extending the Range of Beer's Law in FT-IR Spectrometry. Part II: Theoretical Study of Continuous Apodization Functions. *Applied Spectroscopy*, 52 (11): (1998) p. 1409-1413.

- [134] <http://www.chemistry.nmsu.edu/Instrumentation/AAS1.htm>
- [135] M. M. Cross. Relation between viscoelasticity and shear-thinning behavior in liquids. *Rheologica Acta*, 18 (5) 1979, 609-614.
- [136] R. W. Whorlow. *Rheological techniques*, 2nd edition, Ellis Horwood, (1992).
- [137] M. Reiner and R. Rivlin, (1927) *Kolloid Z*, 43 1.
- [138] W.A. Hyman, (1976) *Ind. Eng. Chem. Fundasn.* 15215-218.
- [139] <http://www.hanssummers.com/electronics/viscometer/mech.htm>
- [140] Michael E. Brown, *Introduction to thermal analyses: Techniques & Applications*. Kluwer Academic Publishers, (1988).
- [141] Cooley J. W. John W. Tukey. An Algorithm for the Machine Calculation of Complex Fourier Series. *Mathematics of Computation*, 19 (90): (1965) 297-301.
- [142] Francis M. Mirabella. *Modern techniques in applied molecular spectroscopy*. Wiley-Interscience, (1998).
- [143] Brian Smith. *Infrared spectral interpretation. A systematic approach*. CRC Press, (1999).
- [144] Bohdan Schatschneider and Eric L. Chronister. High-resolution FTIR study of the para-terphenyl phase transition at high pressure. *Journal of Luminescence*, 127 (1): (2007) 34-40.
- [145] Andreas Fredriksson and Allan Holmgren. An in-situ ATR-FTIR study of the adsorption kinetics of xanthate on germanium. *Colloids and Surfaces A: Physicochemical and Engineering Aspects*, 302 (1-3): (2007) 96-101.
- [146] Anastasios Antonakos, Efthymios Liarokapis and Theodora Leventouri. Micro-Raman and FTIR studies of synthetic and natural apatites *Biomaterials*, 28 (19): (2007) 3043-3054.
- [147] Noel P.G. Roeges. *A Guide to the Complete Interpretation of Infrared Spectra of Organic Structures*. John Wiley & Sons, (1994).
- [148] John. R. Ferraro, K. Krishnan. *Practical Fourier Transform Infrared Spectroscopy. Industrial and Laboratory Chemical Analyses*. Academic Press, (1990).
- [149] Katarzyna Kudlaty. *Attenuated Total Reflection technique for on-line oil monitoring by means of a FTIR fiber-optic probe*. (2004). PhD dissertation,

- submitted to the faculty for electrokinetic and information technology, Technical University Munchen, Germany.
- [150] N. Rashidnia and R. Balasubramaniam "Thermocapillary Migration of Liquid Droplets in a Temperature Gradient in a Density Matched System," *Experiments in Fluids*, Vol 11 (1999), 167- 174.
- [151] A. W. Adamson (1960),"Physical Chemistry of Surfaces," Interscience Publishers Inc.
- [152] C. A. Miller and P. Neogi (1985),"Interfacial Phenomena," Marcel Dekker Inc., New York.
- [153] S. B. Reddy Kani and V. K. Mathur (1988),"Measurement of Interfacial Tension of Immiscible Liquids of Equal Density," *AIChE J.*, Vol 34, NO 1, pp 155-157.
- [154] Defay R. and G Pe'tre', (1991) "Dynamic Surface Tension" in: *Surface and Colloid Science*, Vol. 3, (Editor) E. Matijevic, Wiley-Interscience, New York.
- [155] Roberson .A, C.T. Crowe (1993), *Engineering Fluid Mechanics*, 5th edition, Houghton Mifflin Company, Boston, USA.
- [156] Du Noúy P. Lecomte (1919), "A new apparatus for measuring surface tension", *Gen. Physio.*, 1, 521-524.
- [157] Harkins W .D. and H. Jordon (1930), "A Method for the Determination of Surface and Interfacial Tension from the Maximum Pull on a Ring", *Amer. Chem. Soc.*, 52, 1751-1772.
- [158] Freund B .B. and H.Z. Freund (1930), "A Theory of the Ring Method for the Determination of Surface Tension", *Amer. Chem. Soc.*, 52, 1772-1782.
- [159] D.S. Ambwani and F. Tomlinson, in: *Surface and Colloid Science*, vol. 11, Eds. R.J. Good and R.R. Stromberg, (1965) 2255. Plenum, New York, 1979.
- [160] F. K. Hansen. *Surface Tension by Image Analyses: Fast and Automatic Measurements of Pendant and Sessile Drops and Bubbles* *Journal of Colloid and Interface Science*, 160 (1), 1993, 209-217.
- [161] Harkins, W. D., and Brown, F. E., *J. Am. Chem. Soc.*, 1919, 41, 499; *J. Clin. Inv.*, 1929, 7, 263.

- [162] Tai L. Huo. The Effect of Dynamic Surface Tension on Oxygen Transfer Coefficient in Fine Bubble Aeration System. PhD Dissertation submitted to Civil Engineering Department, University of California, 1998.
- [163] Pierson F.W. and S. Whitaker (1975), "Studies of the Drop-Weight Method for Surfactant Solutions, I. Mathematical Analyses of the Adsorption of Surfactants at the Surface of a Growing Drop", *Journal of Colloid and Interface Science*, 54, 2, 203-218.
- [164] M. Simon, *Ann. Chim. Phys.* 32 (1851) 5.
- [165] http://www.kruss.info/index.php?content=http%3A//www.kruss.info/techniques/bubble_pressure_e.html
- [166] Vibhor K. Srivastava, Gautam Kini, Deeleep Rout. Detergency in spontaneously formed emulsions. *Journal of Colloid and Interface Science* 304 (2006) 214-221.
- [167] Vonnegut B. Rotating bubble method the determination of surface and interfacial tensions. *Rev. Sci. Instr.* 13 (1942) 6-16.
- [168] Princen H. M., Zia I. Y. Z., Mason S. G. Measurement of interfacial tension from the shape of a rotating drop. *J. Colloid Interface Sci.* 23 (1967) 99-107.
- [169] Binnig, G. H. Rohrer, Ch. Gerber and E. Weibel, *Surface Studies by Scanning Tunneling Microscopy*, *Phys. Rev. Lett.*, 49 (1982) 57.
- [170] Binnig, G., Quate, C. F., and Gerber, C. H. Atomic force microscopy. *Physical Review Letters*, 56 (1986) 930-933).
- [171] D errick Rousseau, Shane M. Hodge. Stabilization of water-in-oil emulsions with continuous phase crystals. *Colloids and Surfaces A: Physicochemical and Engineering Aspects*, 2005, 260 (1-3), 229-237.
- [172] F.L. Leite, L.G. Paterno, C.E. Borato, P.S.P. Herrmann, Jr, O.N. Oliveira, L.H.C. Mattoso. Study on the adsorption of poly(o-ethoxyaniline) nanostructured films using atomic force microscopy. *Polymer*, 46 (26): (2005) 12503-12510.
- [173] Fengzhou Zhao, Bing Wang, Xuefeng Cui, Nan Pan, Haiqian Wang, J.G. Hou. Buckle delamination of textured TiO₂ thin films on mica *Thin Solid Films*, 489 (1-2): (2005) 221-228.

- [174] M.A. Beckmann, S. Venkataraman, M.J. Doktycz, J.P. Nataro, C.J. Sullivan, J.L. Morrell-Falvey and D.P. Allison. Measuring cell surface elasticity on enteroaggregative *Escherichia coli* wild type and dispersin mutant by AFM, *Ultramicroscopy*, 106 (8-9): (2006) 695-702.
- [175] A.R. Phani, F.J. Gammel and T. Hack. Structural, mechanical and corrosion resistance properties of $\text{Al}_2\text{O}_3\text{-CeO}_2$ nanocomposites in silica matrix on Mg alloys by a sol-gel dip coating technique. *Surface and Coatings Technology*, 201 (6): (2006) 3299-3306.
- [176] http://www.molec.com/what_is_afm.html
- [177] Brunauer, S., Emmett, P. H. & Teller, E. (1938) Adsorption of gases in multimolecular layers. *J. Am. Chem. Soc.* 60, pp. 309-319.
- [178] Legagneux, L., Cabanes, A. & Dominé, F. (2002) Measurement of 176 snow samples using methane adsorption at 77 K. *J. G. R.* 107, D17, p. 4335.
- [179] Zeller, A. (2004) Measuring the specific surface area of gas hydrates. Master Thesis, University of Göttingen, Germany.
- [180] E. Kowalewski, T. Boassen and O. Torsaeter. Wettability alterations due to aging in crude oil; wettability and Cryo-ESEM analyses. *Journal of Petroleum Science and Engineering* 39 (3-4): (2003) 377-388.
- [181] Goodhew, P.J. and Humphreys, F.J., *Electron Microscopy and Analyses*, 2nd Edition, Taylor & Francis, (1988).
- [182] Chescoe, D. and Goodhew, P.J., *The Operation of Transmission and Scanning Electron Microscopes*, Oxford University Press/Royal Microscopical Society, (1990).
- [183] <http://www.nlectc.org/assistance/edx.html>
- [184] Reid B. Grigg, Baojun Bai. Calcium lignosulfonate adsorption and desorption on Berea sandstone. *Journal of Colloid and Interface Science* 279 (2004) 36-45.
- [185] E. Ayranci, O. Duman, Removal of anionic surfactants from aqueous solutions by adsorption onto high area activated carbon cloth studied by in-situ UV spectroscopy, *Journal of Hazardous Materials* 148 (2007) 75-82.

- [186] W.J. Weber Jr., J.C. Morris, Kinetics of adsorption on carbon from solution, *J. Sanit. Eng. Div. ASCE* 89 (SA2) (1963) 31–59.
- [187] Rahimah Abd. Karim, M. Shaufi Dahlan, Khairul Annuar Noordin, Harun M. Noor, Successful Application of Six Key Elements in Integrating People and Technology Toward Quality Achievements of Angsi Field Development Team. SPE 102804. SPE Annual Technical Conference and Exhibition, San Antonio, Texas, U.S.A., 24–27 September (2006).
- [188] Sorbie, K.S.: *Polymer-Improved Oil Recovery*, Blackie, Glasgow and London, CRC Press Inc., Boca Raton, Florida (1991) 45-48.
- [189] Ahmad Rabieel, M. Ebrahim Zeynali, and Habibollah Baharvand. Synthesis of High Molecular Weight Partially Hydrolyzed Polyacrylamide and Investigation on its Properties. *Iranian Polymer Journal* 14 (7): (2005) 603-608.
- [190] Laishun Shi. An approach to the flame retardation and smoke suppression of ethylene–vinyl acetate copolymer by plasma grafting of acrylamide. *Reactive & Functional Polymers* 45 (2000) 85–93.
- [191] Zeynali M.E., Rabii A., Alkaline hydrolysis of polyacrylamide and study on poly(acrylamide-co-sodium acrylate) properties, *Iranian Polymer Journal*, 11, (2002) 269-275.
- [192] Ayşe Kuleyin. Removal of phenol and 4-chlorophenol by surfactant-modified natural zeolite. *Journal of Hazardous Materials*, 144 (1-2): (2007) 307-315.
- [193] Robert E. C. Wildman, *Handbook of Nutraceuticals and Functional Foods*, 2nd edition, p-472, CRC press, (2006).
- [194] Guangming Liu, Shourong Zheng, Daqiang Yin, Zhaoyi Xu, Jie Fan, Fang Jiang, Adsorption of aqueous alkylphenol ethoxylate surfactants by mesoporous carbon CMK-3. *Journal of Colloid and Interface Science* 302 (2006) 47–53.